

COMPLEXATION AND BIOAVAILABILITY OF DISSOLVED MERCURY  
EVALUATION BY HPLC AND A NOVEL Au-HYDROGEL ANALYTICAL  
SENSOR PROTOCOL.

SHIRLEY THEODORA ROSE LE ROUX



A thesis submitted in partial fulfillment of the requirements for the degree of  
Doctor Philosophiae in Department of Chemistry, University of Western  
Cape

Supervisor: Prof. P G Baker

Co-supervisor: Prof. A M Crouch

March 30, 2017

## Keywords

Mercury

Humic acid

Bioavailability

Cyclic voltammetry

Hydrogel

Sensor



## Declaration

I declare that the entirety of the work: ***Complexation and bioavailability of dissolved mercury evaluation by HPLC and a novel Au-hydrogel analytical sensor protocol*** is my own original work, and that I have not previously in its entirety submitted it for obtaining any qualification, and all sources I have used or quoted was acknowledged as complete references.

Shirley Theodora Rose Le Roux

March 30, 2017

Signature:



Supervisor: Prof. Priscilla Baker

Signature:



Co supervisor: Prof. Andrew Crouch

Signature:

## Acknowledgements

I would like to thank and give praise to the Almighty Father whose love is never ending, for giving me the strength not to give up and to complete the thesis.

Thanks to my beloved family. My husband Roger, for his love, understanding during the most difficult of times and endless support. Thanks to my daughters Liane and Laura for their help, understanding and encouragement.

Many thanks to my supervisor Professor Priscilla Baker for her excellent supervision, help, advice and encouragement. Thanks Prof. Baker, I learned so much from you.

Sincere thanks to Professor A M Crouch for his support, patience, help and encouragement throughout the study.

Dr M Hurndall for her advice with editing the thesis.

Prof. S Reinecke for her help and support with the bioavailability experiments.

All the staff of the Department of Chemistry at CPUT for their advice and assistance.

Ms N Yozana and Mr Mabuwa, students who gave technical assistance.

Thanks to the staff and students of the Sensor Research Laboratory, your friendliness, help and support made the work so much easier.

Prof. Somerset and Ms. Williams from the CSIR for their assistance and support.

CSIR for their financial and technical support.

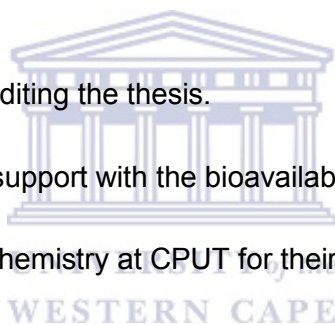


## TABLE OF CONTENTS

Keywords	ii
Declaration	iii
Acknowledgements	iv
Table of contents	v
List of figures	ix
List of tables	xv
List of appendixes	xvii
List of abbreviations	xxi
Nomenclature	xxii
Abstract	xxiii

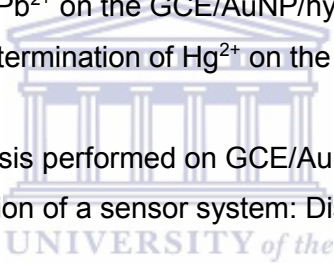
### CHAPTER 1 INTRODUCTION AND OBJECTIVES

1.1	Background to the study	1
1.2	Formation and complexing ability of humic substances	3
1.3	Interactions of mercury in the environment	6
1.4	Anthropogenic sources of mercury and status of mercury research in South Africa	7
1.5	Research objectives	10
1.6	Conceptual diagram	12
1.7	Layout of manuscript	13

### CHAPTER 2 EXPERIMENTAL: ESTABLISHMENT OF AN ANALYTICAL METHOD FOR THE DETERMINATION AND COMPLEXATION OF MERCURY

2.1	Introduction	14
2.2	Experimental protocols	15
2.2.1	Reagents and materials used	15
2.2.2	High -performance liquid chromatography conditions	15
2.2.3	Best conditions for separation and detection of Hg by high–performance liquid chromatography with electrochemical detection	16
2.2.4	Modification of HPLC-EC method for determination of the complexation of Hg <sup>2+</sup> and MeHg with HA	22
2.3	Determination of the complexation of Hg <sup>2+</sup> and MeHg with HA in aqueous phase with HPLC-EC	25

2.3.1	Introduction	25
2.3.2	Investigation of the influence of $\text{Hg}^{2+}$ -to-HA ratio	25
2.3.3	The study of the complexation of $\text{Hg}^{2+}$ and MeHg with HA monitored with HPLC-EC	27
<b>CHAPTER 3 DETERMINATION OF THE KINETICS OF THE COMPLEXATION OF <math>\text{Hg}^{2+}</math> WITH HA IN AN AQUEOUS PHASE</b>		
3.1	Water exposure: Complexation of $\text{Hg}^{2+}$ with HA at selected conditions of pH and temperature using HPLC-EC	32
3.2	Water exposure: Complexation of $\text{Hg}^{2+}$ with HA monitored at 293.15 K	33
3.2.1	Water exposure: Complexation of $\text{Hg}^{2+}$ with HA at 298.15 K	34
3.2.2	Water exposure: Complexation of $\text{Hg}^{2+}$ with HA at 303.15 K	35
3.3	Kinetics of the Hg-HA complexation	37
3.3.1	Kinetics for the complexation of $\text{Hg}^{2+}$ with HA in aqueous phase	37
3.3.2	Determination of the rate constants for the complexation of $\text{Hg}^{2+}$ with HA in aqueous phase for first-order reaction with HPLC-EC	37
3.3.3	Determination of the rate constants for the complexation of $\text{Hg}^{2+}$ with HA in aqueous phase for first-order reaction using hydride generation atomic absorption spectroscopy	40
3.3.4	Rate constants for the complexation of $\text{Hg}^{2+}$ with HA in aqueous phase using the van't Hoff equation	42
3.4	Relationship between rate constant and time	45
3.5	Complexation processes in aqueous phase: Discussion	46
<b>CHAPTER 4 DEVELOPMENT AND OPTIMIZATION OF A NOVEL SENSOR SYSTEM</b>		
4.1	Introduction	50
4.2	Preparation of gold nanoparticles (AuNP)	52
4.3	Preparation and characterization of hydrogel	53
4.3.1	Preparation of hydrogel	53
4.3.2	Characterization of hydrogel	54
4.4	Synthesis and characterization of GCE/AuNP	55
4.4.1	Synthesis of GCE/AuNP	55
4.4.2	Characterization of GCE/AuNP	58

4.5	Synthesis and characterization of GCE/AuNP/hydrogel	63
4.5.1	Synthesis of GCE/AuNP/hydrogel	63
4.5.2	Characterization of GCE/AuNP/Hydrogel	64
4.6	Synthesis and characterization of GCE/AuNP/hydrogel/HA	68
4.7	Summary of results for characterization performed on GCE/AuNP, GCE/AuNP/Hydrogel and GCE/AuNP/Hydrogel/HA	69
4.8	Determination of Hg <sup>2+</sup> on the GCE/AuNP/hydrogel/HA sensor	70
4.8.1	Determination of Hg <sup>2+</sup> on an unmodified GCE	70
4.8.2	Determination of Hg <sup>2+</sup> on the GCE/AuNP/hydrogel/HA sensor	72
4.8.3	Spectroscopic determination of Hg <sup>2+</sup> on the GCE/AuNP/hydrogel/HA sensor	76
4.9	Determination of Pb <sup>2+</sup> on the GCE/AuNP/hydrogel/HA sensor	78
4.9.1	Determination of Pb <sup>2+</sup> on an unmodified GCE	78
4.9.2	Determination of Pb <sup>2+</sup> on the GCE/AuNP/hydrogel/HA sensor	80
4.9.3	Spectroscopic determination of Hg <sup>2+</sup> on the GCE/AuNP/hydrogel/HA sensor	83
4.10	Summary of result for analysis performed on GCE/AuNP/Hydrogel/HA	86
4.11	Development and optimization of a sensor system: Discussion	89
		
<b>CHAPTER 5</b>	<b>DETERMINATION OF INTERACTION OF Hg<sup>2+</sup> WITH HA IN SOIL</b>	
5.1	Introduction	90
5.2	Experimental	90
5.2.1	Recovery studies for Hg <sup>2+</sup> in soil with DMA	91
5.3	Water and soil exposure: Complexation of Hg <sup>2+</sup> with HA monitored over 28 hours at 293.15 K	92
5.3.1	Changes in the total concentration of Hg <sup>2+</sup> in aqueous phase and soil after 28 hours	95
5.4	Kinetics of the Hg <sup>2+</sup> with HA complexation in aqueous phase and soil	96
5.4.1	Rate constant determination for the complexation of Hg <sup>2+</sup> with HA in aqueous phase and soil	97
5.4.2	Rate constants for the complexation of Hg <sup>2+</sup> with HA in aqueous phase and soil, for first-order reaction	97
5.4.3	Rate constants for the complexation of Hg <sup>2+</sup> with HA in aqueous phase and soil using the van't Hoff equation	100
5.5	Complexation processes in aqueous phase and soil: Discussion	103

## CHAPTER 6

## SUMMARY AND CONCLUSIONS

6.1	Introduction	111
6.2	Summary of the complexation of Hg <sup>2+</sup> with HA in aqueous phase/soil/biota	111
6.3	Development of hydrogel sensor	114
6.4	Recommendations	115
<b>BIBLIOGRAPHY</b>		<b>117</b>





## LIST OF FIGURES

Figure 1.1	Hypothetical molecule of fulvic acid.	5
Figure 1.2	Presentation of the binding that can occur between humic substances and metal ions ( $M^{2+}$ ).	5
Figure 1.3	Dissertation conceptual diagram	12
Figure 2.1	Effect of the change the MeOH/THF ratio on the HPLC retention times of MeHg, EtHg, PhHg and $Hg^{2+}$ .	16
Figure 2.2	Effect of concentration of sodium acetate on the HPLC retention time of MeHg, EtHg, PhHg and $Hg^{2+}$ .	17
Figure 2.3	Effect of the pH on the HPLC retention times of MeHg, EtHg, PhHg and $Hg^{2+}$ .	17
Figure 2.4	Chromatogram of a 5 $\mu\text{g/L}$ standard solution of MeHg, EtHg, PhHg and $Hg^{2+}$ determined with HPLC-EC and using best conditions established (Table 2.2).	18
Figure 2.5	Calibration curve of $Hg^{2+}$ determined with HPLC-EC obtained with operating conditions as reported in Table 2.1. Results are the mean of three determinations and insert shows the linear range from 0.5 – 30 $\mu\text{g/L}$ (std deviation, $n = 3$ ).	19
Figure 2.6	Calibration curve of MeHg determined with HPLC-EC obtained with operating conditions as reported in Table 2.1. Results are the mean of three determinations and insert shows the linear range from 0.2 – 30 $\mu\text{g/L}$ (std deviation, $n = 3$ ).	20
Figure 2.7	Calibration curve of MeHg determined with HPLC-EC obtained with operating conditions as reported in Table 2.1. Results are the mean of three determinations and insert shows the linear range from 0.2 – 30 $\mu\text{g/L}$ (std deviation, $n = 3$ ).	20
Figure 2.8	Chromatogram of a mixed 60 $\mu\text{g/L}$ standard solution of MeHg and $Hg^{2+}$ determined with HPLC – EC and using best conditions established (Table 2.1). Retention times for MeHg at 350s and 500s for $Hg^{2+}$ .	23
Figure 2.9	Calibration curve of MeHg determined with HPLC-EC obtained with operating conditions as reported in Table 2.3. Results are the mean of three determinations and insert shows the linear range from 20 – 150 $\mu\text{g/L}$ (std deviation, $n = 3$ ).	23
Figure 2.10	Calibration curve of $Hg^{2+}$ determined with HPLC-EC obtained with operating conditions as reported in Table 2.3. Results are the mean of three	

	determinations and insert shows the linear range from 20 – 150 µg/L (std deviation, n = 3).	24
Figure 2.11	The role of the Hg <sup>2+</sup> /HA ratio on the complexation of Hg <sup>2+</sup> with HA (error bars representing standard error).	26
Figure 2.12	Chromatogram of the complexation of MeHg with HA after 72 hr.	27
Figure 2.13	Complexation of MeHg with HA after 72 hr with HPLC-EC (conditions as described in Paragraph 2.2.5) (std deviation, n = 3).	29
Figure 2.14	Chromatogram of the complexation of Hg <sup>2+</sup> with HA after 72 hr.	30
Figure 2.15	Complexation of Hg <sup>2+</sup> with HA after 72 hr with HPLC-EC (conditions as described in Table 3.1) (error bars representing standard error).	31
Figure 3.1	Complexation of Hg <sup>2+</sup> at 293.15 K (error bars representing standard error).	34
Figure 3.2	Complexation of Hg <sup>2+</sup> at 298.15 K (error bars representing standard error).	35
Figure 3.3	Complexation of Hg <sup>2+</sup> at 303.15 K (error bars representing standard error).	36
Figure 3.4	Rate constant determination of the complexation of Hg <sup>2+</sup> with HA at pH 5.5 at 293.15 K.	38
Figure 3.5	Rate constants (hr <sup>-1</sup> ) vs pH of the complexation of Hg <sup>2+</sup> with HA.	39
Figure 3.6	Rate constants (hr <sup>-1</sup> ) vs temperature of the complexation of Hg <sup>2+</sup> with HA.	39
Figure 3.7	Rate constants (hr <sup>-1</sup> ) vs pH of the complexation of Hg <sup>2+</sup> with HA using Hydride generation atomic absorption spectroscopy.	41
Figure 3.8	Rate constants ( hr <sup>-1</sup> ) vs temperature of the complexation of Hg <sup>2+</sup> with HA using Hydride generation method.	41
Figure 3.9	Rate constants (log K) vs pH of the complexation of Hg <sup>2+</sup> with HA	43
Figure 3.10	Rate constants ( log K) vs temperature of the complexation of Hg <sup>2+</sup> with HA	44
Figure 3.11	Log of the rate constant vs 1/T at pH 7.0.	45
Figure 3.12	Log of the rate constant vs 1/T at pH 5.5 and pH 8.0.	46
Figure 3.13	Graphical representation of a hypothetical HA molecule (Livens, 1991)	48
Figure 3.14	Graphical representation of the complexation of Hg <sup>2+</sup> with HA	48
Figure 3.15	A summary of the complexing processes in this study of Hg <sup>2+</sup> with HA in aqueous phase.	49
Figure 4.1	Graphical representation of the synthesis and characterization of the GCE/AuNP/Hydrogel/HA sensor as planned in this study.	51
Figure 4.2	Graphical representation of the determination of Hg <sup>2+</sup> on the GCE/AuNP/Hydrogel/HA sensor as planned in this study.	52
Figure 4.3	UV/Vis Absorption spectra of AuNP prepared as described in paragraph 5.2.	52

Figure 4.4	UV/Vis Absorption spectra of AuNP before synthesis of the GCE/AuNP.	53
Figure 4.5	FTIR spectrum of the PSF-PVA hydrogel.	54
Figure 4.6	Cyclic Voltammetry of polysulfone hydrogel at a GCE in a 0.1 M HCl solution for characterization of the hydrogel. Cathodic reduction peaks at 0.5 V and -1.0 V.	55
Figure 4.7	Cyclic voltammetry of the 1 mM AuNP deposited on the GCE in 0.1 M NaNO <sub>3</sub> (pH = 3) solution and cycling (n = 10) at a scan rate of 50 mVs <sup>-1</sup> .	56
Figure 4.8	Cyclic voltammetry of the 1 mM AuNP deposited on the GCE in 0.1 M NaNO <sub>3</sub> (pH = 3) solution and cycling (n = 10) at a scan rate of 50 mVs <sup>-1</sup> .	57
Figure 4.9	Cyclic voltammetry of the activation of GCE/AuNP in 0.1 M HCl and cycling (n = 10) at a scan rate of 50 mVs <sup>-1</sup> .	58
Figure 4.10	Cyclic voltammetry of the characterization of the GCE/AuNP in 0.1 M HCl solution at increasing scan rates from 5 – 400 mVs <sup>-1</sup> .	59
Figure 4.11	Determination of diffusion coefficient for GCE/AuNP in 0.1 M HCl with data (n=4) obtained from Figure 5.5.	59
Figure 4.12	Square wave voltammetry of reduction at GCE/AuNP in 0.1 M HCl solution. Peaks appeared at 0.34 V and at 0.8 V.	60
Figure 4.13	Square wave voltammetry of reduction at GCE/AuNP in 0.1 M HCl solution after CV cycles (n = 10).	61
Figure 4.14	Raman spectra representing an unmodified GCE(black), a synthesized GCE/AuNP electrode(red) and another synthesized GCE/AuNP electrode(blue).	61
Figure 4.15	AFM image of an unmodified GCE.	62
Figure 4.16	AFM image of a modified GCE/AuNP (electrode 1).	62
Figure 4.17	AFM image of a modified GCE/AuNP (electrode 2).	63
Figure 4.18	Cyclic voltammetry recorded during deposition of hydrogel on GCE/AuNP. The hydrogel was added to 0.1 M HCl to deposit on GCE/AuNP by CV and cycling (n = 10) at a scan rate of 50 mVs <sup>-1</sup> . The peak at 0.9 V gradually disappeared with successive scans.	64
Figure 4.19	Cyclic voltammetry for the characterization of GCE/AuNP/Hydrogel in 0.1 M HCl solution as a function of increasing scan rates of 5 – 400 mVs <sup>-1</sup> .	65
Figure 4.20	Determination of scan rates and diffusion coefficient for GCE/AuNP/hydrogel in 0.1 M HCl.	65

Figure 4.21	Square wave voltammetry reduction scan at GCE/AuNP/hydrogel in 0.1 M HCl solution. Peaks appeared at -0.32 V and 1.18 V.	66
Figure 4.22	Square wave voltammetry oxidation scan from at GCE/AuNP/hydrogel in 0.1 M HCl solution. Peaks appeared at -0.32 V and 0.85 V.	67
Figure 4.23	Raman spectra representing an unmodified GCE, a GCE/AuNP and GCE/AuNP/Hydrogel electrodes.	67
Figure 4.24	UV/Vis Absorption spectra of a HA solution.	68
Figure 4.25	The GCE/AuNP/hydrogel/HA electrode was placed in a 0.1 M HCl solution and CV scans was obtained by cycling (n=2) at a scan rate of 50mVs <sup>-1</sup> to obtain a baseline.	69
Figure 4.26	Cyclic voltammetry of Hg <sup>2+</sup> at an unmodified GCE in a 0.1 M HCl solution superimposed on a SWV oxidation scan. Peak of Hg <sup>2+</sup> at 0.2 V of the reduction of Hg <sup>2+</sup> to Hg.	70
Figure 4.27	Square wave voltammetry oxidation scan of increasing concentrations of Hg <sup>2+</sup> at an unmodified GCE in a 0.1 M HCl solution.	71
Figure 4.28	Calibration curve obtained using SWV at an unmodified GCE in a deaerated 0.1M HCl solution. Results are the mean of three determinations and insert shows the linear range from 2 – 16 µM (std deviation, n = 3).	71
Figure 4.29	Cyclic voltammetry of the first detectable Hg <sup>2+</sup> peak in the 0.1M HCl solution at the GCE/AuNP/hydrogel/HA . Peak at 2.2 V.	72
Figure 4.30	Cyclic voltammetry of two additions of a 0.1 µmol/L Hg <sup>2+</sup> standard solution at GCE/AuNP/hydrogel/HA in 0.1M HCl solution. Peak at 2.2 V.	73
Figure 4.31	Square wave voltammetry oxidation of Hg <sup>2+</sup> standard at added in increasing concentration at GCE/AuNP/hydrogel/HA in 0.1M HCl solution.	73
Figure 4.32	Square wave voltammetry oxidation of Hg <sup>2+</sup> standard added in increasing concentration at GCE/AuNP/hydrogel/HA in 0.1M HCl solution. Cathodic peak at 2.0 V of the reduction of Hg <sup>2+</sup> to Hg <sup>0</sup> and a peak at 0.48 V of the complexed Hg-HA.	74
Figure 4.33	Square wave voltammetry reduction of a 3.6 µmol/L Hg <sup>2+</sup> standard added in increasing increments at the GCE/AuNP/hydrogel/HA in 0.1M HCl solution. Cathodic peak at 2.0 V of the reduction of Hg <sup>2+</sup> to Hg <sup>0</sup> and a peak at 0.48 V of the complexed Hg-HA.	74
Figure 4.34	Square wave voltammetry at to the 0.1M HCl solution in the cell with the GCE of the reduction of a 3.6 µmol/L Hg <sup>2+</sup> standard added in increasing increments.	

	Cathodic peak at 2.0 V of the reduction of $\text{Hg}^{2+}$ to $\text{Hg}^0$ and a peak at 0.48 V of the complexed Hg-HA.	75
Figure 4.35	Calibration curve of $\text{Hg}^{2+}$ obtained at SWV GCE/AuNP/Hydrogel/HA in a deaerated 0.1M HCl solution and insert shows the linear range from 0.1 – 5 $\mu\text{mol/L}$ (std deviation, $n = 3$ ).	75
Figure 4.36	UV/Vis absorption spectra of the determination of the $\text{Hg}^{2+}$ at the GCE/AuNP/Hydrogel/HA.	76
Figure 4.37	Comparison of Spectroscopic determination and Square wave voltammetry of the $\text{Hg}^{2+}$ complexed with HA at GCE/AuNP/hydrogel/HA in 0.1 M HCl solution.	77
Figure 4.38	Cyclic voltammetry of increasing concentrations of $\text{Pb}^{2+}$ at an unmodified GCE in 0.1 M HCl solution. Peak of $\text{Pb}^{2+}$ appeared at -0.4 V due to the reduction of $\text{Pb}^{2+}$ to Pb.	78
Figure 4.39	Cyclic voltammetry of increasing concentrations of $\text{Pb}^{2+}$ on an unmodified GCE (higher conc than fig 5.36) in a 0.1 M HCl solution. $\text{Pb}^{2+}$ appeared at -0.4 V due to the reduction of $\text{Pb}^{2+}$ to Pb.	79
Figure 4.40	Square wave voltammetry of reduction of $\text{Pb}^{2+}$ at increasing concentrations at GCE in 0.1M HCl solution.	79
Figure 4.41	Calibration curve obtained using Square wave voltammetry at an unmodified GCE in a deaerated 0.1M HCl solution. Results are the mean of three determinations and insert shows the linear range from 0.1 – 0.5 $\mu\text{mol/L}$ (std deviation, $n = 3$ ).	80
Figure 4.42	Cyclic voltammetry of $\text{Pb}^{2+}$ standard at lower concentrations at GCE/AuNP/hydrogel/HA in 0.1M HCl solution. Reduction peak at -0.39V due to the reduction of $\text{Pb}^{2+}$ to Pb and a peak at -0.41V due to the Pb-HA complexation.	81
Figure 4.43	Cyclic voltammetry of the $\text{Pb}^{2+}$ standards at higher concentrations at the GCE/AuNP/hydrogel/HA in 0.1M HCl solution. Reduction peak at -0.39V due to the reduction of $\text{Pb}^{2+}$ to Pb and a peak at -0.41V due to the Pb-HA complexation. The Pb-HA peak the highest in lower concentrations of $\text{Pb}^{2+}$ added (purple) and smallest in the highest concentration of $\text{Pb}^{2+}$ added (blue).	81
Figure 4.44	Square wave voltammetry the $\text{Pb}^{2+}$ standards at increasing concentrations at GCE/AuNP/hydrogel/HA in 0.1M HCl solution. Reduction peak shifted from -0.46 V to -0.39V with increasing concentrations of $\text{Pb}^{2+}$ added to the cell, due	

	to the Pb-HA complexation before the reduction of the uncomplexed $Pb^{2+}$ is detected.	82
Figure 4.45	Square wave voltammetry of the $Pb^{2+}$ standards at increasing concentrations at GCE/AuNP/hydrogel/HA in 0.1M HCl solution. At higher concentrations of the of $Pb^{2+}$ added to the cell only the reduction peak of the uncomplexed $Pb^{2+}$ is detected.	82
Figure 4.46	Calibration curve obtained at SWV GCE/AuNP/Hydrogel/HA in a deaerated 0.1M HCl solution. Results are the mean of three determinations and insert shows the linear range from 0.1 – 0.6 $\mu\text{mol/L}$ (std deviation, $n = 3$ ).	83
Figure 4.47	UV/Vis spectroscopic spectra of the determination of the $Pb^{2+}$ on the GCE/AuNP/Hydrogel/HA.	84
Figure 4.48	UV/Vis Absorption spectra of the determination of the $Pb^{2+}$ on the GCE/AuNP/Hydrogel/HA.	84
Figure 4.49	Comparison of Spectroscopic determination and Square wave voltammetry of the $Pb^{2+}$ complexed with HA at GCE/AuNP/hydrogel/HA in 0.1 M HCl solution.	85
Figure 5.1	The complexation of $Hg^{2+}$ in aqueous phase and soil of the control sample at 293.15 K.	93
Figure 5.2	The complexation of $Hg^{2+}$ in aqueous phase and soil at pH 5.5 at 293.15 K.	94
Figure 5.3	The complexation of $Hg^{2+}$ in aqueous phase and soil at pH 7.0 at 293.15 K.	94
Figure 5.4	The complexation of $Hg^{2+}$ in aqueous phase and soil at pH 8.0 at 293.15 K.	95
Figure 5.5	Rate constants ( $\text{hr}^{-1}$ ) vs pH of the complexation of Hg with HA in aqueous phase.	98
Figure 5.6	Rate constants ( $\text{hr}^{-1}$ ) vs pH of the complexation of Hg with HA in soil.	99
Figure 5.7	Rate constants ( $\text{hr}^{-1}$ ) vs temperature of the complexation of Hg with HA aqueous phase.	99
Figure 5.8	Rate constants ( $\text{hr}^{-1}$ ) vs. temperature of the complexation of Hg with HA in soil.	100
Figure 5.9	Rate constants ( $\log k$ ) vs pH of the complexation of Hg with HA in aqueous phase.	101
Figure 5.10	Rate constants ( $\log k$ ) vs pH of the complexation of Hg with HA in soil.	101
Figure 5.11	Rate constants ( $\log k$ ) vs temperature of the complexation of Hg with HA in aqueous phase.	102

Figure 5.12	Rate constants (log k) vs temperature of the complexation of Hg with HA in soil.	102
Figure 5.13	Comparison of the control sample and the soil sample at 293.15 K (error bars represent standard error).	103
Figure 5.14	Comparison of the soil sample at 293.15 K at different pH values (std deviation).	104
Figure 5.15	Comparison of the soil sample at different pH values at 298.15 K (error bars represent standard error).	105
Figure 5.16	Comparison of the soil sample at different pH values at 303.15 K (error bars represent standard error).	105
Figure 5.17	Summary of the complexation of Hg <sup>2+</sup> with HA in the aqueous phase and soil.	108

### LIST OF TABLES

Table 2.1	The optimum operating HPLC chromatographic conditions for the determination of Hg compounds.	18
Table 2.2	From the calibration curves, the following statistical results were obtained. Linear regression data of MeHg, EtHg, PhHg and Hg <sup>2+</sup> .	21
Table 2.3	From the calibration curves, the following statistical results were obtained. Relative standard deviation values of MeHg, EtHg, PhHg and Hg <sup>2+</sup> .	22
Table 2.4	From the calibration curves, the following statistical results were obtained. Linear regression data for Hg <sup>2+</sup> and MeHg	24
Table 2.5	From the calibration curves, the following statistical results were obtained. Standard deviation and relative standard deviation values for Hg <sup>2+</sup> and MeHg	25
Table 3.1	Data of the complexation of Hg <sup>2+</sup> with HA at 293.15 K	33
Table 3.2	Data of the complexation of Hg <sup>2+</sup> with HA at 298.15 K	35
Table 3.3	Data of the complexation of Hg <sup>2+</sup> with HA at 303.15 K	36
Table 3.4	Rate constants (hr <sup>-1</sup> ) of the complexation of Hg <sup>2+</sup> with HA	38
Table 3.5	Rate constants of the complexation of Hg <sup>2+</sup> with HA	40
Table 3.6	Rate constant vs time of complexation of Hg <sup>2+</sup> with HA	42
Table 3.7	Rate constant (log k) of the complexation of Hg <sup>2+</sup> with HA	43
Table 3.8	Rate constants (log k) of the complexation of Hg <sup>2+</sup> with HA and FA	44
Table 3.9	Summary of the complexing processes of Hg <sup>2+</sup> in aqueous phase	47

Table 4.1	Results of half wave potentials, formal charges and distribution coefficients for the GCE/AuNP/Hydrogel/HA sensor.	69
Table 4.2	Summary of half wave potentials, formal charges and distribution coefficients (n = 4)	70
Table 4.3	Comparison of concentration $\text{Hg}^{2+}$ on modified and unmodified electrode	86
Table 4.4	Comparison of concentration $\text{Pb}^{2+}$ on modified and unmodified electrode	86
Table 4.5	Comparison of complexation constants obtained in this study and compared to literature values (Miller <i>et al.</i> , 2009).	86
Table 4.6	Rate constant (log k) of the complexation of $\text{Hg}^{2+}$ with HA	87
Table 4.7	Conc and pKa values of ionizable sites determined in HA by potentiometric titration in 0.020 M $\text{NaNO}_3$ and $25 \pm 0.1^\circ\text{C}$ ( Nascimento and Masini, 2012).	87
Table 4.8	Rate constants (pKa) of the complexation of $\text{Hg}^{2+}$ with HA	87
Table 4.9	Comparison of complexation constants for $\text{Hg}^{2+}$ obtained in this study and compared to literature (Miller <i>et al.</i> , 2009).	88
Table 5.1	Recovery values for $\text{Hg}^{2+}$ in soil	91
Table 5.2	Data of the complexation of $\text{Hg}^{2+}$ with HA in aqueous phase at 293.15 K	92
Table 5.3	Data of complexation of $\text{Hg}^{2+}$ with HA in soil samples at 293.15 K	93
Table 5.4	Percentage loss of $\text{Hg}^{2+}$ after 28 hr at different temperatures and pHs	96
Table 5.5	Rate constants ( $\text{hr}^{-1}$ ) of the complexation of $\text{Hg}^{2+}$ with HA in aqueous phase	97
Table 5.6	Rate constants ( $\text{hr}^{-1}$ ) of the complexation of $\text{Hg}^{2+}$ with HA in soil	97
Table 5.7	Rate constants (log k) of the complexation of $\text{Hg}^{2+}$ with HA	100
Table 5.8	Rate constants (log k) of the complexation of $\text{Hg}^{2+}$ with HA in soil	100



## LIST OF APPENDIXES

### APPENDIX A:

#### WATER EXPOSURE: COMPLEXATION OF Hg<sup>2+</sup> WITH HA IN AQUEOUS PHASE MONITORED OVER 72 hr at 293.15 K, 298.15 K AND 303.15 K

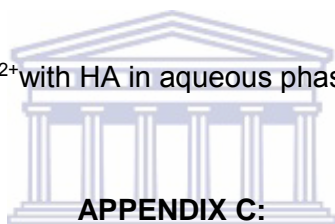
Figure A.1	Complexation of Hg <sup>2+</sup> with HA at pH 5.5 at 293.15 K.	134
Figure A.2	Complexation of Hg <sup>2+</sup> with HA at pH 7.0 at 293.15 K.	134
Figure A.3	Complexation of Hg <sup>2+</sup> with HA at pH 8.0 at 293.15 K.	135
Figure A.4	Complexation of Hg <sup>2+</sup> with HA at pH 5.5 at 298.15 K.	135
Figure A.5	Complexation of Hg <sup>2+</sup> with HA at pH 7.0 at 298.15 K.	136
Figure A.6	Complexation of Hg <sup>2+</sup> with HA at pH 8.0 at 298.15 K.	136
Figure A.7	Complexation of Hg <sup>2+</sup> with HA at pH 5.5 at 303.15 K.	137
Figure A.8	Complexation of Hg <sup>2+</sup> with HA at pH 7.0 at 303.15 K.	137
Figure A.9	Complexation of Hg <sup>2+</sup> with HA at pH 8.0 at 303.15 K.	138
Figure A. 10	Calibration curve of Hg <sup>2+</sup> determined with hydride generation method	138
Table A.1	Calibration curve of Hg <sup>2+</sup> determined with hydride generation method	139
Table A.2	Results of the complexation of Hg <sup>2+</sup> with HA at 293.15 K obtained with hydride generation atomic absorption spectroscopy method	139
Table A.3	Complexation of Hg <sup>2+</sup> with HA at 298.15 K obtained with hydride generation atomic absorption spectroscopy method	140
Table A.4	Complexation of Hg <sup>2+</sup> with HA at 303.15 K obtained with hydride generation method	140

### APPENDIX B:

#### WATER AND SOIL EXPOSURE: COMPLEXATION OF Hg<sup>2+</sup> TO HA IN AQUEOUS PHASE AND SOIL MONITORED OVER 48 hr at 293.15 K, 298.15 K AND 303.15 K

Table B.1	Data of the complexation of Hg <sup>2+</sup> with HA in aqueous phase at 298.15 K	141
Table B.2	Data of the complexation of Hg <sup>2+</sup> with HA in the soil samples at 298.15 K	141
Figure B.1	Complexation of Hg <sup>2+</sup> with HA in aqueous phase and soil of the control at 298.15 K	142

Figure B.2	Complexation of Hg <sup>2+</sup> with HA in aqueous phase and soil at pH 5.5 at 298.15 K.	142
Figure B.3	Complexation of Hg <sup>2+</sup> with HA in aqueous phase and soil at pH 7.0 at 298.15 K.	143
Figure B.4	Complexation of Hg <sup>2+</sup> with HA in aqueous phase and soil at pH 8.0 at 298.15 K.	143
Table B.3	Data of the complexation of Hg <sup>2+</sup> with HA in aqueous phase at 303.15 K	144
Table B.4	Data of the complexation of Hg <sup>2+</sup> with HA in the soil samples at 303.15 K	144
Figure B.5	Complexation of Hg <sup>2+</sup> with HA in aqueous phase and soil of the control at 303.15 K.	145
Figure B.6	Complexation of Hg <sup>2+</sup> with HA in aqueous phase and soil at pH 5.5 at 303.15 K.	145
Figure B.7	Complexation of Hg <sup>2+</sup> with HA in aqueous phase and soil at pH 7.0 at 303.15 K.	146
Figure B.8	Complexation of Hg <sup>2+</sup> with HA in aqueous phase and soil at pH 8.0 at 303.15 K.	146



**APPENDIX C:**

**BIOAVAILABILITY STUDIES: DETERMINATION OF THE COMPLEXATION OF Hg<sup>2+</sup> WITH HA IN AQUEOUS PHASE, SOIL AND EARTHWORMS at 293.15 K, 298.15 K and 303.15 K**

Table C.1	Data of the complexation and adsorption of Hg <sup>2+</sup> in aqueous phase, soil and earthworms of the control at 293.15 K.	147
Figure C.1	Complexation and adsorption of Hg <sup>2+</sup> in aqueous phase, soil and earthworms in the control sample at 293.15 K.	147
Table C.2	Data of the complexation of Hg <sup>2+</sup> with HA in aqueous phase, soil and earthworms pH 7.0 at 293.15 K	148
Figure C.2	Complexation of Hg <sup>2+</sup> with HA in aqueous phase, soil and earthworms at 293.15 K at pH 7.0.	148
Table C.3	Data of the complexation of Hg <sup>2+</sup> with HA in aqueous phase, soil and earthworms at pH 8.0 at 293.15 K	149
Figure C.3	Complexation of Hg <sup>2+</sup> with HA in aqueous phase, soil and earthworms at 293.15 K at pH 8.0.	149

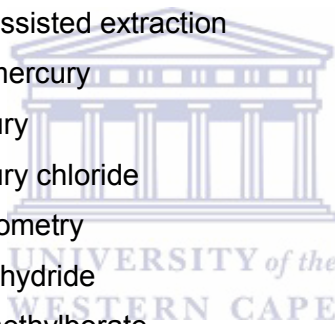
Table C.4	Data of the complexation and adsorption of the $\text{Hg}^{2+}$ in the control in soil and earthworms at 298.15 K	128
Figure C.4	Complexation and adsorption of $\text{Hg}^{2+}$ in soil and earthworms in the control group at 298.15 K.	128
Table C.5	Data of the adsorption and complexation of the $\text{Hg}^{2+}$ in soil and earthworms of the control group at 303.15 K.	129
Figure C.5	Complexation and adsorption of $\text{Hg}^{2+}$ in the control group in soil and earthworms at 303.15 K.	129



## LIST OF ABBREVIATIONS

<b>AAS</b>	Atomic absorption spectroscopy
<b>AES</b>	Atomic emission spectroscopy
<b>AFS</b>	Atomic fluorescence spectroscopy
<b>AFM</b>	Atomic force Microscopy
<b>ATSDR</b>	Agency for Toxic Substances and Disease Registry
<b>AuNP</b>	Gold nanoparticles
<b>BCF</b>	Bioconcentration factor
<b>CAA</b>	Clean Air Act
<b>CAIR</b>	Clean Air Interstate Rule
<b>CDC</b>	Agency for Toxic Substances and Disease Control
<b>CRM</b>	Certified reference material
<b>CSIR</b>	Council for Scientific and Industrial Research
<b>CV</b>	Cyclic voltammetry
<b>CVAAS</b>	Cold vapour atomic absorption spectroscopy
<b>CVAFS</b>	Cold vapour atomic fluorescence spectrometry
<b>DMA</b>	Direct mercury analyser/analysis
<b>DOC</b>	Dissolved organic carbon
<b>DOM</b>	Dissolved organic matter
<b>EC</b>	Electrochemical detector
<b>EDTA</b>	Ethylene diamine tetraacetic acid
<b>EtHg</b>	Ethylmercury
<b>FA</b>	Fulvic acid/s
<b>FDA</b>	Food and Drug Administration
<b>GC</b>	Gas chromatography
<b>GC-ECD</b>	Gas chromatography with an electron capture detector
<b>GC MS</b>	Gas chromatography mass spectrometry
<b>GC-ICP-MS</b>	Gas chromatography inductively coupled plasma mass spectrometry
<b>GFAAS</b>	Graphite furnace atomic absorption spectroscopy
<b>HGAAS</b>	Hydride generation atomic absorption spectroscopy
<b>HA</b>	Humic acid/s

<b>Hg</b>	Mercury
<b>HPLC</b>	High-performance liquid chromatography
<b>HPLC-EC</b>	High-performance liquid chromatography with an electrochemical detector
<b>HPLC-ICP MS</b>	High-performance liquid chromatography inductively coupled plasma mass spectrometry
<b>HPLC-MS</b>	High-performance liquid chromatography mass spectrometry
<b>HS</b>	Humic substance/s
<b>LC-ICP-MS</b>	Liquid chromatography inductively coupled plasma mass spectrometry
<b>ICP</b>	Inductively coupled plasma
<b>ICP-MS</b>	Inductively coupled plasma mass spectrometry
<b>LLE</b>	Liquid-liquid extraction
<b>LOD</b>	Limit of detection
<b>LOQ</b>	Limit of quantification
<b>MAE</b>	Microwave assisted extraction
<b>MeEtHg</b>	Methylethylmercury
<b>MeHg</b>	Methylmercury
<b>MeHgCl</b>	Methylmercury chloride
<b>MS</b>	Mass spectrometry
<b>NaBH<sub>4</sub></b>	Sodium borohydride
<b>NaBEt<sub>4</sub></b>	Sodium tetraethylborate
<b>NaBPh<sub>4</sub></b>	Sodium tetraphenylborate
<b>NaBPr<sub>4</sub></b>	Sodium tetrapropylborate
<b>NOM</b>	Natural organic matter
<b>PE</b>	Polyethylene
<b>PhHg</b>	Phenylmercury
<b>PP</b>	Polypropylene
<b>PTFE</b>	Polytetrafluoroethylene
<b>RSD</b>	Relative standard deviation
<b>SAMA</b>	South African mercury assessment
<b>SWV</b>	Square wave voltammetry
<b>THg</b>	Total mercury
<b>US-EPA</b>	United States Environmental Protection Agency



## NOMENCLATURE

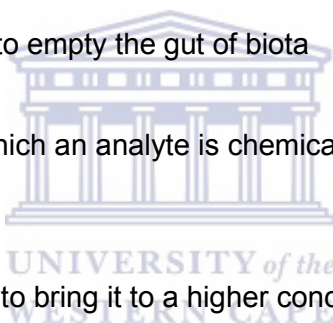
**Abiotic** components or factors are non-living chemical and physical factors in the environment which affects ecosystems.

**Bioaccumulation** is defined as the accumulation of chemicals in the tissue of organisms through any route, including respiration, ingestion, or direct contact with contaminated water, sediment, and pore water in the sediment. These toxic chemicals attain concentrations in biota several orders of magnitude greater than their aqueous concentrations.

**Bioindicators** are biological indicators of soil contamination.

**Deputation** is a starvation period, to empty the gut of biota

**Derivatization** is a procedure in which an analyte is chemically modified to make it easier to detect or separate.



**Preconcentration** of an analyte is to bring it to a higher concentration prior to analysis.

**Physio-chemical parameters** include both physical and chemical properties such as pH, temperature, dissolved oxygen content etc., that influence the properties of aqueous systems.

**Speciation** is the identification and quantification of specific forms of an element, e.g. the analysis of edible fish tissue to determine the concentrations of methylmercury and inorganic mercury present.

## ABSTRACT

Anthropogenic sources as well as natural contributions (e.g. volcanic activity and evaporation from the oceans) have increased mercury levels in the environment. Mercury deposits mainly in sediments, and it finally ends up in aquatic systems. Sediments are capable of immobilising toxic metals but this does not guarantee that the metals are safely removed from aquatic systems. Metals can be reintroduced into aquatic systems if the solubility, mobility and bioavailability of metals change due to environmental factors, such as pH, salt concentration, the presence of complexing agents and changes in redox potential. A metal's mobility, accumulation, bioavailability and toxicity depend on the chemical form of the metal. Dissolved humic acid (HA), play an important role in the speciation and bioavailability of mercury in freshwater systems. Previous studies on both zooplankton and fish indicate that HA reduces the bioavailability of Hg by complexation, yet mercury levels in fish often increase with increasing concentration of humic substance (HS). It is important to fully understand the role that dissolved HA play in the bioavailability of mercury.

The objective of the study was to investigate the impact of HA on the bioavailability of Hg<sup>2+</sup> by: determining the complexation of Hg<sup>2+</sup> with HA in aquatic systems, under different physical conditions; then in aqueous systems and soil, and then to study the uptake of Hg<sup>2+</sup> by selected invertebrates, (e.g. earthworms *Eisenia andrei*) in a controlled laboratory environment, to quantify the impact of HA on Hg bioavailability processes.

Experiments were performed to first determine the best analytical method to use for the separation of Hg<sup>2+</sup>, MeHg, EtHg and PhHg. This analytical method developed for Hg speciation was then used to study the complexation of Hg<sup>2+</sup> with HA in aquatic media, soil and earthworms *Eisenia andrei* under various physical conditions. Rate constants of the complexation reactions were calculated to gain an understanding of the kinetics of the reactions. Rate constants increased with increases in pH and temperature. Rate constants for the complexation of Hg<sup>2+</sup> with HA in aqueous phase were 0.04–0.11 hr<sup>-1</sup>, depending on pH and temperature. Complexation of Hg<sup>2+</sup> in soil was fast and most of the Hg<sup>2+</sup> concentration was transferred from the aqueous phase to the soil within the 24 hr. Rate constants for the complexation of Hg<sup>2+</sup> with HA in soil were 0.087–0.154 hr<sup>-1</sup>.

A novel hydrogel sensor (GCE/Au/Hydrogel/HA) was developed for the study of the complexation of Hg with HA by entrapment of HA into the hydrogel. The stable hydrogel system

was used to determine  $\text{Hg}^{2+}$ . To verify robustness of the system  $\text{Pb}^{2+}$  was also determined. The cyclic voltammetry (CV) and square wave voltammetry (SWV) of both  $\text{Hg}^{2+}$  and  $\text{Pb}^{2+}$  clearly showed the development of  $\text{Hg}^{2+}$ --HA and  $\text{Pb}^{2+}$ --HA complexes at a unique potential compared to the standard redox potential of the free metal. The sensor also shows excellent results for Hg and Pb with LOD (limit of detection) of  $0.02 \mu\text{mol/L}$  and sensitivity of  $0.1\text{-}0.3 \mu\text{mol/L}$ . The disappearance of the free metal, from the electrolytic solution that the GCE/Au/Hydrogel/HA sensor was exposed to, was followed by UV/Vis analysis. An increase in UV/Vis absorbance trend, for  $\text{M}^{2+}$  ion concentration, provided complimentary corroboration for the electrochemically driven complexation of  $\text{M}^{2+}$  ion by the HA ligand entrapped in the sensor matrix. The complexation of  $\text{Hg}^{2+}$  by HA ligand entrapped in the GCE/Au/Hydrogel/HA sensor showed strong affinity for  $\text{Hg}^{2+}$  and  $\text{Pb}^{2+}$  as evident by the high complexation values,  $\log K = 4.75$  and  $\log K = 3.04$  respectively. The complexation values for Hg using the sensor are in good agreement with values established by High-performance liquid chromatography (HPLC)  $\log K = 2.9$  to  $4.80$  (at different temperatures) in this study.





## CHAPTER 1

### INTRODUCTION AND OBJECTIVES

#### 1.1 BACKGROUND TO THE STUDY

The toxicity of mercury (Hg) and its organic compounds is well known and documented (Clarkson, 1993; Davidson *et al.*, 2006; van Wijngaarden *et al.*, 2006; Hassan *et al.*, 2015; Ghanei-Motlagh *et al.*, 2016). It is known to persist in the environment, and has the potential for global atmospheric transport with air masses (Pacyna *et al.*, 2006; Pacyna *et al.*, 2010). Evidence of this atmospheric transport over long distances is reflected in Hg levels in the Arctic that cannot be attributed to natural or local sources (Wilson *et al.*, 2006; Channa *et al.*, 2013). The chemistry of Hg is very complex, making it difficult to predict its behaviour in the environment despite the many investigations on the subject. The biochemical cycle of Hg has been widely studied but uncertainties still exist as to how MeHg (methylmercury) is formed in the environment (Ullrich *et al.*, 2001; Minganti *et al.*, 2007). It is widely accepted that sulphate-reducing bacteria (SRBs) are the primary methylators of Hg<sup>2+</sup> to the more toxic MeHg in freshwater and estuarine anoxic sediments (Rabenstein, 1978; Clarkson, 1993; Walcarius *et al.*, 2004; Davidson *et al.*, 2006; Minganti *et al.*, 2007; Monperrus *et al.*, 2007). Other studies have however demonstrated that abiotic methylation of Hg is possible (Minganti *et al.*, 2007; Monperrus *et al.*, 2007). Factors that have an important impact on abiotic methylation are pH, ionic strength and dissolved organic carbon (DOC) (Gabriel and Williamson, 2004). The more toxic MeHg form is released into the water column, where it bioaccumulates and bioconcentrates up the trophic food chain (Boudou and Ribeyre, 1985; Davidson *et al.*, 2006). Even at low concentrations it can cause severe bioaccumulation problems (Gabriel and Williamson, 2004). The bioaccumulation kinetics of the two forms of Hg, via direct uptake or ingestion, and the transformations of Hg<sup>2+</sup> and MeHg via methylation and demethylation reactions, are difficult to study separately under natural conditions (Odin *et al.*, 1997).

Biomethylation of Hg occurs in all sediments, depending on the environment, and all fish have some level of Hg in their muscle tissue (Davidson *et al.*, 2006). Ninety-four percent of human exposure to Hg is due to dietary intake (Myers *et al.*, 2000; Cabañero *et al.*, 2004) of methyl mercury (MeHg) in fish and seafood products (Maury-Brachet *et al.*, 2006; Hight and Cheng, 2006; van Wijngaarden *et al.*, 2006). The high nutritional value of fish in terms of minerals,

unsaturated lipids, phospholipids and proteins makes it an ideal component of a healthy and balanced diet. Mercury accumulation in humans is a serious health hazard because of the high stability of Hg and the long time it takes before it is eliminated from tissues. It is also known to accumulate in protein-laden tissue rather than in fat (Spiro and Stigliani, 1996). Typical health hazards include immunotoxic and neurotoxic effects in humans. Typical symptoms experienced by those who consumed the contaminated fish included numbness in the limbs, blurring/vision loss, and loss of hearing and muscle coordination, all associated with brain dysfunction caused by MeHg crossing the blood–brain barrier (Clarkson, 1993; Ipolyi *et al.*, 2004). Results of a study of prenatal exposure suggested that levels as low as 10 µg/mL Hg in maternal hair, that grows during pregnancy, can be associated with adverse foetal consequences (Myers *et al.*, 2000). The recommended limit for Hg in fish for human consumption has been set at 0.1–0.4 µg/kg/day by health and environmental authorities such as the United States Environmental Protection Agency (US-EPA) as well as the Agency for Toxic Substances and Disease Control (CDC) (van Wijngaarden *et al.*, 2006). It has been recommended that suitable measures be taken to monitor the health risks associated with consumption of Hg-contaminated fish (Cabañero *et al.*, 2004).

Sediments are an important location as storage reservoirs and for Hg methylation, resulting in high MeHg levels in organisms living in aquatic systems (Inza *et al.*, 1997; Lawrence and Mason, 2001). The speciation and thus bioavailability of Hg depends on a number of physical and biological parameters: DOM and pH have been determined to be two very important factors (Ullrich *et al.*, 2001; Gui-fen *et al.*, 2006; Yang *et al.*, 2007). Both Hg<sup>2+</sup> and MeHg interact strongly with DOM and natural organic matter (NOM) present in sediments (Walcarius *et al.*, 2004). The study of these interactions of Hg<sup>2+</sup> with DOM is important because dissolved Hg<sup>2+</sup> is the main form available for methylation and subsequently bioavailability (Skylberg, 2006). Most of the dissolved organic matter (DOM) in sediments consists of humic and/or fulvic materials. There is a general lack of reliable data of the complexation of Hg<sup>2+</sup> with humic acids (HA) and/or fulvic acids (FA) (do Nascimento and Masini, 2012). The complexity of humics and its variety of potential binding sites make such studies difficult. Most of the natural organic matter (NOM) in sediments consists of HA hence a study of the influence of HA becomes important. The role of HA in the complexation of metals in natural waters is not well known. It has been suggested that, on the physico-chemical and biological conditions, Hg compounds can be changed and released from sediments to the water phase, taken up by biota or freed into the atmosphere or transported to new locations. They may thus keep some of the

biologically important transition-metal ions in solution and are involved in solubilisation and transport (Manahan, 1996).

Metal–organic interactions such as complexation and reduction depend on the soil characteristics and the types of functional groups present (Serudo *et al.*, 2007). These reactions can affect the transportation, accumulation and bioavailability of heavy metals. The abiotic reduction of  $\text{Hg}^{2+}$  by HA may be an important process in the volatilisation of Hg from soils (Serudo *et al.*, 2007). The degree of bioaccumulation and bioavailability depends on the physical and chemical composition of particles (Álvarez *et al.*, 2004). The study of the speciation and complexation of Hg is essential to the understanding and prediction of its availability for absorption.

There is a need for an analytical method that is sensitive, efficient, accurate, and can differentiate between the different forms of Hg. High-efficiency analytical techniques are available to determine different chemical forms rapidly and with good sensitivity. The more widely used methods are gas chromatography(GC) and high-performance liquid chromatography (HPLC), which provide the separating power coupled with element sensitive detectors that provide the necessary sensitivity. For analysis of trace levels of different Hg species, the most widely used methods are chromatographic methods with spectrometric detectors (Capitán-Vallvey *et al.*, 2004). As is evident from a number of studies, cold vapour atomic fluorescence spectroscopy (CVAFS) is a very popular technique for the determination of total mercury analysis (Inza *et al.*, 1997; Morita *et al.*, 1998; Cabañero *et al.*, 2004; Durrieu *et al.*, 2005; Maury-Brachet *et al.*, 2006; Hight and Cheng, 2006; Fitzgerald *et al.*, 2007). Hyphenated techniques are popular for Hg speciation because of their improved analytical performance (Kubáň *et al.*, 2007). However some of these methods are expensive, time-consuming and require numerous sampling handling and separation steps (Priyadarshini & Pradhan, 2017). Voltammetric sensors are popular because they species specific, are relatively inexpensive, have a fast response time, low cost and excellent sensitivity (Ghanei-Motlagh *et al.*, 2016; Asadpour-Zeynali & Amini, 2017).

## **1.2 FORMATION AND COMPLEXING ABILITY OF HUMIC SUBSTANCES**

The amount and origin of organic carbon can be considered to be one of the most important factors in determining biotic functioning in aquatic ecosystems, with the dissolved fraction of organic matter playing a key role in energy flow. Organic matter is a vital resource, affecting

food webs directly, by either uptake from organisms or indirectly by metal chelation and transport of contaminants.

Dissolved organic carbon consists of a non-humic fraction made up of bio-molecular compounds such as lipids, carbohydrates, proteins, and a humic fraction (McDonald *et al.*, 2004). The humic fraction is the main component of organic matter that occurs naturally in soils and waters; it is acidic, classified on the basis of solubility, has a high molecular weight and is generically termed 'humic substances' (HS) (Manahan, 1996; McDonald *et al.*, 2004; Wu *et al.*, 2007). Humic substances occur as depositions in coniferous forest soil, marsh sediments, peat lands, coal, lignite, or in almost any location where large quantities of vegetation have decayed (Sjöblom *et al.*, 2000; McDonald *et al.*, 2004; Moreda-Piñeiro *et al.*, 2004).

Humic substances are a complex mix of substances and have not yet been fully chemically defined (Lehtonen *et al.*, 2000; McDonald *et al.*, 2004; Wu *et al.*, 2007). Although HS have been known since before the 1800s, their structural and chemical characteristics are still being investigated. These substances contain a carbon skeleton with a high degree of aromatic character and with a large percentage of the molecular weight incorporated in functional groups, most of which contain oxygen. If a material containing HS is extracted with a strong base, and the resulting solution is acidified, the products are the following: (a) a nonextractable plant residue called humin; (b) a material that precipitates from the acidified extract, called humic acid (HA); and (c) an organic material that remains in the acidified solution, called fulvic acid (FA). Because of their acid–base, sorptive, and complexing properties, both the soluble and insoluble HS have a strong effect upon the properties of water. Mercury toxicity is greatly influenced by the nature of the sorption/desorption reactions that take place (Gabriel and Williamson, 2004).

In general, FA dissolves in water and exerts its effects as the soluble species. Fulvic acid-type compounds are associated with the yellow colour of water. The functional groups that may be present in HA are carboxyl, phenolic, alcoholic hydroxyl, and carbonyl groups (Figure 1.1). Humin and HA remain insoluble and affect water quality through exchange of cations or organic materials with water (Manahan, 1996). The molecular weights of HS range from a few hundred for FA to tens of thousands for the HA and humin fractions. The elementary composition of most HS is within the following ranges: C, 45–55%; O, 30–45%, H, 3–6%; N, 1–5%; and S, 0–1%. Therefore, the terms humin, HA and FA do not refer to a single compound but to a wide range of compounds of generally similar origin, and with many common properties.

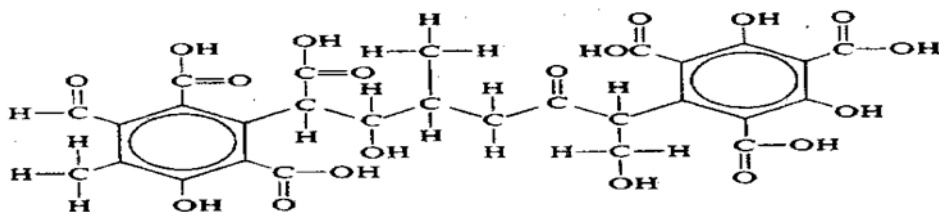


**Figure 1.1** Hypothetical molecule of humic acid (Manahan, 1996).

The insoluble HS, humins and HA, effectively exchange cations with water and may complex large quantities of metals. The binding of metal ions by HA is one of its most important environmental characteristics. This binding can occur as chelation between a carboxyl group and a phenolic hydroxyl group, as chelation between two carboxyl groups, or as complexation with a carboxyl group (see Figure 1.2) or via S-containing groups.

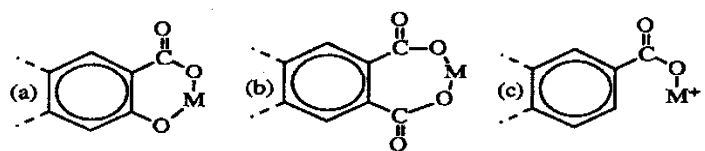


**Figure 1.2** Presentation of the binding that can occur between humic substances and metal ions ( $M^{2+}$ ) (Manahan, 1996).

Studies using X-ray spectroscopy have shown that reduced organic sulphur as well as oxygen and nitrogen are involved in the complexation of Hg with HA. Mercury was found to be complexed by two reduced organic S groups (thiols) at a distance of 2.33 Å in a linear configuration and a third reduced sulphur (most likely an organic sulphide) in a weaker bond at a further distance of 2.92–3.08 Å. When these sites were saturated another bond with carbonyl–O and amino–N was formed at a distance of 2.07 Å, and one at 2.84 Å for carbonyl–O. There is thus powerful confirmation that S-containing groups (thiol) are important binding sites in the complexation of HA to Hg (Haitzer *et al.*, 2002; Khwaja *et al.*, 2006; Skyllberg *et al.*, 2006).

Humic acid is regarded as the most important complexing agents in soil and the strongest Hg sorbent in the aqueous and terrestrial environment (Gabriel and Williamson, 2004; Gui-fen *et al.*, 2006; Yang *et al.*, 2007; do Nascimento *et al.*, 2012). The role of HA in the complexation of metals in natural waters is not well known. It has been suggested that HA keeps some of the biologically important transition metal ions in solution and are involved in solubilisation and

transport (Manahan, 1996). Metal–organic interactions can be by complexation or reduction, depending on the soil characteristics and the types of functional groups present (Serudo *et al.*, 2007). These reactions can affect the transportation, accumulation and bioavailability of heavy metals. The abiotic reduction of  $\text{Hg}^{2+}$  by HA may be an important process in the volatilisation of Hg from soils (Serudo *et al.*, 2007).

### 1.3 INTERACTIONS OF MERCURY IN THE ENVIRONMENT

The inorganic form of Hg and the organic forms clearly have different physicochemical properties and bioaccumulation capacities (Simon and Boudou, 2001). The toxicity of Hg is highly dependent on its chemical form; MeHg is considered more toxic than the inorganic form of Hg (Ipolyi *et al.*, 2004). Methylmercury has a neurotoxic effect, especially for a developing foetus (Clarkson, 1993). Inorganic Hg salts may cause kidney damage when ingested (Jarosinska *et al.*, 2006). Exposure to Hg vapour can have severe health effects because  $\text{Hg}^0$  is highly toxic when inhaled as it can pass into the bloodstream and also cross the blood-brain barrier. In the brain it can presumably be oxidized and bound to protein sulfhydryl groups where it produces the same neurological effects as MeHg (Spiro and Stigliani, 1996). Methylmercury is more readily bioaccumulated than  $\text{Hg}^{2+}$  despite contaminated levels in sediments being one or two thousand times greater for  $\text{Hg}^{2+}$  (Inza *et al.*, 1997; Simon and Boudou, 2001). Results of bioaccumulation in fish showed accumulation factors of 1000 for  $\text{Hg}^{2+}$  and 13 000 for MeHg (Simon and Boudou, 2001). Accumulated MeHg is eliminated slowly because of its high affinity for sulfur ligands, thus contributing to its bioaccumulation in the food chain (Spiro and Stigliani, 1996). Methylmercury can originate from anthropogenic sources, but the  $\text{Hg}^{2+}$  species can be converted to the methylated form in algae and humic substance (HS). The rate and extent of methylation of  $\text{Hg}^{2+}$  in water and sediments is affected by several factors such as the pH, oxygen content and the chemistry of the sediments and water (Ipolyi *et al.*, 2004).

The degree of bioaccumulation and bioavailability depends on the physical and chemical composition of absorbed particles (Álvarez *et al.*, 2004). The study of the speciation of Hg is essential to the understanding and prediction of its availability for absorption. The differences in absorption, distribution and toxicity between  $\text{Hg}^0$ ,  $\text{Hg}^{2+}$  and MeHg are such that detailed studies are required to establish a full picture of bioavailable Hg uptake. While information on the Hg content of foods is reasonably adequate, knowledge of Hg availability and bioavailability is incomplete. Seafood consumption is the predominant pathway of Hg exposure in humans (Clarkson, 1993; Spiro and Stigliani, 1996; Lawrence and Mason, 2001; Ipolyi *et al.*, 2004; Hight

and Cheng, 2006). The total Hg content in food does not provide information about its bioavailability, i.e. the percentage of the ingested amount of the element that can be absorbed during digestion and be transformed into metabolically active species (Cabañero *et al.*, 2004).

Mercury deposits mainly in sediments, where it finally ends up in aquatic systems (Inza *et al.*, 1997; Lawrence and Mason, 2001). Sediments are capable of immobilising toxic metals but this does not guarantee that the metals are safely removed from aquatic systems. Metals can be reintroduced into the aquatic systems if the solubility, mobility and bioavailability increase due to different environmental factors, such as pH, salt concentration, presence of complexing agents and changes in redox potential or chemical form (Minganti *et al.*, 2007). Sediments can be a long-term source of Hg to surface waters (Gabriel and Williamson, 2004). Aquatic organisms are exposed to Hg through direct uptake from the water phase, indirect uptake via food (trophic uptake), or both, and bioaccumulate up the food chain (Clarkson, 1993; Laporte *et al.*, 1997; Maury-Brachet *et al.*, 2006). Bioaccumulation in aquatic organisms is influenced by the total Hg concentrations and the bioavailability of Hg, as well as the physiological properties of the organisms themselves (Grieb *et al.*, 1990; Sjöblom *et al.*, 2000).

The behaviour and transformations of Hg into other forms, as well as the distribution mechanisms in the environment, are still inadequately understood despite the extensive amount of literature on the subject (Ullrich *et al.*, 2001). The study of the transformation and distribution of Hg in water/air, water/soil and subsequent uptake in biota, and the physio-chemical parameters that influence this partitioning, thus becomes important (Ullrich *et al.*, 2001; Miretzky *et al.*, 2005). Combined with appropriate models, such data may also be useful to quantify the chemical partitioning of Hg<sup>2+</sup> and MeHg in humic-rich waters.

#### **1.4 ANTHROPOGENIC SOURCES OF MERCURY AND STATUS OF MERCURY RESEARCH IN SOUTH AFRICA**

Mercury is one of the most toxic contaminants emitted into the atmosphere; it has serious toxic effects on the environment and human health. Metallic Hg is used in many industries and different types of equipment, e.g., in household goods such as batteries, switches, lamps, and other electrical equipment, as a catalyst in the manufacture of sodium hydroxide, in gold mining where the mercury amalgamation method is used (Durrieu *et al.*, 2005), manufacture of batteries and thermometers, and as fungicides, herbicides and disinfectants (Spiro and Stigliani, 1996; Ipolyi *et al.*, 2004). The improper usage and disposal of many of these products in

municipal incinerators, the atmosphere and aquatic systems add to the global load of Hg to the environment. Other anthropogenic sources that contribute significantly to the overall atmospheric Hg emissions are fossil fuel combustion and the incineration of waste materials. It is estimated that fossil fuel combustion contributes  $\pm 25\%$  of global Hg emission. Where high Hg emissions occur in regions such as Southeast Asia, South Africa, Central and Eastern Europe, and the eastern parts of the USA, the main source of electricity and heat production is coal combustion (Pacyna *et al.*, 2003).

South Africa is the world's sixth largest producer of coal (Wagner and Hlatshwayo, 2005); coal provides about 75% of the country's primary energy needs and over 90% of its electricity is coal-driven (Kading *et al.*, 2009; Oosthuizen *et al.*, 2010). Almost all the Hg present in the coal, >90% (Pone *et al.*, 2007) is vaporised and released in the form of elemental Hg. The largest emissions of Hg in South Africa are from coal-fired power plants, with an estimated contribution of 78% (Masekoameng *et al.*, 2010). Anthropogenic Hg emissions are likely to increase as human dependency or demand for energy increases. Masekoameng *et al.*, (2010) studied the trends in the anthropogenic mercury emission for South Africa and showed a general increase in emissions with a contribution of up to 2% of total global emissions.

There are not many reported studies (Davies and Mundalamo, 2010) about the Hg emissions from natural sources although they could be an important contribution to total Hg emission (Masekoameng *et al.*, 2010). The highest natural causes of death in South Africa could debatably be linked to some geo-environmental co-factor such as heavy metal exposure. Health impacts of potentially harmful elements, stemming from sulphide mineralization, mining or ore processing and mine waste disposal are generally not well documented (Davies and Mundalamo, 2010).

Disposal of mine waste in tailing dams could be a large risk to the adjacent environment due to the potential of migration of these toxic, heavy metals to the surrounding area. Inadequate management of these tailing dams has led to serious environmental problems (Rashed, 2010). Dam tailing disasters such as the one at Merriespruit in 1994, when the tailing dam failed and the nearby suburb flooded could have a large impact on the environment (van Niekerk and Viljoen, 2005). South Africa as the world's largest gold producer, discards mine waste in these tailing dams. It is important to understand the environmental impact of heavy metals entering the surrounding area from these tailing dams (Cukrowska *et al.*, 2004). In South Africa and neighbouring countries there is an increase in illegal small-scale mining of disused gold mines



(Channa *et al.*, 2013). These mining operations use entirely Hg extraction methods for gold recovery.

Thor Chemicals (Pty) Ltd., who commissioned a large Hg incinerator in KwaZulu-Natal (South Africa) come to public attention following the death of employees due to Hg poisoning. Further environmental concerns were raised when it was reported that unknown quantities of effluent had been discharged into the Mngceweni River from a holding pond (Oosthuizen and Ehrlich, 2001). An investigation by Greenpeace determined that gross environmental contamination occurred at the site and subsequently the senior management of the plant was prosecuted for negligence in not enforcing proper occupational health control measures (Oosthuizen and Ehrlich, 2001). Although the recycling operation was closed, stockpiles of Hg remain on the premises (Oosthuizen and Ehrlich, 2001). Investigation by Johnston *et al.* (1991) revealed Hg levels in the soil and sediment a few hundred meters from the boundary of the plant that were 8600 times higher than the USA limit for toxic waste (Barratt and Combrink, 2002). The plant was built in close proximity to the Mngceweni River, a tributary of the U'Mgeni River, which flows into the Inanda Dam and provides the city of Durban with drinking water.

Oosthuizen and Ehrlich (2001) determined the human health impact associated with fish consumption in a contaminated area downstream of Thor Chemicals (Pty) Ltd. The authors reported that the level of total Hg concentrations in hair samples was below  $0.5 \mu\text{g g}^{-1}$ , which is below the reference dose set by the US-EPA of  $11 \text{ mg g}^{-1}$ . This study concluded that the fish-eating community has not yet consumed dangerous quantities of Hg, but that if Hg continues to be mobilized from the contaminated sediments into the local ecosystem, could pose a risk to human health (Oosthuizen and Ehrlich, 2001). Barratt and Combrink (2002) investigated the area between Thor Chemicals (Pty)Ltd. and the Inanda Dam. The study showed that Hg levels were similar in magnitude to levels obtained by Johnston *et al.* (1991) eight years prior to the study by Barratt and Combrink (2002). An increase of 98% in Hg in sediment levels was found in a site 10 km downstream from the chemical plant. Possible reasons for this increase may be that bio magnification could have taken place (Barratt and Combrink, 2002). A recent study in the same area by Papu-Zamxaka *et al.*, (2010) found sediment levels with Hg concentrations of 2-10  $\mu\text{g/g}$ , levels severe enough to require remedial action; Hg levels in fish exceeding the WHO and South African guidelines and Hg levels in hair above the WHO guideline level. In the same study it was found that the ratio of MeHg to total Hg in human hair ranged between 75% and 100 %, which implies contamination through diet (Papu-Zamxaka *et al.*, 2010; Channa *et al.*, 2013). The authors conclude that the pollutant

remained at high contamination levels decades after the polluting incident took place. There is a pressing need to address the problem of Hg exposure to the communities living in the area, for remedial action to address the Hg contamination and a ban on fish from the Inanda Dam (Papu-Zamxaka *et al.*, 2010).

Other possible sources of Hg emissions include products of the incineration and treatment of waste at a municipal waste site and medical waste incinerator. Kuhn (2003) found excessive levels of Hg in some of the residents of an area in Cape Town (South Africa) living in close proximity to a waste disposal site, an industrial site that housed a brick factory that burned fossil fuels, and to an oil reclamation plant (potentially resulting in airborne Hg) (Dalvie and Ehrlich, 2005). Dalvie and Ehrlich (2005) found that the urinary Hg levels of residents in the exposure area however were not a major health factor as the levels determined were below levels associated with adverse health effects. In the population in three sites along the South Africa coast Channa *et al.*, (2013) determined Hg levels of 1.15 µg/L and 1.67 µg/L in maternal and cord blood respectively.

Recent legislation in South Africa (e.g. the National Air Quality Act) requires monitoring of the distribution of metals, including Hg species, as part of controlling pollution from industrial processes. There are a number of very efficient analytical techniques capable of determining Hg levels in different matrices. However, most techniques in South Africa measure only total Hg levels, and are often not sensitive enough to determine Hg levels in natural waters. The US-EPA has published methods for measuring low levels of Hg and MeHg in water and biota, using gas chromatography (GC) and cold-vapour atomic fluorescence spectrophotometry (CVAFS) (US-EPA methods 1631 and 1630, 1999).

## 1.5 RESEARCH OBJECTIVES

The purpose of this investigation was to determine the impact of complexation of Hg and dissolved HA, the physio-chemical parameters that influence the complexation and transformation as well as the bioavailability of Hg<sup>2+</sup> by exposing invertebrates in controlled laboratory experiments. Voltammetry, Impedance and High performance liquid chromatography with inductively coupled plasma mass spectroscopy (HPLC-ICP-MS), high performance liquid chromatography with an electrochemical detector (HPLC-EC), or a diode array detector (HPLC-DA) will be used for analysis of aqueous samples. A direct mercury analyser (DMA) will be used to analyse total Hg levels in different substrates: sediments, biota and aqueous media.

General objectives:

- determining the best analytical method for the separation of  $\text{Hg}^{2+}$ , MeHg, EtHg and PhHg by developing methods for Hg speciation
- determine how  $\text{Hg}^{2+}$  and MeHg are affected by the presence of dissolved HA
- study the complexation of  $\text{Hg}^{2+}$  with HA in aquatic systems under different physical conditions;
- validate an analytical method for the analysis of  $\text{Hg}^{2+}$  in sediments
- study the complexation of  $\text{Hg}^{2+}$  with HA in water and sediments under different physical conditions;
- study the uptake of  $\text{Hg}^{2+}$  by selected invertebrates (e.g. earthworms *Eisenia andrei*) in order to quantify the impact of HS on Hg bioavailability processes;
- development of a sensor system and optimization. Functionalization of Humic acid into the hydrogel and characterization.
- verify the data obtained in the study by using appropriate rate speciation data on the chemical partitioning of inorganic Hg in humic waters as well as soil under different physical conditions.

The following conditions will apply; concentrations:  $0.15\text{--}5\ \mu\text{g g}^{-1}$ , pH: 5.5: 7.0 and 8.0, salinity:  $35\ \mu\text{g/mL Cl}^{-1}$  and temperatures: 293.15 K: 298.15 K and 303.15 K.

The purpose of this study was to determine the impact of complexation of Hg and dissolved HA in aqueous media, soil and biota. The investigation of the complexation of Hg and HA is intricate and involves many simultaneous ligand exchanges. It was necessary to develop and modify many analytical methods to use in the study. Voltammetry, High performance liquid chromatography with inductively coupled plasma mass spectroscopy (HPLC-ICP-MS), high performance liquid chromatography with an electrochemical detector (HPLC-EC), or a diode array detector (HPLC-DA) and direct mercury analyser (DMA) was used to analyse total Hg and MeHg levels in different substrates: sediments, biota and aqueous media. A novel hydrogel sensor was developed for the study of the complexation of Hg with HA by functionalization of HA into the hydrogel.

## 1.6 CONCEPTUAL DIAGRAM

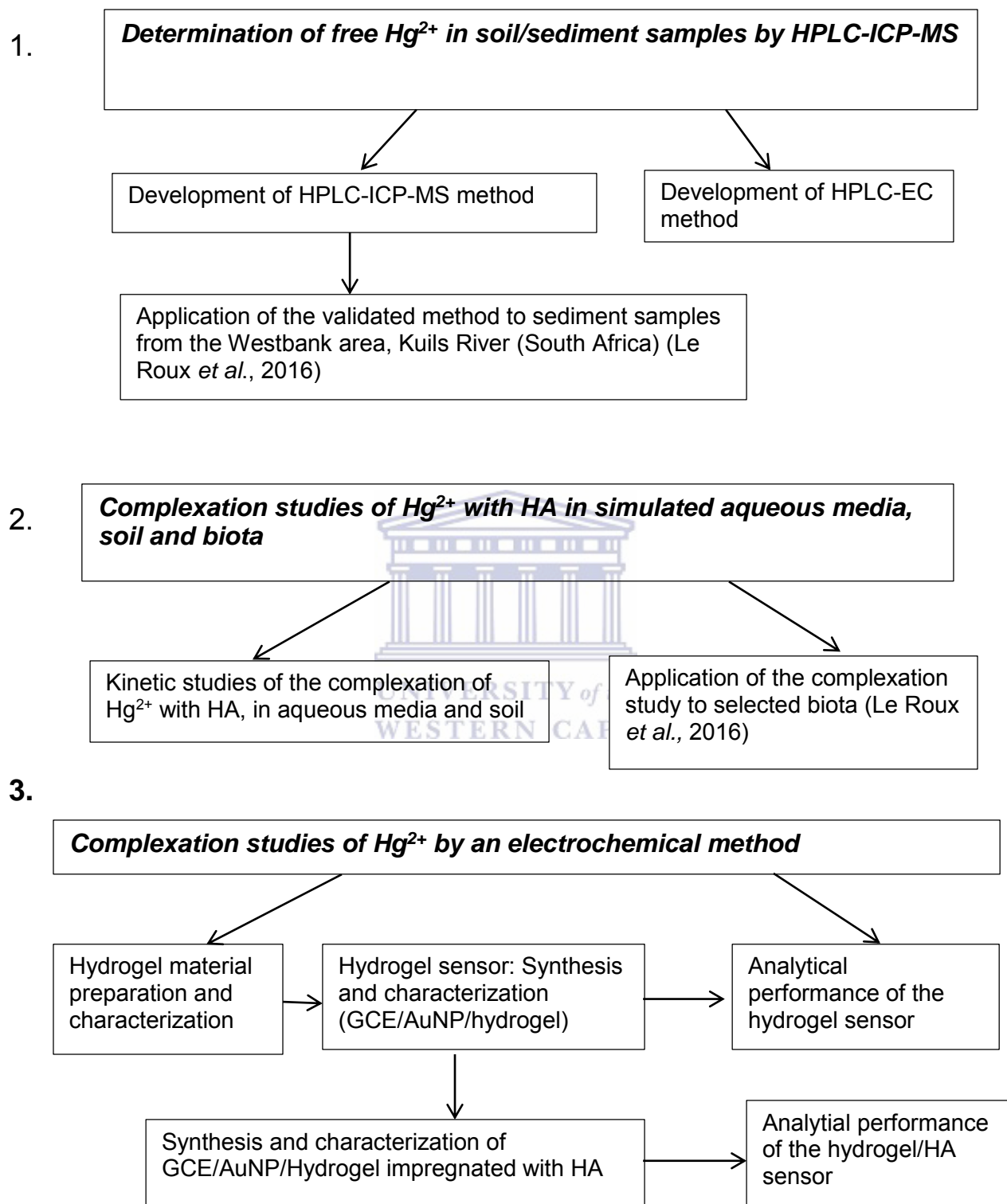


Figure 1.3 Dissertation conceptual diagram

## 1.7 LAYOUT OF MANUSCRIPT

These aspects as laid out in the conceptual diagram (Figure 1.3) are addressed in the following chapters. Determination of free  $\text{Hg}^{2+}$  in soil/sediment samples by HPLC-ICP-MS is laid out in Chapter 1. Chapter 1 introduces the problem of Hg in the environment, and the research objectives of the study are formulated. It describes a practical investigation to study the complexation of  $\text{Hg}^{2+}$  and MeHg with HA in aqueous media. It describes the modification of the HPLC-ICP-MS and HPLC-EC analytical method for the analysis of Hg in aqueous media and soil/sediments. The methods were validated, and tested on sediment samples from the Kuils River system, Kuils River, Western Cape (South Africa). It was published in *S. Afr. J. Chem.*, 2016, 69: *Determination of mercury in selected polluted sediments using HPLC-ICP-MS in Westbank area, Western Cape, South Africa* by authors Shirley Le Roux, Priscilla Baker and Andrew Crouch.

Complexation studies of  $\text{Hg}^{2+}$  with HA in simulated aqueous media, soil and biota is addressed in Chapter 3 and describes the complexation and kinetics of  $\text{Hg}^{2+}$  with HA in water, soil and biota. Results of the complexation of Hg with HA and bioaccumulation of Hg in earthworms *Eisenia andrei* study were published in SpringerPlus Open, DOI10.1186/s40064-016-2282-6 as *Bioaccumulation of total mercury in the earthworm Eisenia Andrei* by authors Shirley Le Roux, Priscilla Baker and Andrew Crouch.

Complexation studies of  $\text{Hg}^{2+}$  by an electrochemical method are addressed in Chapter 4. Chapter 4 describes the hydrogel sensor system that was developed and optimized. The hydrogel sensor system is for the study of Hg complexation with HA by functionalization of HA into the hydrogel. The study is to understand the surface morphology and Electrochemistry principles governing the complexation process. The system will be studied using cyclic voltammetry. As a comparison the complexation of Pb with HA by functionalization of HA into the hydrogel will also be studied.

Chapter 6 presents a summary of the study, the conclusions are drawn to the objectives mentioned at the outset (in Chapter 1).

## CHAPTER 2

### EXPERIMENTAL: ESTABLISHMENT OF AN ANALYTICAL METHOD FOR THE DETERMINATION AND COMPLEXATION OF MERCURY

#### 2.1 INTRODUCTION

It was necessary to develop, from information in previous studies (Sánchez *et al.*, 2000; Hight and Cheng, 2006), a suitable analytical method for the detection and separation of  $\text{Hg}^{2+}$ , MeHg, EtHg and PhHg in environmental samples. The analytical method developed was used to study the complexation of  $\text{Hg}^{2+}$  with HA. The analytical method must be selective, rapid and simple with no time-consuming sample preparation steps to be suitable for the present study. The analytical technique chosen was HPLC that can rapidly and efficiently separate a variety of mercury compounds, but it lacks sufficient concentration detection sensitivity (Dabek-Zlotorzynska *et al.*, 1998; Sánchez *et al.*, 2000; Hight and Cheng, 2006; Houserová *et al.*, 2007). Detectors have been developed that can substantially increase the sensitivity of this analytical technique.

The two analytical methods chosen for use in this study were HPLC-EC and HPLC-ICP-MS. These methods have shown high selectivity, excellent linearity and reproducibility in the analysis of  $\text{Hg}^{2+}$  and other forms of Hg (Dabek-Zlotorzynska *et al.*, 1998). The HPLC-ICP-MS method reported previously by Hight and Cheng (2006) for mercury in biota analysis was adapted in this study and applied to mercury determination in riverbed sediments. Analysis was performed using an HPLC-ICP-MS with mobile phase consisting of aqueous 0.1% w/v L-cysteine HCl-H<sub>2</sub>O + 0.1% L-cysteine and a reverse phase C<sub>18</sub> chromatographic column Synergi Hydro-RP, 150 mm x 4.6 mm, 4 µm (Phenomenex Inc.). Sediments were sampled in the Eerste Kuil River, Westbank area, Kuils River, Western Cape (South Africa) which is located at close proximity to a landfill site. These samples were analysed by HPLC-ICP-MS and the results compared to those obtained by DMA in order to verify the results (Le Roux *et al.*, 2016). The developed method was applied to the recovery of Hg species from sediments. This was necessary because analysis of Hg in soil was important for the present study (Chapter 3–4).

The chromatographic conditions for the separation of  $\text{Hg}^{2+}$ , MeHg, EtHg and PhHg using HPLC-EC method was adapted from a previous study by Sánchez *et al.*, (2000). The modified method was applied to the complexation of  $\text{Hg}^{2+}$  and MeHg with HA.

## 2.2 EXPERIMENTAL PROTOCOLS

To ensure the accuracy of results, MeHg and Hg standards, laboratory duplicates, and standard reference materials of known Hg and MeHg concentrations was analyzed. Detection limits for  $\text{Hg}^{2+}$ , MeHg, EtHg and PhHg were based on three times the standard deviation of the blank measurements, and the average value of triplicate measurements were reported for all analyses. For trace metal analysis of Hg, important procedures must be put in place to avoid contamination of the samples. Special attention was given to the correct cleaning of glassware, sampling method, sample preparation, storage of samples and suitable analytical techniques for the determination of Hg.

### 2.2.1 REAGENTS AND MATERIALS USED

The  $\text{HNO}_3$  (65%), HCl and sodium acetate were reagent grade purity and purchased from Merck. HPLC grade THF and methanol were obtained from Sigma-Aldrich (Sigma-Aldrich, Cape Town, South Africa). Stock solutions of MeHg, EtHg and  $\text{Hg}^{2+}$  were prepared from the respective chloride salts obtained from Aldrich-Sigma at a concentration of  $1.0 \text{ g L}^{-1}$  each. A stock solution of  $\text{Hg}^{2+}$  was prepared by dissolving its chloride salt in 0.1% HCl. Stock solutions of MeHg, EtHg and PhHg were prepared by dissolving the respective salts in HPLC grade methanol and diluting with ultrapure water purified by a Milli-Q (Millipore) system. All stock solutions were stored in a refrigerator. The standard solutions were prepared daily by appropriate dilutions with purified water.

The dithizone (1,5-diphenylthiocarbazone;  $\text{H}_2\text{Dz}$ ) used was ACS grade, obtained from Sigma-Aldrich, and used without further purification. The solution was prepared by dissolving 5.0 mg dithizone in 0.5 mL 25% ammonium hydroxide. Dithizone is almost insoluble in water but dissolves at high pH. The pH was adjusted to 9.0 with acetic acid before diluting to a final volume of 100 mL with Milli-Q purified water (Sánchez *et al.*, 2000).

### 2.2.2 HIGH-PERFORMANCE LIQUID CHROMATOGRAPHY CONDITIONS

Analysis was performed on a 600E Waters System Controller and a 481 Photodiode Array Detector as well as an EC detector. Separation was achieved by using a Nova Pac  $\text{C}_{18}$  column,  $150 \times 4.6 \text{ mm}$ ,  $4 \mu\text{m}$  (Waters Corp., Milford, MA). The detector was set at 475 nm for peak area determinations (Sánchez *et al.*, 2000). The DAX3 Data Acquisition and Analysis Software were used to acquire and process all the chromatographic data obtained. The Hg complexes were detected in the amperometric mode at -0.8V.

The mobile phase consisted of methanol, tetrahydrofuran and sodium acetate buffer. Ethylene diamine tetraacetic acid (EDTA) was added as a complexing agent to eliminate interference of any other ions that may be present. Dithizone forms stable chelates with inorganic as well as organic mercury compounds. Inorganic mercury forms a red-orange 1:2 chelate of the form  $[\text{Hg}(\text{HDz})_2]$ , when complexed in a mildly alkaline solution with excess dithizone. Under similar conditions, MeHg, EtHg, and PhHg form orange-yellow 1:1 chelates of the form  $[\text{RHg}(\text{HDz})]$ . The wavelength of maximum absorbance is about 475 nm as determined in previous studies (Sánchez *et al.*, 2000).

### 2.2.3 BEST CONDITIONS FOR SEPARATION AND DETECTION OF Hg BY HIGH-PERFORMANCE LIQUID CHROMATOGRAPHY WITH ELECTROCHEMICAL DETECTION

The mobile phase that gave the best separation of the mercury species in the shortest retention time was established and illustrated in Figures 2.1–2.3. Conditions were established at a wavelength of 475 nm with a spectroscopic detector (Sanchez *et al.*, 2000). The best conditions for separation were determined by changing the composition of the mobile phase. The effect of the change in the percentage MeOH/THF, the buffer and pH on the retention times of MeHg, EtHg, PhHg and  $\text{Hg}^{2+}$  can be seen in these figures.

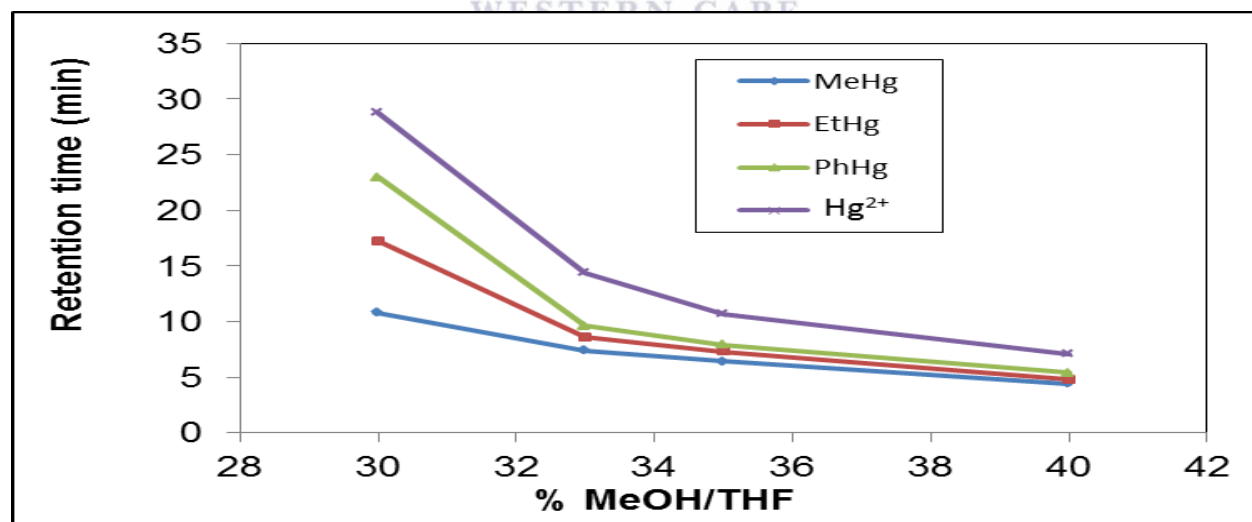


**Figure 2.1** Effect of change of the ratio of MeOH/THF on the HPLC retention times of MeHg, EtHg, PhHg and  $\text{Hg}^{2+}$ .



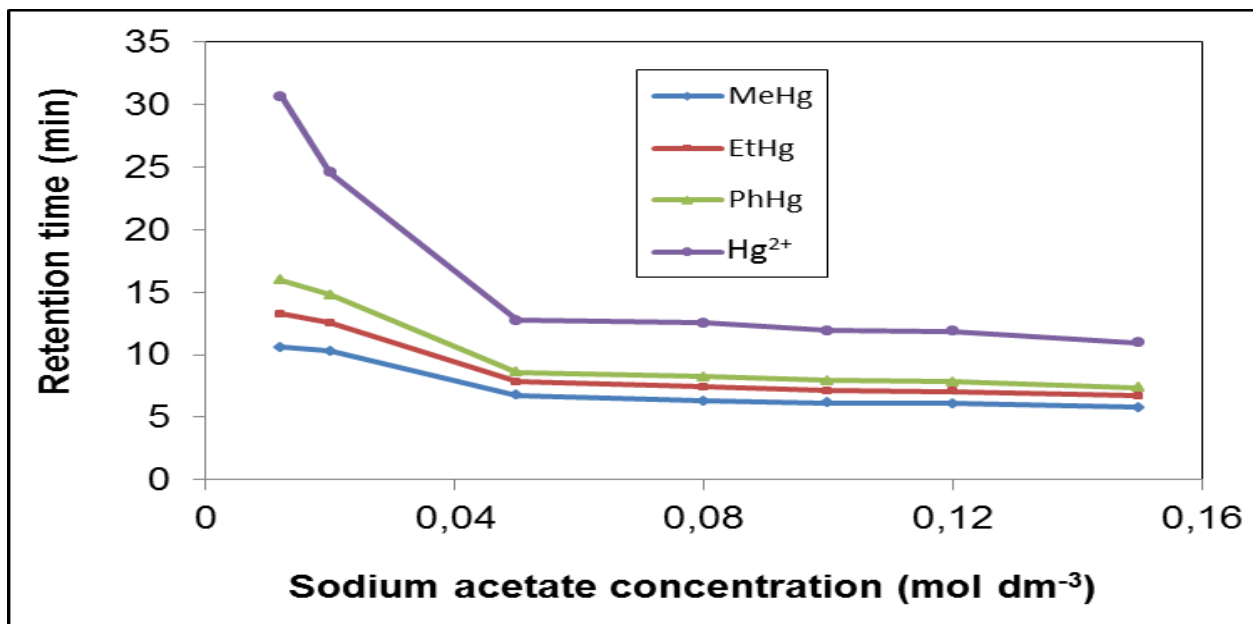


**Figure 2.2** Effect of concentration of sodium acetate on the HPLC retention times of MeHg, EtHg, PhHg and Hg<sup>2+</sup>.

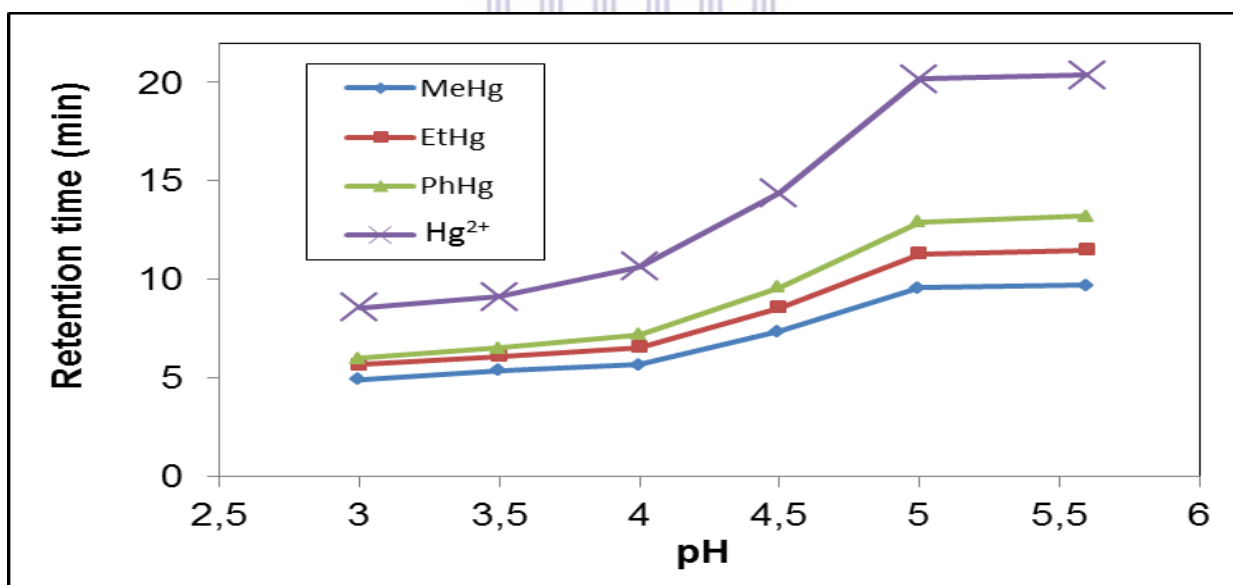


**Figure 2.3** Effect of the pH on the HPLC retention times of MeHg, EtHg, PhHg and Hg<sup>2+</sup>.

With an increase in the pH, better separation of the MeHg, EtHg, PhHg and Hg<sup>2+</sup> peaks were obtained but the retention times increased as well. At pH 3.5 analysis run-time was 10 min and this increased to 24 min at pH of 5.5. Retention times were shorter with an increase in the

concentration of the buffer and the percentage methanol/tetrahydrofuran but with poor separation of peaks. The optimum conditions were determined to be a mixture of 33% (v/v) methanol, 33%(v/v) tetrahydrofuran, 34%(v/v) 0.1 M sodium acetate–acetic acid and pH 4.5. This was based on the best separation with the shortest retention times.

**Table 2.1** The optimum operating HPLC chromatographic conditions for the determination of Hg compounds

	HPLC-EC
Column	Nova Pac C <sub>18</sub> , 150 x 4.6 mm, 4 µm
Column temperature	Ambient
Detection	Electrochemical detector
Wavelength (nm)	475
Injection volume (µl)	20
Flow rate (mL min <sup>-1</sup> )	0.8
Pump mode	Isocratic
Mobile phase	(33/33/34%) Methanol/tetrahydrofuran/ sodium acetate–acetic acid, pH 4.5
Analysis run time (min)	15

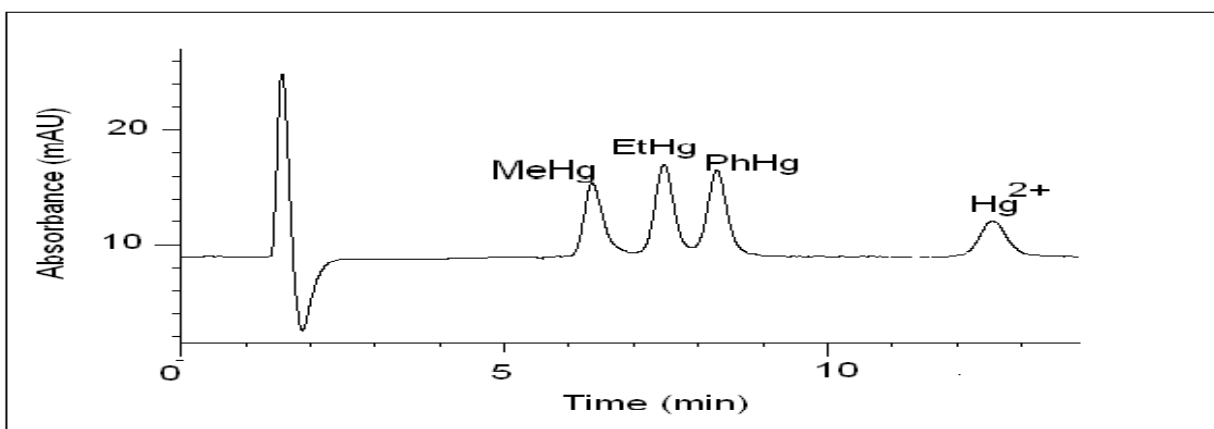


**Figure 2.4** Chromatogram of a 5 µg/L standard solution of MeHg, EtHg, PhHg and Hg<sup>2+</sup> determined with HPLC-EC and using best conditions established (Table 2.2).

The retention time of MeHg, EtHg, PhHg and inorganic Hg was verified by single standard analysis. A cocktail standard was prepared by mixing MeHg, EtHg, PhHg and inorganic Hg. A 20  $\mu\text{L}$  of the prepared standard was injected and analysed. The peaks of the mixed standards were well resolved and the different mercury species all elute within 15 minutes (Figure 2.4). The retention time of MeHg was 6.8 min, EtHg appears at 7.5 min, PhHg at 8.7 min and  $\text{Hg}^{2+}$  at 12.9 min.

Calibration curves for each mercury species were constructed. The calibration graphs containing the information for the determination of the mercury species is illustrated in Figure 2.5 -2.7. The optimum conditions for separation as mentioned in Table 2.1 were used to obtain the required data.

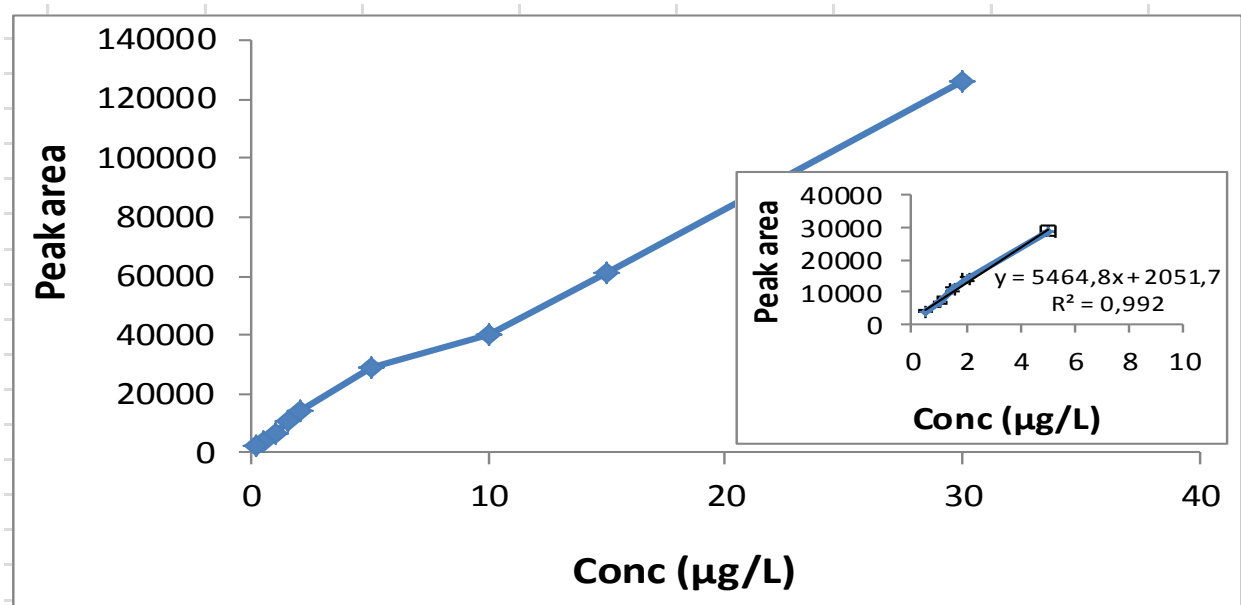


**Figure 2.5** Calibration curve of  $\text{Hg}^{2+}$  determined with HPLC-EC obtained with operating conditions as reported in Table 2.1. Results are the mean of three determinations and insert shows the linear range from 0.5 – 30  $\mu\text{g/L}$  (std deviation,  $n = 3$ ).

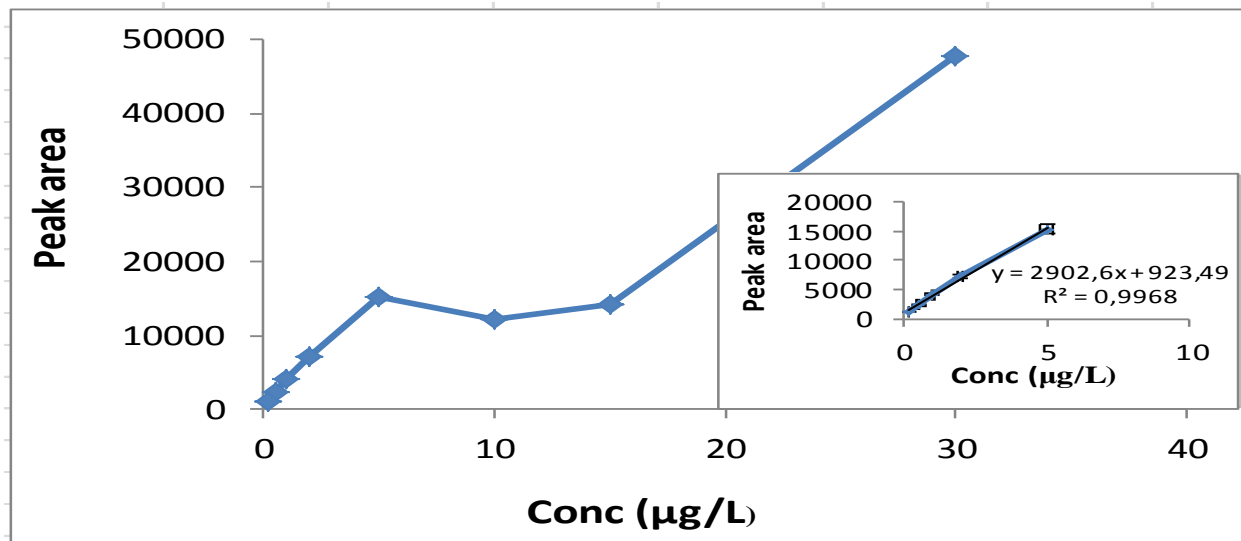


**Figure 2.6** Calibration curve of MeHg determined with HPLC-EC obtained with operating conditions as reported in Table 2.1. Results are the mean of three determinations and insert shows the linear range from 0.2 – 30 µg/L (std deviation, n = 3).

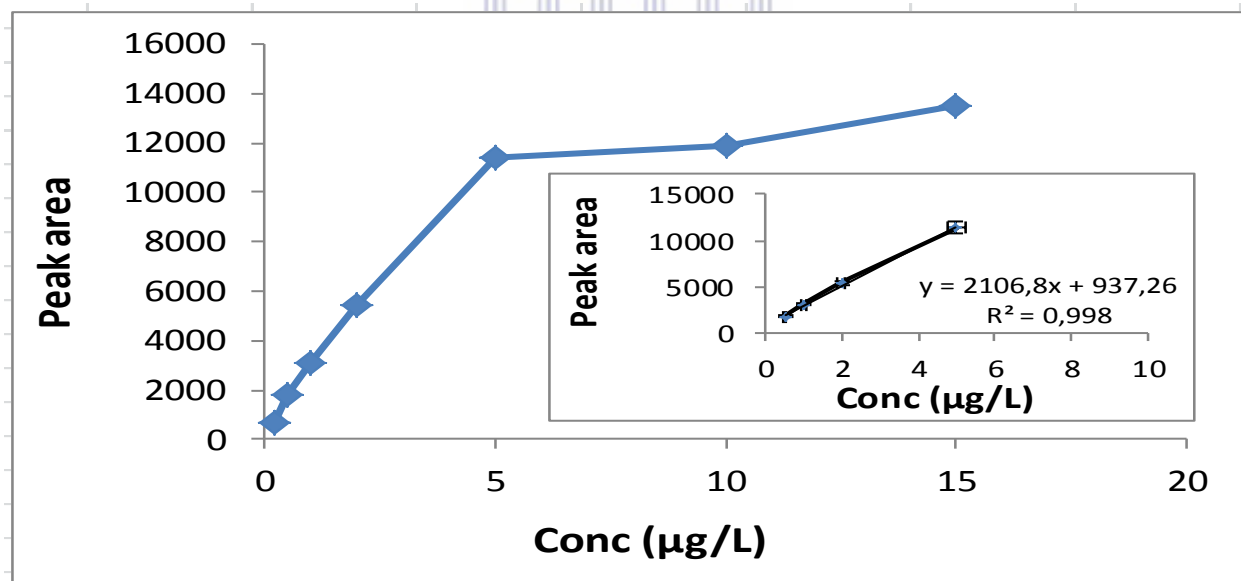


**Figure 2.7** Calibration curve of EtHg determined with HPLC-EC obtained with operating conditions as reported in Table 2.1. Results are the mean of three determinations and insert shows the linear range from 0.2 – 30 µg/L (std deviation, n = 3).

Chromatographic separation of the three compounds was achieved within 12 min at ambient temperature. Retention times were 2.5 min, 4.5 min and 10.8 min for  $Hg^{2+}$ , MeHg and EtHg

respectively. Linear regression data for  $\text{Hg}^{2+}$ , MeHg and EtHg are presented in Table 2.2 below. A calibration curve for each of the four mercury species were obtained from three standards and were found to be linear over the concentration range 0.5 – 20  $\mu\text{g/L}$ . The correlation coefficient was higher than 0.99 for the three compounds.

The analytical protocols produced calibration data which leads to the statistic results as presented in Table 2.2 and 2.3. All statistical data were reported at 95 % confidence level. The detection limit defined as the calculated amount of the analyte which corresponds to a signal equal to three times the standard deviation of six representative blank samples is listed in Table 2.2 and was found to be 2  $\mu\text{g/mL}$  or less for all the species. The limit of detection (LOD) and limit of quantification (LOQ) values were determined using a signal-to-noise ratio of 3 and 10 respectively.

**Table 2.2** From the calibration curves, the following statistical results were obtained. Linear regression data of MeHg, EtHg, PhHg and  $\text{Hg}^{2+}$ .

Compound	Range $\mu\text{g/mL}$	Linear regression equation	Correlation Coefficient ( <i>r</i> )	LOD $\mu\text{g/L}$	LOQ $\mu\text{g/L}$	Sensitivity $\mu\text{g/L}$
MeHg	0.2–5	2903x + 924	0.997	0.2	2.0	0.29
EtHg	0.2–5	2106x + 937	0.998	0.2	2.0	0.21
PhHg	0.2–5	5175x – 276	0.993	0.2	2.0	0.52
$\text{Hg}^{2+}$	0.5–5	5465x + 205	0.998	0.5	1.0	0.55

Linear regression data for MeHg, EtHg, PhHg and  $\text{Hg}^{2+}$  are tabulated in Table 2.2. Calibration curves for each of the four mercury species were obtained from five standards, and were found to be linear over the concentration range 0.2–5  $\mu\text{g/mL}$ . The correlation coefficient was higher than 0.99 in all the calibration curves. The limit of detection for a 20  $\mu\text{L}$  manual injection was 4 ng/  $\mu\text{L}$  for MeHg, EtHg and PhHg and 2 ng/ $\mu\text{L}$  for  $\text{Hg}^{2+}$ . The repeatability for each of the mercury species was examined by injecting eight times with the same standard at two different concentrations. The LOQ values for MeHg and  $\text{Hg}^{2+}$  were lower than for EtHg and PhHg.

**Table 2.3** From the calibration curves, the following statistical results were obtained. Relative standard deviation values of MeHg, EtHg, PhHg and Hg<sup>2+</sup>.

	Relative standard deviation (%) Concentration (2 µg/mL)	Relative standard deviation (%) Concentration (4 µg/mL)
MeHg	3.35	4.26
EtHg	2.99	4.46
PhHg	3.41	4.04
Hg <sup>2+</sup>	2.37	3.89

The detection limit is defined as the calculated amount of the analyte which corresponds to a signal equal to three times the standard deviation of six representative blank samples (Malesuik *et al.*, 2006). The limit of detection (LOD) and limit of quantification (LOQ) values were determined using a signal-to-noise ratio of 3 and 10, respectively. The detection limits for MeHg, EtHg, PhHg were determined to be 4 ng/µL and 2 ng/µL for Hg<sup>2+</sup> for a 20 µL injection. The standard deviation was found to be acceptable with all values less than 10.

#### 2.2.4 MODIFICATION OF HPLC-EC METHOD FOR DETERMINATION OF THE COMPLEXATION OF Hg<sup>2+</sup> AND MeHg WITH HA

A repeat of separation of only Hg<sup>2+</sup> and MeHg was performed with an HPLC-EC by modified conditions as described in Table 2.1 to decrease retention times and make the chromatographic run shorter. The mobile phase was prepared by volume and consisted of a mixture of methanol 40% + tetrahydrofuran 40% + (0.1 M sodium acetate-acetic acid, pH 4) 20%. As the concentration of MeOH/THF increased the analytes eluted more quickly (Figure 2.8).

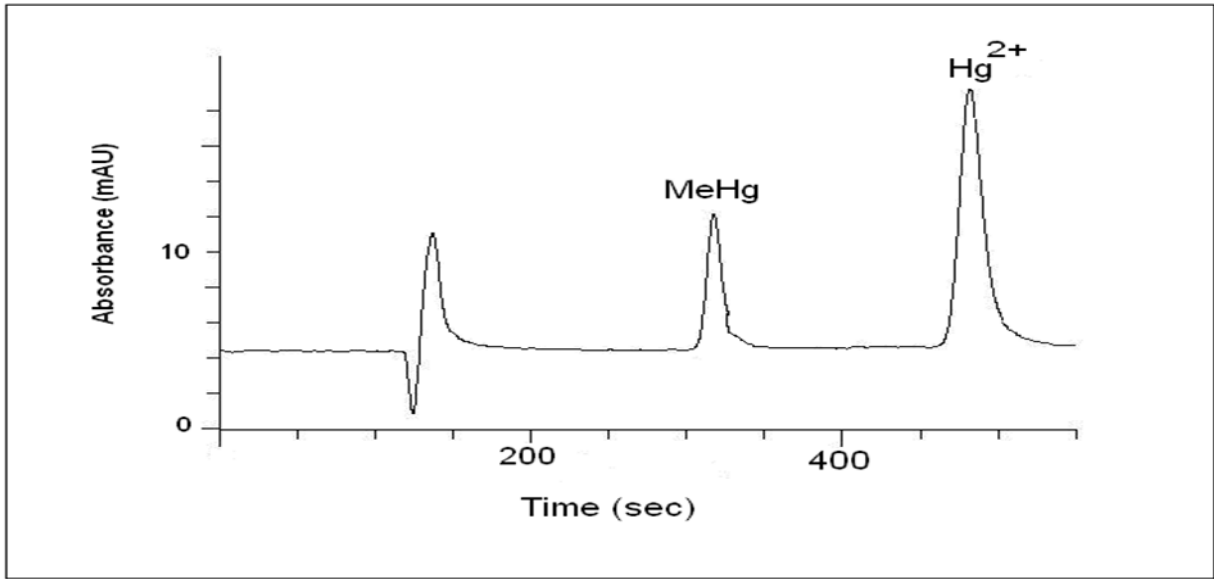


**Figure 2.8** Chromatogram of a mixed 60 µg/L standard solution of MeHg and Hg<sup>2+</sup> determined with HPLC – EC and using best conditions established (Table 2.1). Retention times for MeHg at 350s and 500s for Hg<sup>2+</sup>.

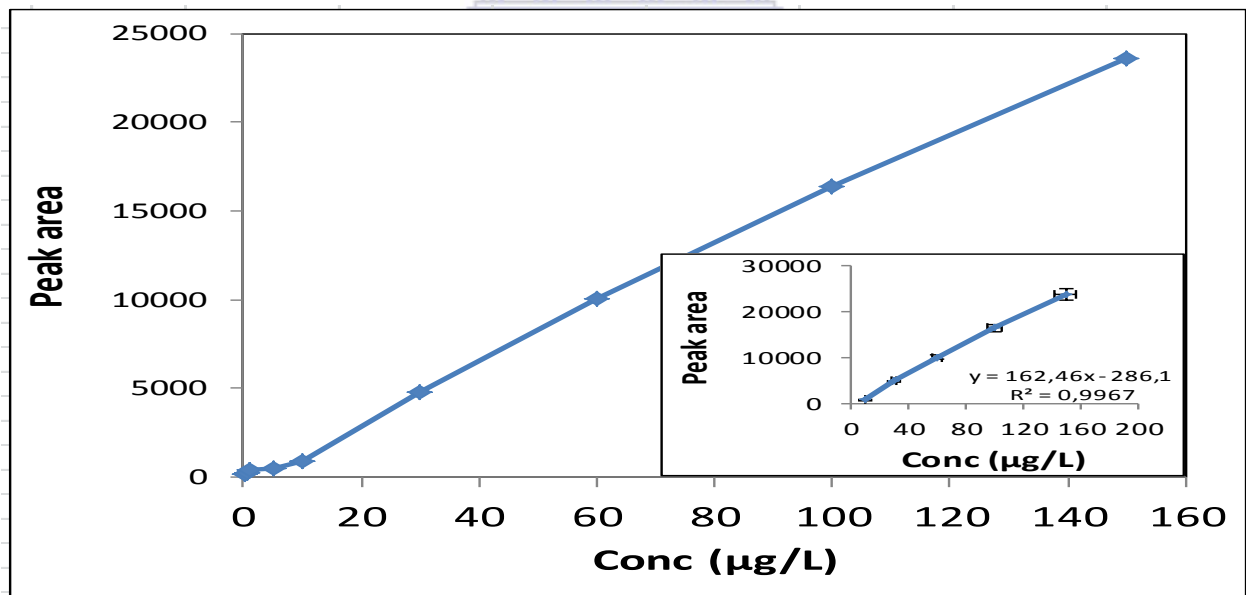


**Figure 2.9** Calibration curve of MeHg determined with HPLC-EC obtained with operating conditions as reported in Table 2.3. Results are the mean of three determinations and insert shows the linear range from 20 – 150 µg/L (std deviation, n = 3).

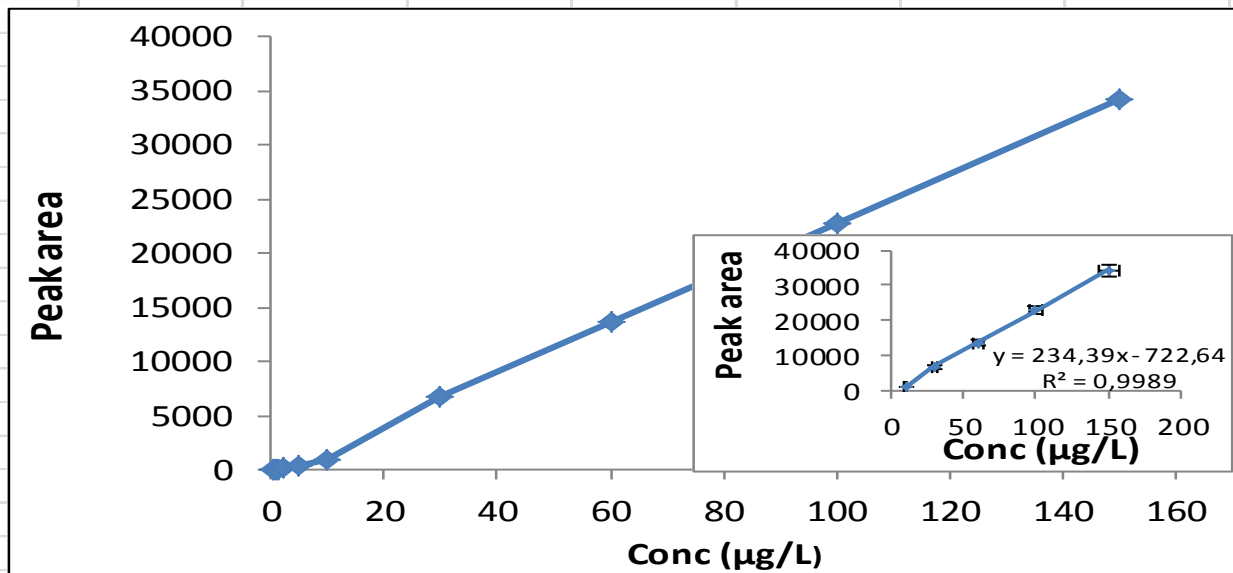


**Figure 2.10** Calibration curve of  $\text{Hg}^{2+}$  determined with HPLC-EC obtained with operating conditions as reported in Table 2.3. Results are the mean of three determinations and insert shows the linear range from 20 – 150  $\mu\text{g/L}$  (std deviation,  $n = 3$ ).

Calibration curves for the two mercury species were obtained from ten standards, and were found to be linear over the concentration range 0.2–20  $\mu\text{g/L}$  (Figure 2.9 and 2.10). The result of the linear regression, correlation coefficient, LOD, LOQ and the standard deviation are tabulated (Tables 2.4 and 2.5). These results were obtained using conditions as described in Section 2.2.5

**Table 2.4** From the calibration curves, the following statistical results were obtained. Linear regression data for  $\text{Hg}^{2+}$  and MeHg

Compound	Range ( $\mu\text{g/L}$ )	Linear Regression equation	Correlation Coefficient, ( $r$ )	LOD ( $\mu\text{g/L}$ )	LOQ ( $\mu\text{g/L}$ )	Sensitivity $\mu\text{g/L}$
MeHg	10 – 150	$162.7x - 286.1$	0.997	0.4	4	0.12
$\text{Hg}^{2+}$	10 – 150	$234.4x - 722.6$	0.999	0.5	5	0.23



**Table 2.5** From the calibration curves, the following statistical results were obtained. Standard deviation and relative standard deviation values for Hg<sup>2+</sup> and MeHg

	Standard deviation Concentration (80 µg/L)	Relative standard deviation Concentration (80 µg/L) (%)
MeHg	0.316	3.16
Hg <sup>2+</sup>	0.270	2.70

## 2.3 DETERMINATION OF THE COMPLEXATION OF Hg<sup>2+</sup> AND MeHg WITH HA IN AQUEOUS PHASE WITH HPLC-EC

### 2.3.1 INTRODUCTION

In recent years a considerable amount of research has been devoted to the understanding of Hg and its compounds because of the very toxic nature of these compounds and thus the potential threat to human health. Different forms of Hg differ in toxicity and the speciation of Hg is of particular importance. Speciation determines toxicity, bioavailability, residence time and transport pathways in the environment (Gui-fen *et al.*, 2006; Yang *et al.*, 2007). The speciation and thus availability of Hg depends on a number of physical and biological parameters: DOM and pH have been determined to be two very important factors (Ullrich *et al.*, 2001; Gui-fen *et al.*, 2006; Yang *et al.*, 2007). The most important ligand of DOM is HA and it plays a very important role because of the strong binding between Hg and HA.

The role of the complexation of Hg<sup>2+</sup> and MeHg with HA was investigated. The complexation process was initially monitored over a period of 72 hr and various concentrations at room temperature to obtain optimum conditions. The concentrations selected for this initial investigation (not shown) of MeHg and Hg<sup>2+</sup> respectively were 150 µg/L, 100 µg/L, 80 µg/L, 60 µg/L and 30 µg/L. After the sequential injections of the different concentrations a decision was made to use 80 µg/L concentration for the subsequent experiments as it gave a good signal to noise ratio of 2 or more.

### 2.3.2 INVESTIGATION OF THE INFLUENCE OF Hg<sup>2+</sup>-to-HA RATIO

The complexation of Hg<sup>2+</sup> with HA could be influenced by the ratio of Hg<sup>2+</sup>/HA. Spectroscopic evidence (Skylberg *et al.*, 2006) found evidence of Hg binding to reduced organic sulphur

groups in organic matter. These interactions between compounds containing sulphur and Hg can be very strong and such interactions are expected to dominate interactions between Hg<sup>2+</sup> and HA. However the oxygen containing groups are present in much higher concentrations than the sulphur containing groups and at lower ratio of Hg<sup>2+</sup>-to-HA could saturate bonding sites.

The influence of the concentration ratio of Hg<sup>2+</sup>/HA was investigated and reported in Figure 2.11. The concentration of Hg<sup>2+</sup> used was 80 µg/L and the Hg<sup>2+</sup>/HA ratios were 1:1; 1:100: and 1:1000. A control sample (no HA added) was also determined.

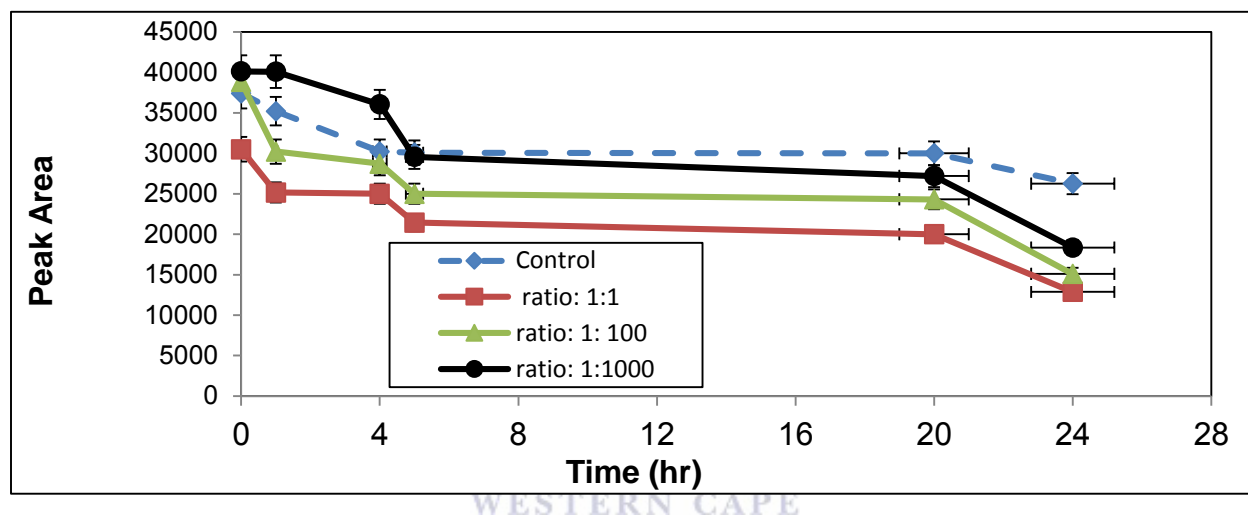


**Figure 2.11** The role of the Hg<sup>2+</sup>/HA ratio on the complexation of Hg<sup>2+</sup> with HA (error bars representing standard error).

The same concentration of Hg<sup>2+</sup> was used for all experimental values and the first analysis was performed after addition of reagents. Initially there was a sharp decrease for all values. The samples with lower concentration of HA decreased more rapidly than the one with highest concentration of HA. Between 5 hr and 25 hr there is a steady state where the concentration remained constant. After 24 hr there was a rapid decrease for all values except the control. Although more constant the control also decreased and that could be due to Hg<sup>2+</sup> evaporation and adsorption on the container walls.

Previous studies (Haitzer *et al.*, 2002., Haitzer *et al.*, 2003; Khwaja *et al.*, 2006; Helal *et al.*, 2007) have found that the Hg-HA complexation was found to be influenced by the ratio of Hg<sup>2+</sup>/HA. For the present study it was decided to use the same concentration of HA as that of the Hg<sup>2+</sup> and MeHg i.e. 80 µg/L.

### 2.3.3 THE STUDY OF THE COMPLEXATION OF Hg<sup>2+</sup> AND MeHg WITH HA, MONITORED by HPLC-EC UNDER AMBIENT CONDITIONS

The complexation process was initially monitored over a period of 72 hr at room temperature. The mixed solution of MeHg and HA was prepared to a final concentration of 80 µg/L. The HA solution was prepared from a soluble form of HA (Sigma Aldrich Catalogue number H1, 675-2 Lot.:S33786-057). A control sample was prepared using the same conditions but without HA added. Mercury compounds are unstable and degrade with time, hence control samples were also prepared and analysed over the same period and under the same conditions.

The MeHg complexes were detected with HPLC-EC in the amperometric mode at -0.8V with optimum conditions for the HPLC. This optimum voltage for the EC determination was determined by cyclic voltammetry with the chromatograms of the results shown in Figures 2.13 and 2.14.

The chromatogram in Figure 2.12 represents three different chromatographic runs showing the difference in concentration as the complexation proceeds. The line in the chromatogram labelled 1 (green) is of the uncomplexed MeHg, line 2 (black) five min after addition of HA to MeHg and 3 (red) 72 hr after the addition of HA to MeHg.

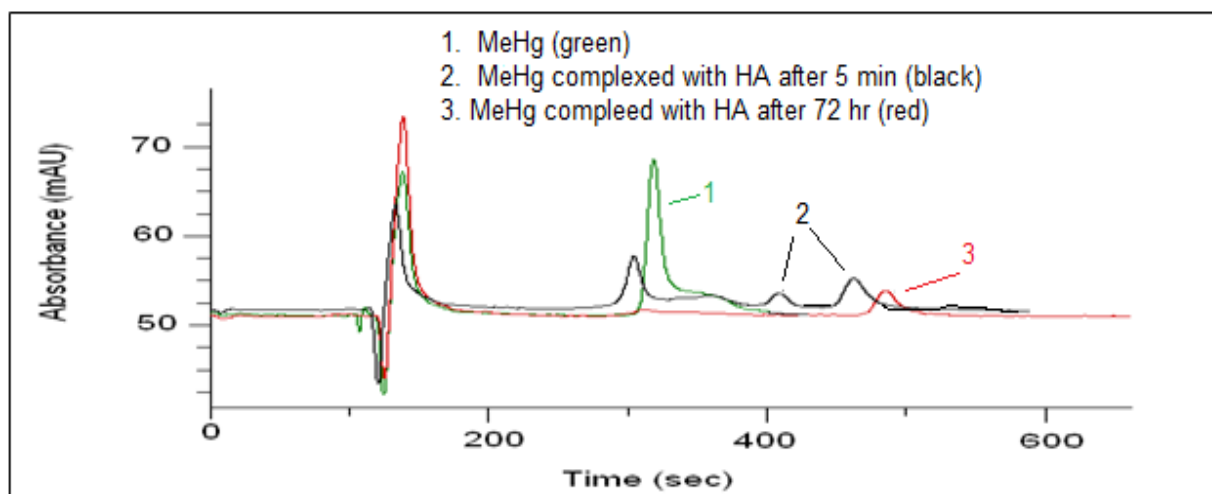


**Figure 2.12** Chromatogram of the complexation of MeHg with HA after 72 hr.

The complexation of MeHg with HA in the initial investigation was evaluated (t = 0) green, (t = 5 min) black and (t = 72 hr) red. Line 1 (green) of the uncomplexed compound shows the biggest

peak at a retention time of 325 sec and the highest concentration of MeHg. Line 2 (black), was of a chromatographic run immediately after addition of HA and shows a decrease in the concentration of the uncomplexed MeHg and two new peaks were observed. One of the new peaks had the same retention time as  $Hg^{2+}$  (at 475 sec). Line 3 (red) shows the results 72 hr after addition of HA. The peak representing the uncomplexed MeHg (retention time at about 330 sec) had disappeared and a new peak was formed at the same retention time as  $Hg^{2+}$ , at 500 sec (Figure 2.11) as represented by the reactions a - c. This confirmed a conversion from MeHg to the inorganic form. Previous studies have also showed that abiotic methylation/demethylation can occur (Gabriel *et al.*, 2004; Rodríguez Martín-Doimeadios *et al.*, 2004; Gui-fen *et al.*, 2006).

The chemical transformations corresponding to the different time intervals may be represented as follows:

(a) MeHg (uncomplexed) or  $CH_3Hg^+$

(b)  $MeHg + HA \rightarrow MeHg \text{ (amount still uncomplexed)} + MeHg-HA + Hg-HA$

or

$CH_3Hg^+ + HA \rightarrow CH_3Hg^+ + CH_3Hg^+ - HA \rightarrow CH_3---Hg--HA \rightarrow CH_3^{\cdot} + Hg^{2+} + Hg-HA$

(c)  $MeHg + HA \rightarrow Hg^{2+} \text{ (72 hr)}$

or  $CH_3Hg^+ + HA \rightarrow Hg^{2+} \text{ (72 hr)}$

The ability of MeHg to form multidentate bonds with ligands is limited. The affinity of HA for MeHg is thus considerably weaker than for  $Hg^{2+}$ , so the  $CH_3Hg^+ - HA$  bond is weaker than the  $Hg^{2+}-HA$  bond. Hence it binds preferentially to the carbonyl group of the HA (Tipping, 2007).

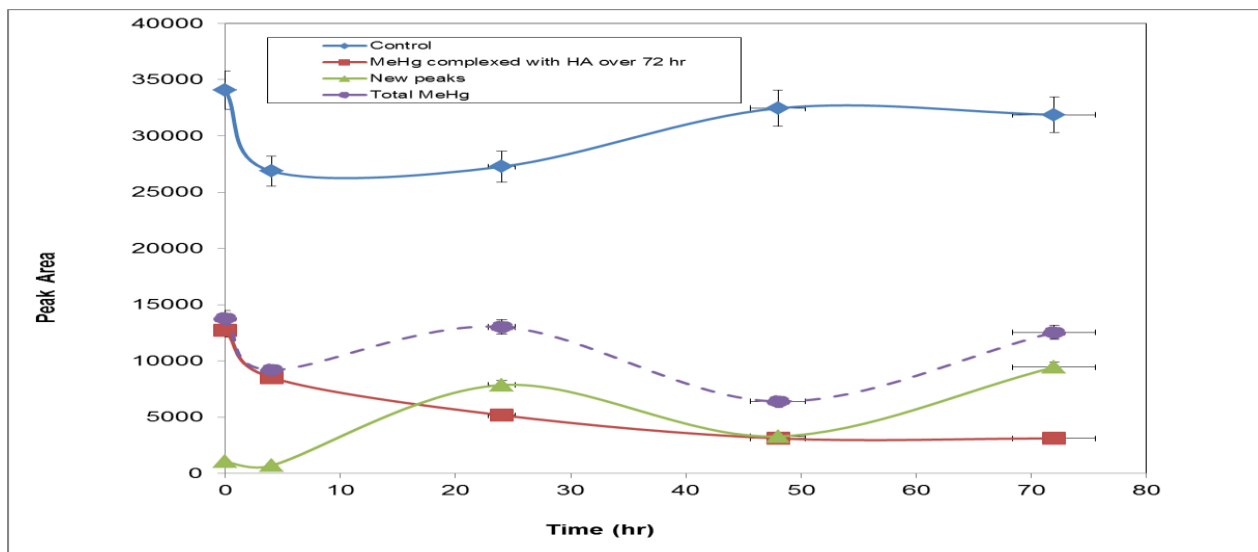


**Figure 2.13** Complexation of MeHg with HA after 72 hr with HPLC-EC (conditions as described in Paragraph 2.2.5) (error bars representing standard error).

Figure 2.13 illustrates the change in the concentration of MeHg complexed with HA and in the control (without HA) over a 72 hr period. The initial experiment was performed at room temperature. From the first determination there is a difference between the control and the solution of MeHg with HA. Analysis of the variance (ANOVA) was done to determine if the difference was significant or not. Statistical comparison between the control and the solution of MeHg and HA was determined and shows a significant difference between the two determinations ( $p < 0.05$ ). From the first determination it was found that the concentrations of MeHg and HA are much lower than that of the control, which indicates that complexation occurred almost immediately. A new peak was observed after 4 hr with the same retention time as  $Hg^{2+}$  (Figure 2.12) and the concentration of this peak increased over the 72 hr period. The total amount of MeHg (MeHg complexed with HA over 72 hr + new peaks formed) does not add up to the concentration in the control. Statistically the difference was found not to be significant with  $P > 0.05$ . The difference in concentration could be losses due to adsorption on container walls or reduction of  $MeHg$  to  $Hg^0$ .

The same complexation process was followed in the study of the complexation of  $Hg^{2+}$  with HA (Figure 2.14). The process was monitored over a period of 72 hr, using a mixed aqueous solution of  $80\mu g/L$   $Hg^{2+}$  and the same concentration of HA at room temperature.

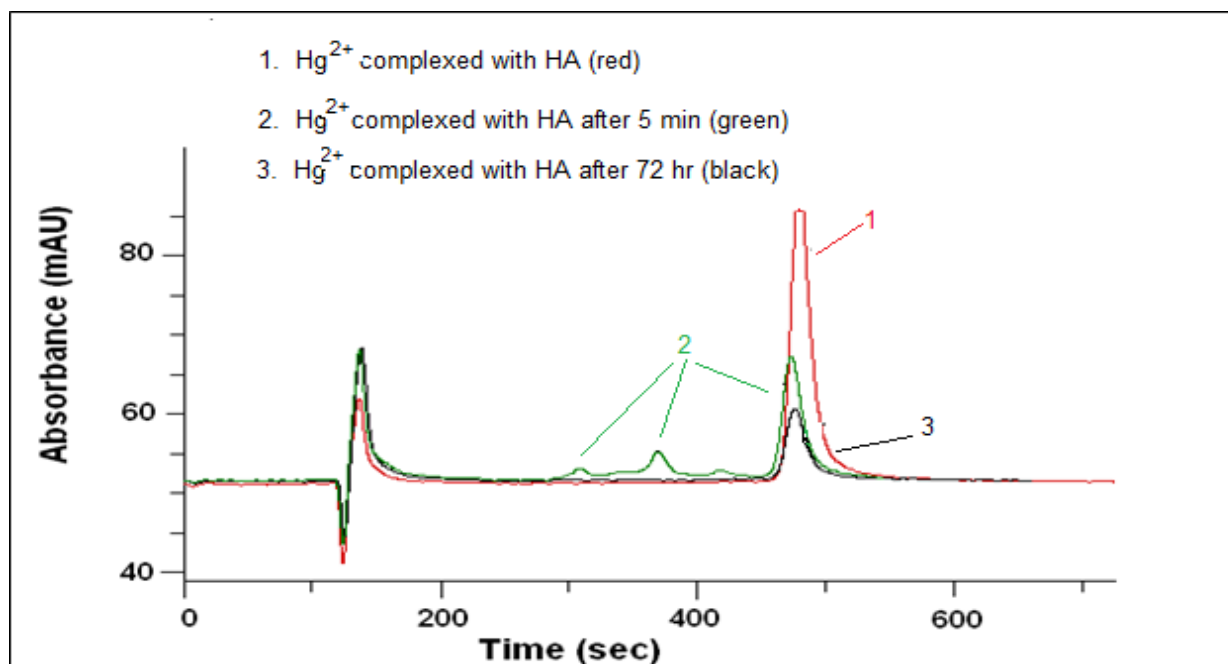
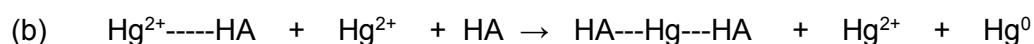


**Figure 2.14** Chromatogram of the complexation of  $\text{Hg}^{2+}$  with HA after 72 hr.

The complexation of  $\text{Hg}^{2+}$  with HA in the initial investigation was evaluated ( $t = 0$ ) red, ( $t = 5$  min) green and ( $t = 72$  hr) black. The chromatogram above illustrates the complexation of  $\text{Hg}^{2+}$  with HA in the initial investigation. The chromatogram represents three different chromatographic runs that show the difference in concentration as the complexation proceeds. Line 1 (red) is that of the uncomplexed compound and shows the highest concentration and thus the biggest peak at retention time of 490 sec. Line 2 (green) shows the change in  $\text{Hg}^{2+}$  concentration after addition of HA and thus the complexation of  $\text{Hg}^{2+}$  with HA. The concentration of  $\text{Hg}^{2+}$  decreases and new peaks are observed. The new peak has the same retention time as MeHg (Figure 2.8). Line 3 (black) shows the complexation 72 hr after addition of HA. The peak that represents the uncomplexed  $\text{Hg}^{2+}$  decreased to almost a third of the initial concentration, signifying a stable complex of  $\text{Hg}^{2+}$  that persists after 72 hours as represented by the reactions a-b.



The complexation of  $\text{Hg}^{2+}$  with HA involves the formation of complexes  $\text{Hg}^{2+}$ -HA via Hg and carbonyl and thiolate bonds. The affinity of thiols for mercury is well documented (Fitzgerald *et al.*, 2007, Gu *et al.*, 2011). The concentration of the  $\text{Hg}^{2+}$  (first chromatogram) was reduced to almost a third of the size after complexation (third chromatogram). In addition to the  $\text{Hg}^{2+}$ -HA some of the Hg may also have been lost to the reduction of  $\text{Hg}^{2+}$  to  $\text{Hg}^0$ .

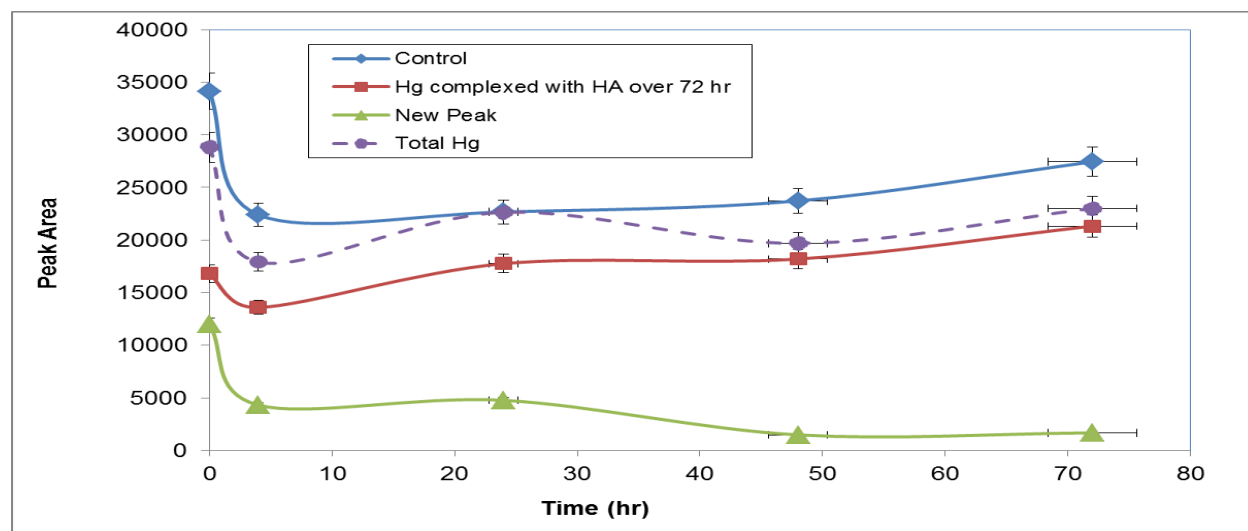


**Figure 2.15** Complexation of  $\text{Hg}^{2+}$  with HA after 72 hr with HPLC-EC (conditions as described in Table 3.1) (error bars representing standard error).

Figure 2.15 illustrates the results of the complexation of  $\text{Hg}^{2+}$  with HA over a 72 hr period. The initial experiment was performed at room temperature and the pH was not controlled. Statistical comparison between the control and the solution of  $\text{Hg}^{2+}$  and HA was determined and the difference found to be significant with  $P < 0.05$ . From the first determination there is a difference in concentration of the control and that of the solution of  $\text{Hg}^{2+}$  and HA. The initial lower concentrations of  $\text{Hg}^{2+}$  and HA compared to the control was an indication that complexation occurred immediately. After an initial decrease the concentration of the control remained reasonably stable. The total amount of  $\text{Hg}^{2+}$  ( $\text{Hg}^{2+}$  complexed with HA over 72 hr + new peaks formed) are very close to that of the control and the difference was found to be not significant at  $P > 0.05$ . The difference could be due to absorption to container walls or abiotic reduction of  $\text{Hg}^{2+}$  to  $\text{Hg}^0$ . After about 30 hr the concentration of the new peak formed decreased and then remained fairly constant over the 72 hr period.

## CHAPTER 3

### DETERMINATION OF THE KINETICS OF THE COMPLEXATION OF $\text{Hg}^{2+}$ WITH HA IN AN AQUEOUS PHASE

#### 3.1 WATER EXPOSURE: COMPLEXATION OF $\text{Hg}^{2+}$ WITH HA AT SELECTED pH AND TEMPERATURE USING HPLC-EC

After optimization of experimental conditions the role of the complexation of HA with  $\text{Hg}^{2+}$  in water was investigated, under selected conditions of temperature, pH and salinity. The conditions were chosen to be as close as possible to conditions in fresh water systems in the environment e.g. rivers and lakes. A salinity of 35  $\mu\text{g}/\text{mL}$  was selected in order to maintain natural conditions. Natural waters contain dissolved solids and have a concentration of 30–40  $\mu\text{g}/\text{mL}$   $\text{Cl}^-$  (Buell and Girard, 1994). In natural water  $\text{Cl}^-$  plays a very important role in the speciation of  $\text{Hg}^{2+}$ . Literature (Schuster, 1991; Davis *et al.*, 1997, Fitzgerald *et al.*, 2007) have reported that  $\text{Cl}^-$  concentrations of > 14  $\mu\text{g}/\text{mL}$   $\text{Hg}^{2+}$  is enough for most of the available Hg to be in the  $\text{HgCl}_2$  form, and that at higher pH values  $\text{Cl}^-$  can act as a desorbing agent. It is regarded as one of the most mobile and persistent complexing agents for Hg. As  $\text{Cl}^-$  occurs in all natural soil and water systems, it was added to the experimental systems.

The temperature range was based on the mean annual temperature in South Africa, Southern Hemisphere, which is an average summer temperature of 301.15 K and 291.15 K for average winter temperature ([www.worldweatheronline.com](http://www.worldweatheronline.com), [www.weathersa.co.za/climate](http://www.weathersa.co.za/climate)). The concentration of HA is much higher than  $\text{Hg}^{2+}$  in natural systems (Haitzer *et al.*, 2002) but the HA concentration was kept constant for the present study to decrease the number of variables impacting on the evaluation of the complexation of  $\text{Hg}^{2+}$  with HA.

To control the temperature the complexation experimental setup was held in a waterbath in a temperature controlled room. After the complexation process was initialized, samples were taken immediately and at set intervals over a nine-day period for analysis. Only the first 72 hr were deemed important and reported in the study. For all experiments in this study Teflon containers were used since they are the most suitable for Hg investigations. Parker and Bloom (2005) reported that total Hg is stable for 300 days if Teflon containers are used as they give the lowest contamination and lowest amount of  $\text{Hg}^0$  diffusing through the container walls.

The conditions were chosen to simulate conditions in a fresh water lake i.e. salinity 35  $\mu\text{g}/\text{mL}$ ; pHs 5.5, 7.0 and 8.0; and temperatures 293.15 K, 298.15 K and 303.15 K. The data for



complexation of HA with Hg<sup>2+</sup> are given in Tables 3.1–3.3, Figures 3.1–3.3 and Appendix A, Figures 1–12). Results were for an average of three injections. A control sample was prepared in the same way but without addition of HA.

It was necessary to verify the results obtained for the above experiments using HPLC-EC with another Analytical technique. The method selection was the hydride generation atomic absorption spectroscopy (HGAAS). Results for the rate constants were verified by repeating the Hg–HA complexation in aqueous phase under same conditions (Section 2.2.5) but determining the complexation of Hg with HA using the HGAAS method (Section 3.3.3).

### 3.2 WATER EXPOSURE: COMPLEXATION OF Hg<sup>2+</sup> WITH HA MONITORED AT 293.15 K

The first experiment was performed at 293.15 K at a concentration of 80 µg/L, using conditions as stated above. The results obtained are tabulated in Table 3.1 and shown in Figure 3.1 and Appendix A, Figures 1–3. The aqueous phase was prepared by taking a saline solution, prepared from distilled water and NaCl to a final concentration of 35 µg/mL, spiking it with Hg<sup>2+</sup> to a final concentration of 80 µg/L. The HA solution, prepared from a soluble form of HA (Sigma Aldrich Catalogue number H1, 675-2 Lot.:S33786-057) was added to a final calculated concentration of 80 µg/L. A control sample was prepared using the same conditions but without HA added.

**Table 3.1** Data of the complexation of Hg<sup>2+</sup> with HA at 293.15 K

Time (hr)	Control (Hg <sup>2+</sup> )/80 µg/L		Hg <sup>2+</sup> and HA at a salinity of 35 µg/mL and pH 5.5		Hg <sup>2+</sup> and HA at a salinity of 35 µg/mL and pH 7.0		Hg <sup>2+</sup> and HA at a salinity of 35 µg/mL and pH 8.0	
		New peak		New peak		New peak		New peak
0	18012	0	18175	0	11966	0	12217	0
24	15426	0	5474	2567	5516	2315	8931	3955
48	4905	0	4036	3759	3837	3141	3328	4490
72	3403	1320	1836	3158	893	5145	1681	5119

The results showed a decrease in the concentration of Hg<sup>2+</sup> over the 72 hours. New peaks were also observed, which may be the formation of Hg in another oxidation state. The data are represented in Figure 3.1.

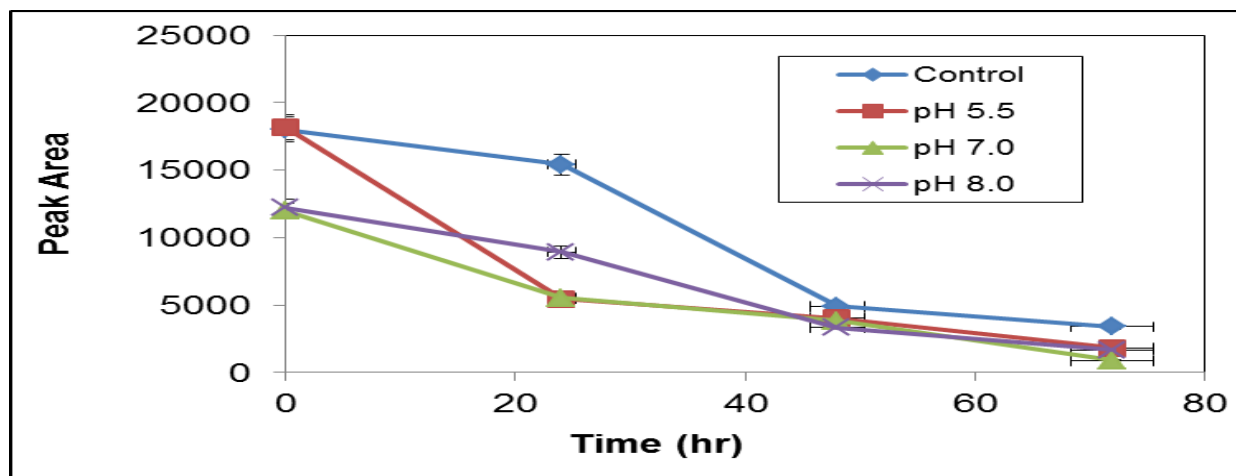


**Figure 3.1** Complexation of  $\text{Hg}^{2+}$  at 293.15 K (error bars representing standard error).

Figure 3.1 illustrates the complexation of  $\text{Hg}^{2+}$  and HA at 293.15 K as determined under the conditions mentioned in Section 2.2.5. The first determination was recorded immediately after the solutions had been mixed and the pH set. Although all samples were spiked with the same concentration of  $\text{Hg}^{2+}$ , the concentration at the first determination of the solutions at pH 7.0 and pH 8.0 were lower than the control and solution of pH 5.5. This may indicate that complexation had taken place almost immediately. The concentration of  $\text{Hg}^{2+}$  decreased to 22% within the first 48 hr. The concentration of control sample was consistently higher than the other solutions although it also decreased quite rapidly after the first 24 hr. In aqueous media the  $\text{Hg}^{2+}$  will complex HA as well as the  $\text{OH}^-$  and the  $\text{Cl}^-$  in the system. Low pH values are more favourable for the formation of  $\text{HgCl}_2(\text{aq})$ ,  $\text{HgCl}_4^{2-}$  as well as  $\text{HgOHCl}(\text{aq})$  and  $\text{Hg}(\text{OH})_2(\text{aq})$  at higher pH values (Allard *et al.*, 1991; Gabriel and Williamson, 2004). The decrease in concentration, in the control sample (no HA, low pH) could be that  $\text{Hg}^{2+}$  complexed with  $\text{Cl}^-$ . After 72 hr the concentrations at all the pH values had decreased considerably and were fairly constant. The results at different pH values are shown in Appendix A, Figures 1–3.

### 3.2.1 WATER EXPOSURE: COMPLEXATION OF $\text{Hg}^{2+}$ WITH HA AT 298.15 K

The next set of experiments was performed at 298.15 K (Section 2.2.5 and 2.7.1). The results obtained are tabulated in Table 3.2, and shown in Figure 3.2 and in Appendix A, Figures 4–6. A control sample of  $\text{Hg}^{2+}$  was also monitored over the same period and under the same conditions but without the HA added.

**Table 3.2** Data of the complexation of Hg<sup>2+</sup> with HA at 298.15 K

Time (hr)	Control (Hg <sup>2+</sup> )/ 100 µg/L		Hg <sup>2+</sup> and HA at a salinity of 35 µg/mL and pH 5.5		Hg <sup>2+</sup> and HA at a salinity of 35 µg/mL and pH 7.0		Hg <sup>2+</sup> and HA at a salinity of 35 µg/mL and pH 8.0	
		New peak		New peak		New peak		New peak
0	24607	0	22147	0	16503	0	16959	0
24	19480	0	17149	0	13147	0	14099	0
48	19589	0	14257	0	10224	0	9294	0
72	14532	0	12104	1444	6809	0	6170	808

Figure 3.2 illustrates the complexation of Hg<sup>2+</sup> and HA at 298.15 K. The trends are similar to those observed in the previous experiment at 293.15 K, but with the concentration decreasing more gradually.

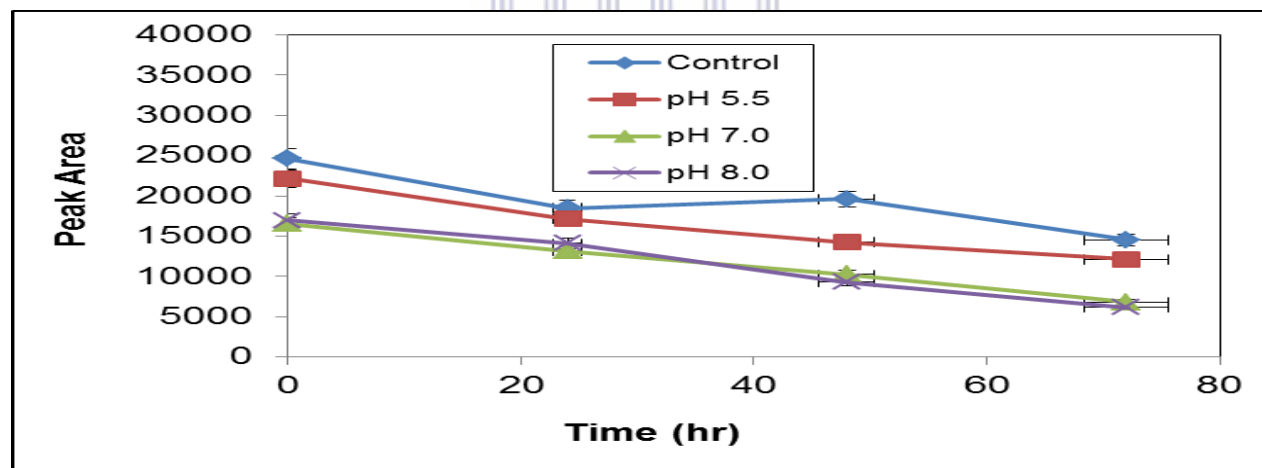


**Figure 3.2** Complexation of Hg<sup>2+</sup> at 298.15 K (error bars representing standard error).

### 3.2.2 WATER EXPOSURE: COMPLEXATION OF Hg<sup>2+</sup> WITH HA AT 303.15 K

The next experiments are performed under the same conditions as mentioned above but at 303.15 K. Analyses were performed by HPLC-EC using optimum conditions (Section 2.2.5 and 2.3.3). The results obtained are tabulated Table 3.3, and shown in Figure 3.3 and in Appendix A, Figures 7–9. A control sample of Hg<sup>2+</sup> was also monitored over the same period and under the same conditions, but without the HA added.

**Table 3.3** Data of the complexation of Hg<sup>2+</sup> with HA at 303.15 K

Time (hr)	Control (Hg <sup>2+</sup> )/100 µg/L		Hg <sup>2+</sup> and HA at a salinity of 35 µg/mL and pH 5.5		Hg <sup>2+</sup> and HA at a salinity of 35 µg/mL and pH 7.0		Hg <sup>2+</sup> and HA at a salinity of 35 µg/mL and pH 8.0	
		New peak		New peak		New peak		New peak
0	28185	0	12853	0	26905	0	25403	0
24	10327	0	2829	0	2358	0	6333	0
48	8772	0	2154	0	1553	0	5129	0
72	4752	0	1312	0	3218	1098	1042	0

The complexation of Hg<sup>2+</sup> and HA at 303.15 K is illustrated in Figure 3.3. The trends are similar to those observed in the previous experiment at 293.15 K and 298.15 K, but with the concentration decreasing more rapidly at this higher temperature. The results at different pH values as well as any new peaks that were formed are shown in Appendix A, Figures 7–9.

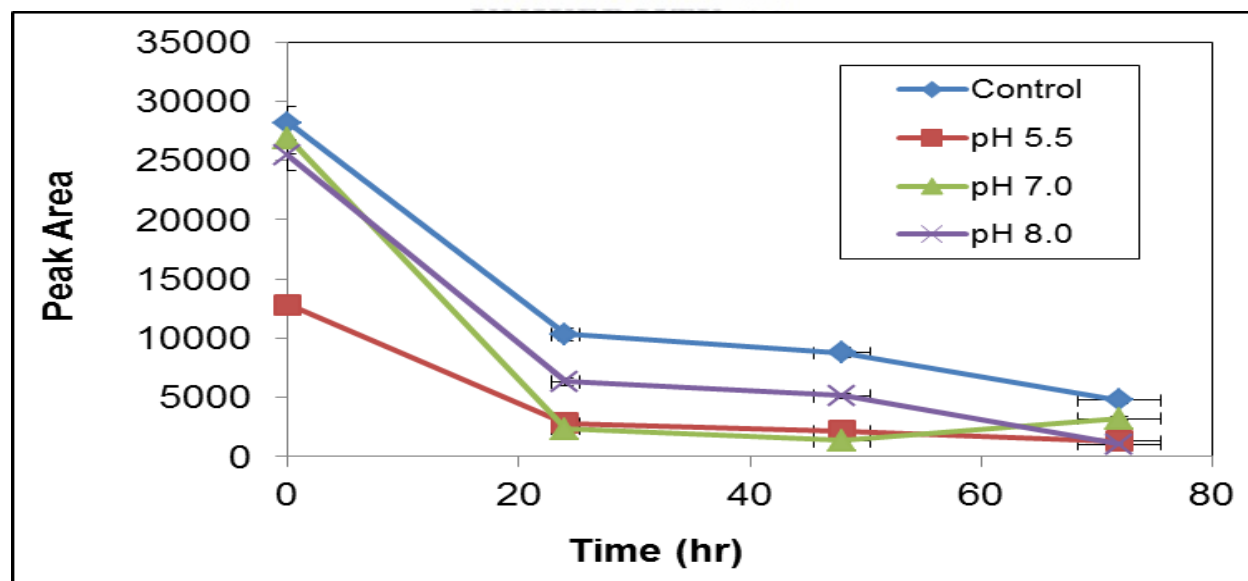


**Figure 3.3** Complexation of Hg<sup>2+</sup> at 303.15 K (error bars representing standard error).

### 3.3 KINETICS OF THE Hg–HA COMPLEXATION

The kinetics of the complexation of Hg<sup>2+</sup> with HA was calculated to get a sense of how the different complexation rates are affected by different pH and temperature values. The determination of the rate constants of the Hg–HA complexation is made difficult by the lack of stoichiometric and structural information of HA. In previous studies, The Hg–HA complexation was found to be influenced by the ratio of Hg<sup>2+</sup>/HA, the type and origin of the HA and the pH (Haitzer *et al.*, 2002., Haitzer *et al.*, 2003; Han *et al.*, 2005; Khwaja *et al.*, 2006; Helal *et al.*, 2007). Although numerous studies report rate/binding constants, the values differ considerably and reliable rate constants are still unavailable. Constants with log K values ranging from log 2.6 to 38 have been reported. Comparing values are hampered by the different techniques and conditions used in the different studies (Haitzer *et al.*, 2002., Haitzer *et al.*, 2003; Han *et al.*, 2005; Khwaja *et al.*, 2006; Skyllberg *et al.*, 2006; Miller *et al.*, 2009).

#### 3.3.1 KINETICS FOR THE COMPLEXATION OF Hg<sup>2+</sup> WITH HA IN AQUEOUS PHASE

Interactions between Hg and HA are complex and involve many different interactions. It was found that neither first-order nor second-order kinetics provide a good fit. However, in a previous study a relatively short reaction time of 1–7 hr was used and found to follow pseudo-first-order kinetics (Miller *et al.*, 2009). In some previous studies interaction between Hg–NOM was found to complex with thiol functional groups on HS, and that the reaction was slow, and that a time of 9 hr is needed for the reaction (Miller *et al.*, 2009).

However, in this study, complexation was found to be very swift. Interaction could take place on all available functional groups, such as the strongly bound reduced thiols, which are present in low abundance, and the weakly bound carbonyl, phenolic and amine functional groups, which are more abundant. The Hg–HS complexes could be formed initially with these more abundant groups like the carbonyl and amine groups and these would then slowly be replaced by transfer of the Hg to stronger binding sites (Miller *et al.*, 2009).

#### 3.3.2 DETERMINATION OF THE RATE CONSTANTS FOR THE COMPLEXATION OF Hg<sup>2+</sup> WITH HA IN AQUEOUS PHASE FOR FIRST-ORDER REACTION WITH HPLC-EC

Rate constants were calculated for first-order reaction processes (Gårdfeldt *et al.*, 2003; Rodríguez Martín-Doimeadios *et al.*, 2004). The rate constant was calculated for a

4 hr period. A graph of  $\ln$  area vs time(hr) was constructed with the rate constant  $k = -\text{slope}$ . This provides a good fit with  $r^2 > 0.99$ . Figure 3.4 shows how the rate constant values were obtained. The rate constant value determined in Figure 3.4 was for the complexation of  $\text{Hg}^{2+}$  with HA at pH 5.5 at 293.15 K. Results are tabulated in Table 3.4 and shown in Figures 3.5–3.6.

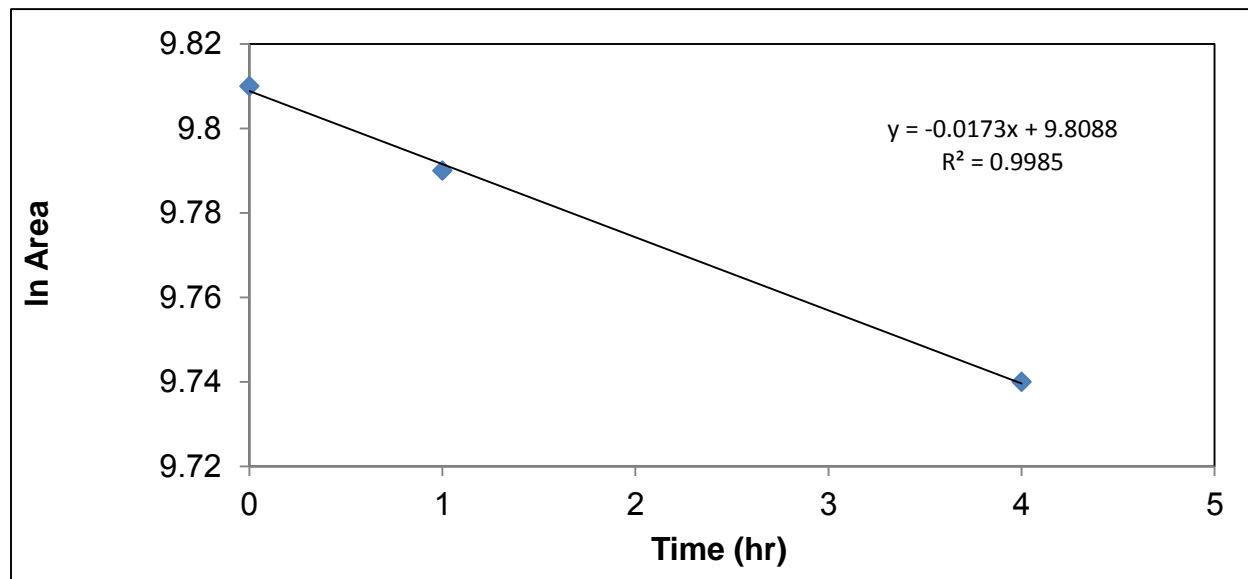


**Figure 3.4** Rate constant determination of the complexation of  $\text{Hg}^{2+}$  with HA at pH 5.5 at 293.15 K.

**Table 3.4** Rate constants ( $\text{hr}^{-1}$ ) of the complexation of  $\text{Hg}^{2+}$  with HA

Temp (K)	pH 5.5	pH 7.0	pH 8.0
293.15 K	0.032	0.014	0.014
298.15 K	0.011	0.011	0.011
303.15 K	0.100	0.110	0.100

These values are in agreement with values obtained in a previous study by Miller *et al.*, (2009), whose data was obtained over a reaction time of 1–7 hr (Table 3.6). In the present study the data used for calculation was obtained over a reaction time of 0–24 hr. The reported rate constant values ( $\text{hr}^{-1}$ ) from the study by Miller *et al.*, (2009) ranged from 0.05 to 0.29, depending on the type of HS used. The values of the rate constants ( $\text{hr}^{-1}$ ) in the present study ranged from 0.032 to 0.11, depending on the pH and temperature used. Although within range it is slightly lower than the reported values but the difference could be due to different techniques and conditions used.

Figure 3.5 shows how the rate constants vary with increasing pH. Previous studies found that the rate constants increase with increasing pH (Haitzer *et al.*, 2003; Helal *et al.*, 2007). The rate constants at 303.15 K were much higher than that at other temperatures (Figure 3.5).

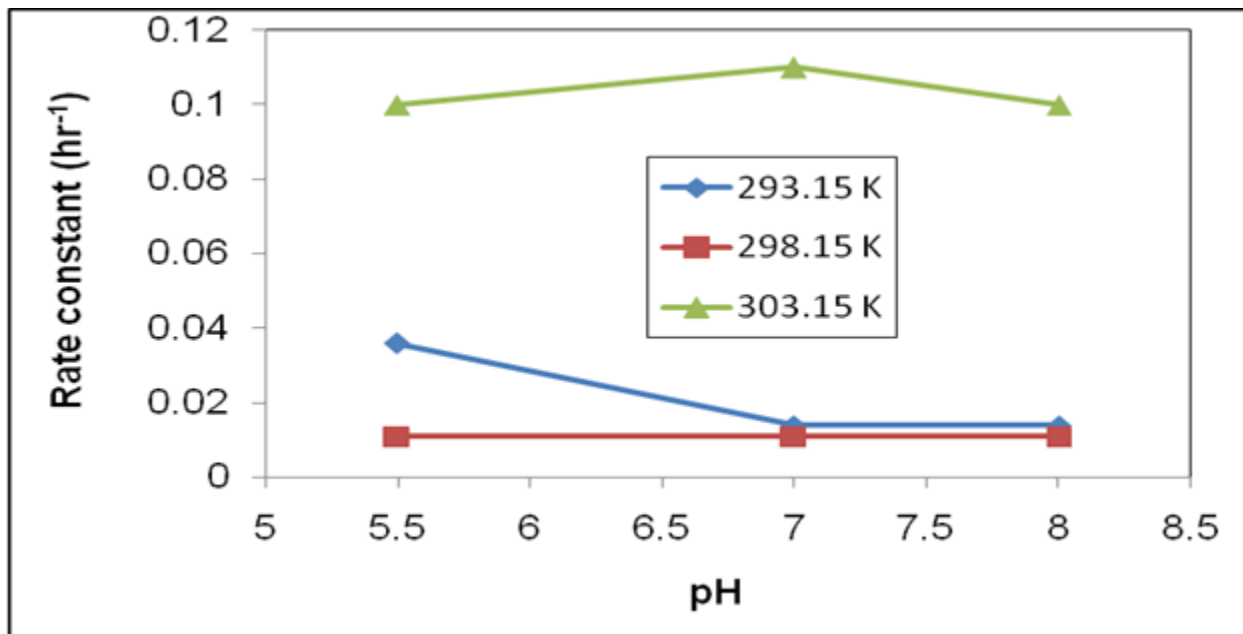


Figure 3.5 Rate constants (hr<sup>-1</sup>) vs pH of the complexation of Hg<sup>2+</sup> with HA.

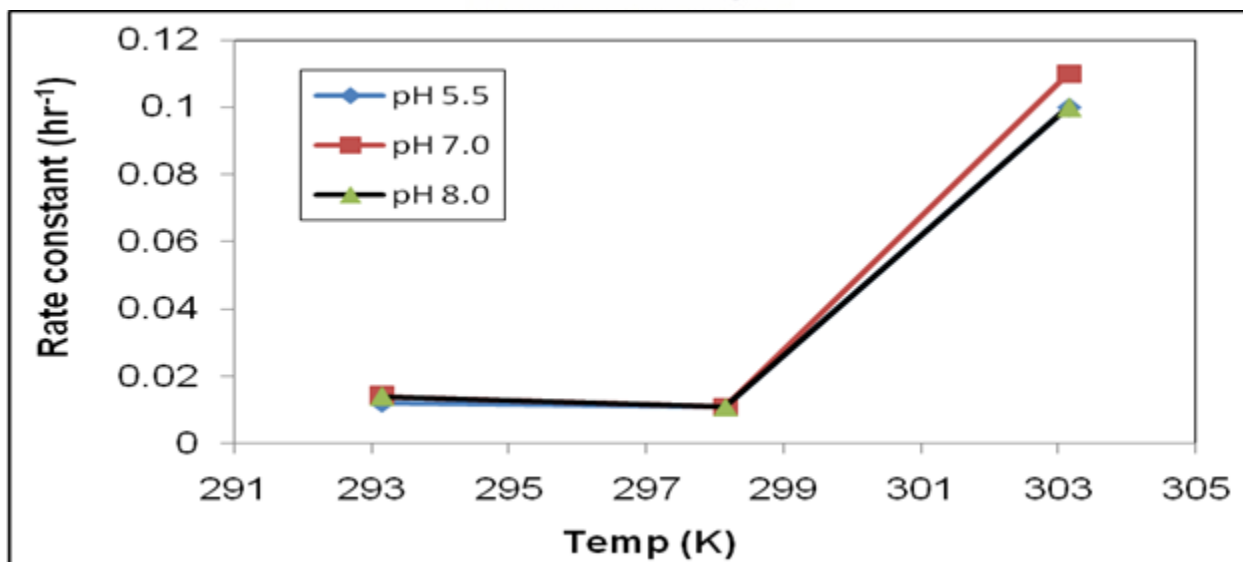


Figure 3.6 Rate constants (hr<sup>-1</sup>) vs temperature of the complexation of Hg<sup>2+</sup> with HA.

Figure 3.6 shows how the rate constants vary with increasing temperature. No previously reported results could be found for the effects of temperature on the complexation of  $\text{Hg}^{2+}$  with HA. To verify results, the analyses were repeated using the hydride generation method, (Section 3.3.4) with same conditions as reported in Section 3.1.1, but with determination over four hours.

### 3.3.3 DETERMINATION OF THE RATE CONSTANTS FOR THE COMPLEXATION OF $\text{Hg}^{2+}$ WITH HA IN AQUEOUS PHASE FOR FIRST-ORDER REACTION USING THE HYDRIDE GENERATION ATOMIC ABSORPTION SPECTROSCOPY METHOD

Results for the rate constants were verified by repeating the Hg–HA complexation in aqueous phase under same conditions (Section 2.2.5) but determining the Hg by the HGAAS method. The correlation coefficient was higher than 0.99 in the calibration curves and limit of detection 0.004  $\mu\text{g}/\text{mL}$  (Appendix A, Figure A10). The experiments were run for 4 hr and the results are listed in (Appendix A, Tables 1–4). Pseudo-first-order was assumed and a graph of  $\ln$  area vs time was constructed with the rate constant = -slope.

**Table 3.5** Rate constants of the complexation of  $\text{Hg}^{2+}$  with HA

Temp (K)	Control	pH 5.5	pH 7.0	pH 8.0
293.15	0.176	0.193	0.192	0.242
298.15	0.243	0.210	0.212	0.253
303.15	0.404	0.487	0.521	0.501

In the Figure 3.7 the trend shows a general increase in the rate constants with an increase in temperature.



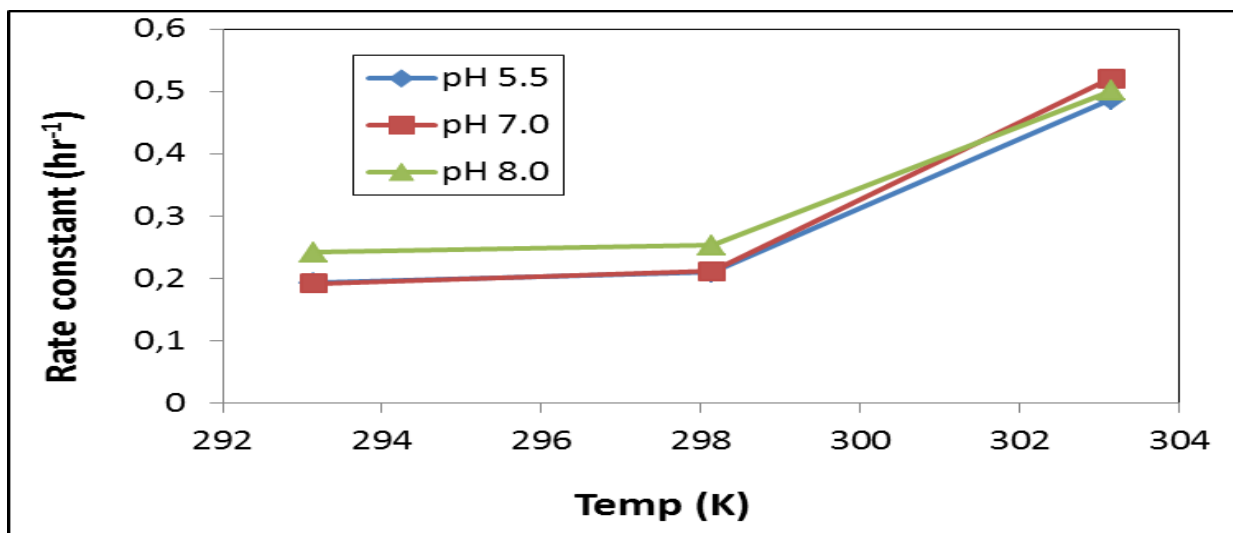


**Figure 3.7** Rate constants ( $\text{hr}^{-1}$ ) vs temperature of the complexation of  $\text{Hg}^{2+}$  with HA obtained with HGAAS method.

In Figure 3.7 there is a general increase in rate constant with an increase in pH at 293.15 K and 298.15 K. This trend is the same as the previously reported data (Figure 3.5). There is an increase in rate constant with an increase in temperature, with rate constants at 303.15 K larger than at 293.15 K and 298.15 K, also similar to previously reported values (Figure 3.6).

Figure 3.7 and 3.8 showed, more clearly than the previous results that there is a general increase of rate constant with an increase in pH and temperature.

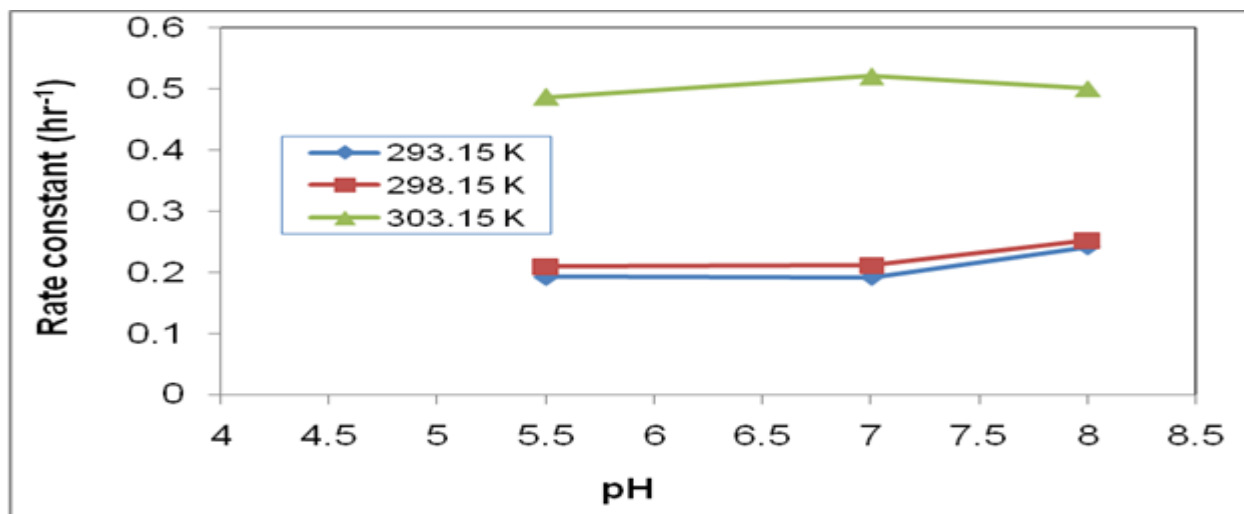


**Figure 3.8** Rate constants ( $\text{hr}^{-1}$ ) vs pH for the complexation of  $\text{Hg}^{2+}$  with HA using HGAAS method.

In Table 3.6 is a comparison of the rate constants in the different studies which shows a decrease in rate constant with increasing time of complexation. The results support the finding of Miller *et al.*, 2009, that a relatively short reaction time follows pseudo-first-order kinetics.

**Table 3.6** Rate constant vs time of complexation of Hg<sup>2+</sup> with HA

	Method	Time (hr)	Rate constant (hr <sup>-1</sup> )
Present study	HGAAS	0–4	0.176–0.532
(Miller <i>et al.</i> , 2009)	CVAFS	1–7	0.050–0.290
Present study	(HPLC-EC)	0–24	0.010–0.100

There is a need for better understanding of the rate at which Hg<sup>2+</sup> complexes to HA because it can influence the interpretation of complexation processes. In previously reported studies, it was found that formation of Hg–HA was slow, and an equilibrium time of 9 hr should be allowed before analysis, while others reported complexation to be within 20 sec (Miller *et al.*, 2009). The extent which time of the formation of complexes influences rate constants is tabulated in Table 3.9. Thus from the values in Table 3.9, the reaction rate decreases over time. This supports the previously mentioned reason that the Hg–HA complexes could be formed initially weaker, more abundant groups, like the carbonyl and amine groups and these would then slowly be replaced by transfer of the Hg to stronger binding sites (Miller *et al.*, 2009).

### 3.3.4 RATE CONSTANTS FOR THE COMPLEXATION OF Hg<sup>2+</sup> WITH HA IN AQUEOUS PHASE USING THE VAN'T HOFF EQUATION

Rate constant values tabulated in Table 3.7 was calculated using the same experimental values as those reported in Section 3.3.3 but plotting  $\log(-\Delta A/\Delta t)$  vs  $\log \Delta A$  with the intercept the rate constant and slope the order of the reaction. The Van't Hoff plot was constructed in an attempt to deduce the order of the reaction. The results of the order determination were inconclusive (not shown). The results of the rate constants are shown in Figures 3.9–3.10.

**Table 3.7** Rate constant (log k) of the complexation of Hg<sup>2+</sup> with HA

Temp (K)	pH 5.5	pH 7.0	pH 8.0
293.15	2.90	3.90	6.70
298.15	3.67	5.00	6.50
303.15	4.80	2.98	6.00

In previous studies (Helal *et al.*, 2007), the rate constant was found to increase with an increase in pH (Table 3.8). This trend was only observed at the temperature 293.15 K and 298.15 K (Figures 3.9 and 3.10). At 308.15 K a deviation from this trend occurred at pH 7.0.

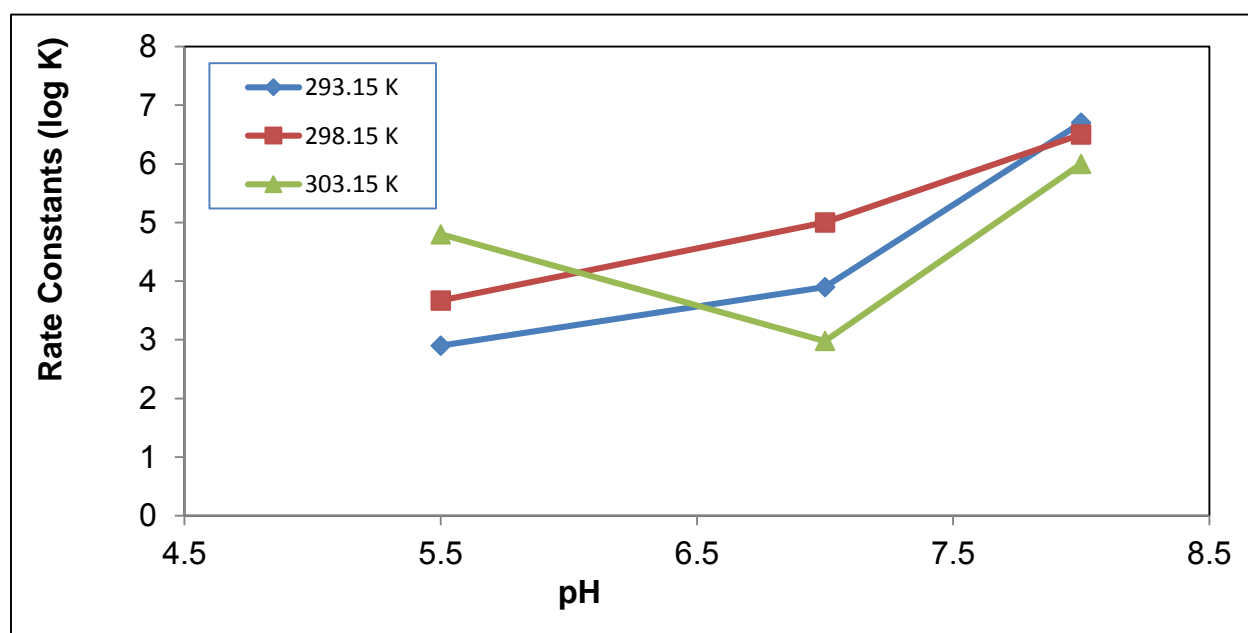


**Figure 3.9** Rate constants (log k) vs pH of the complexation of Hg<sup>2+</sup> with HA.

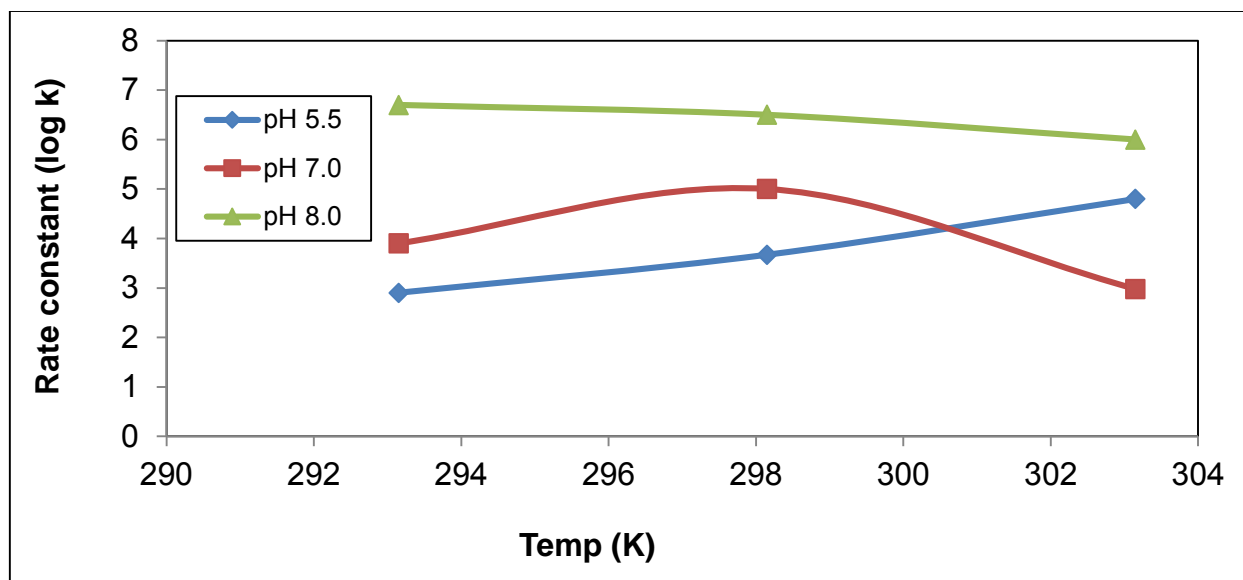


**Figure 3.10** Rate constants (log k) vs temperature of the complexation of  $\text{Hg}^{2+}$  with HA.

There is generally an increase in rate constant with an increase in temperature except in the case of pH 7.0; there was a decrease at 303.15 K.

Confirmation that the initial complexation may mostly occur between Hg and the carboxylic groups on HS is that the binding constants determined in the present study most closely resemble those reported in a study by Helal *et al.*, 2007 (Table 3.8).

**Table 3.8** Rate constants (log k) of the complexation of  $\text{Hg}^{2+}$  with HA and FA

	pH 4.26		pH 5.42		pH 6.69	
	$\beta_1$	$\beta_2$	$\beta_1$	$\beta_2$	$\beta_1$	$\beta_2$
Humic acid	2.34	2.83	2.59	3.08	3.80	3.29
Fulvic acid	3.23	3.28	3.32	3.37	3.48	3.53

Values reported in Table 3.8 are from the study by Helal *et al.*, (2007).

The study by Helal *et al.*, (2007) was based on potentiometric titration with HA and FA at pH of 4.26–6.69 (Table 3.8). Different concentrations of HS were compared and  $\beta_1$  and  $\beta_2$  calculated to fit the binding as a function of carboxylate concentration, with the metal ion forming 1:1 and 1:2 complexes. The binding constants  $\beta_1$  and  $\beta_2$  were calculated by plotting  $(C_m - [\text{M}^{2+}]/[\text{M}^{2+}][\text{A}^-])$

against  $1/[A^{-1}]$ . The value of the binding constants was obtained from the slopes,  $K_1$  ( $\beta_1$ ) and the intercepts,  $K_1K_2$  ( $\beta_2$ ). The value  $C_m$  (total concentration of the divalent metal) =  $[M^{2+}] + [MA^+] + [MA_2]$ . Differences in reported values and those of the present study could be explained by the difference in concentration of HS, the temperature and technique used.

### 3.4 RELATIONSHIP BETWEEN RATE CONSTANT AND TIME

Reaction rates of most chemical reactions increase with an increase in temperature. The log of the rate constant was plotted against  $1/T$ , and should give a straight line if the trends in the present study were consistent with the theory of Arrhenius i.e.,

$$\text{Rate constant} = A10^{(E_c/RT)}$$

High activation energy ( $E_c$ ) corresponds to a reaction rate that is very sensitive to temperature, while a positive or negative slope is characteristic of the reaction (Atkins, 1996).

From the graph of log of the rate constant vs  $1/T$ , it was determined that the graphs were linear, with some exceptions (see Figures 3.11 and 3.12). The graphs of pH 5.5 and pH 8.0 were linear. The graph of pH 7.0 was linear except at 293.15 K. The slope at pH 5.5 differs from that of pH 7.0 and pH 8.0. This is an indication that different complexation processes may dominate at lower pH values (see Table 3.9). Activation energies obtained from the graph are high ( $E_c = \text{slope} \times R$ ) and it is an indication that the complexation reactions of Hg are temperature sensitive.

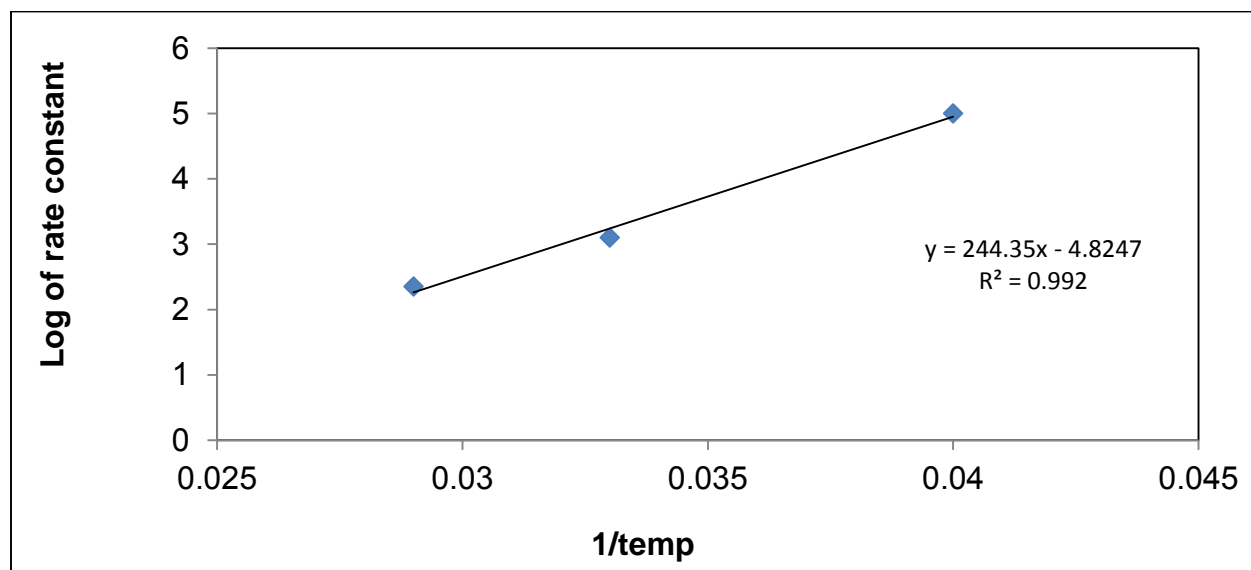
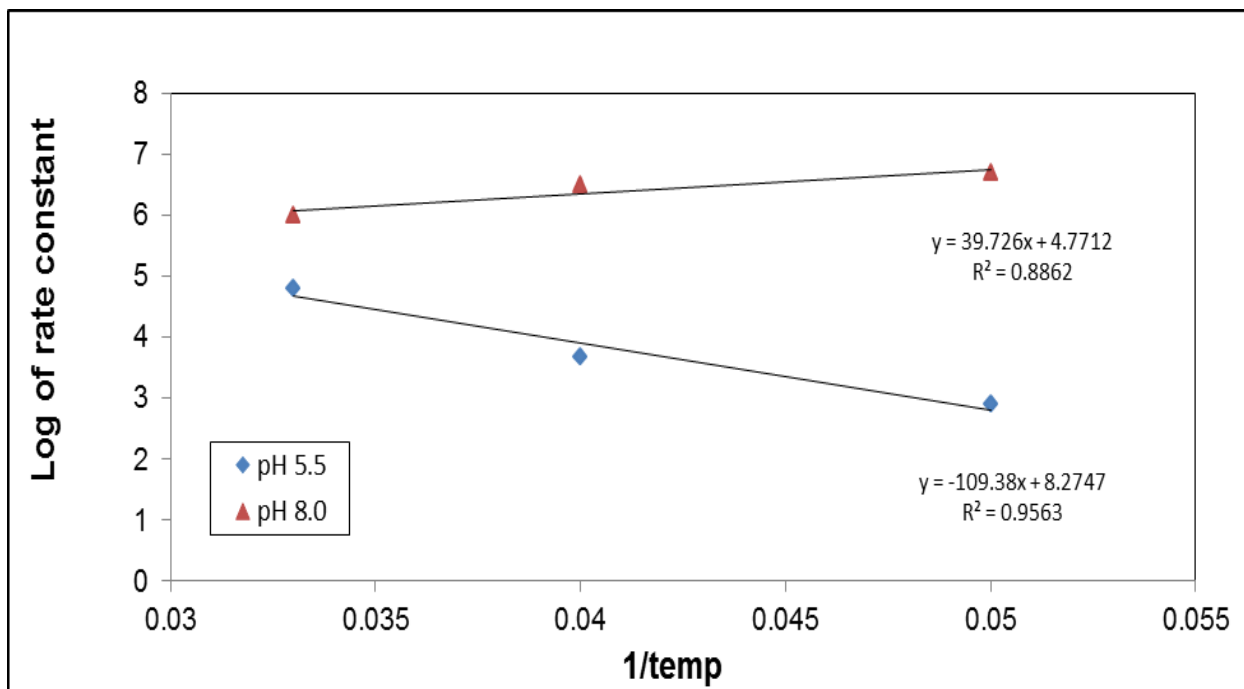


Figure 3.11 Log of the rate constant vs  $1/T$  at pH 7.0.



**Figure 3.12** Log of the rate constant vs 1/T at pH 5.5 and pH 8.0.

### 3.5 COMPLEXATION PROCESSES IN AQUEOUS PHASE: DISCUSSION

Speciation of Hg in aquatic systems is strongly influenced by pH, temperature, redox conditions and the concentrations of complexing ligands. Generally the expected trend, of an increase in rate constant with an increase in pH and temperature, seem to change at higher pH values and higher temperatures. At these higher pH and temperature values, there may be more reactions and processes involved than only the complexation of  $\text{Hg}^{2+}$  with HA. Serudo *et al.*, (2007) found that there is competition between complexation and reduction processes ( $\text{Hg}^{2+}$  to  $\text{Hg}^0$ ). The processes that may occur in aqueous phase are summarised in Table 3.9.

**Table 3.9** Summary of the complexing processes of Hg<sup>2+</sup> in aqueous phase

	Low pH	High pH
Low temperature	<ul style="list-style-type: none"> <li>• Complexation to Cl<sup>-</sup></li> <li>• <math>\text{Hg}^{2+} + 2\text{Cl}^- \rightarrow \text{HgCl}_2</math> (k = 0.193)</li> </ul>	<ul style="list-style-type: none"> <li>• Complexation to OH<sup>-</sup> <math>\text{Hg}^{2+} + 2\text{OH}^- \rightarrow \text{Hg}(\text{OH})_2</math></li> <li>• Precipitation</li> <li>• Demethylation (k = 0.242)</li> </ul>
High temperature	<ul style="list-style-type: none"> <li>• Complexation to Cl<sup>-</sup></li> <li>• Hg complexation with HA</li> <li>• Methylation (k = 0.404)</li> </ul>	<ul style="list-style-type: none"> <li>• Complexation to OH<sup>-</sup> <math>\text{Hg}^{2+} + 2\text{OH}^- \rightarrow \text{Hg}(\text{OH})_2</math></li> <li>• Precipitation</li> <li>• Evaporation</li> <li>• Reduction of Hg<sup>2+</sup> to Hg<sup>0</sup> (k = 0.501)</li> </ul>

(Low and high pH and temperature as defined in this study ie pH 5.5 and 8.0 temperature of 293.15 and 303.15K)

Most of the processes take place at high temperatures and high pH values. This supports the results recorded in this study where there is a deviation from the general trend at higher pH (Figure 3.5 and Figure 3.10). Although it could be due to processes such as reduction it could also be due to the change of the structure of HA. There is a slow transition from a fibrous structure at low pH to a more sheet-like one at higher pH values. Schnitzer and Khan (1978) found that HA, if viewed under a scanning electron microscope, occurs as elongated fibres and bundles of fibres in a relative open structure. If the pH is increased the fibres mesh into a finely woven network which gives a sponge-like structure. At about a pH of 7 and above a distinct change in the structural arrangement and orientation was observed. At a higher pH sheets tend to form which then thickens. At high pH and exposed sunlight there is the formation of a high concentration of free radicals. They cleave the HA molecules and the molecular weight of HA change with increasing pH (Schnitzer and Khan, 1978). New peaks are also generally more evident at low pH and higher temperature (Appendix A, Figures 1–12).

At all the different concentrations the control sample is consistently higher than the other solutions although it also decreased over time. This decrease in Hg concentration could be due to sorption on container walls. Miller *et al.*, (2009) reported that sorption to container walls could

be up to 25% within the first 7 hr. However, teflon containers were used, which should minimize such losses, thus the most probable cause is due to complexation of  $\text{Hg}^{2+}$  to  $\text{Cl}^-$ . In the initial study to determine best results, no  $\text{Cl}^-$  was added and the control did not show this sharp decrease.

The diagram represented in Figure 3.13 was constructed from the data in the table, to gain and understanding of the complexing processes in an aqueous phase. Reactions between Hg and HA is intricate and there are multiple interactions between Hg and the many different binding sites on HA. Although complexation of  $\text{Hg}^{2+}$  with HA dominates, other complexing processes play an important role in the chemistry of Hg in the aqueous phase. In the present study, complexation was found to be fast, with most of the free Hg present in the complexed form within 24 hr. Reaction rates increased with pH and temperature. The rate constant increased from 0.193 to 0.501 with increasing pH and temperature. Competing complex processes also occur and mixed complexes may increase the reaction rate. The summary in Table 3.9 and Figure 3.13 shows most favourable conditions under which such complexation takes place.

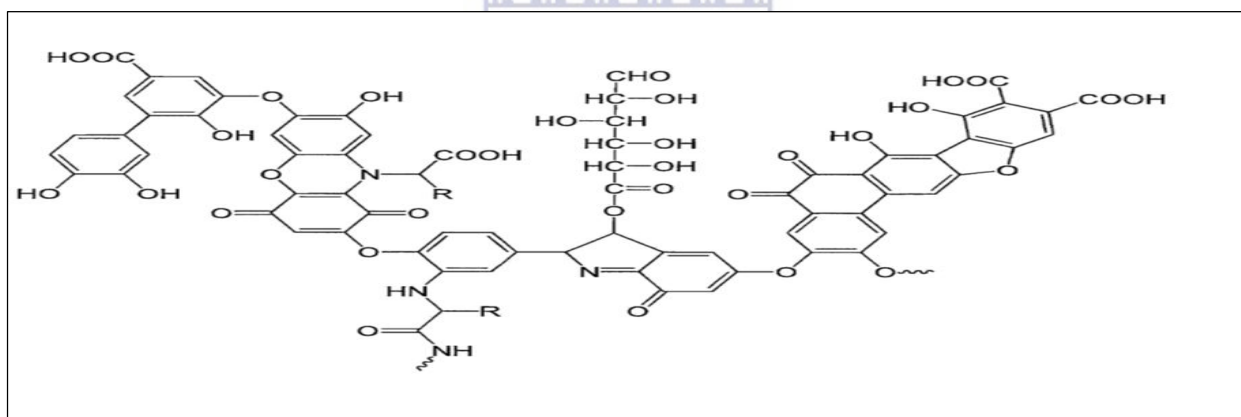


Fig 3.13 Graphical representation of a hypothetical HA molecule (Livens, 1991)

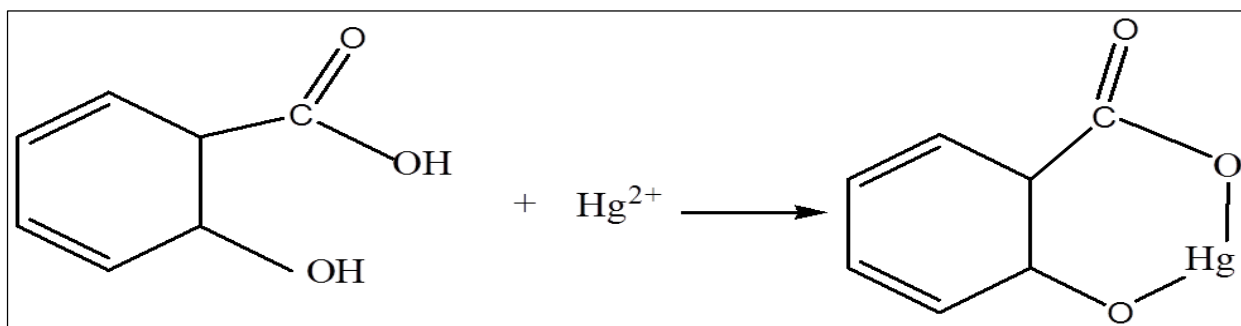
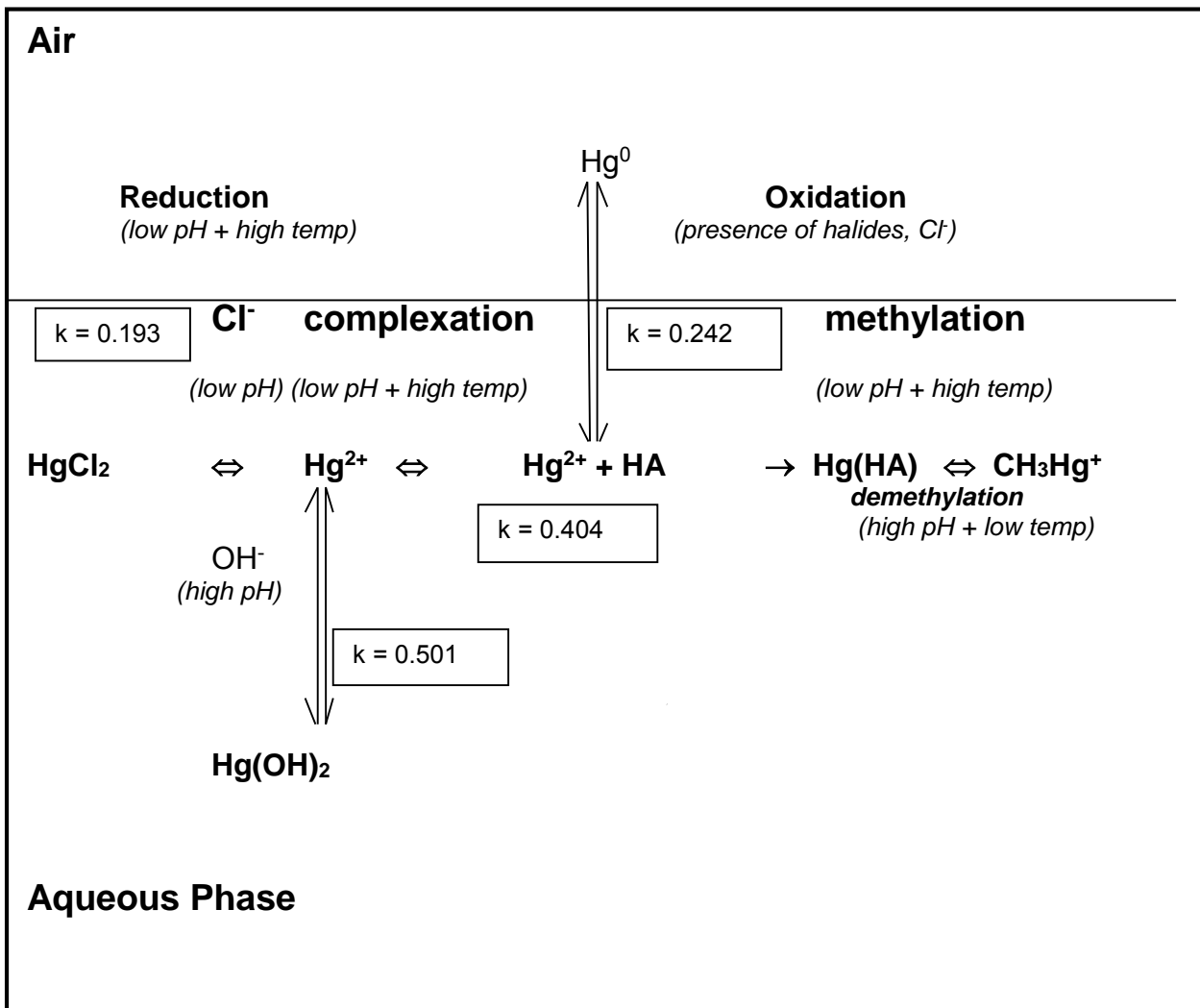


Fig 3.14 Graphical representation of the complexation of  $\text{Hg}^{2+}$  with HA





**Figure 3.15** A summary of the complexing processes in this study of  $\text{Hg}^{2+}$  with HA in aqueous phase

UNIVERSITY of the  
WESTERN CAPE

## CHAPTER 4

### DEVELOPMENT AND OPTIMIZATION OF A NOVEL SENSOR SYSTEM

#### 4.1.1 Introduction

Electrochemical sensors are affordable and easily transportable devices for determination of metals that can be used in a laboratory or for on site assessment. Chemical modification of the sensor is frequently employed to enhance performance. The use of nanoparticles has generated a lot of interest because of their physio-chemical properties that significantly improve mass transport, interface roughening determination and the study of catalytic and conductive properties. The strong affinity of Au for Hg makes the use of gold nanoparticles (AuNP) highly favourable in the development of new modified electrodes (Hezard *et al.*, 2012, Gao and Huang, 2013, Hassan *et al.*, 2015). The advantages of nanomaterial application made substantial contributions to the voltammetric determination of  $\text{Hg}^{2+}$  (Gao and Huang, 2013).

In the present study AuNP, hydrogel and humic acid (HA) were successively electrodeposited on a glassy carbon electrode using voltammetry to develop a cost effective sensor for  $\text{Hg}^{2+}$  trace analysis (Figure 4.1-4.2). In related work Au electrodes was used but AuNP's onto GCE results in a more cost effective high surface area functionalised electrode. Hydrogel sensors have quick and very sensitive detection capabilities for the detection of heavy metals. Because of their excellent loading capacity and low detection limit for detecting heavy metals, developing hydrogel sensors are very important (Muya *et al.*, 2017). PSF-PDA hydrogel contains sulphate groups which forms chemical bonds with Au, thus without the AuNP the hydrogel is only physisorbed and may simply fall off the electrode. Cyclic voltammetry (CV) was employed in the modification of GCE with AuNP and AuNP with hydrogel. The electrode was prepared by the deposition of AuNP on glassy carbon electrode (GCE). The AuNP was added to 0.1 M  $\text{NaNO}_3$  (pH 3) and deposited on GCE using CV. The GCE/AuNP electrode was further modified by the deposition of the prepared hydrogel, using CV. The GCE/AuNP/hydrogel electrode was placed in a 1000 ppm HA solution for 30 min for incubation, after which the electrode was removed, rinsed and transferred to fresh HCl solution for CV ( $n=2$ ) to obtain a baseline. A calibration curve was constructed for the absorption of  $\text{Hg}^{2+}$  onto the hydrogel sensor in the concentration range 0.1- 5  $\mu\text{mol/L}$ . The  $\text{Hg}^{2+}$  calibration curve was also determined on an unmodified GCE. A second metal ion,  $\text{Pb}^{2+}$ , was introduced into the study for validation of the sensor performance. The  $\text{Pb}^{2+}$  calibration at unmodified GCE and GCE/AuNP/Hg/HA electrode was done, under the

same analytical conditions as for  $\text{Hg}^{2+}$ . All solutions were prepared using ultra pure water and chemicals used were of analytical grade and purchased from Sigma- Aldrich.

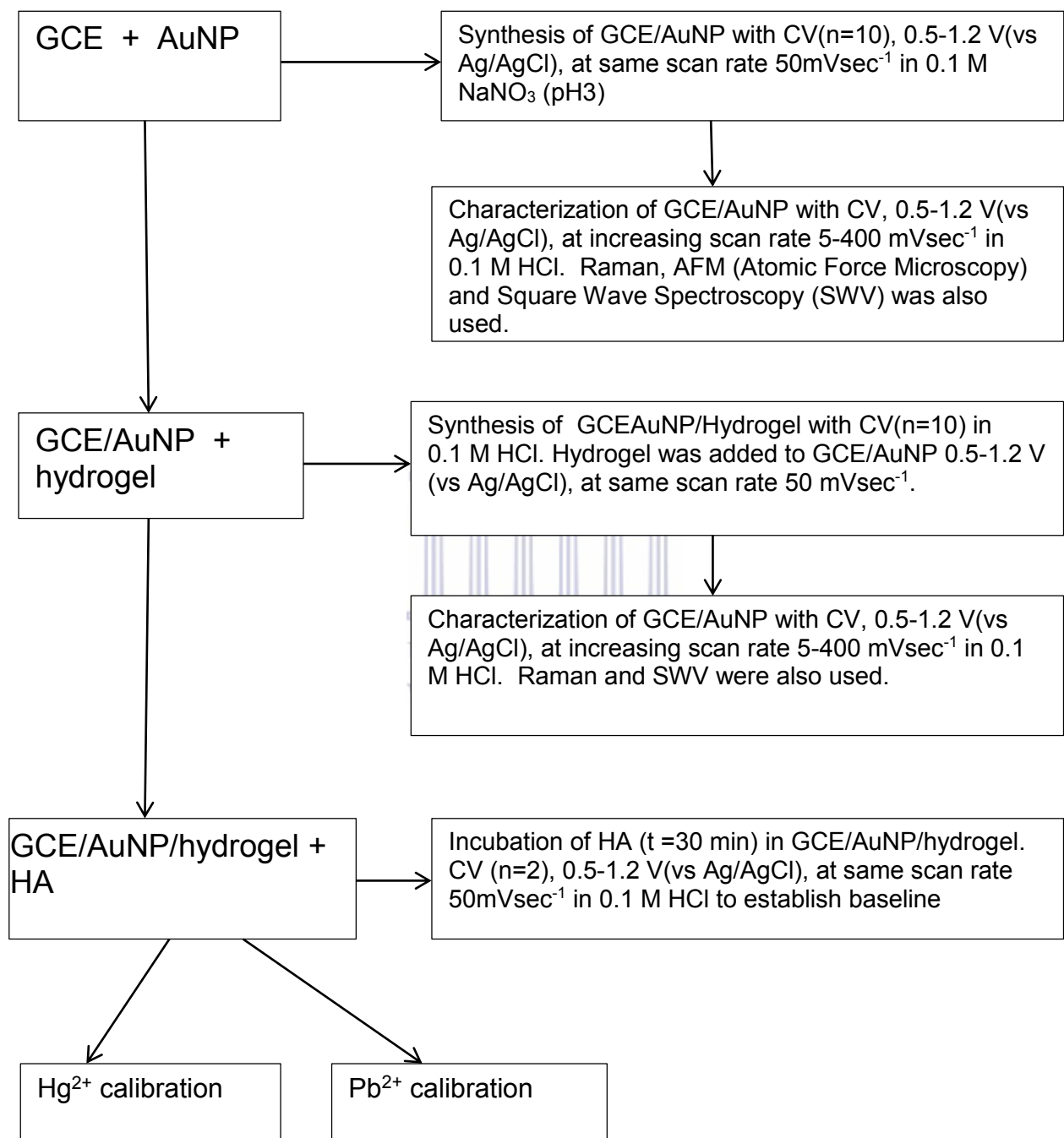


**Figure 4.1** Graphical representation of the synthesis and characterization of the GCE/AuNP/Hydrogel/HA sensor.

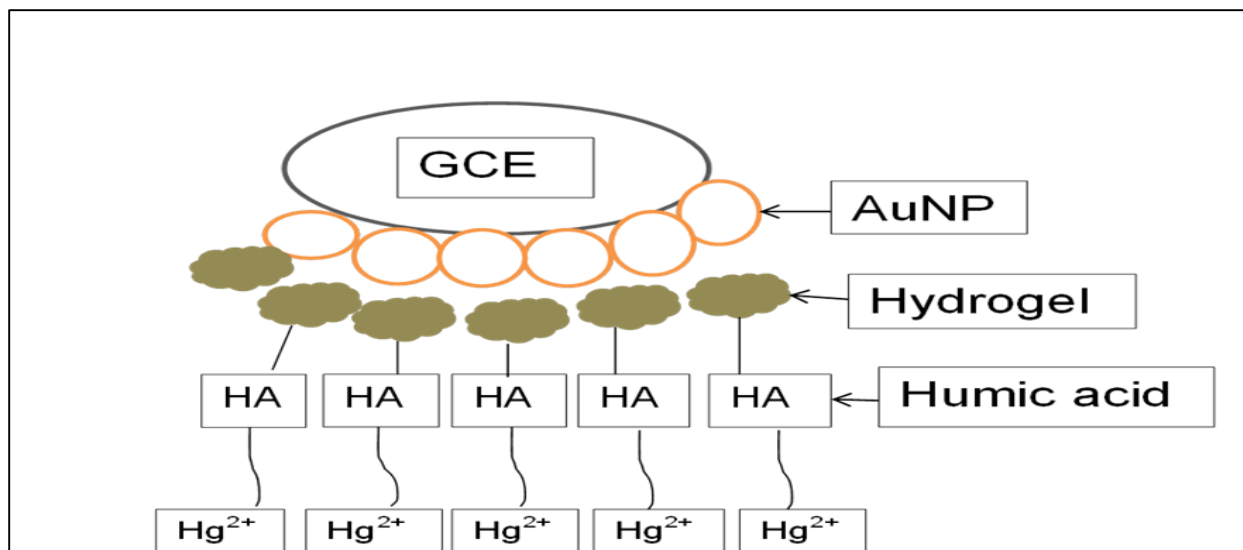


**Figure 4.2** Graphical representation of the determination of  $\text{Hg}^{2+}$  on the GCE/AuNP/Hydrogel/HA sensor as planned in this study.

#### 4.2.1 Preparation of gold nanoparticles (AuNP)

Gold nanoparticles (AuNPs) were prepared through the reduction of 1.0 mM  $\text{HAuCl}_4$  using sodium citrate as the reducing agent. 20 mL of 1.0 mM  $\text{HAuCl}_4$  solution was added to a 50 mL Erlenmeyer flask on a stirring hot plate. A magnetic stirrer was added into the solution and the solution heated to boil. To the boiling solution, 2 mL of 1% solution of sodium citrate, ( $\text{C}_6\text{H}_5\text{O}_7\text{Na}_3$ ) was added. Gold sol gradually formed as the citrate reduced  $\text{Au}^{3+}$  to  $\text{Au}^0$ . The solution was heated until a deep red colour was observed (Mailu *et al.*, 2010).

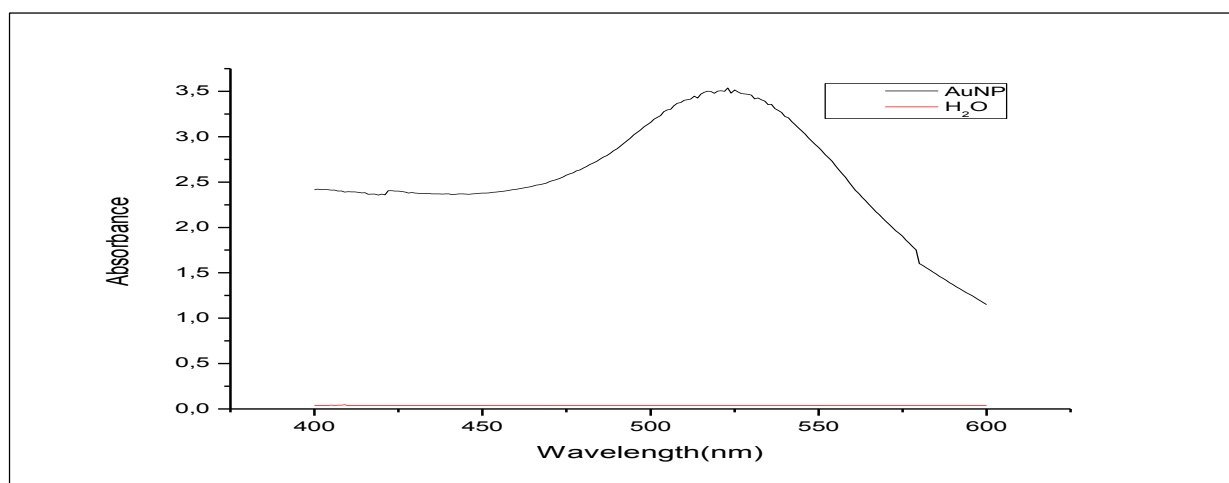


**Figure 4.3** UV/Vis Absorption spectra of AuNP prepared as described in paragraph 4.2.1.

The shape of gold nanoparticles plays an important role in their optical properties. AuNPs absorb in the visible spectrum, 450-600 nm (Bahram *et al.*, 2014). By synthesizing gold nanoparticles of different shapes, the surface plasmon resonance can easily be tuned to give absorption maxima from 500 nm to the near-infrared part of the spectrum (Figure 4.3). Spherical colloidal gold of size 13 nm has absorbance maxima between 515-570 nm (Frost *et al.*, 2017; Priyadarshini & Pradhan, 2017). It was more cost effective to synthesize than to use commercially purchased AuNP particles. A UV/Vis Absorption spectra of the prepared gold particles was run each day before the electro deposition step to confirm that the particles were not degraded or amalgamated and separated (Figure 4.4).

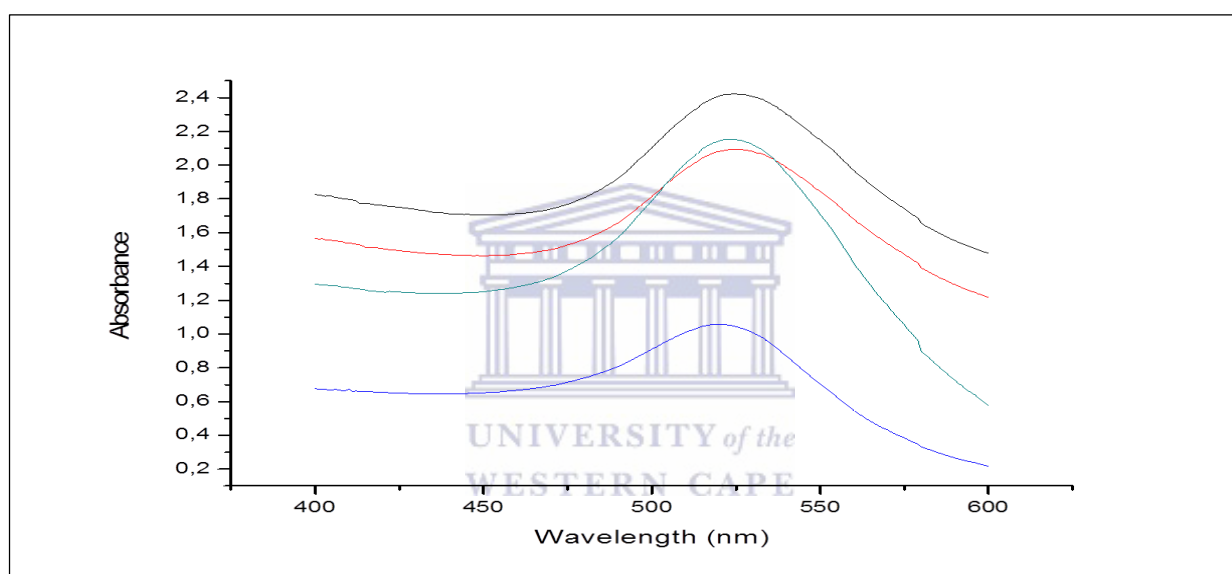


**Figure 4.4** UV/Vis Absorption spectra of AuNP before synthesis of the GCE/AuNP.

### 4.3 Preparation and characterization of hydrogel

#### 4.3.1 Preparation of hydrogel

To prepare the hydrogel 0.8842 g of polysulfone beads (PSV) (MW = 34. 000) was dissolved in 50 ml N,N-dimethyl acetamide. The reaction mixture was sonicated in a water bath for an hour and yielded 0.0520 M PSF-solution. To prepare the polysulfone -hydrogel, 5 mL of 0.0520 M PSF-solution was added to 2.5895 g PVA in a 100 mL round bottom flask. To this mixture 1 mL glutaraldehyde cross-linker solution was added followed by 1 mL of 2mL HCl as catalyst. The mixture was refluxed for 3 hr at 75°C with constant stirring. The reaction was stopped after 3 hrs and the mixture stored at room temperature for 10 days in order for the crosslinking to reach completion (Muya *et al.*, 2014).

### 4.3.2 Characterization of hydrogel

#### (a) Swelling characteristics

The swelling characteristics of the hydrogel were determined (Kayalvizhy & Pazhanisamy, 2016). 1g of the dried hydrogel was placed in a clean weighed test tube, weighed and 10 mL of deionised water added. The test tube was closed with polystyrene film and the mixture left to equilibrate for 24 hr. The water was found to be significantly reduced in volume. The water was removed with a Pasteur pipette and the weight of the hydrogel determined. The amount of swelling was determined to be 35 % (n =3).

#### (b) Characterization of hydrogel with FTIR

The hydrogel was characterised with FTIR. To prepare the disk for FTIR scan, a small amount of the dried hydrogel and KBr was mixed by grinding a mixture of the two compounds and then placing 1% of the mixture in a hydraulic press. For the CV characterization the hydrogel was added to 10 mL of 0.1 M HCl and scan rates determined at an increasing rate from 10 – 700 mVs<sup>-1</sup>.

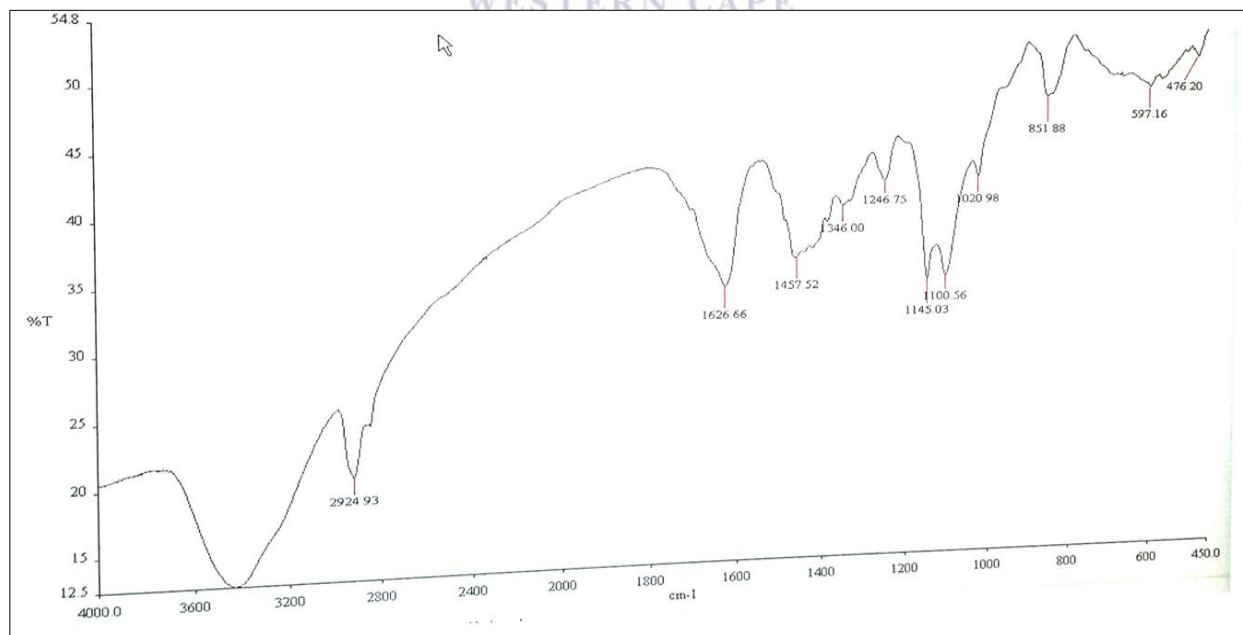


**Figure 4.5** FTIR spectrum of the PSF-PVA hydrogel.

The FTIR spectrum in Figure 4.5 shows C-H stretching bands at 1457 and 2924  $\text{cm}^{-1}$ ,  $\text{SO}_2$  at 1346  $\text{cm}^{-1}$ , and C-C at 1100  $\text{cm}^{-1}$  confirming the presence of those groups in the hydrogel.

## (b) Characterization of hydrogel with CV

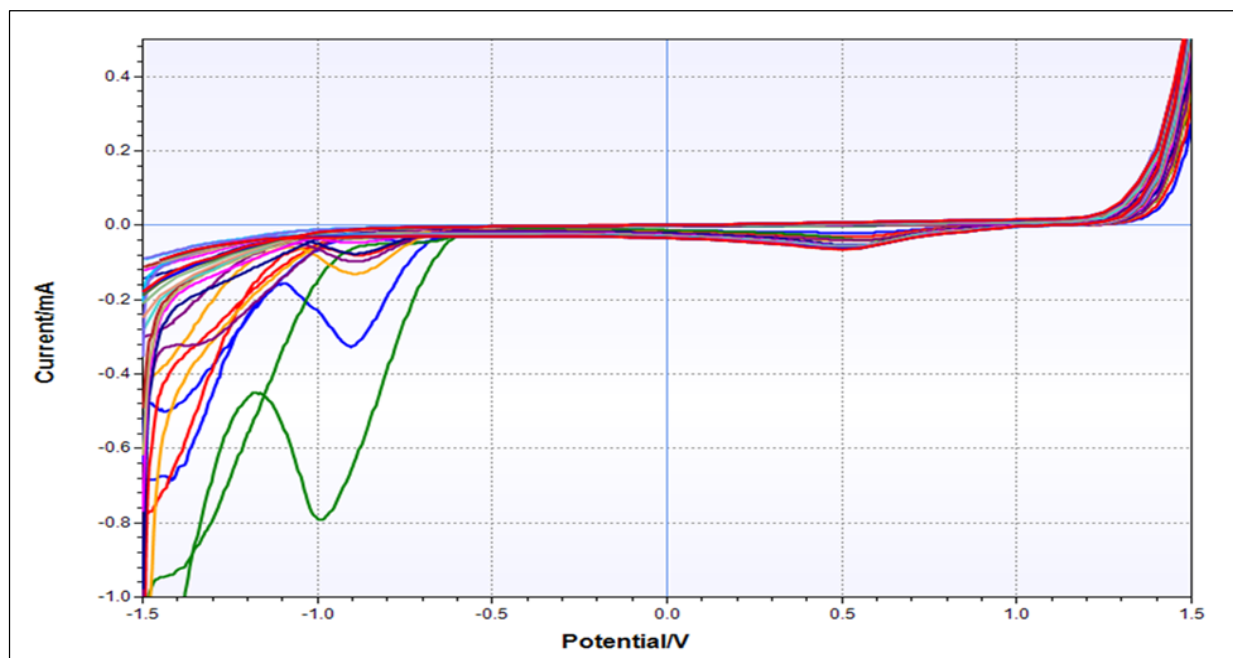


**Figure 4.6** Cyclic Voltammetry of polysulfone hydrogel at a GCE in a 0.1 M HCl solution for the characterization of hydrogel.

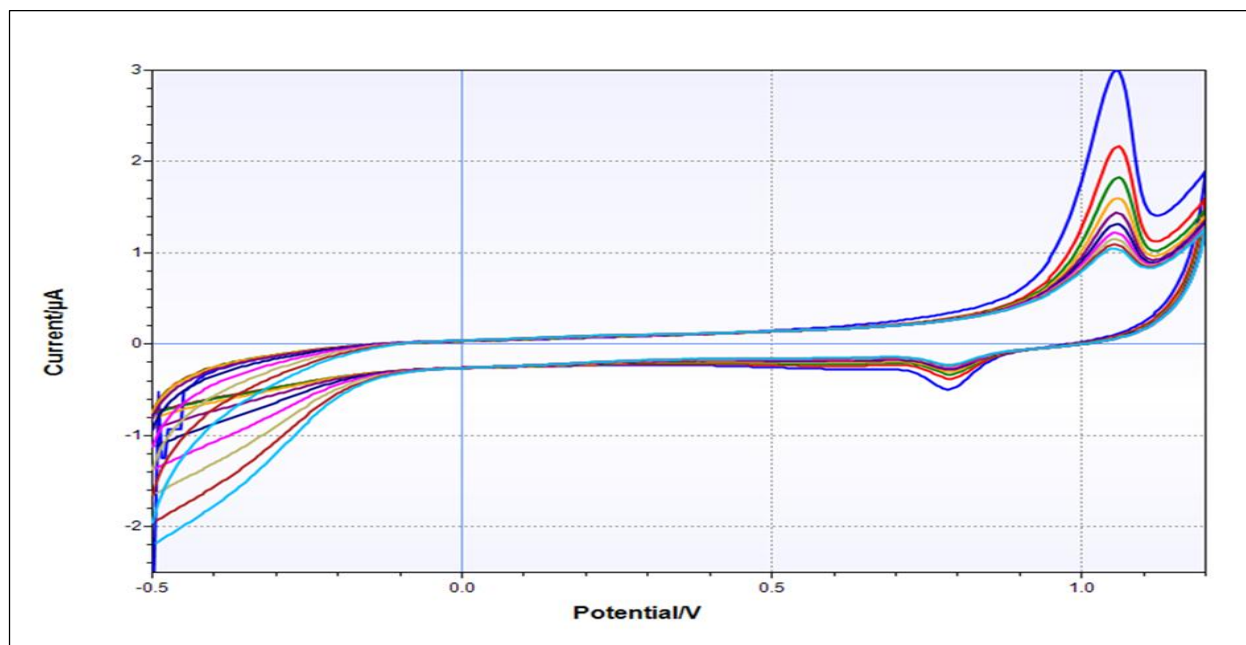
Cyclic voltammetry was used to characterize the hydrogel (Figure 4.6) in 0.1 M HCl. Cathodic reduction peaks of the hydrogel was found at 0.5 V and -1.0 V.

## 4.4 Synthesis and characterization of GCE/AuNP

### 4.4.1 Synthesis of GCE/AuNP

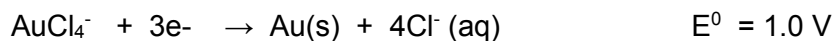
Before each modification, the GC surfaces were cleaned by polishing successively on cloth polishing pad with 1  $\mu\text{m}$ , 0.3  $\mu\text{m}$  and 0.05  $\mu\text{m}$  alumina slurry. Between polishing steps the electrodes were cleaned in ethanol in an ultrasonic bath. The GCE/AuNP were prepared by CV ( $n=10$ ) scanning from -0.1 V -1.5 V in a deaerated 0.1 M  $\text{NaNO}_3$  (pH 3) (Hezard *et al.*, 2012) solution containing 1 mM AuNP particles (preparation and used in the synthesis of GCE/AuNP without further quantification as described in section 4 .2) at a scan rate of 50  $\text{mVs}^{-1}$ (Figure 4.7-

4.8). The resulting electrodes were activated using CV (n=10) in 0.1 M HCl scanning from -0.1 and 1.5 V at a scan rate of 50 mVs<sup>-1</sup>.



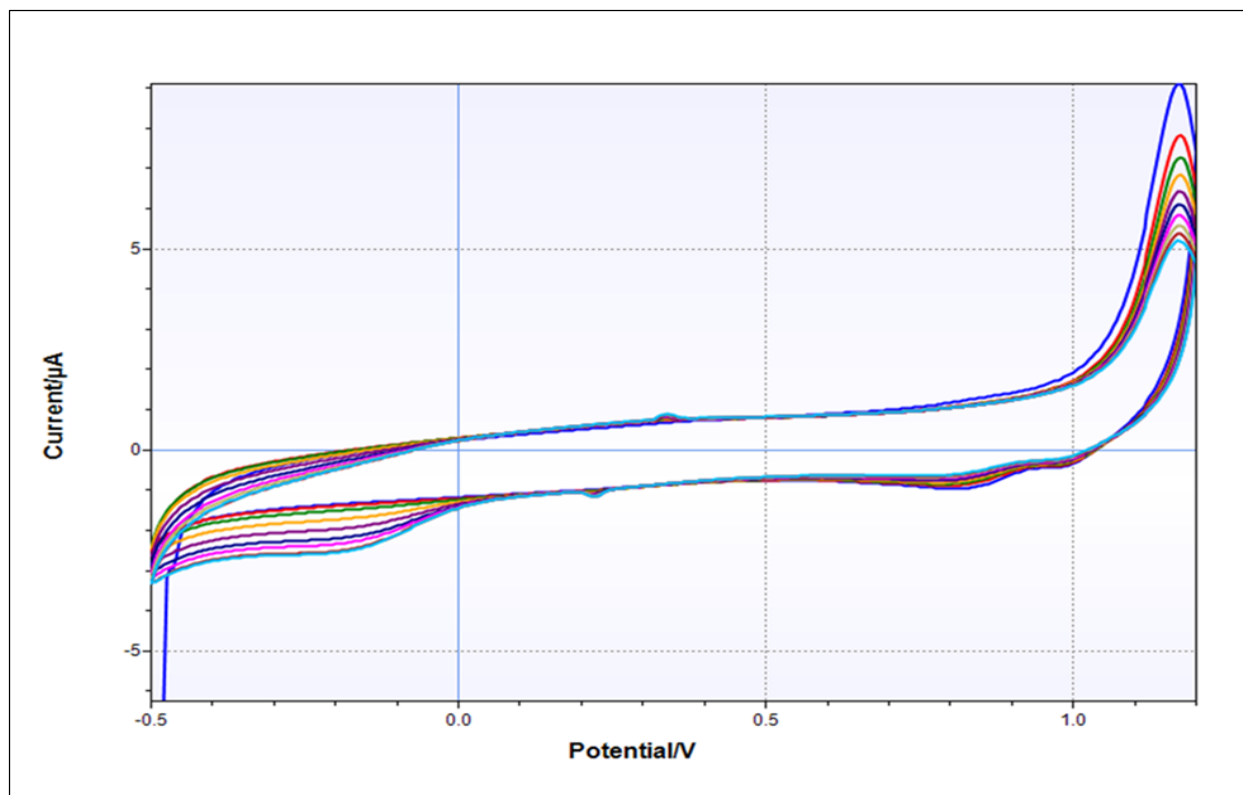
**Figure 4.7** Cyclic voltammetry of the 1 mM AuNP deposited on the GCE in 0.1 M NaNO<sub>3</sub> (pH = 3) solution and cycling (n = 10) at a scan rate of 50 mVs<sup>-1</sup>.

Figure 4.7 shows a oxidation peak at 1.1 V in the cyclic voltammogram and a cathodic peak at 0.85 V in the reverse scan. The peaks are associated with the reduction of Au<sup>3+</sup> to Au<sup>0</sup>.



Formal potential = (E<sub>pa</sub> + E<sub>pc</sub>)/2 = (1.1 V + 0.8 V)/2 = 1.0 V (from Figure 4.7)





**Figure 4.8** Cyclic voltammetry of the 1 mM AuNP deposited on the GCE in 0.1 M NaNO<sub>3</sub> (pH = 3) solution and cycling (n = 10) at a scan rate of 50 mVs<sup>-1</sup>.

The anodic peak shifts from 0.85 V to 0.5 V with successive scans, supporting the fact that Au deposition occurred on the NP's created during the first scans (Hezard *et al.*, 2012). The peak currents gradually decreased with successive scans as the AuNP particles are electrodeposited on the GCE.

A reduction peak at 0.35 V and 1.2 V (Figure 4.8) as observed in the forward scan and an oxidation peak at 0.85 V and 0.22 V. The cathodic peak at 0.35 V could be the reduction of Au<sup>3+</sup> to Au<sup>+</sup>. The cathodic peak at 1.2 V is due to the reduction of Au<sup>3+</sup> to Au<sup>0</sup>, inducing the deposition of AuNP/s onto the GCE surface (Hezard *et al.*, 2012).

#### 4.4.2 Characterization of GCE/AuNP

##### (a) Characterization of GCE/AuNP with Cyclic Voltammetry (CV)

The modified GCE/AuNP electrode was activated in 0.1 M HCl solution by running 10 ten scans between -0.5 – 1.2 V at a scan rate of 50 mVs<sup>-1</sup>.

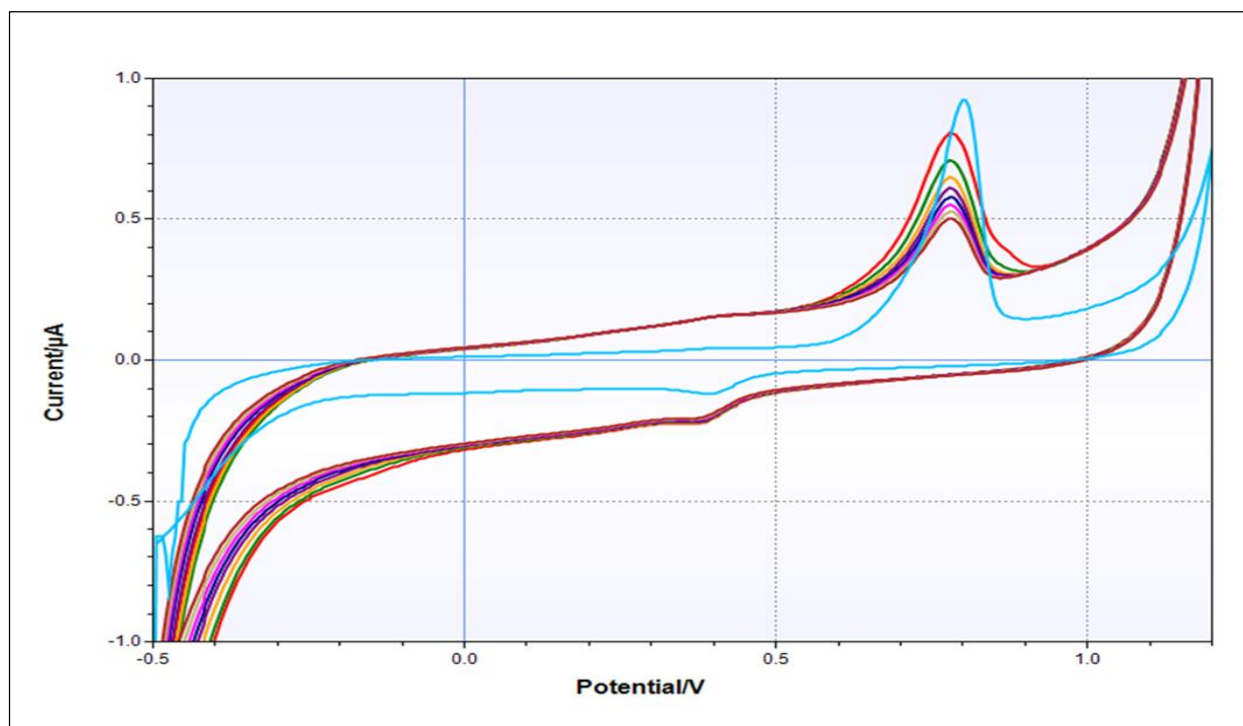


**Figure 4.9** Cyclic voltammetry of the activation of GCE/AuNP in 0.1 M HCl and cycling (n = 10) at a scan rate of 50 mVs<sup>-1</sup>.

To characterise the GCE/AuNP electrode was placed in 10 mL in a 0.1 M HCl solution and the scan rates were determined by scanning at an increased scan rate from 5- 400 mVs<sup>-1</sup> (Figure 4.9). The scan rates and diffusion coefficient were determined. For further characterization SWV scans were also obtained (Figure 4.12-4.13).

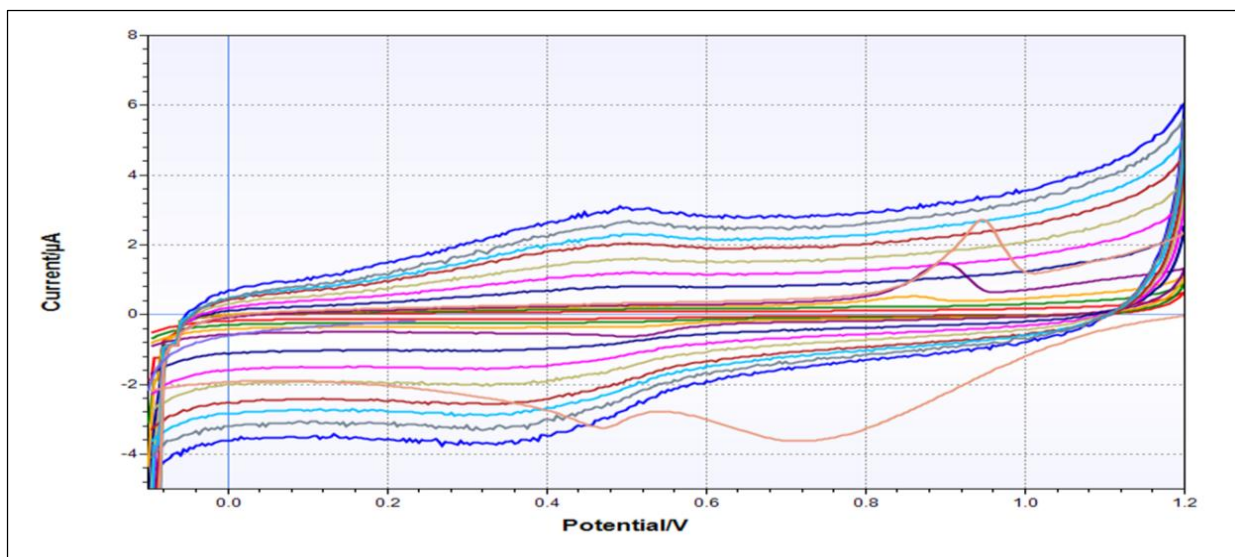


**Figure 4.10** Cyclic voltammetry of the characterization of the GCE/AuNP in 0.1 M HCl solution at increasing scan rates from 5 – 400 mVs<sup>-1</sup>.

The peaks at 0.92 V (Figure 4.10) are associated to the oxidation of Au and possibly the formation of oxides resulting from intricate sorption mechanism of OH<sup>-</sup> on different crystallographic faces and the peak at 0.7 and 0.48 V due to the reduction of the previously formed oxides (Hezard *et al.*, 2012). The increases scan rate data was used to determine the diffusion coefficients, number of electrons and the formal charge as illustrated below.

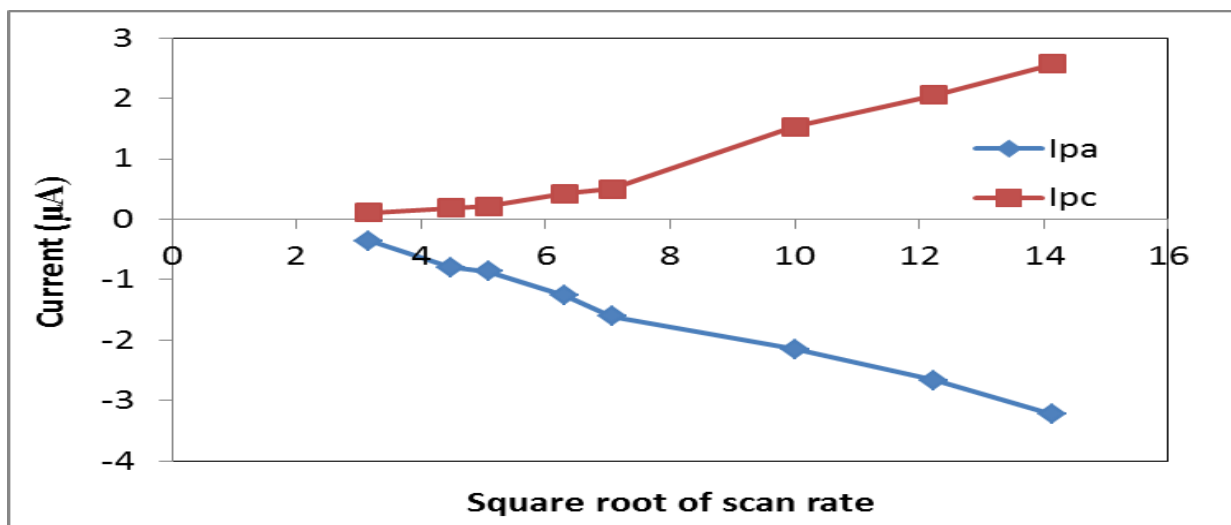


**Figure 4.11** Determination of diffusion coefficient for GCE/AuNP in 0.1 M HCl with data (n=4) obtained from Figure 4.10.

**Sample calculation of the determination of Formal charge:**

$$\Delta E = (E_{pa} + E_{pc})/2 = (0.92 \text{ V} + 0.52)/2 = 0.72 \text{ V}$$

$$E = 0.0592/n$$

$$N = 0.059/(0.92 - 0.52) = 0.15$$

**Sample calculation of the determination of diffusion coefficient:**

$$\text{Slope} = (2.69 \text{ e}^5) n^{3/2} A C D^{1/2}$$

$$D^{1/2} = \text{slope}/[(2.69 \text{ e}^5) n^{3/2} A C]$$
$$= 0.24/[(2.69 \text{ e}^5) 1^{3/2} \cdot 0.07 \cdot 1 \times 10^{-3}]$$

$$D = 1.62 \times 10^{-4} \text{ cm}^2 \text{ s}^{-1}$$

Summary for determinations (n =4) reported in table 5.1.

**(b) Characterization of GCE/AuNP with SWV**

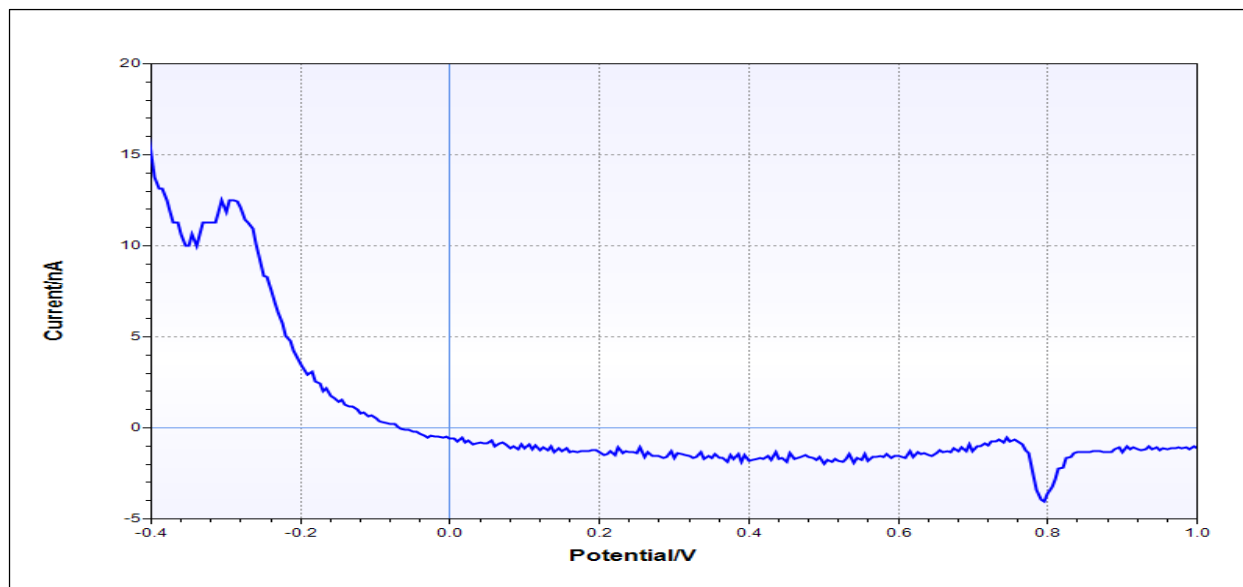


**Figure 4.12** Square wave voltammetry of reduction at GCE/AuNP in 0.1 M HCl solution. Peaks appeared at 0.34 V and at 0.8 V.

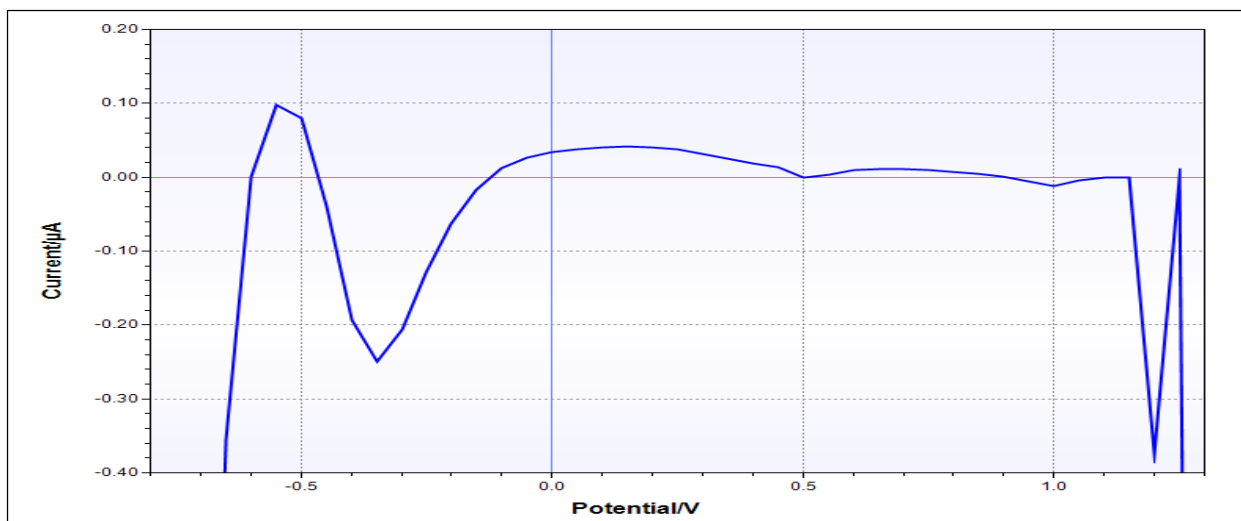


**Figure 4.13** Square wave voltammetry of reduction at GCE/AuNP in 0.1 M HCl solution after CV cycles ( $n = 10$ ).

**(c) Characterization of GCE/AuNP with Raman**

The GC/AuNP was characterised with Raman (Figure 4.14). The electrode was prepared as described above and allowed to dry overnight at room temperature before Raman and AFM analysis.

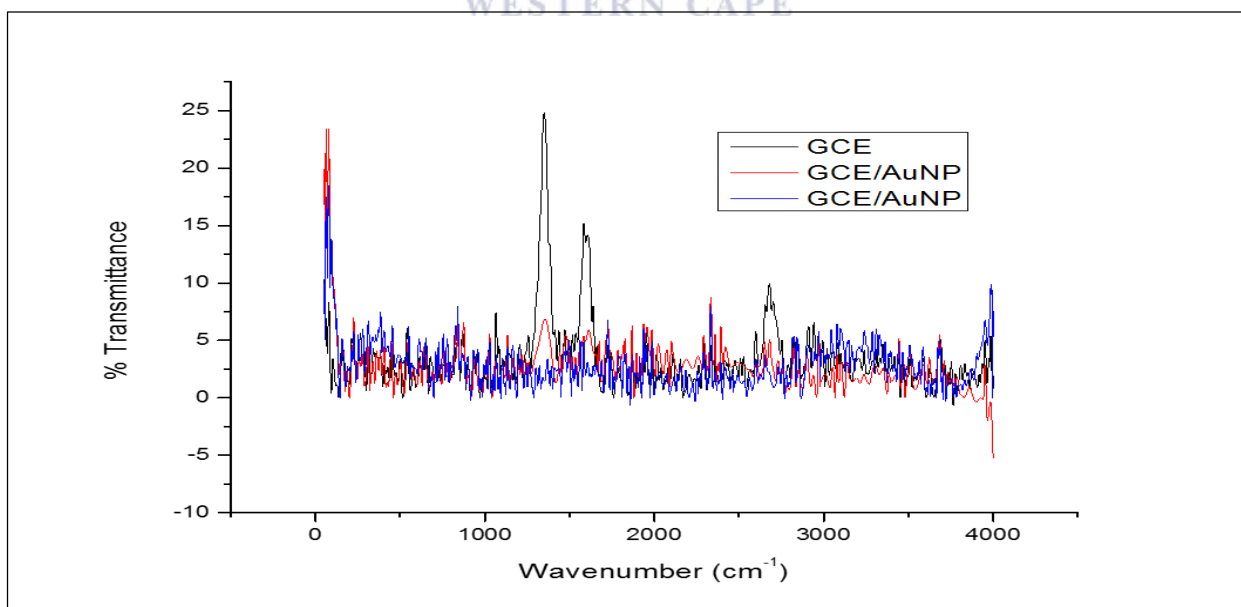


**Figure 4.14** Raman spectra representing an unmodified GCE(black), a synthesized GCE/AuNP electrode(red) and another synthesized GCE/AuNP electrode(blue).

The two peaks in the spectra are due to the D band at  $1354\text{ cm}^{-1}$  due to the disordered in the  $\text{sp}^2$  carbon systems and the G band which arises from the stretching of the C-C at  $1583\text{ cm}^{-1}$ . The  $\text{G}^1$  band appears at  $2700\text{ cm}^{-1}$ . The peaks that clearly appeared in the unmodified GCE are significantly reduced in the Raman scan of the GCE/AuNP.

**(d) Characterization of GCE/AuNP with Atomic Force Microscopy (AFM)**

Atomic Force Microscopy is widely used to characterise surface roughness which gives important information on the surface properties that plays a vital part in membrane permeability and fouling behaviour (Muya *et al.*, 2014).

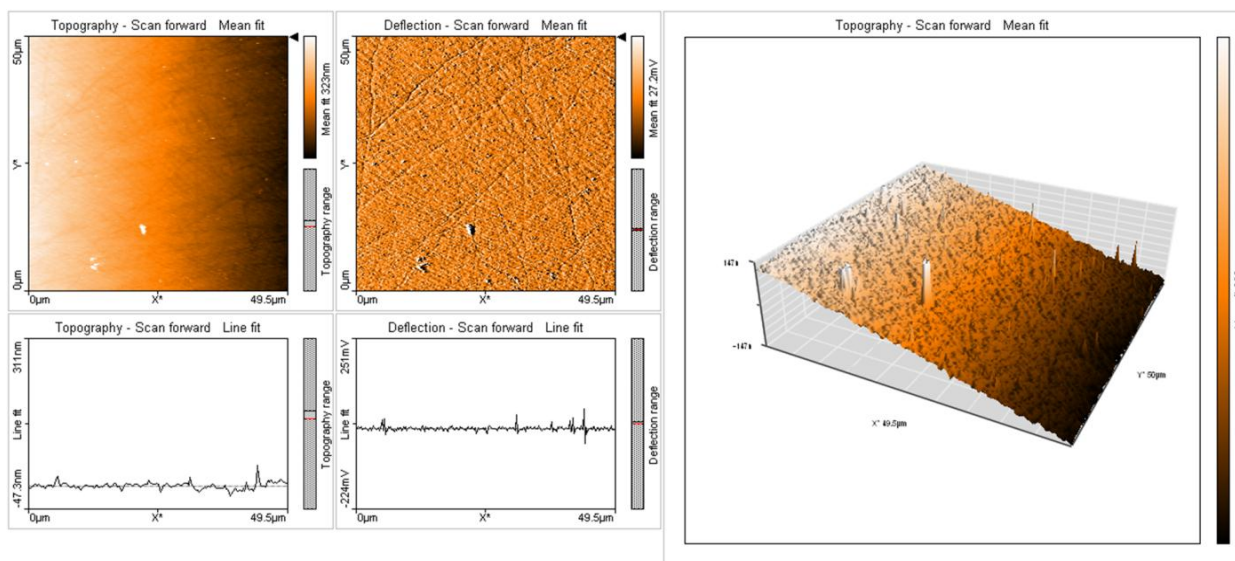


**Figure 4.15** AFM image of an unmodified GCE.

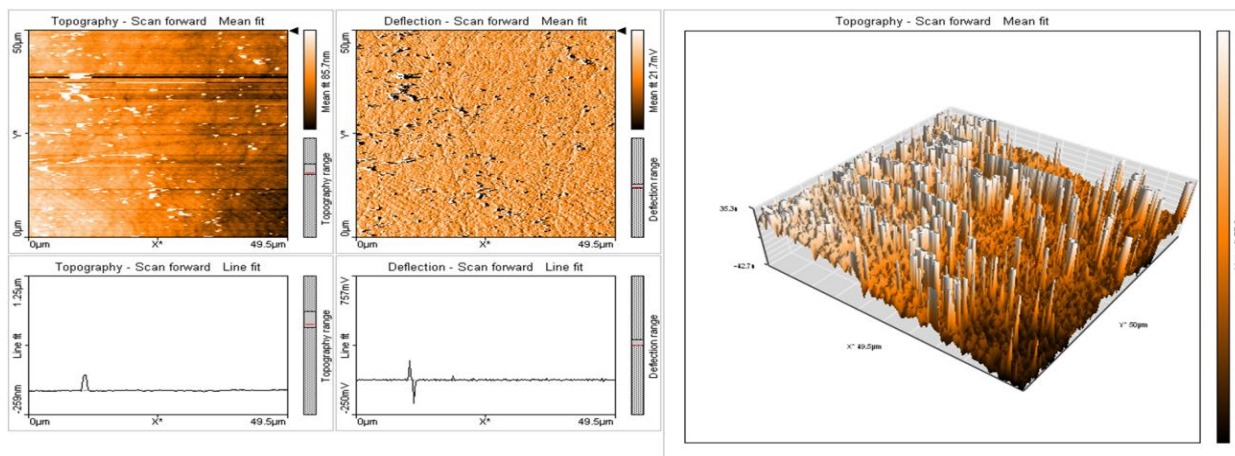


**Figure 4.16** AFM image of a modified GCE/AuNP (electrode 1).

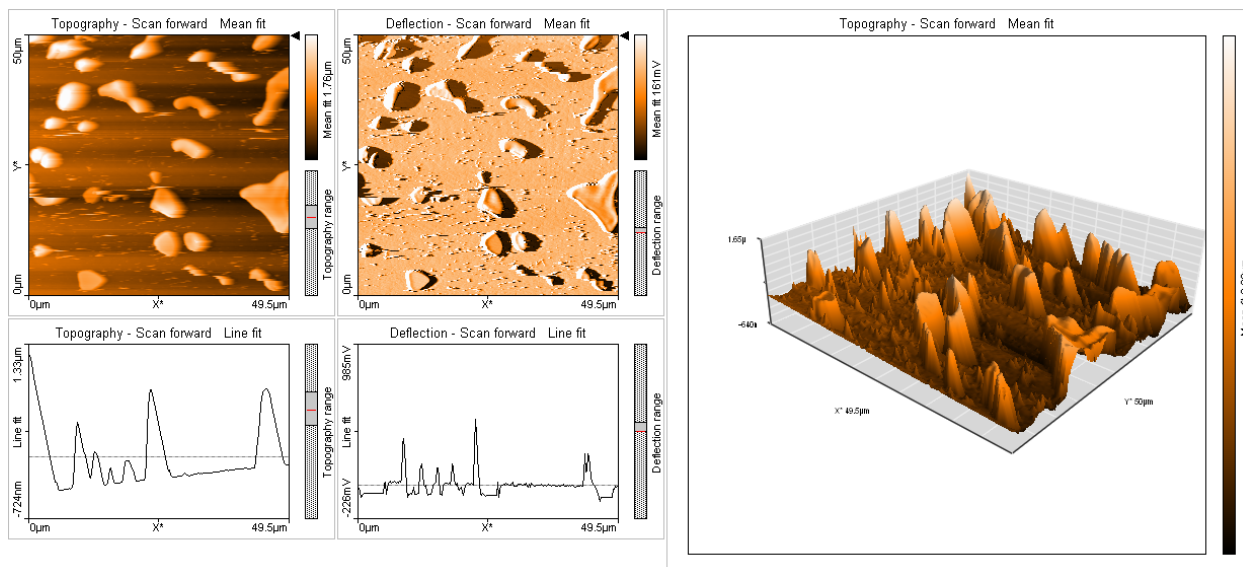


**Figure 4.17** AFM image of a modified GCE/AuNP (electrode 2).

The AFM scan of the unmodified GCE shows a rough topography (Figure 4.15). Sobri *et al.* (2008) found that initial deposit of Au yields a number of large nuclei which initially grows independent from one another with an average size of 120 nm. The particles can coalesce to particles of size 550 nm. The growth of gold nuclei than exhibit needle-like structures (Sobri *et al.* 2008). The AFM scans (Figure 4.16-4.17) shows an increasing surface roughness, with the GCE/AuNP exhibiting the needle-like structures as described by Sobri *et al.* (2008).

## 4.5 Synthesis and characterization of GCE/AuNP/hydrogel

### 4.5.1 Synthesis of GCE/AuNP/hydrogel

The synthesized and characterised AuNP/GCE was placed in a fresh 0.1 M HCl solution and after deaeration the hydrogel was added. To deposit the hydrogel CV scans ( $n=10$ ) at a scan rate  $50 \text{ mVs}^{-1}$ , was obtained in the range  $-0.5 \text{ V} - 1.2 \text{ V}$ . The GCE/Au/Hydrogel was placed in fresh 0.1 M HCl for characterization, the scan rates and diffusion coefficient was determination. Square wave voltammetry scans were also obtained (Figure 4.18).

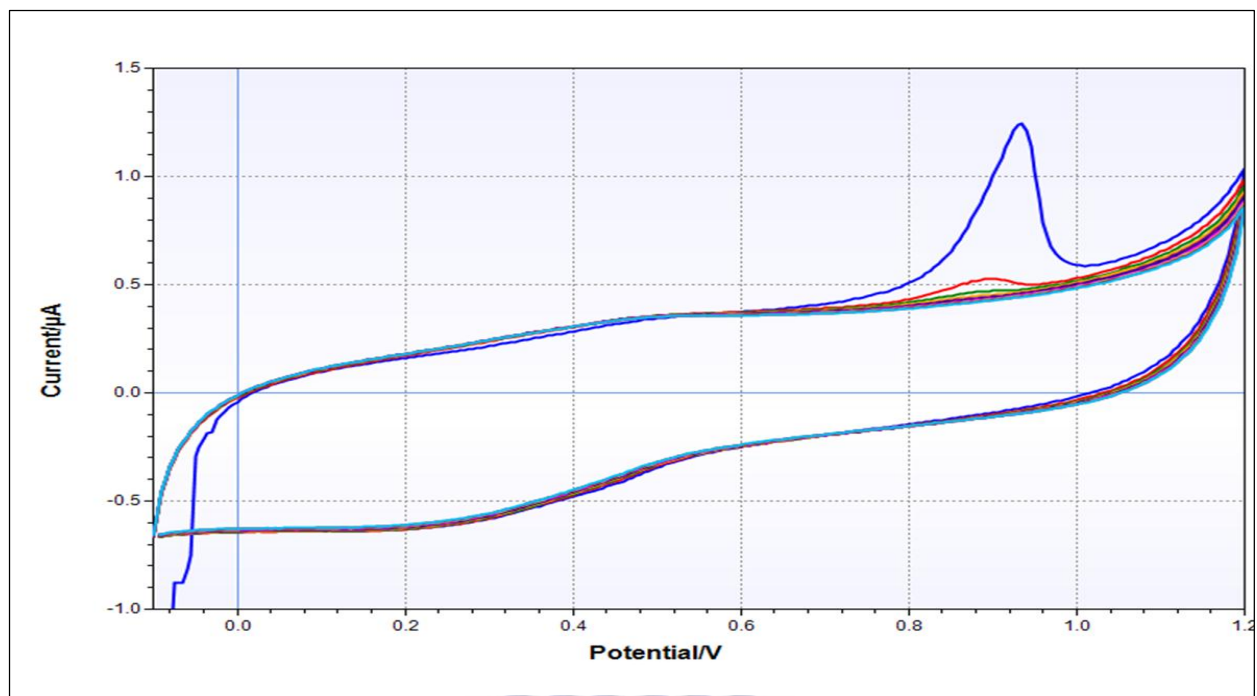


**Figure 4.18** Cyclic voltammetry recorded during deposition of hydrogel on GCE/AuNP. The hydrogel was added to 0.1 M HCl to deposit on GCE/AuNP by CV and cycling ( $n = 10$ ) at a scan rate of  $50 \text{ mVs}^{-1}$ . The peak at 0.9 V gradually disappeared with successive scans.

#### 4.5.2 Characterization of GCE/AuNP/Hydrogel

To characterise the GCE/AuNP/Hydrogel electrode was placed in 10 mL of a fresh 0.1 M HCl solution and the scan rates were determined by scanning at an increasing scan rate from  $5 \text{ mV} - 400 \text{ mVs}^{-1}$ . The scan rates and diffusion coefficient was determined. For further characterization SWV scans were also obtained.



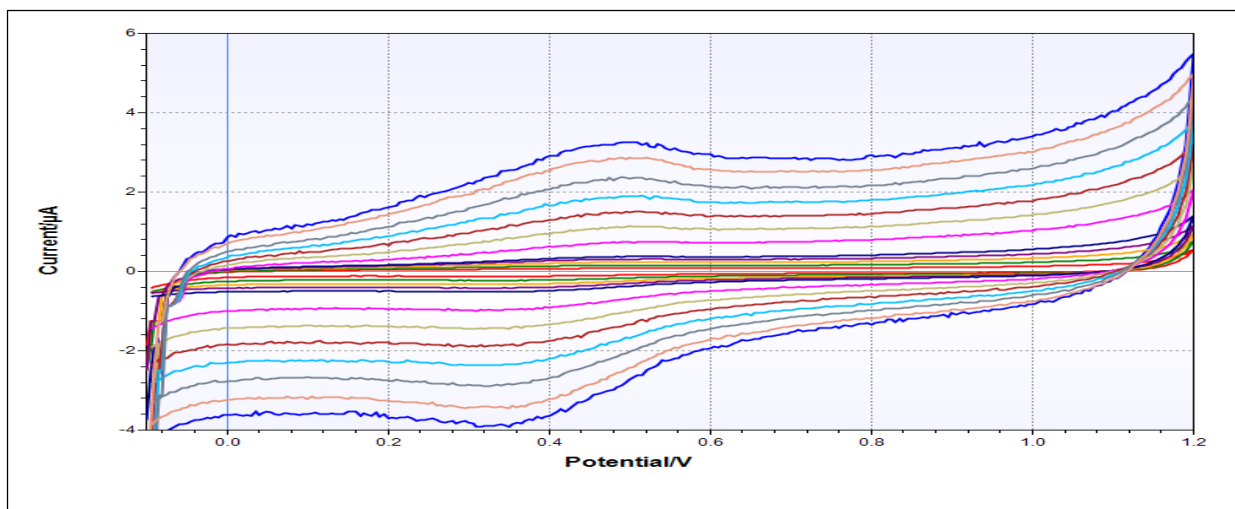


**Figure 4.19** Cyclic voltammetry for the characterization of GCE/AuNP/Hydrogel in 0.1 M HCl solution as a function of increasing scan rates of 5 – 400 mVs<sup>-1</sup>. Reduction peaks appear at 0.48 V and 1.2 V and an anodic peak at 0.34 V.

To characterise the GCE/AuNP/hydrogel electrode it was placed in 0.1 M HCl solution, CV obtained at increasing scan rates of 5 - 400 mVs<sup>-1</sup> to determine the diffusion coefficient (Figure 4.19 and 4.20).

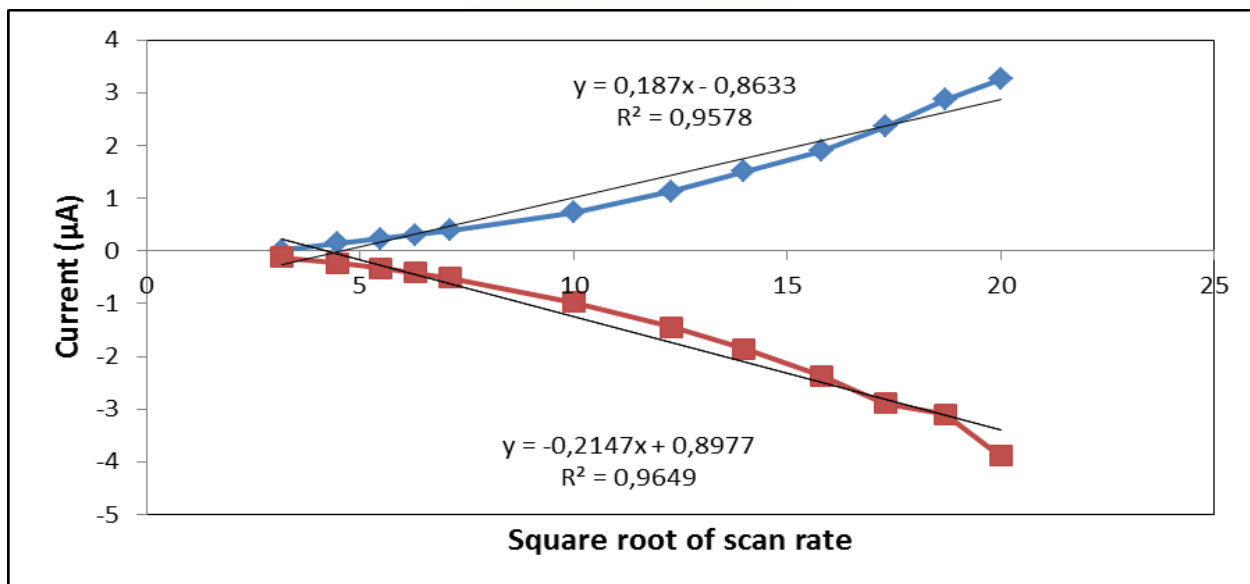


**Figure 4.20** Determination of scan rates and diffusion coefficient for GCE/AuNP/hydrogel in 0.1 M HCl solution.

**Sample calculation of the determination of Formal charge:**

$$\Delta E = (E_{pa} + E_{pc})/2 = (0.4 \text{ V} + 0.52)/2 = 0.46 \text{ V}$$

$$\Delta E = 0.0592/n$$

$$N = 0.059/(0.52 - 0.4) = 0.49 \approx 1$$

**Sample calculation of the determination of Diffusion coefficient:**

$$\text{Slope} = (2.69 \text{ e}^5) n^{3/2} A C D^{1/2}$$

$$D^{1/2} = \text{slope}/[(2.69 \text{ e}^5) n^{3/2} A C]$$
$$= 0.187/[(2.69 \text{ e}^5) 1^{3/2} \cdot 0.07 \cdot 1 \times 10^{-3}]$$

$$D = 9.86 \times 10^{-5} \text{ cm}^2 \text{ s}^{-1}$$

**Sample calculation of the determination Diffusion coefficient:**

$$\text{Slope} = (2.69 \text{ e}^5) n^{3/2} A C D^{1/2}$$

$$D^{1/2} = \text{slope}/[(2.69 \text{ e}^5) n^{3/2} A C]$$
$$= 0.2147/[(2.69 \text{ e}^5) 1^{3/2} \cdot 0.07 \cdot 1 \times 10^{-3}]$$

$$D = 1.30 \times 10^{-4} \text{ cm}^2 \text{ s}^{-1}$$

Summary for determinations ( $n = 4$ ) reported in table 5.1.

For further characterization a SWV of GCE/AuNP/ hydrogel placed in 0.1 M HCl with a scan rate of  $50 \text{ mVs}^{-1}$  was obtained (Figure 4.21-4.22).

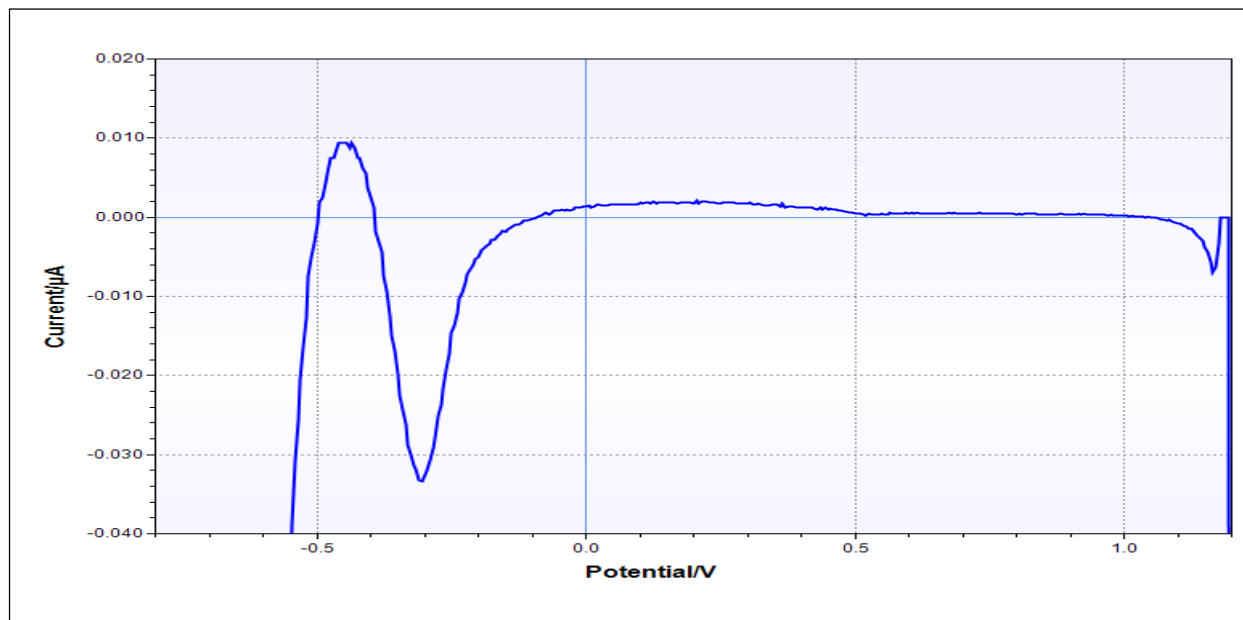


**Figure 4.21** Square wave voltammetry reduction scan at GCE/AuNP/hydrogel in 0.1 M HCl solution. Peaks appeared at -0.32 V and 1.18 V.

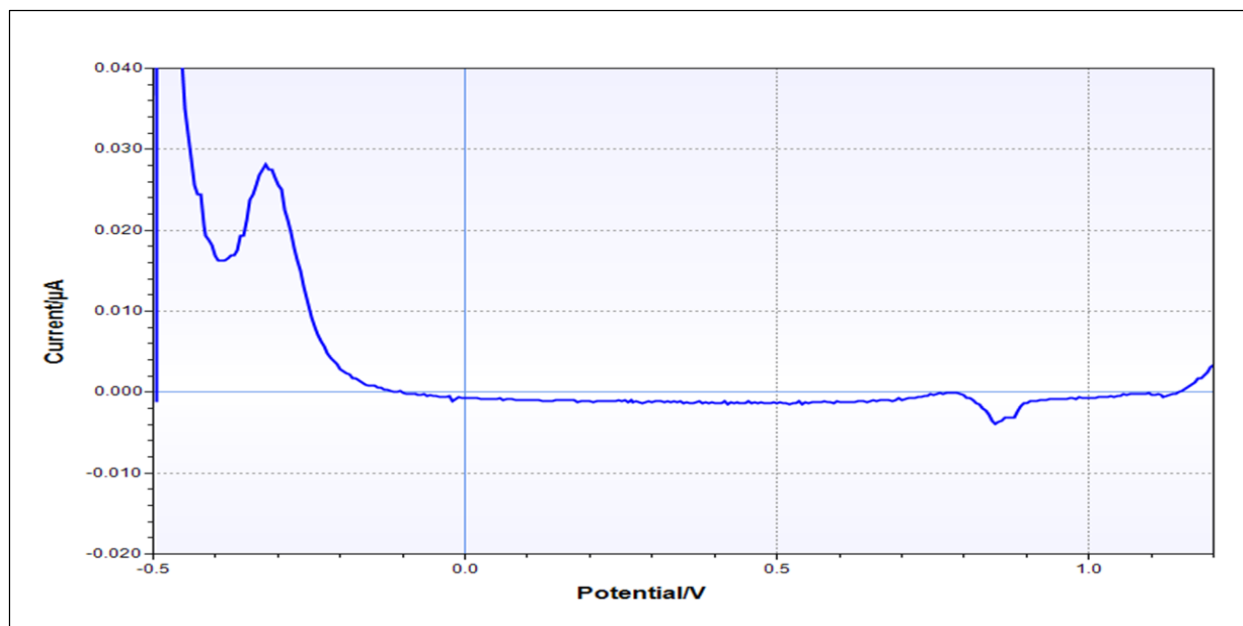


**Figure 4.22** Square wave voltammetry oxidation scan from at GCE/AuNP/hydrogel in 0.1 M HCl solution. Peaks appeared at -0.32 V and 0.85 V.

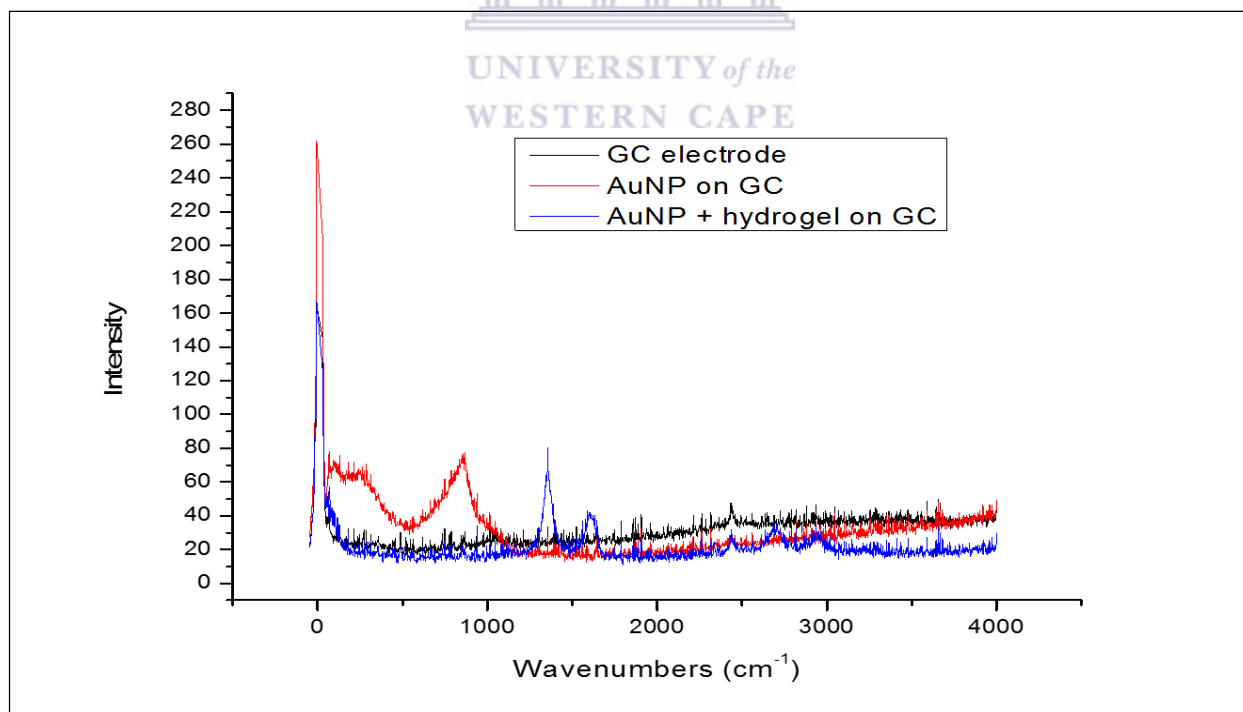


**Figure 4.23** Raman spectra representing an unmodified GCE, a GCE/AuNP and GCE/AuNP/Hydrogel electrodes

The GC/AuNP was characterised with Raman and AFM analysis. The electrode was prepared as described above, allowed to dry overnight at room temperature before Raman and AFM analysis.

The Raman scan shows increased intensity between 0- 1000  $\text{cm}^{-1}$  for GCE/AuNP (Figure 4.23).

For GCE/AuNP/hydrogel peaks appeared at:

2 peaks at 1650  $\text{cm}^{-1}$  and 1800  $\text{cm}^{-1}$ , C=C stretch at 1650 – 1638  $\text{cm}^{-1}$ , C=C stretch at 1800  $\text{cm}^{-1}$  or C=O at 1750  $\text{cm}^{-1}$ ,

2 peaks at 2400  $\text{cm}^{-1}$  and 2900  $\text{cm}^{-1}$ , C-H at 2900  $\text{cm}^{-1}$

#### 4.6 Synthesis and characterization of GCE/AuNP/hydrogel/HA

The HA solution was prepared from a soluble form of HA (Sigma- Aldrich Catalogue number H1, 675-2 Lot.:S33786-057). A UV/Vis spectra of the HA was obtained (Figure 4.24) and shows absorption in UV range.

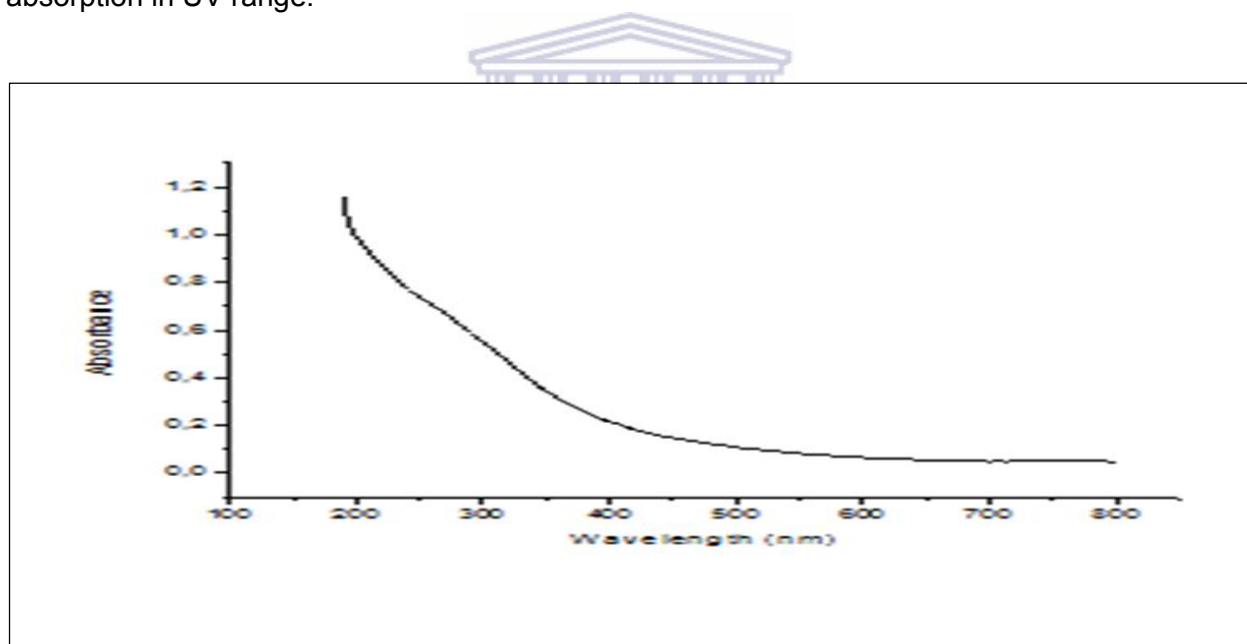


**Figure 4.24** UV/Vis Absorption spectra of a HA solution

The GCE/AuNP/hydrogel electrode was placed in a 1000 ppm HA solution for 30 min. After the 30 min incubation period the electrode was removed, rinsed down and transferred to fresh 0.1 M HCl solution. Two CV scans were obtained by cycling at 50 $\text{mVs}^{-1}$  from -0.5 - 1.2 V (Figure 4.25). The prepared sensor was then used for the determination of Hg and Pb.

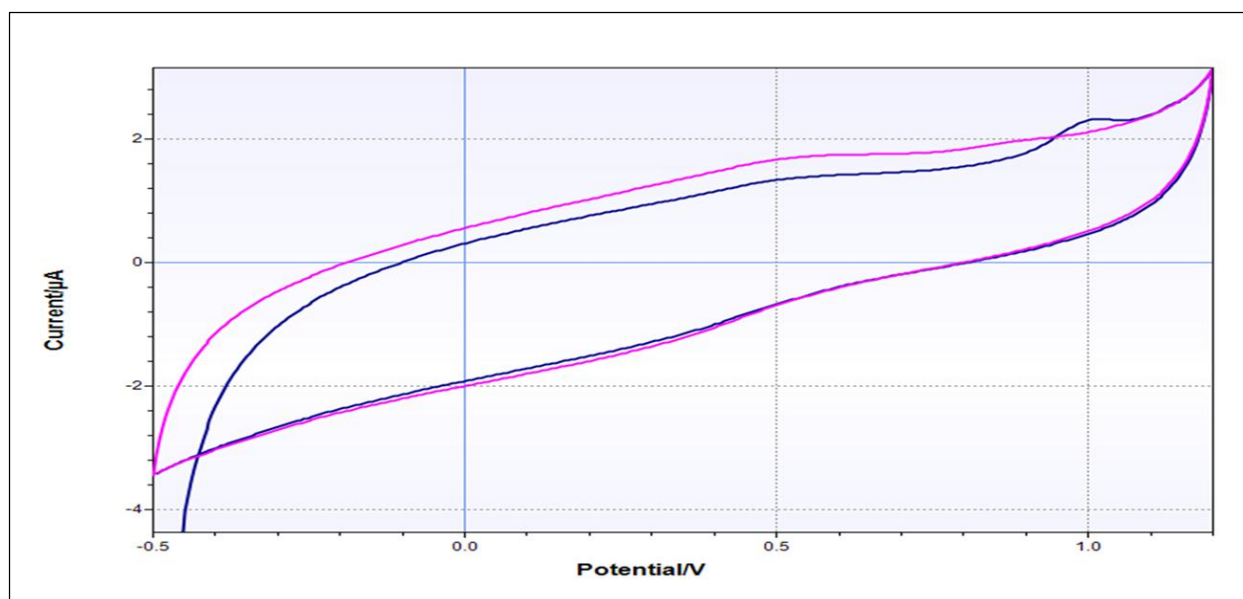


**Figure 4.25** The GCE/AuNP/hydrogel/HA electrode was placed in a 0.1 M HCl solution and CV scans was obtained by cycling (n=2) at a scan rate of 50 mVs<sup>-1</sup> to obtain a baseline.

#### 4.7 Summary of results for characterization performed on GCE/AuNP, GCE/AuNP/Hydrogel and GCE/AuNP/Hydrogel/HA

**Table 4.1** Results of half wave potentials, formal charges and distribution coefficients for the GCE/AuNP/Hydrogel/HA sensor (n=4).

Electrode	E <sub>1/2</sub> (V)		Formal Charge (V)	Distribution Coefficient (cm <sup>2</sup> s <sup>-1</sup> )	
	I <sub>pc</sub>	I <sub>pa</sub>		I <sub>pc</sub>	I <sub>pa</sub>
GCE/AuNP	0.52	0.92	0.72	1.3 x 10 <sup>-4</sup>	1.02 x 10 <sup>-4</sup>
GCE/AuNP (repeat)	0.48	0.80	0.64	1.26 x 10 <sup>-4</sup>	8.2 x 10 <sup>-5</sup>
GCE/AuNP (repeat)	0.48	0.98	0.73	1.59 x 10 <sup>-4</sup>	1.72 x 10 <sup>-4</sup>
GCE/AuNP (repeat)	0.48	0.98	0.73	1.34 x 10 <sup>-4</sup>	1.12 x 10 <sup>-4</sup>
GCE/AuNP/hydrogel	0.48	0.91	0.70	9.75 x 10 <sup>-5</sup>	2.19 x 10 <sup>-4</sup>
GCE/AuNP/hydrogel	0.40	0.52	0.46	9.86 x 10 <sup>-5</sup>	1.30 x 10 <sup>-4</sup>
GCE/AuNP/hydrogel	0.34	0.52	0.46	9.86 x 10 <sup>-5</sup>	1.30 x 10 <sup>-4</sup>
GCE/AuNP/hydrogel	0.36	0.48	0.42	1.71 x 10 <sup>-5</sup>	2.51 x 10 <sup>-4</sup>
GCE/AuNP/Hydrogel/HA	0.49	0.95	0.72	1.75 x 10 <sup>-4</sup>	2.29 x 10 <sup>-4</sup>
GCE/AuNP/hydrogel/HA	0.48	0.98	0.72	1.75 x 10 <sup>-4</sup>	2.29 x 10 <sup>-4</sup>
GCE/AuNP/hydrogel/HA	0.48	0.98	0.72	1.75 x 10 <sup>-4</sup>	3.48 x 10 <sup>-3</sup>
GCE/AuNP/hydrogel/HA	0.48	0.98	0.72	1.75 x 10 <sup>-4</sup>	3.48 x 10 <sup>-3</sup>

**Table 4.2** Summary of half wave potentials, formal charges and distribution coefficients (n = 4)

Electrode	E <sub>1/2</sub> (V)		Formal Charge (V)	Distribution Coefficient (cm <sup>2</sup> s <sup>-1</sup> )	
	I <sub>pc</sub>	I <sub>pa</sub>		I <sub>pc</sub>	I <sub>pa</sub>
GCE/AuNP	0.48	0.94	0.71	1.37 x 10 <sup>-4</sup>	1.17 x 10 <sup>-4</sup>
GCE/AuNP/hydrogel	0.40	0.87	0.45	9.82 x 10 <sup>-5</sup>	1.83 x 10 <sup>-4</sup>
GCE/AuNP/Hydrogel/HA	0.48	0.95	0.45	1.75 x 10 <sup>-4</sup>	1.85 x 10 <sup>-4</sup>

St dev = 0.05

Summary of the half wave potentials, formal charges and distribution coefficients (n = 4) obtained from the characterization by CV and SWV are reported in Table 4.1-4.2.

## 4.8 Determination of Hg<sup>2+</sup> on the GCE/AuNP/hydrogel/HA sensor

### 4.8.1 Determination of Hg<sup>2+</sup> on an unmodified GCE

The Hg<sup>2+</sup> standards were prepared from a 1000 ppm stock solution and added to the 0.1M HCl solution, in the analytical concentration range 0.1-16 μmol/L, to the cell with the GCE/AuNP/hydrogel/HA sensor. For comparison the same analysis was performed on an unmodified GC electrode. Figure 4.26 shows a CV and Figure 4.27 a SWV scan of the Hg<sup>2+</sup> uncomplexed solution. A calibration curve of the Hg<sup>2+</sup> was constructed to determine the LOD and LOQ. Results are for an average of three determinations.

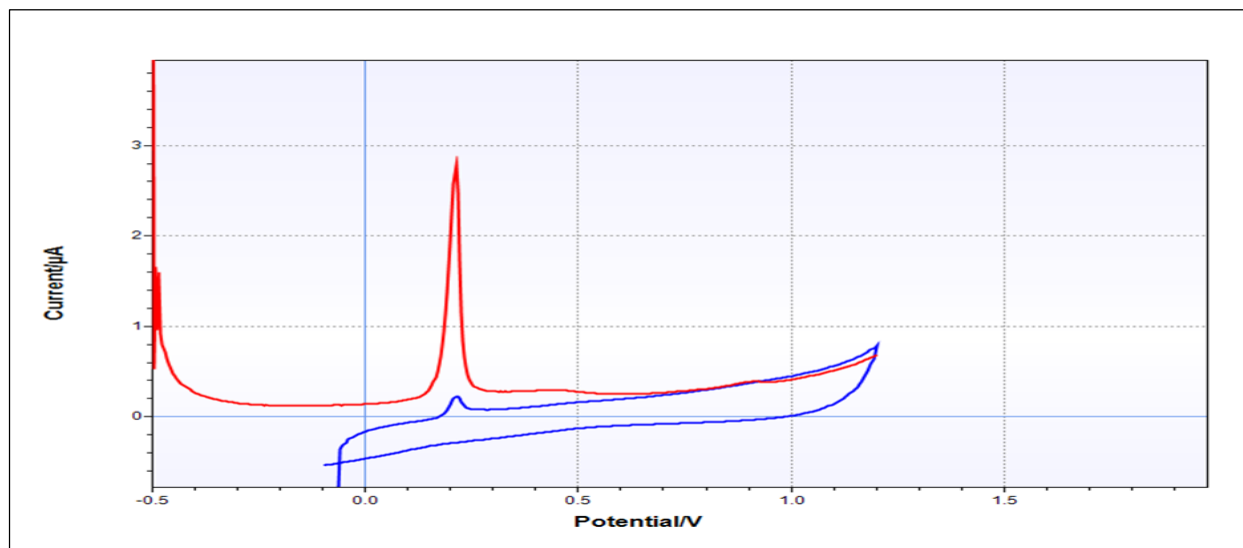


**Figure 4.26** Cyclic voltammetry of Hg<sup>2+</sup> at an unmodified GCE in a 0.1 M HCl solution superimposed on a SWV oxidation scan. Peak of Hg<sup>2+</sup> at 0.2 V of the reduction of Hg<sup>2+</sup> to Hg.

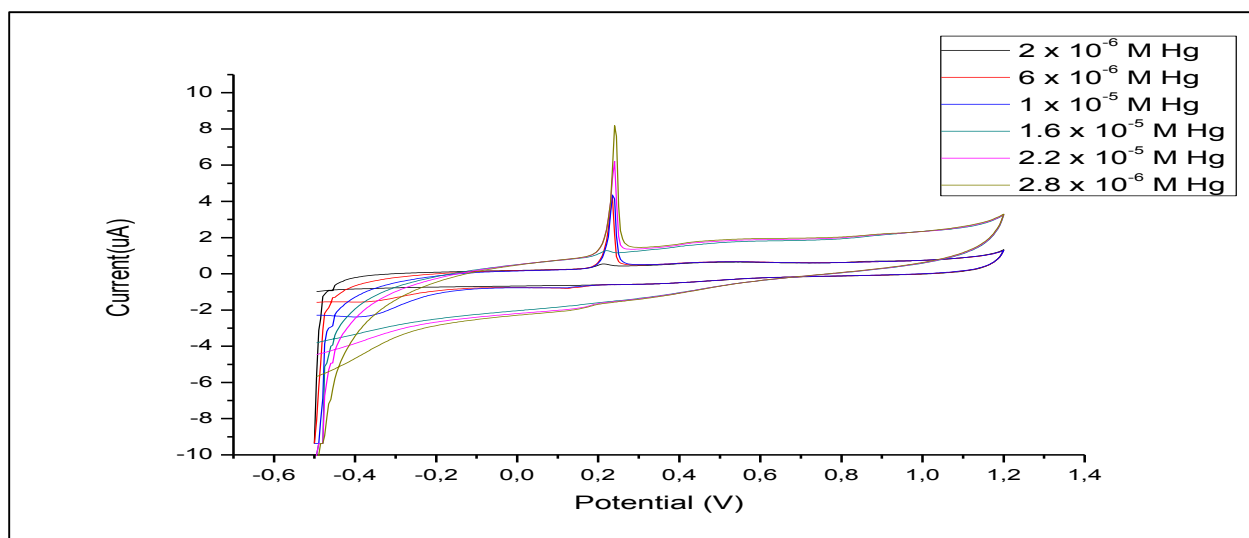


**Figure 4.27** Square wave voltammetry oxidation scan of increasing concentrations of  $\text{Hg}^{2+}$  at an unmodified GCE in a 0.1 M HCl solution.

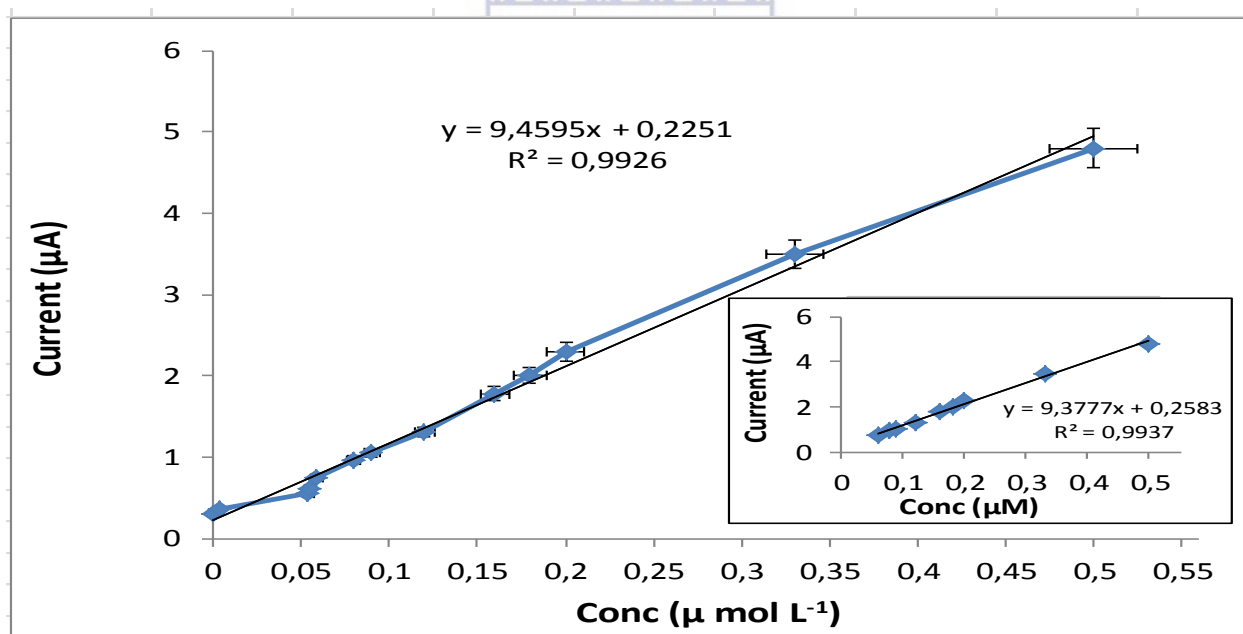


**Figure 4.28** Calibration curve obtained using SWV at an unmodified GCE in a deaerated 0.1 M HCl solution. Results are the mean of three determinations and insert shows the linear range from 0.1 – 0.5  $\mu\text{mol/L}$  (std deviation,  $n = 3$ ).

The calibration curves showed a dynamic range that exhibited two narrow linear ranges. The analytical protocols produced calibration data which leads to the statistic results as presented in

Table 4.3. All statistical data were reported at 95 % confidence level. Under these conditions the statistical data showed sensitivity of 9.4  $\mu\text{mol/L}$ , limit of detection (LOD) and limit of quantification (LOQ) respectively 0.02  $\mu\text{mol/L}$  and 0.17  $\mu\text{mol/L}$  and a linearity  $r^2 = 0.994$ .

#### 4.8.2 Determination of $\text{Hg}^{2+}$ on the GCE/AuNP/hydrogel/HA sensor

The  $\text{Hg}^{2+}$  standards added in increments in the concentration range 0.1-5  $\mu\text{mol/L}$  to the cell with the GCE/AuNP/hydrogel/HA sensor with 0.1M HCl solution. For characterization CV and SWV scans were obtained to determine the LOD and LOQ. Results are for an average of three determinations.

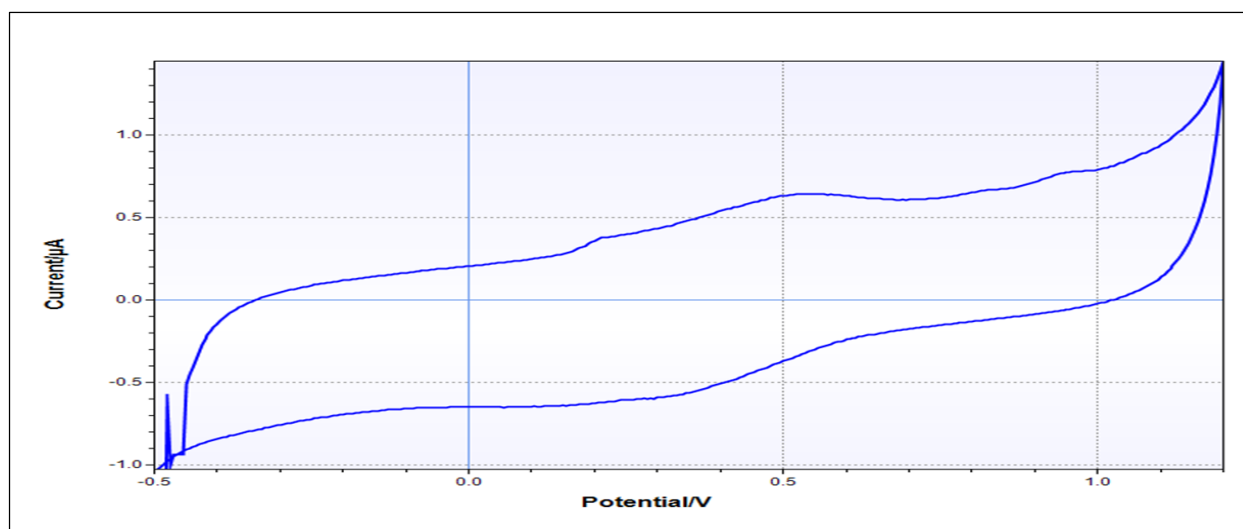


**Figure 4.29** Cyclic voltammetry of the first detectable  $\text{Hg}^{2+}$  peak in the 0.1M HCl solution at the GCE/AuNP/hydrogel/HA . Peak at 0.22 V.

The first detectable  $\text{Hg}^{2+}$  peak appeared in Figure 4.29 at a potential of 0.2 V, the standard reduction potential for the reduction of  $\text{Hg}^{2+}$  to  $\text{Hg}^0$ . The peak due to the Hg-HA complexation is evident at 0.5 V. Figure 4.30 showed an increased concentration of  $\text{Hg}^{2+}$  solution added to the 0.1 M HCl electrolyte in the cell containing the sensor. Figure 4.30 of the SWV illustrated more clearly the peak due to the free  $\text{Hg}^{2+}$  (0.2V) and Hg-HA complex at 0.5V.



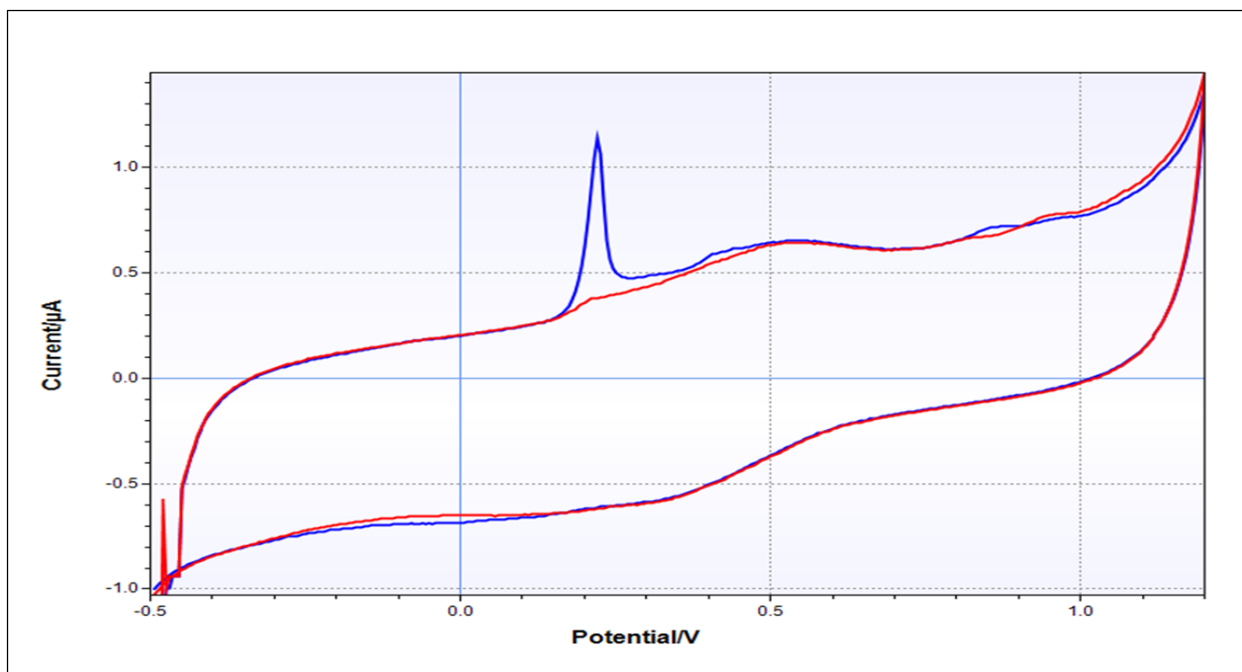


**Figure 4.30** Cyclic voltammetry of two additions of a 0.1  $\mu\text{mol/L}$   $\text{Hg}^{2+}$  standard solution at GCE/AuNP/hydrogel/HA in 0.1M HCl solution. Peak at 0.2 V.

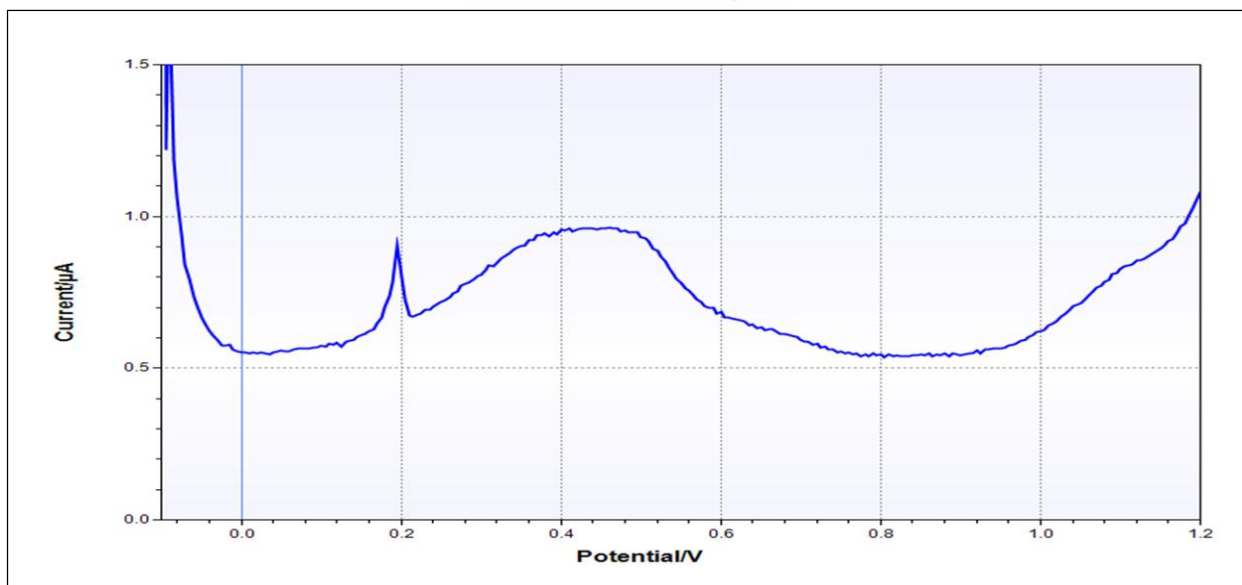
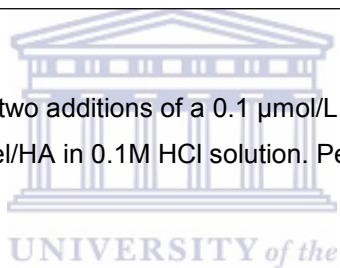


**Figure 4.31** Square wave voltammetry oxidation of  $\text{Hg}^{2+}$  standard at added in increasing concentration at GCE/AuNP/hydrogel/HA in 0.1M HCl solution. Cathodic peak at 0.20 V of the reduction of  $\text{Hg}^{2+}$  to  $\text{Hg}^0$  and a peak at 0.48 V of the complexed Hg-HA.

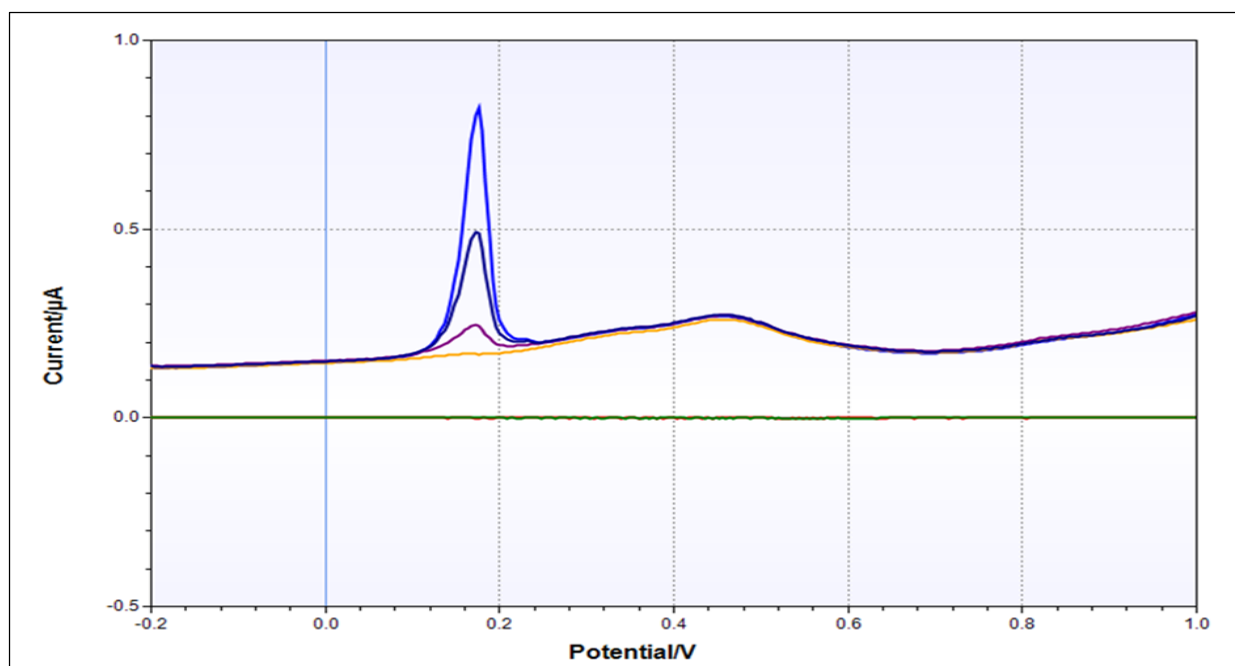


**Figure 4.32** Square wave voltammetry oxidation of  $\text{Hg}^{2+}$  standard added in increasing concentration at GCE/AuNP/hydrogel/HA in 0.1M HCl solution. Cathodic peak at 0.20 V of the reduction of  $\text{Hg}^{2+}$  to  $\text{Hg}^0$  and a peak at 0.48 V of the complexed Hg-HA.

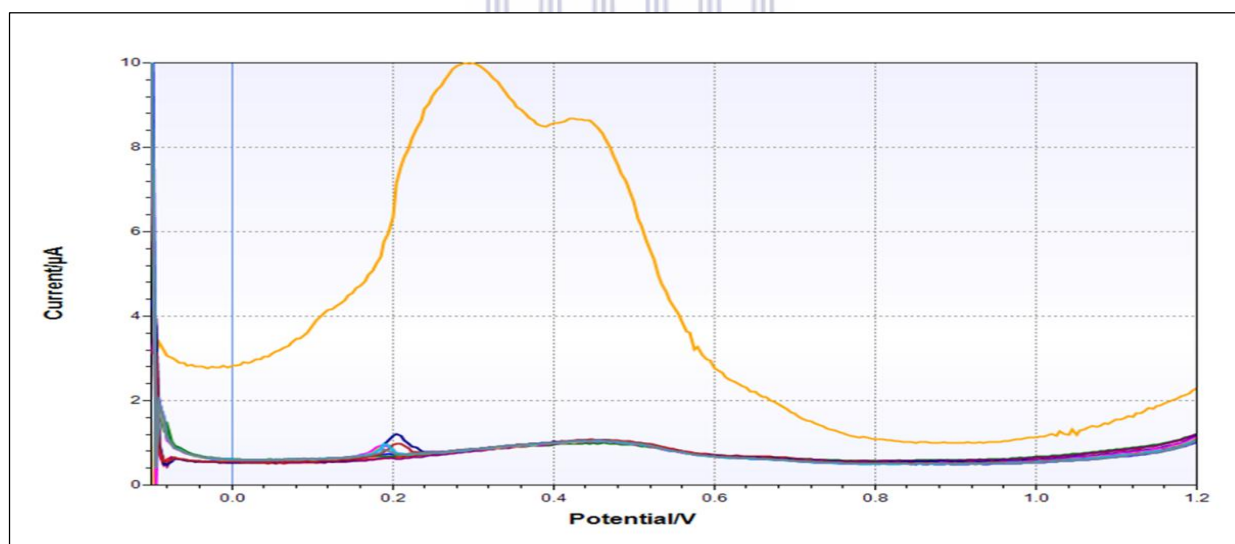


**Figure 4.33** Square wave voltammetry reduction of a  $3.6 \mu\text{mol/L}$   $\text{Hg}^{2+}$  standard added in increasing increments at the GCE/AuNP/hydrogel/HA in 0.1M HCl solution. Cathodic peak at 0.20 V of the reduction of  $\text{Hg}^{2+}$  to  $\text{Hg}^0$  and a peak at 0.48 V of the complexed Hg-HA.

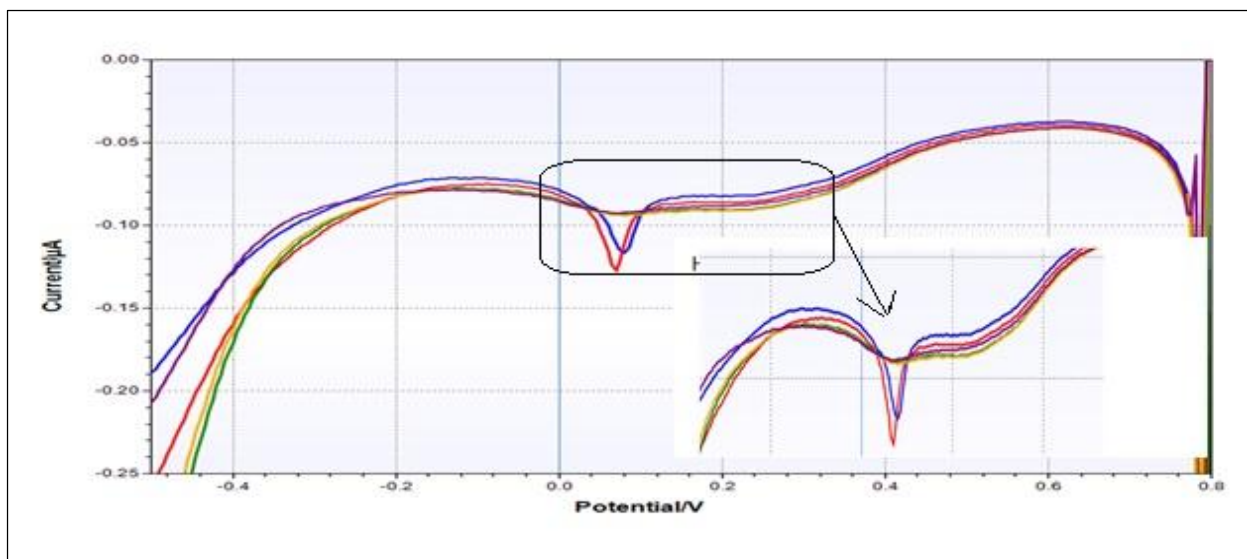


**Figure 4.34** Square wave voltammetry at to the 0.1M HCl solution in the cell with the GCE of the reduction of a 3.6  $\mu\text{mol/L}$   $\text{Hg}^{2+}$  standard added in increasing increments. Cathodic peak at 0.20 V of the reduction of  $\text{Hg}^{2+}$  to  $\text{Hg}^0$  and a peak at 0.48 V of the complexed  $\text{Hg-HA}$ .

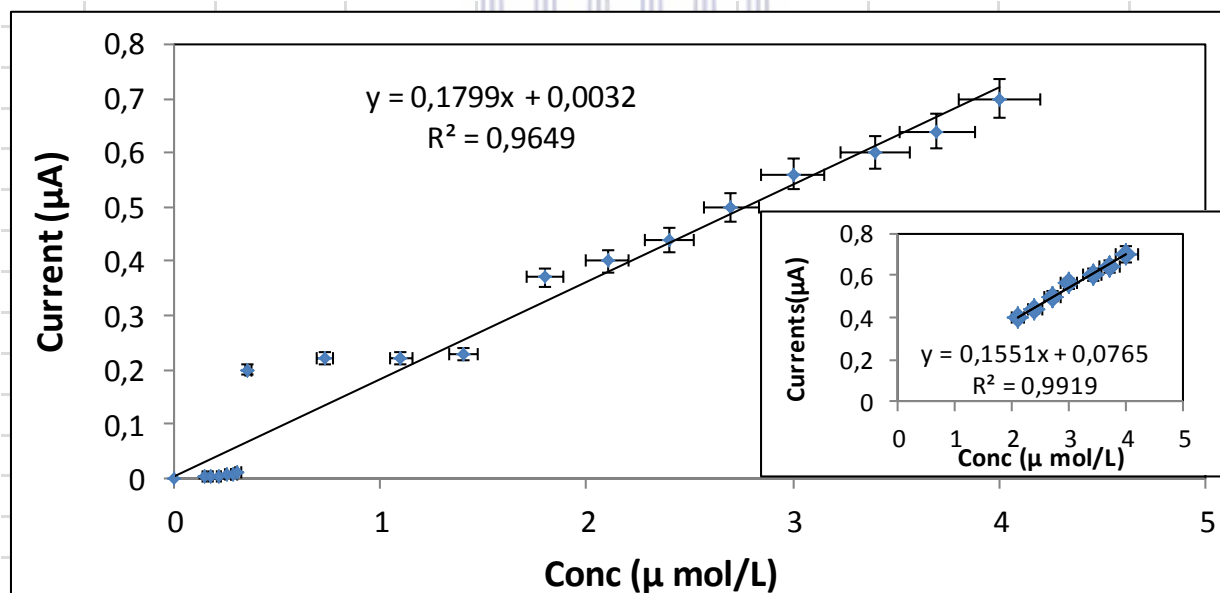


**Figure 4.35** Calibration curve of  $\text{Hg}^{2+}$  obtained at SWV GCE/AuNP/Hydrogel/HA in a deaerated 0.1M HCl solution and insert shows the linear range from 0.1 – 5  $\mu\text{mol/L}$  (std deviation,  $n = 3$ ).

The calibration curves showed a narrow linear dynamic range. The analytical protocols produced calibration data which leads to the statistic results as presented in Table 5.3. All

statistical data were reported at 95 % confidence level. Under these conditions the statistical data showed sensitivity of 0.2  $\mu\text{mol/L}$ , limit of detection (LOD) and limit of quantification (LOQ) respectively 0.002  $\mu\text{mol/L}$  and 0.03  $\mu\text{mol/L}$  and a linearity  $r^2 = 0.992$ .

#### 4.8.3 Spectroscopic determination of $\text{Hg}^{2+}$ on the GCE/AuNP/hydrogel/HA sensor

The disappearance of the free metal during SWV analysis, from the electrolytic solution that the GCE/Au/Hydrogel/HA sensor was exposed to, was followed by UV/Vis analysis (Figure 4.36). An increase in UV/Vis absorbance trend, for  $\text{M}^{2+}$  ion concentration, provided complimentary corroboration for the electrochemically driven complexation of  $\text{M}^{2+}$  ion by the HA ligand entrapped in the sensor matrix.

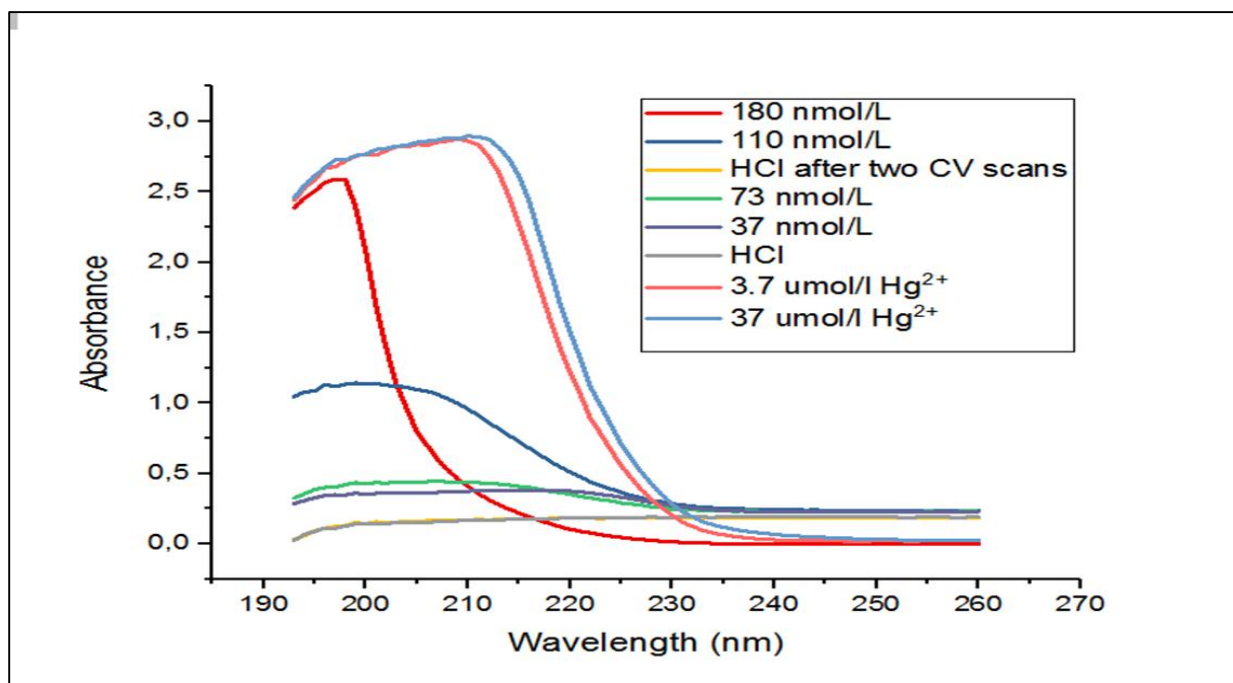


**Figure 4.36** UV/Vis Absorption spectra of the determination of the  $\text{Hg}^{2+}$  at the GCE/AuNP/Hydrogel/HA.

After the 30 min incubation period to entrap the HA into the GCE/AuNP/Hydrogel, CV ( $n=2$ ) in 0.1 M HCl was obtained. After the CV was completed a sample of the 0.1 M HCl was extracted from the electrochemical cell and the absorbance measured to obtain a baseline. Aliquots of a  $\text{Hg}^{2+}$  standard was then added in increasing concentrations (0.03-3.7  $\mu\text{mol/L}$ ) the 0.1 M HCl solution in the electrochemical cell containing the GCE/AuNP/Hydrogel sensor. SWV was run after each addition. After the SWV run a sample of the solution was taken and the absorbance

measured. This was done for seven additions of  $\text{Hg}^{2+}$  standard in increasing concentration from 0.03-3.7 nmol/L. The absorbance increased with increasing concentrations of  $\text{Hg}^{2+}$ . The absorbance of an uncomplexed  $\text{Hg}^{2+}$  standard was also measured i.e. without adding it to the cell for SWV analysis. This solution of 3.7  $\mu\text{mol/L}$   $\text{Hg}^{2+}$  had the highest absorbance of 3.8.

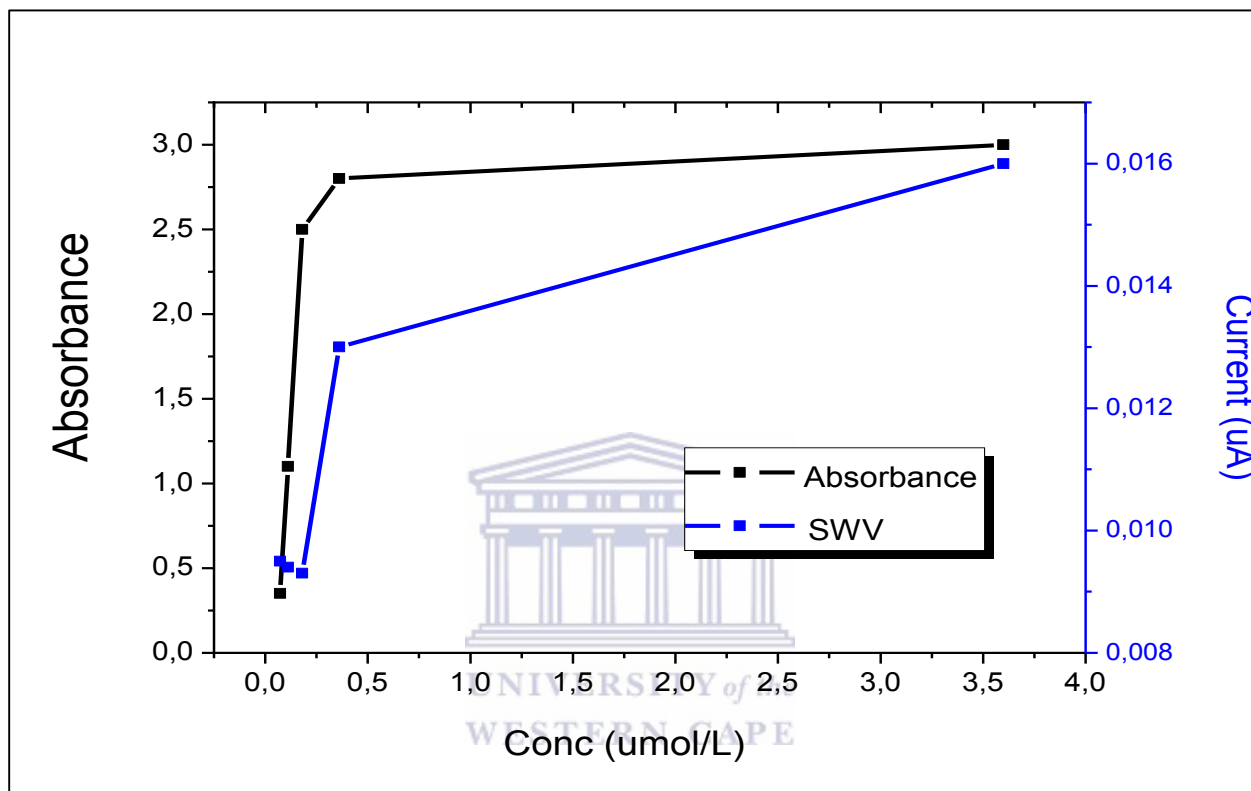


**Figure 4.37** Comparison of UV/Vis Absorption determination and Square wave voltammetry of the  $\text{Hg}^{2+}$  complexed with HA at GCE/AuNP/hydrogel/HA in 0.1 M HCl solution.

A comparison of the data obtained from the two techniques is represented in Figure 4.37. The blue line in the graph (SWV) showed a constant, non linear behaviour at the lower concentration range. This clearly demonstrated that complexation took place. Only after all sites in the ligand were filled, was the free metal detected by SWV. This is corroborated by the UV spectra in Figure 4.36 by the low absorbance of the lower concentration ie no free metal because they were complex with the HA entrapped in the sensor.

## 4.9 Determination of $\text{Pb}^{2+}$ on the GCE/AuNP/hydrogel/HA sensor

### 4.9.1 Determination of $\text{Pb}^{2+}$ on an unmodified GCE

The  $\text{Pb}^{2+}$  standards added in increments in the concentration range 0.1-5  $\mu\text{mol/L}$  to the cell with the GCE with 0.1M HCl solution. For comparison the same analysis was performed on an unmodified GCE as well as the GCE/AuNP/Hydrogel/HA sensor.

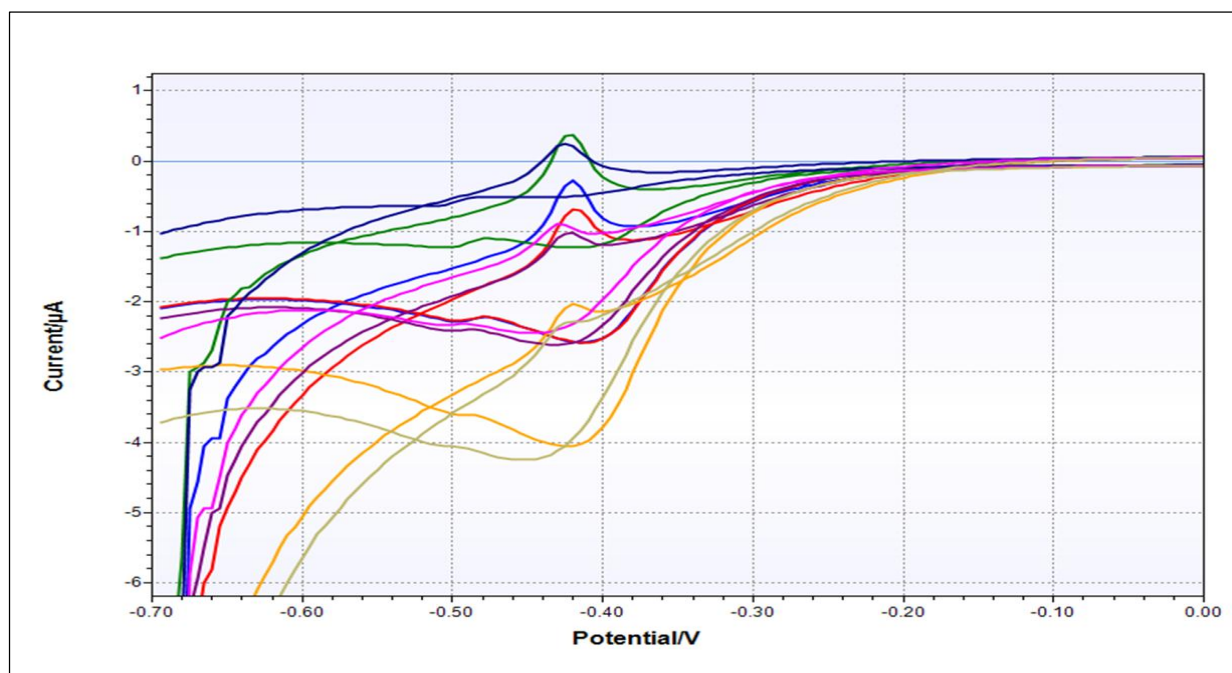


**Figure 4.38** Cyclic voltammetry of increasing concentrations of  $\text{Pb}^{2+}$  at an unmodified GCE in 0.1 M HCl solution. Peak of  $\text{Pb}^{2+}$  appeared at -0.4 V due to the reduction of  $\text{Pb}^{2+}$  to  $\text{Pb}$ .

Figures 4.38- 4.39 show the effect of increasing concentration of  $\text{Pb}^{2+}$  with CV in 0.1 M HCl using an unmodified GCE. The analysis was repeated with SWV (Figure 4.40).

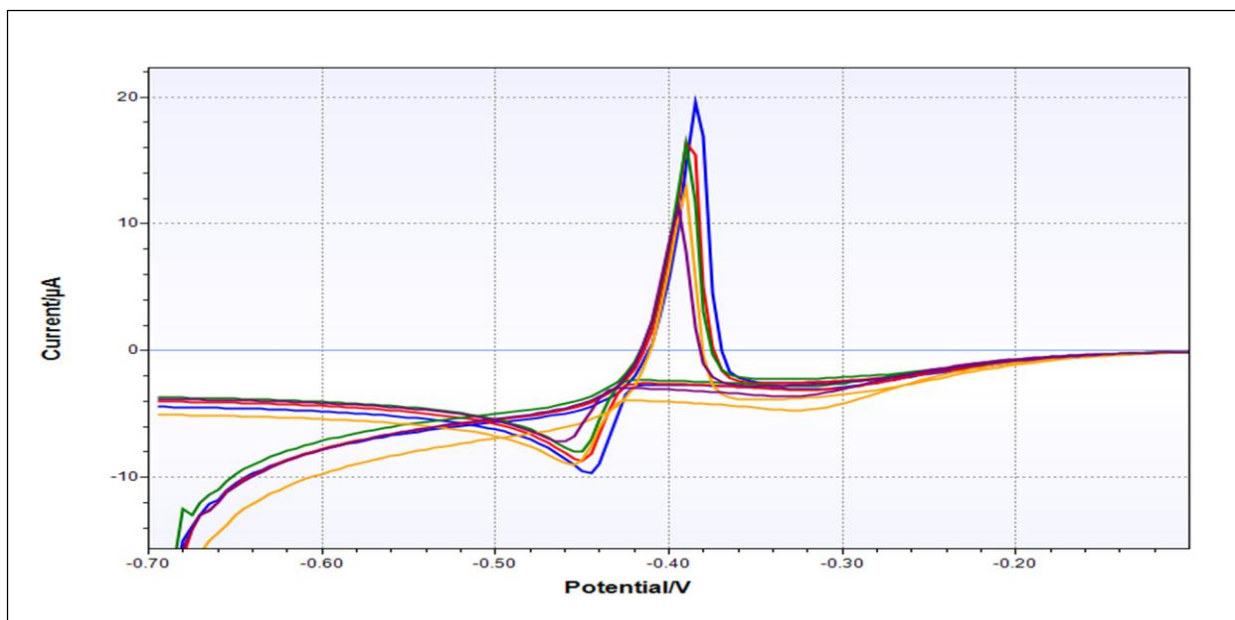


**Figure 4.39** Cyclic voltammety of increasing concentrations of  $Pb^{2+}$  on an unmodified GCE (higher conc than fig 4.38) in a 0.1 M HCl solution.  $Pb^{2+}$  appeared at -0.4 V due to the reduction of  $Pb^{2+}$  to Pb.

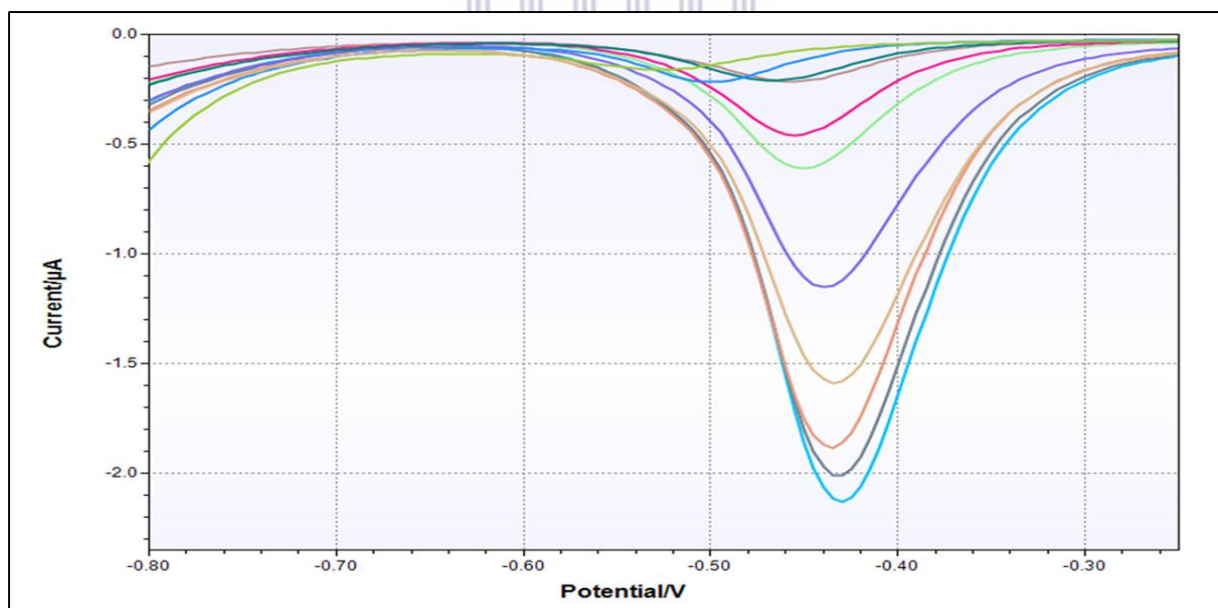


**Figure 4.40** Square wave voltammety of reduction of  $Pb^{2+}$  at increasing concentrations at GCE in 0.1M HCl solution.

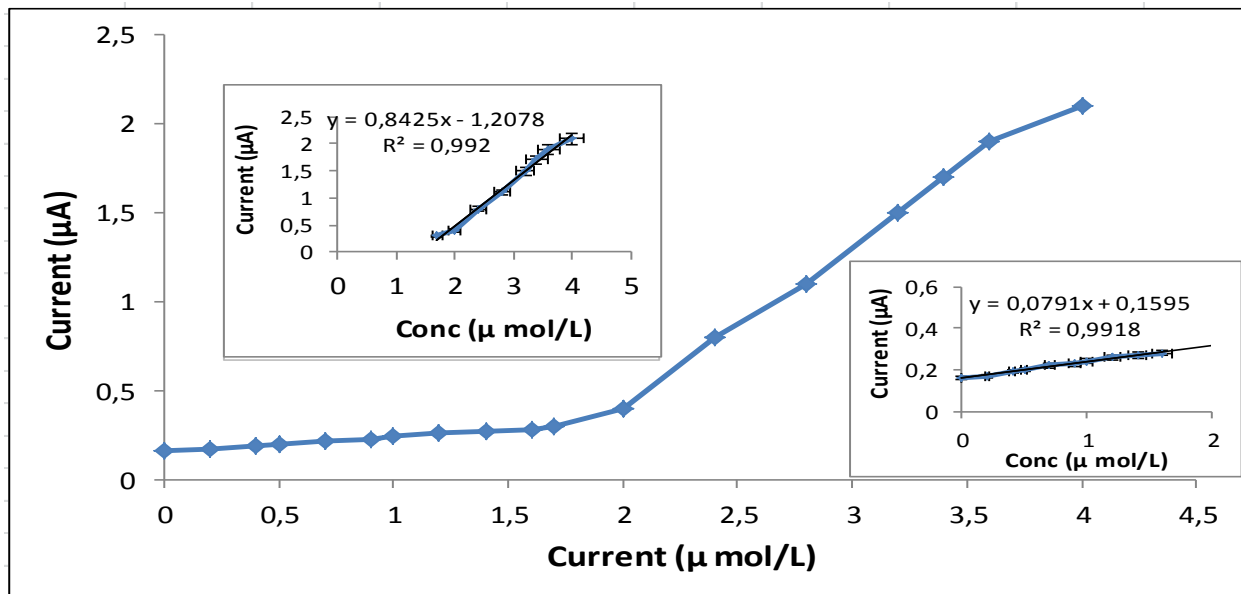


**Figure 4.41** Calibration curve obtained using Square wave voltammetry at an unmodified GCE in a deaerated 0.1M HCl solution. Results are the mean of three determinations and insert shows the linear range from 0.1 – 0.5 µ mol/L (std deviation, n = 3).

The calibration curves showed a dynamic range that exhibited two narrow linear ranges. The analytical protocols produced calibration data which leads to the statistic results as presented in Table 4.3. All statistical data were reported at 95 % confidence level. Under these conditions the statistical data showed sensitivity of 0.08 µmol/L, limit of detection (LOD) and limit of quantification (LOQ) respectively 0.01 µmol/L and 0.15 µmol/L and a linearity  $r^2 = 0.994$ .

### 3.9.2 Determination of Pb<sup>2+</sup> on the GCE/AuNP/hydrogel/HA sensor

The Pb<sup>2+</sup> standards added in increments in the concentration range 0.1-5 µmol/L to the cell with the GCE/AuNP/hydrogel/HA sensor with 0.1M HCl solution. Cyclic voltammetry of Pb<sup>2+</sup> standard at lower concentrations at GCE/AuNP/hydrogel/HA in 0.1M HCl solution was obtained (Figure 4.42-4.43). Reduction peak at -0.39V due to the reduction of Pb<sup>2+</sup> to Pb and a peak at -0.41V clearly due to the Pb-HA complexation. Figures 4.44-4.45 shows the effect of the complexation of Pb<sup>2+</sup> and HA with SWV. With increasing concentrations of Pb<sup>2+</sup> the peak at -0.41V (reduction of uncomplexed (Pb<sup>2+</sup>)) increased with a corresponding decrease of the peak due to the complex Pb-HA. This happens as the sites of the ligand become saturated.



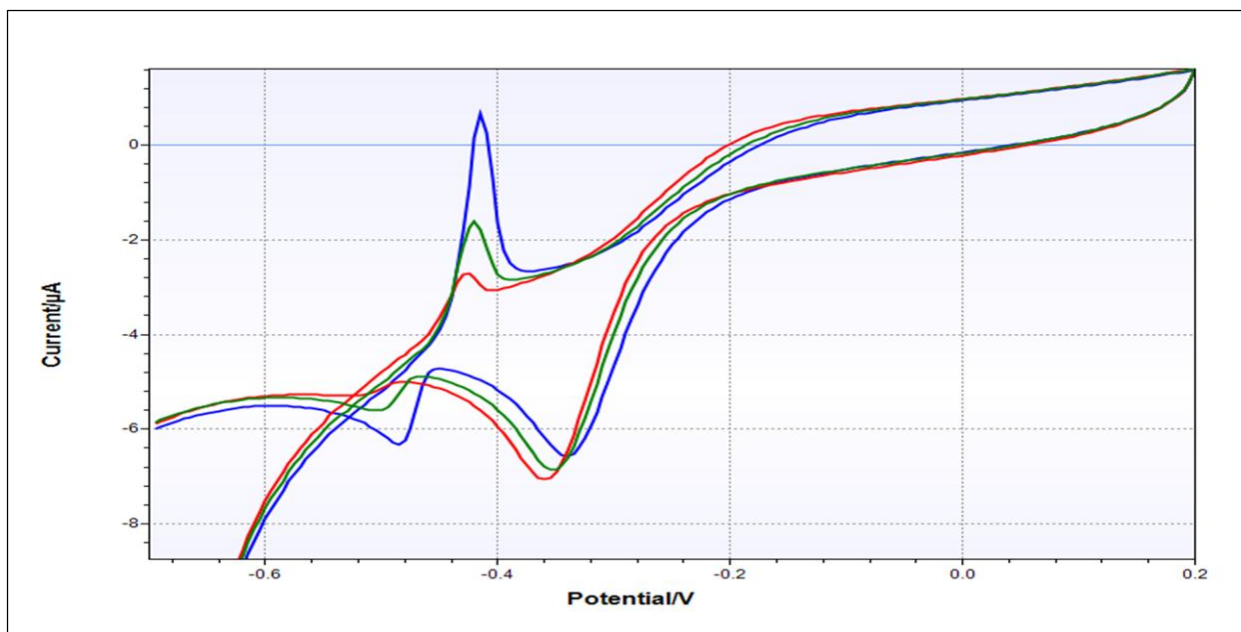


**Figure 4.42** Cyclic voltammetry of  $Pb^{2+}$  standard at lower concentrations at GCE/AuNP/hydrogel/HA in 0.1M HCl solution. Reduction peak at -0.41V due to the reduction of  $Pb^{2+}$  to Pb and a peak at -0.30V due to the Pb-HA complexation.

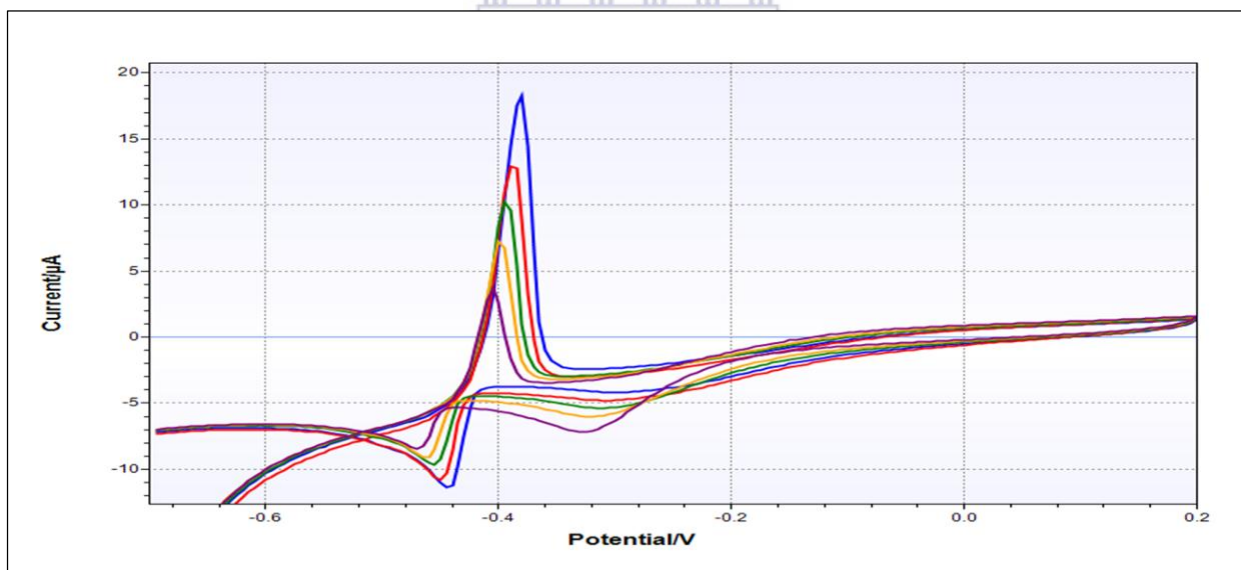


**Figure 4.43** Cyclic voltammetry of the  $Pb^{2+}$  standards at higher concentrations at the GCE/AuNP/hydrogel/HA in 0.1M HCl solution. Reduction peak at -0.41V due to the reduction of  $Pb^{2+}$  to Pb and a peak at -0.30V due to the Pb-HA complexation. The Pb-HA peak the highest in lower concentrations of  $Pb^{2+}$  added (purple) and smallest in the highest concentration of  $Pb^{2+}$  added (blue).

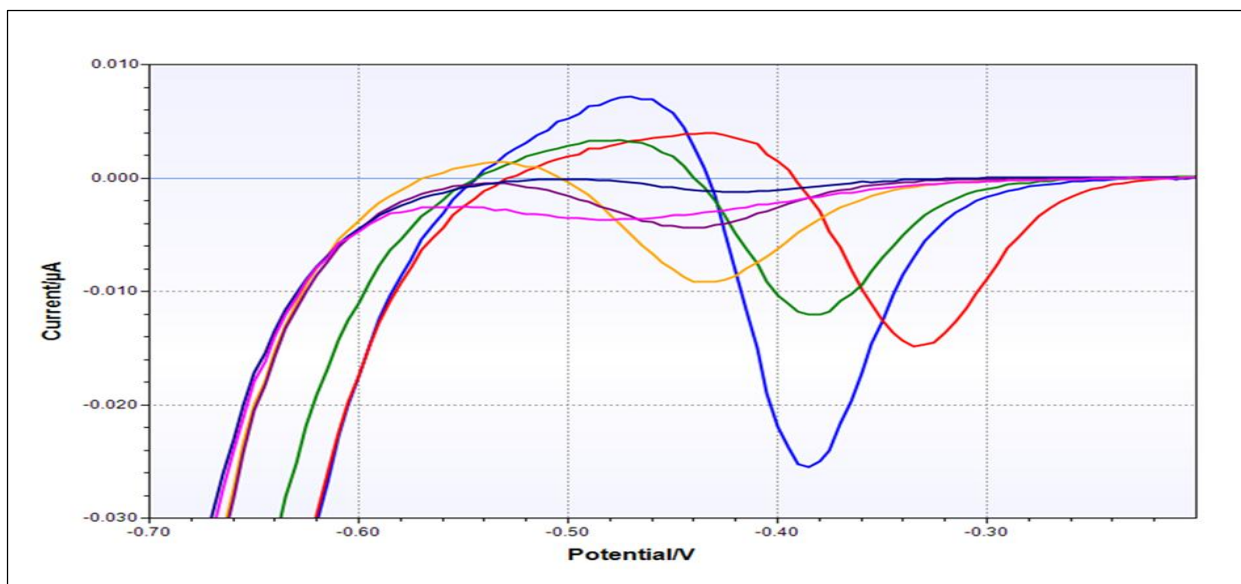


**Figure 4.44** Square wave voltammetry the  $\text{Pb}^{2+}$  standards at increasing concentrations at GCE/AuNP/hydrogel/HA in 0.1M HCl solution. Reduction peak shifted from -0.46 V to -0.39V with increasing concentrations of  $\text{Pb}^{2+}$  added to the cell, due to the Pb-HA complexation before the reduction of the uncomplexed  $\text{Pb}^{2+}$  is detected.

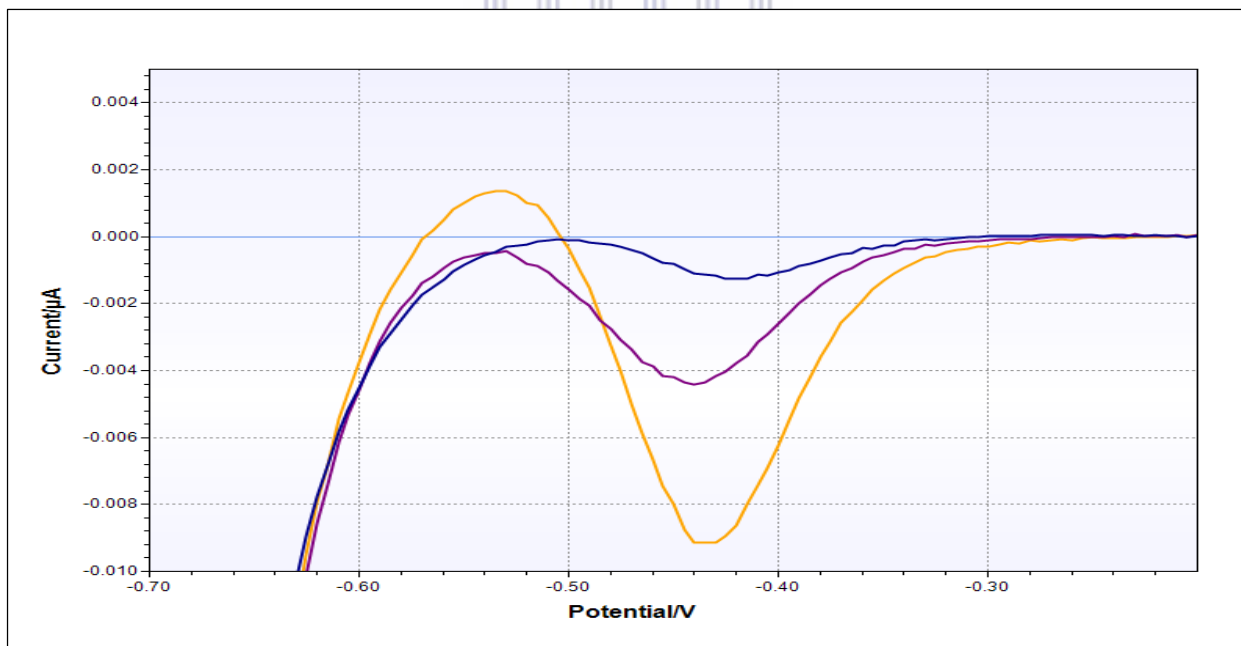


**Figure 4.45** SWV scan of the  $\text{Pb}^{2+}$  standards at increasing concentrations added to the 0.1M HCl solution in the cell with the GCE/AuNP/hydrogel/HA. At higher concentrations of the of  $\text{Pb}^{2+}$  added to the cell only the reduction peak of the uncomplexed  $\text{Pb}^{2+}$  is detected.

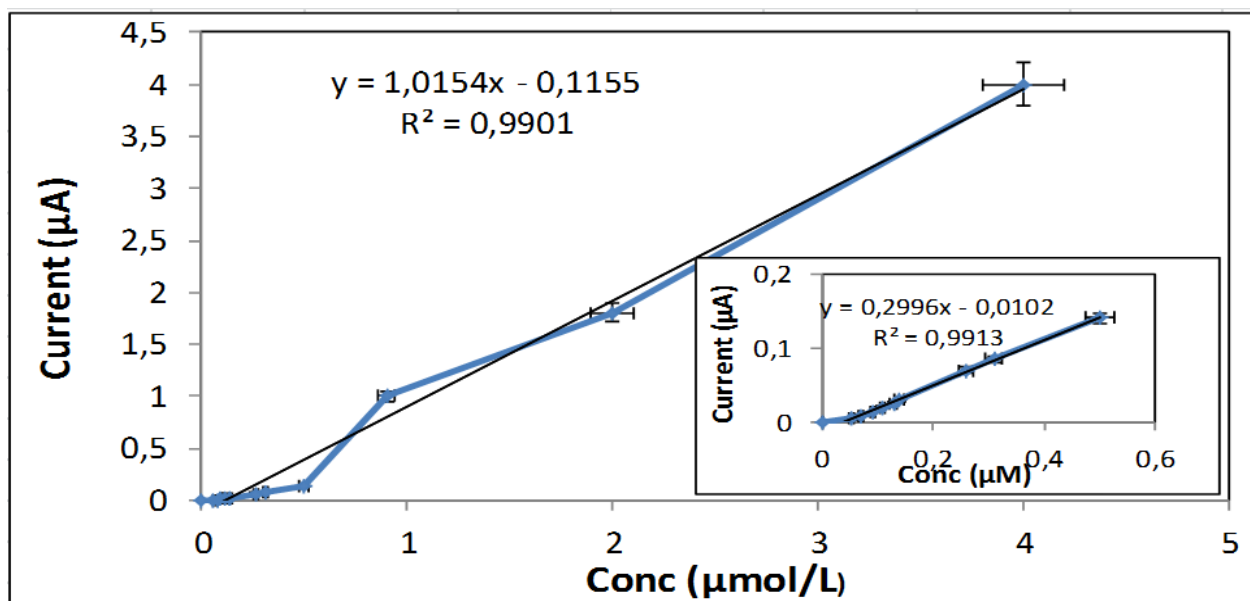


**Figure 4.46** Calibration curve obtained using SWV GCE/AuNP/Hydrogel/HA in a deaerated 0.1M HCl solution. Results are the mean of three determinations and insert shows the linear range from 0.1 – 0.6  $\mu\text{mol/L}$  (error bars represent standard error,  $n = 3$ ).

The calibration curves showed a narrow linear dynamic range. The analytical protocols produced calibration data which leads to the statistic results as presented in Table 4.3. All statistical data were reported at 95 % confidence level. Under these conditions the statistical data showed sensitivity of 0.30  $\mu\text{mol/L}$ , limit of detection (LOD) and limit of quantification (LOQ) respectively 0.001  $\mu\text{mol/L}$  and 0.01  $\mu\text{mol/L}$  and a linearity  $r^2 = 0.992$ .

#### 4.9.3 Spectroscopic determination of $\text{Pb}^{2+}$ on the GCE/AuNP/hydrogel/HA sensor

The disappearance of the free metal during SWV analysis, from the electrolytic solution that the GCE/Au/Hydrogel/HA sensor was exposed to, was followed by UV/Vis analysis (Figure 4.47-4.48). An increase in UV/Vis absorbance trend, for  $\text{M}^{2+}$  ion concentration, provided complimentary corroboration for the electrochemically driven complexation of  $\text{M}^{2+}$  ion by the HA ligand entrapped in the sensor matrix.

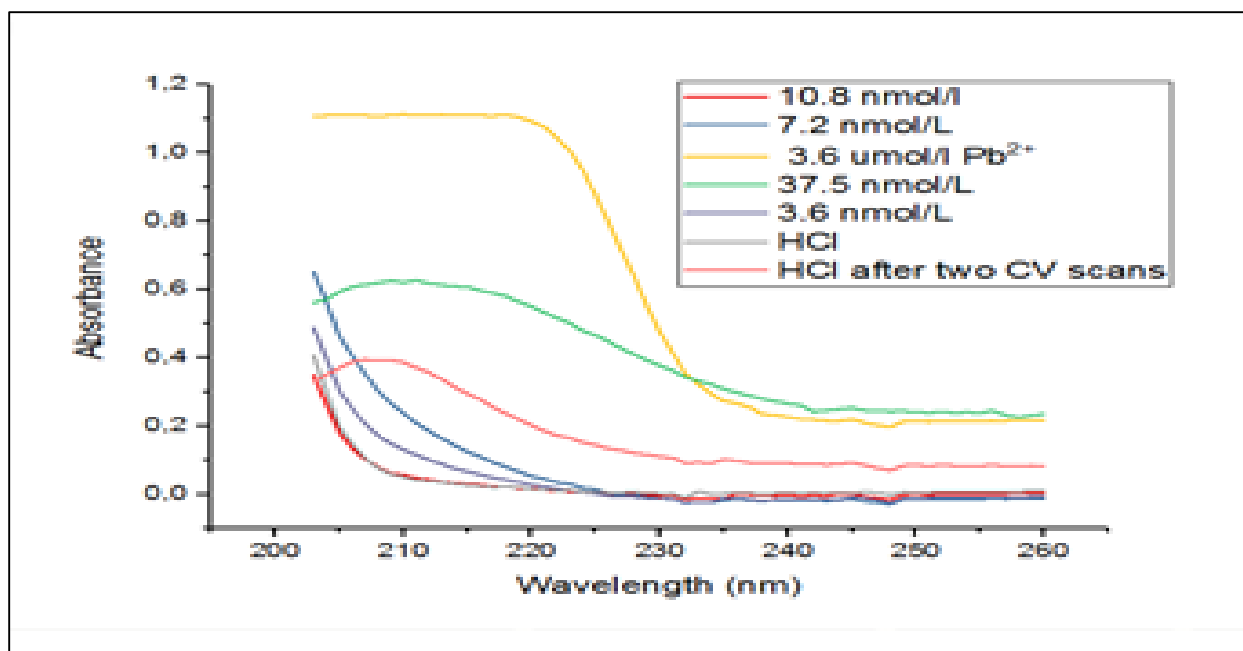


**Figure 4.47** UV/Vis spectroscopic spectra of the determination of the  $Pb^{2+}$  on the GCE/AuNP/Hydrogel/HA.

After the 30 min incubation period to entrap the HA into the GCE/AuNP/Hydrogel, CV ( $n=2$ ) in 0.1 M HCl was obtained. After the CV was completed a sample of the 0.1 M HCl was extracted from the electrochemical cell and the absorbance measured to obtain a baseline.

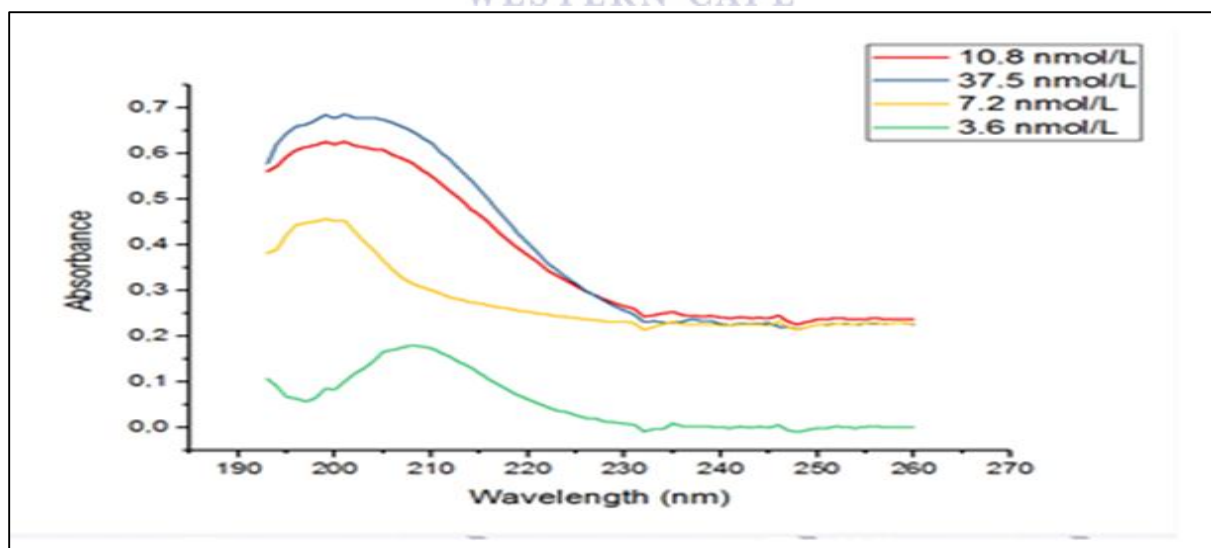


**Figure 4.48** UV/Vis Absorption spectra of the determination of the  $Pb^{2+}$  on the GCE/AuNP/Hydrogel/HA.

Aliquots of a  $\text{Pb}^{2+}$  standard was then added in increasing concentrations (0.03-3.7  $\mu\text{mol/L}$ ) the 0.1 M HCl solution in the electrochemical cell containing the GCE/AuNP/Hydrogel sensor. SWV was run after each addition. After the SWV run a sample of the solution was taken and the absorbance measured. This was done for seven additions of  $\text{Pb}^{2+}$  standard in increasing concentration from 0.03-3.7  $\mu\text{mol/L}$ . The absorbance increased with increasing concentrations of  $\text{Pb}^{2+}$ . The absorbance of an uncomplexed  $\text{Pb}^{2+}$  standard was also measured i.e. without adding it to the cell for SWV analysis. This solution of 3.7  $\mu\text{mol/L}$   $\text{Pb}^{2+}$  had the highest absorbance of 1.1.

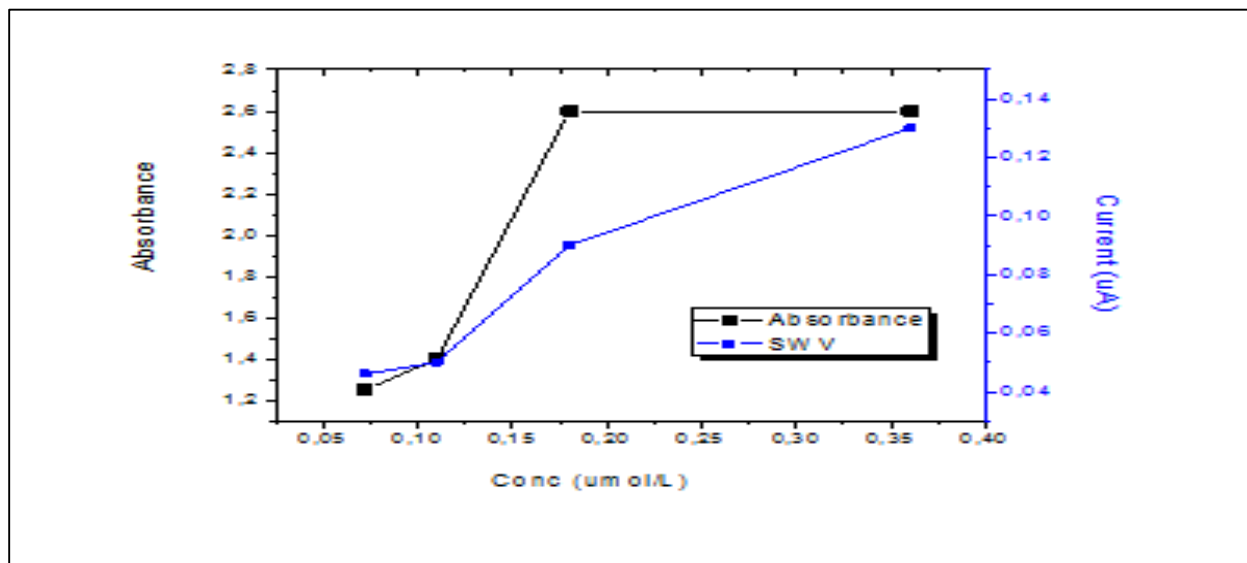


**Figure 4.49** Comparison of UV/Vis Absorption determination and Square wave voltammetry of the  $\text{Pb}^{2+}$  complexed with HA at GCE/AuNP/hydrogel/HA in 0.1 M HCl solution.

A comparison of the data obtained from the two techniques is represented in Figure 4.49. The blue line in the graph (SWV) showed a constant, non linear behaviour at the lower concentration range. This clearly demonstrated that complexation took place. Only after all sites in the ligand was filled, was the free metal detected by SWV. This is corroborated by the UV spectra in Figure 4.49 by the low absorbance of the lower concentration ie no free metal because they were complex with the HA entrapped in the sensor.

#### 4.10 Summary of result for analysis performed on GCE/AuNP/Hydrogel/HA for Hg<sup>2+</sup> and Pb<sup>2+</sup>

**Table 4.3** Comparison of concentration Hg<sup>2+</sup> on modified and unmodified electrode

Electrode	Linear range (µmol/L)	Sensitivity (µmol/L)	LOD (µmol/L)	R <sup>2</sup>
GCE	0 – 0.55	10.052	0.020	0.979
	0.1 -0.55	9.377	0.026	0.994
GCE/AuNP/Hydrogel/HA	0 – 5	0.178	0.003	0.965
	2 - 5	0.155	0.007	0.992

The analytical protocols produced calibration data which leads to the statistic results as presented in Table 4.3. All statistical data were reported at 95 % confidence level, n = 3).

**Table 4.4** Comparison of concentration Pb<sup>2+</sup> on modified and unmodified electrode

Electrode	Linear range (µmol/L)	Sensitivity (µmol/L)	LOD (µmol/L)	R <sup>2</sup>
GCE	0 - 5	0.843	0.012	0.992
	0 - 2	0.079	0.002	0.992
GCE/AuNP/Hydrogel/HA	0 – 5	1.015	0.001	0.990
	0 – 0.6	0.300	0.001	0.991

The analytical protocols produced calibration data which leads to the statistic results as presented in Table 4.3. All statistical data were reported at 95 % confidence level, n = 3)

**Table 4.5** Comparison of complexation constants obtained in this study and compared literature (Miller *et al.*, 2009).

	Method	Time (hr)	Rate constant (hr <sup>-1</sup> )
Present study	HGAAS	0–4	0.176–0.532
(Miller <i>et al.</i> , 2009)	CVAFS	1–7	0.050–0.290
Present study	HPLC-EC	0–24	0.010–0.100

Rate constant values tabulated in Table 4.6 was calculated using the same experimental values as those reported above but plotting  $\log \Delta A/\Delta t$  vs  $\log \Delta A$  with the intercept the rate constant.

**Table 4.6** Rate constant (log k) of the complexation of  $\text{Hg}^{2+}$  with HA

Temp (K)	pH 5.5	pH 7.0	pH 8.0
293.15	2.90	3.90	6.70
298.15	3.67	5.00	6.50
303.15	4.80	2.98	6.00

**Table 4.7** Rate constants (log k) of the complexation of  $\text{Hg}^{2+}$  with HA and FA

	pH 4.26		pH 5.42		pH 6.69	
	$\beta 1$	$\beta 2$	$\beta 1$	$\beta 2$	$\beta 1$	$\beta 2$
Humic acid	2.34	2.83	2.59	3.08	3.80	3.29
Fulvic acid	3.23	3.28	3.32	3.37	3.48	3.53

Values reported in Table 4.7 are from the study by Helal *et al.*, (2007).

**Table 4.8** Conc and pKa values of ionizable sites determined in HA by potentiometric titration in 0.020 M  $\text{NaNO}_3$  by SWV at screen-printed electrodes at  $25 \pm 0.1^\circ\text{C}$  (do Nascimento and Masini, 2012).

Site	Concentration ( $\text{mmol g}^{-1}$ )	pKa
HA1	1.1 $\pm$ 0.1	4.4 $\pm$ 0.2
HA2	0.64 $\pm$ 0.04	5.8 $\pm$ 0.2
HA3	0.26 $\pm$ 0.08	7.23 $\pm$ 0.01
HA4	0.45 $\pm$ 0.07	8.26 $\pm$ 0.04
HA5	0.46 $\pm$ 0.08	9.9 $\pm$ 0.2

Log K of HA-Hg was found to vary from 4.2-3.6.

Values reported in Table 4.8 are from the study by do Nascimento and Masini (2012). HA1 - HA5 representing different complexation sites on the HA structure.

In this study:

Using the complexation values for Hg:

$$E_{1/2}(\text{complexed}) - E_{1/2}(\text{complexed}) = -0.0591/n \log K - 0.0591/n \log C_L$$

$$0.48V - 0.2 V = 0.059/1 \log K - 0.059/2 \log 1$$

$$\log K = 4.75$$

Using the complexation values for Pb:

$$E_{1/2}(\text{complexed}) - E_{1/2}(\text{complexed}) = -0.0591/n \log K - 0.0591/n \log C_L$$

$$-0.48V - (-0.39 V) = 0.059/2 \log K - 0.059/2 \log 1$$

$$\log K = -3.04$$

**Table 4.9** Comparison of complexation constants for Hg<sup>2+</sup> obtained in this study and compared to literature ( Miller *et al.*, 2009).

	Method	Time (hr)	Rate constant (hr <sup>-1</sup> )	Rate constant (log K)
This study	HGAAS	0–4	0.176–0.532	
This study	HPLC-EC	0–24	0.010–0.100	
(Miller <i>et al.</i> , 2009)	CVAFS	1–7	0.050–0.290	
This study	HPLC-EC	0–24	-	2.90-6.70
This study	EC-SWV using GCE/AuNP/Hydrogel/HA	-		4.75
(Helal <i>et al.</i> , 2007)	Potentiometric titrations and Spectrophotometry	-	-	2.34-3.80
(do Nascimento and Masini, 2012)	EC-SWASV at screen-printed Au electrode	-	-	4.4-9.9



#### 4.11 Development and optimization of a sensor system: Discussion

A hydrogel sensor was developed and optimized. The hydrogel sensor system was used for the study of Hg complexation with HA by functionalization of HA into the hydrogel. The study was to understand the surface morphology and Electrochemistry principles governing the complexation process. The system was studied using cyclic voltammetry. As a comparison the complexation of Pb with HA by functionalization of HA into the hydrogel was also studied.

The increasing contamination of ground water and soil due to potentially toxic heavy metals pollutants has created many environmental problems and health hazards (Muya *et al.*, 2016; Hughes *et al.*, 2017, Asadpour-Zeynali & Amini, 2017). The GCE/AuNP/Hydrogel/ HA was developed and successfully applied to the determination of Hg and Pb. The sensor showed excellent sensitivity and linearity. The complexation constant for the complexation of Hg to HA calculated from data obtained using the sensor are in good agreement to the results obtained using the HPLC-EC and HGAAS method. It is also in good agreement to studies done by Helal *et al.* (2007) and do Nascimento and Masini, (2012). This novel sensor can be successfully applied to the determination of these toxic metals in environmental samples.

## CHAPTER 5

### DETERMINATION OF COMPLEXATION OF Hg<sup>2+</sup> WITH HA IN AQUEOUS PHASE, SOIL and BIOTA

#### 5.1 INTRODUCTION

The role of the complexation of HA with Hg<sup>2+</sup> in an aqueous phase and soil was also determined. Metal–organic interactions such as complexation and reduction depend on the soil characteristics and the types of functional groups present (Serudo *et al.*, 2007). These reactions can affect the transportation, accumulation and bioavailability of heavy metals. The abiotic reduction of Hg<sup>2+</sup> by HA may be an important process in the volatilisation of Hg from soils (Serudo *et al.*, 2007). The degree of bioaccumulation and bioavailability depends on the physical and chemical composition of particles (Álvarez *et al.*, 2004). The study on the speciation of Hg is essential to the understanding and prediction of its availability for absorption.

#### 5.2 Experimental

Further experiments were carried out to study the complexation of Hg with HA under varying physical conditions, e.g., temperature and salinity but with soil added. The experimental set-up used was as described previously (Section 3.1.1) but now soil was added to the water. The type of soil selected for use was sandy soil because it contains little or no organic matter. The soil used was collected from a relatively unpolluted reference site. The soil was acid leached, rinsed thoroughly with distilled water and dried in an oven for 48 hr. A weighed quantity of the soil (50.00 g) was spiked with HA and left for 12 hr to equilibrate at 4°C. The aqueous phase was prepared by taking a fixed volume of 35 µg/mL saline solution, spiking it with Hg<sup>2+</sup> to 5 µg/mL and then fixing the required pH using an acetic acid/ammonium solution. The total volume was then adjusted to 50.0 mL in order to obtain the initial desired concentrations. A control sample was prepared in the same way but without the HA. Samples were held in a waterbath in a temperature controlled room. Water and sand samples were taken initially and at set intervals until the termination of the experiment. If analysis could not be done immediately the samples were stored in acid-cleaned Teflon storage containers and refrigerated until subsequent analysis.

Results of the previous experiments (aqueous phase only) that were carried out over a 9 day period showed that most of the complexation takes place within the first 28 hr. The selected temperatures were 293.15 K, 298.15 K and 303.15 K, pH values were 5.5, 7.0, 8.0, and a salinity of 35 µg/mL was used in order to maintain natural conditions. Analysis for the aqueous phase was performed on an HPLC-EC under same conditions (Section 2.2.5) and soil by DMA. The complexation process was monitored over a period of 28 hr.

### 5.2.1 RECOVERY STUDIES FOR Hg<sup>2+</sup> IN SOIL WITH DMA

Recovery studies were performed to ensure that the method and analysis for the study of the complexation of Hg<sup>2+</sup> with HA was efficient and accurate. The study was to ensure total Hg recoveries by DMA. Five separate replicate soil samples were used for the study. The HA was added to the preweighed soil (50.00 g) and allowed to equilibrate for 12 hr and then spiked with a known amount of standard Hg<sup>2+</sup> standard solution. Each replicate sample was determined twice with DMA with duplicates within 10% relative difference. Differences between replicate samples values was statistically determined by ANOVA test and t-test (p < 0.05). Statistical analysis shows no significant difference between replicate values.

**Table 5.1** Recovery values for Hg<sup>2+</sup> in soil

Conc (µg/mL)(spiked)		1.5000			
Conc (µg/mL found)	1.4334± 0.06	1.4914±0.05	1.4810±0.05	1.4820±0.02	1.4671±0.03
Recovery (%)	95.6	99.4	98.7	98.8	97.8
Average of 5 replicate samples		1.4670			
Average recovery (%)		97.8			
Relative standard deviation (%)		4.8			
Certified value in Tort-2:		Hg = 270.00 ng/g ± 60.00			
Recovery (%)		98.1± 21.1			

### 5.3 WATER AND SOIL EXPOSURE: COMPLEXATION OF Hg<sup>2+</sup> WITH HA MONITORED OVER 28 HOURS AT 293.15 K

The results of the experiment performed at 293.15 K are tabulated in Tables 5.2–5.3, and shown in Figure 5.1–5.4. The sampling period was 5 days, but only the first 28 hours were considered significant and represented in Figures 5.1-5.4.

Data obtained for the complexation of Hg<sup>2+</sup> with HA at 293.15 K in aqueous phase are tabulated in Table 5.1.

**Table 5.2** Data of the complexation of Hg<sup>2+</sup> with HA in aqueous phase at 293.15 K

Time (hr)	Control (Hg <sup>2+</sup> )/ mg/L	Hg <sup>2+</sup> and HA at a salinity of 35 µg/mL and pH 5.5	Hg <sup>2+</sup> and HA at a salinity of 35 µg/mL and pH 7.0	Hg <sup>2+</sup> and HA at a salinity of 35 µg/mL and pH 8.0
0	3.82	3.00	3.12	3.80
1	2.62	2.60	2.35	3.00
4	2.56	2.30	2.20	2.00
24	2.20	2.00	1.65	1.85
28	0.81	1.40	0.80	1.24

Data obtained for the complexation of Hg<sup>2+</sup> with HA in soil at 293.15 K are tabulated in Table 5.2. Results were obtained on the DMA.

The complexation of Hg<sup>2+</sup> in aqueous phase and soil of the control sample without the addition of HA at 293.15 K is shown in Figure 5.1. The Hg<sup>2+</sup> concentration in aqueous phase decreased rapidly while the concentration in the soil increased. The soil without HA added also had a binding capacity to Hg<sup>2+</sup>. Surface complexation with soil is possible with exposed OH<sup>-</sup> groups of the soil that can bind and release protons, e.g:  $\equiv\text{SOH} \rightarrow \equiv\text{SO}^- + \text{H}^+ \leftrightarrow \equiv\text{SO}^- + \text{Hg}^{2+} \leftrightarrow \text{SOHg}^+$ . It can also occur because of cation-exchange, e.g:  $\text{X}-(\text{Na})_2 + \text{Hg}^{2+} \leftrightarrow \text{X}-\text{Hg} + 2\text{Na}^+$  (Tipping, 2004).

**Table 5.3** Data of the complexation of Hg<sup>2+</sup> with HA in the soil samples at 293.15 K

Time (hr)	Control (Hg <sup>2+</sup> )/µg/g	Hg <sup>2+</sup> and HA at a salinity of 35 µg/mL and pH 5.5	Hg <sup>2+</sup> and HA at a salinity of 35 µg/mL and pH 7.0	Hg <sup>2+</sup> and HA at a salinity of 35 µg/mL and pH 8.0
0	0.046	0.019	0.095	0.014
1	1.662	1.165	1.120	1.239
4	2.402	0.813	2.595	1.457
24	1.740	1.382	2.824	1.567
28	4.146	3.345	3.869	3.405

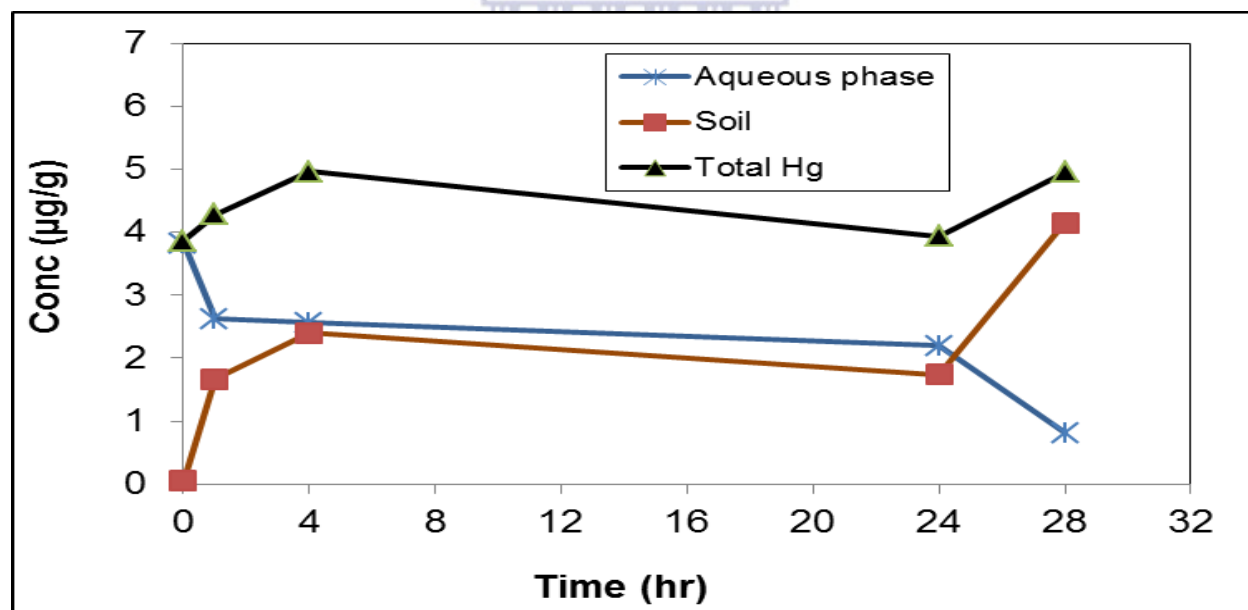


**Figure 5.1** The complexation of Hg<sup>2+</sup> in aqueous phase and soil of the control sample at 293.15 K.

The complexation of Hg<sup>2+</sup> in aqueous phase and soil at different pH values and with the addition of HA at 293.15 K is shown in Figures 5.2–5.4. All the graphs showed the same general trends. The most rapid changes occur within the first 4 hours. There was a general rate condition between 4–24 hr, then a sharp increase in the Hg<sup>2+</sup> concentration in the soil sample between 24 and 28 hr at all pH values.

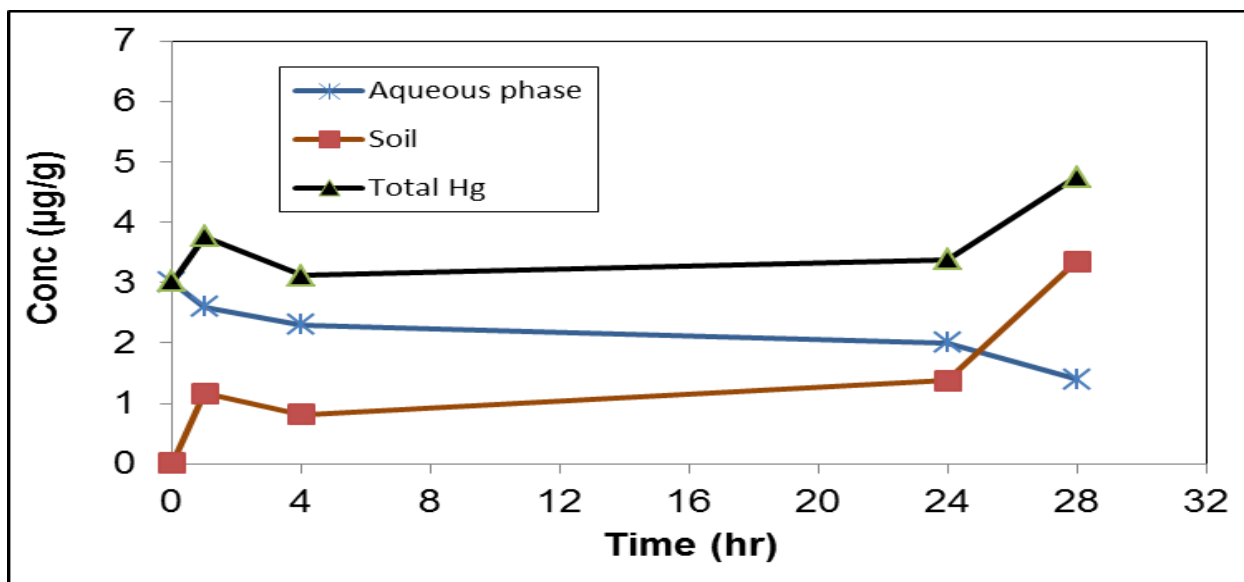


Figure 5.2 The complexation of  $Hg^{2+}$  in aqueous phase and soil at pH 5.5 at 293.15 K.

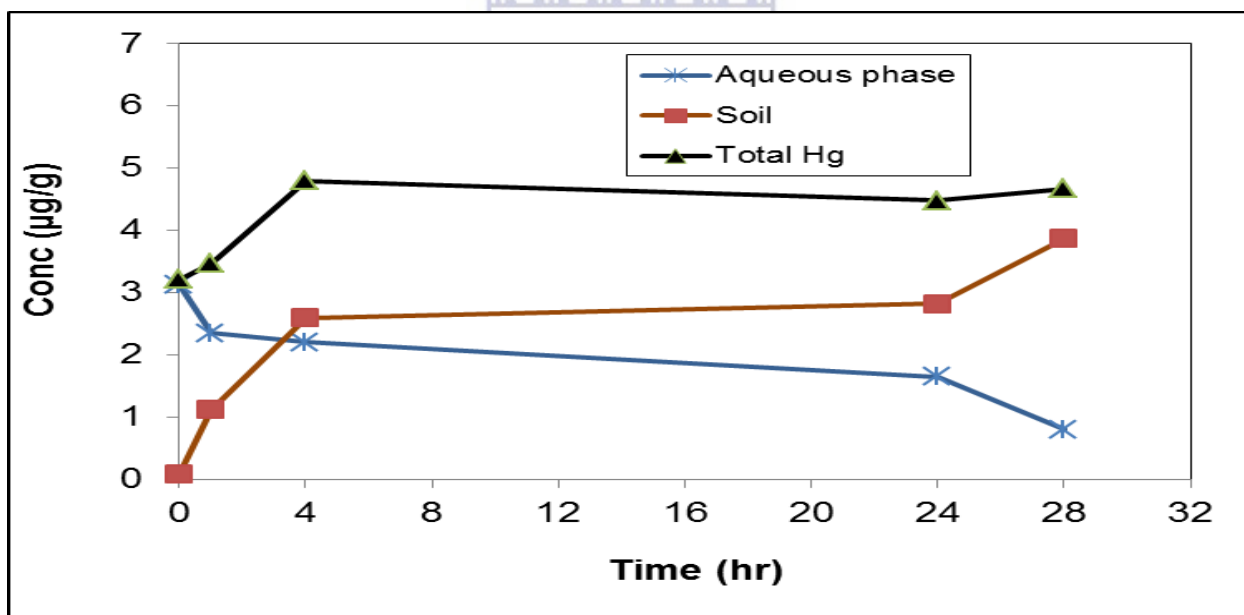
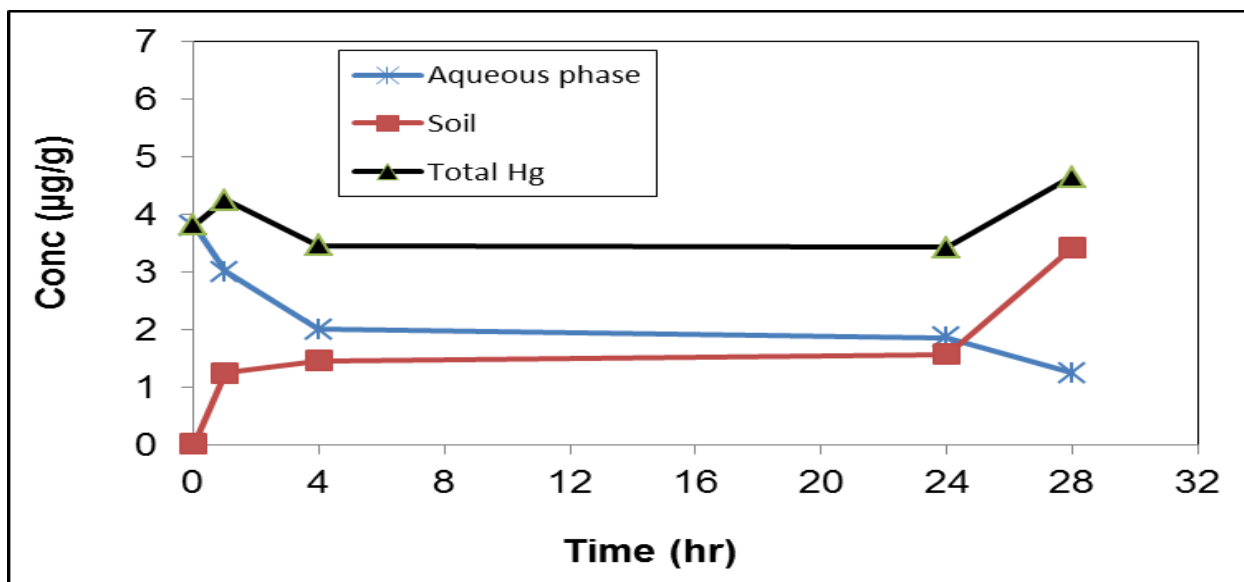


Figure 5.3 The complexation of  $Hg^{2+}$  in aqueous phase and soil at pH 7.0 at 293.15 K.



**Figure 5.4** The complexation of  $\text{Hg}^{2+}$  in aqueous phase and soil at pH 8.0 at 293.15 K.

The fastest increase in  $\text{Hg}^{2+}$  concentration in soil in the first 24 hr was observed at pH 7. At all the different pH values there is a sharp increase in  $\text{Hg}^{2+}$  concentration in soil between 24–28 hr.

The experiment was also performed at pH values of 5.5, 7.0 and 8.0 at 298.15 K and then at 303.15 K under conditions as stated previously (Section 3.3.1 and 4.1.2). The results obtained are in Appendix B, Tables 1–4, Figure 4–8. Similar trends were observed as those at 293.15 K. However at 28 hr there is a clear decrease in Hg concentration in soil with increasing pH at 298.15 K and 303.15 K (Appendix B, Tables 2 and 4). This trend was not observed at a temperature of 293.15 K (Figure 5.1). Studies done by Anderson (1979) and Schuster (1991) also found adsorption to soil decreases with increasing pH, with maximum adsorption around pH 6.0.

### 5.3.1 CHANGES IN THE TOTAL CONCENTRATION OF $\text{Hg}^{2+}$ IN AQUEOUS PHASE AND SOIL AFTER 28 HOURS

In the experiments at different temperatures there were losses of  $\text{Hg}^{2+}$  from the original spiked value. Losses could be due to sorption onto the walls of the container, evaporation of Hg and reduction of  $\text{Hg}^{2+}$  to  $\text{Hg}^0$ . Only the uncomplexed Hg was detected by the HPLC-EC in aqueous phase, thus any complexed Hg in aqueous phase did not contribute to the total Hg shown in the graphs (Figure 5.1–5.4, Appendix B, Figures 4 –6).

Although there were many reported studies on the absorption of Hg to soil, results differ in the different studies. In the following studies (Allard and Arsenie, 1991; Gabriel and Williamson, 2004; Rodríguez Martín-Doimeadios *et al.*, 2004; Yang *et al.*, 2007; Serudo *et al.*, 2007) evaporation of Hg was found to occur especially at higher temperatures and reduction of Hg occurs at low pH in the presence of HS. Other studies (Matthiessen, 1998; Serudo *et al.*, 2007; Yang *et al.*, 2007) have found, however, that reduction of Hg<sup>2+</sup> increases with increasing pH.

These total Hg losses determined in the present study are summarised in the table below.

**Table 5.4** Percentage loss of Hg<sup>2+</sup> after 28 hours at different temperatures and pHs

Temperature , K	Control (%) loss	pH 5.5, (%) loss	pH 7.0, (%) loss	pH 8.0, (%) loss
293.15	1	5	7	7
298.15	14	12	15	20
303.15	15	17	20	34

Generally, the lowest overall losses are in the control samples (low pH values and no HA). At all pH values there is an increase in total Hg loss with increase in temperature. As this trend is observed in the control as well as the samples containing HA, this loss could be due to evaporation and adsorption on container walls. The highest loss was at the highest experimental temperature value of 303.15 K and at pH 8.0. This may be due to evaporation, as well as some reduction of Hg<sup>2+</sup> to Hg<sup>0</sup>. Thus increased heat and pH play a significant role in decreased Hg adsorption and volatilisation from soils. The removal of Hg from soil by evaporation was found to be higher in neutral and alkaline soils (Anderson, 1979). Miretzky *et al.* (2005) found Hg release from soils to be 27–38% of the originally adsorbed Hg into the soil. Desorption first occurred rapidly, depending on conditions, and then at a slower rate.

#### 5.4 KINETICS OF THE Hg WITH HA COMPLEXATION IN AQUEOUS PHASE AND SOIL

As previously mentioned (Section 3.3.1) the determination of the rate constants of the Hg and HA complexation is made difficult by the lack of stoichiometric and structural information of HA. Reported rate/binding constants values differ considerably, and comparing values is hampered



by the different techniques and conditions used in the different studies (Haitzer *et al.*, 2002., Haitzer *et al.*, 2003; Han and Gill, 2005; Khwaja *et al.*,2006; Skyllberg *et al.*,2006; Miller *et al.*, 2009).

#### 5.4.1 RATE CONSTANT DETERMINATION FOR THE COMPLEXATION OF Hg<sup>2+</sup> WITH HA IN AQUEOUS PHASE AND SOIL

In the present study the Hg–HA complexation was found to be influenced by the temperature and pH. Rate and rate constants were calculated for the complexation of Hg and HA in aqueous phase and in soil. In some previous studies interaction between Hg–NOM was found to be slow (Miller *et al.*, 2009). However, complexation in aqueous phase and soil was found to be very fast in the present study.

#### 5.4.2 RATE CONSTANTS FOR THE COMPLEXATION OF Hg<sup>2+</sup> WITH HA IN AQUEOUS PHASE AND SOIL, FOR FIRST-ORDER REACTION

Rate constants were calculated for first- order reaction (Gårdfeldt *et al.*, 2003; Rodríguez Martín-Doimeadios *et al.*, 2004). A graph of ln area vs time (sec) was constructed. This provides a good fit with  $r^2 > 0.9$  and rate constant = -slope. Rate constants were calculated for a 24 hr period, using the method previously mentioned, for the aqueous phase and for complexation in soil and tabulated in Tables 5.1 – 5.2 and Appendix B, Tables 1-4.

**Table 5.5** Rate constant (hr<sup>-1</sup>) of the complexation of Hg with HA in aqueous phase

Temp (K)	pH 5.5	pH 7.0	pH 8.0
293.15	0.0134	0.0203	0.0221
298.15	0.0053	0.0121	0.0211
303.15	0.0253	0.0491	0.0653

**Table 5.6** Rate constant (hr<sup>-1</sup>) of the complexation of Hg with HA in soil

Temp (K)	pH 5.5	pH 7.0	pH 8.0
293.15	0.0851	0.0872	0.0938
298.15	0.0953	0.104	0.116
303.15	0.113	0.130	0.154

The rate constant values obtained in this study, is in agreement with values obtained in a previous study of Miller *et al.*, (2009), that used data obtained between 1–7 hr. This differs from the present study where a data set obtained between 0–24 hr was used for the rate constant calculations. The reported rate constant values ( $\text{hr}^{-1}$ ) from the study by Miller *et al.*, (2009) ranged from 0.05 to 0.29 depending on the type of HS used. Rate constants ( $\text{hr}^{-1}$ ) values in the present study ranged from 0.0053 to 0.065 for the aqueous phase and 0.085–0.154 for soil depending on the pH and temperature used. Although within range, it is lower than the reported values, but consistent with the fact that the rate slows down and complexation occurs more slowly over time (Table 3.6 and Table 3.9). The rate constants values are higher in the soil than the aqueous phase.

In previous studies it was found that the rate constants increase with increasing pH (Haitzer *et al.*, 2003; Helal *et al.*, 2007). In this study there is a deviation from this trend in the aqueous phase at pH 7.0 at temperatures 293.15 K and 298.15 K (Figure 5.5). There is an increase in rate constants for all pH values and temperatures in soil samples (Figure 5.6).

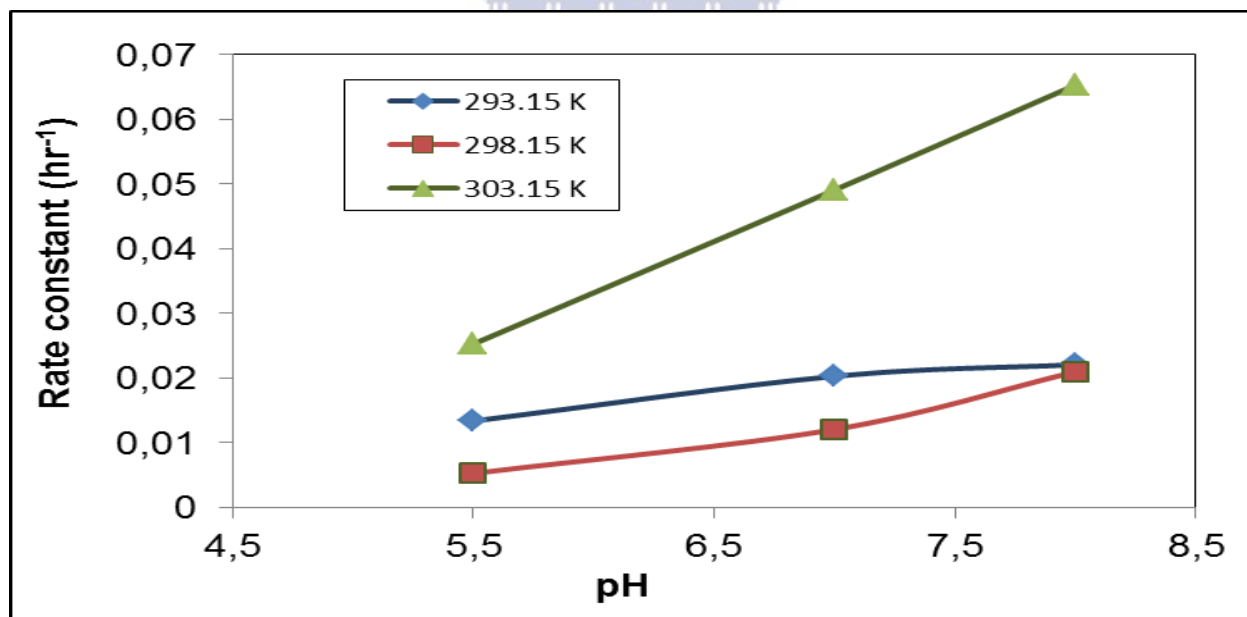


**Figure 5.5** Rate constant ( $\text{hr}^{-1}$ ) vs pH of the complexation of Hg with HA in aqueous phase.

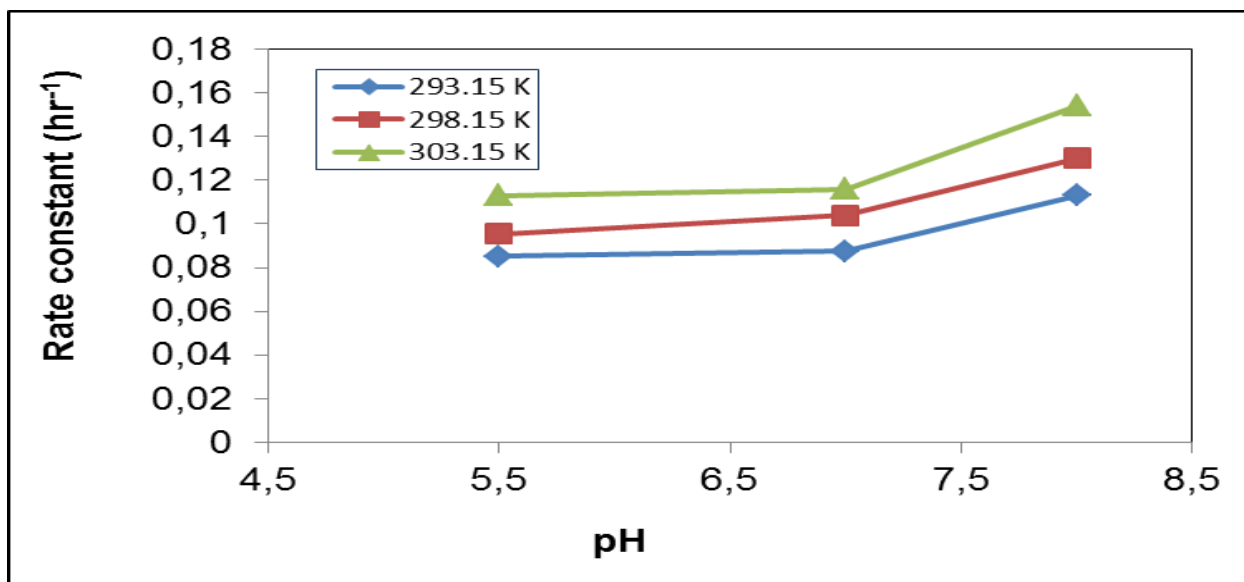


**Figure 5.6** Rate constant ( $\text{hr}^{-1}$ ) vs pH of the complexation of Hg with HA in soil.

There should be a general increase in rate constant with an increase in temperature. No reported values could be found to compare this trend. The aqueous phase shows a slight decrease for all pH values at 298.15 K (Figures 5.7). In the soil samples there is an increase in the rate constants with an increase in temperature.

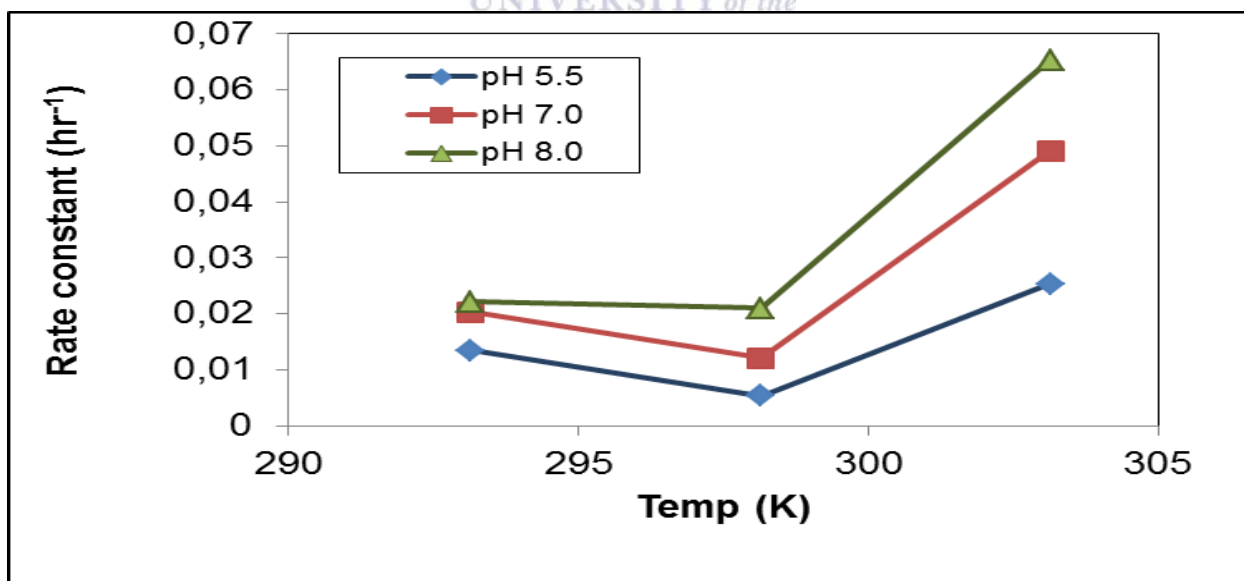


**Figure 5.7** Rate constant ( $\text{hr}^{-1}$ ) vs temperature of the complexation of Hg with HA in aqueous phase.

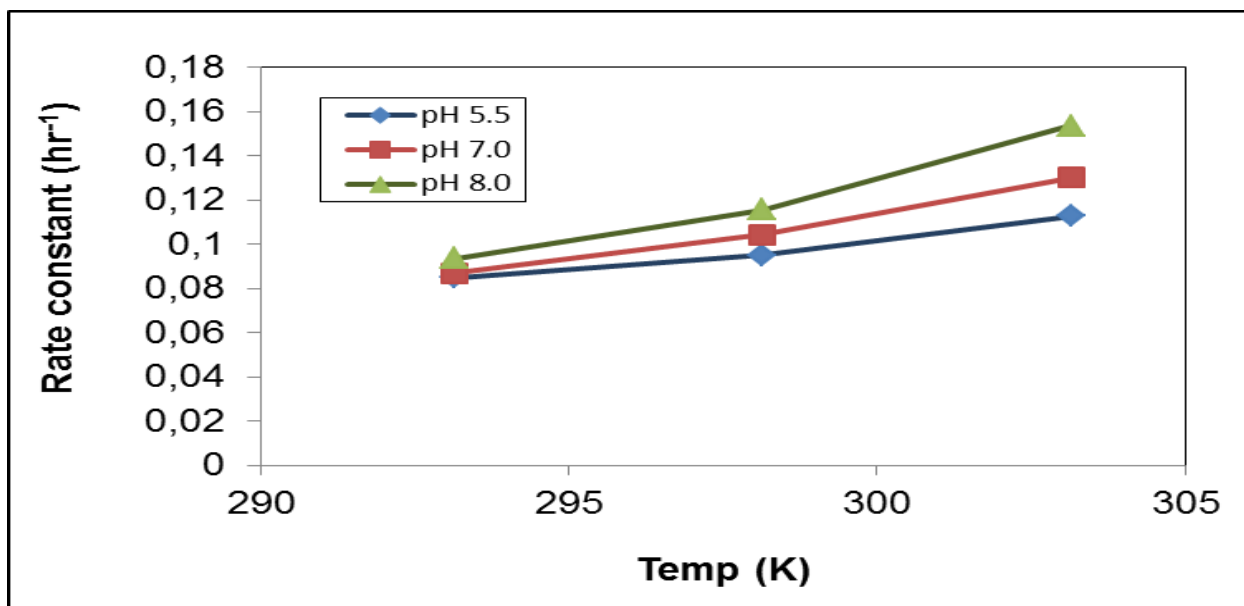


**Figure 5.8** Rate constant ( $\text{hr}^{-1}$ ) vs temperature of the complexation of Hg with HA in soil.

#### 5.4.3 RATE CONSTANTS FOR THE COMPLEXATION OF $\text{Hg}^{2+}$ WITH HA IN AQUEOUS PHASE AND SOIL USING THE VAN'T HOFF EQUATION

The rate constant values tabulated in Tables 5.7 and 5.8 was calculated using the same experimental values as those reported above, but plotting  $\log -(\Delta A/\Delta t)$  vs  $\log \Delta A$  with the intercept as the rate constant.

**Table 5.7** Rate constants ( $\log k$ ) of the complexation of  $\text{Hg}^{2+}$  with HA in aqueous phase

Temp (K)	pH 5.5	pH 7.0	pH 8.0
293.15	0.398	0.427	0.472
298.15	0.515	0.625	0.602
303.15	0.518	0.566	0.504

**Table 5.8** Rate constants ( $\log k$ ) of the complexation of  $\text{Hg}^{2+}$  with HA in soil

Temp (K)	pH 5.5	pH 7.0	pH 8.0
293.15	0.132	0.132	0.148
298.15	0.014	0.148	0.125
303.15	0.055	0.636	0.703

The rate constants in the aqueous phase increased with increasing pH at 293.15 K. At 298.15 K and 303.15 K there was an increase in rate constants at pH 5.5 and pH 7.0 but a decrease at pH 8.0 (Figure 5.9). For the soil samples there was a decrease in rate constants at 298.15 K at pH 8.0 (Figure 5.10).

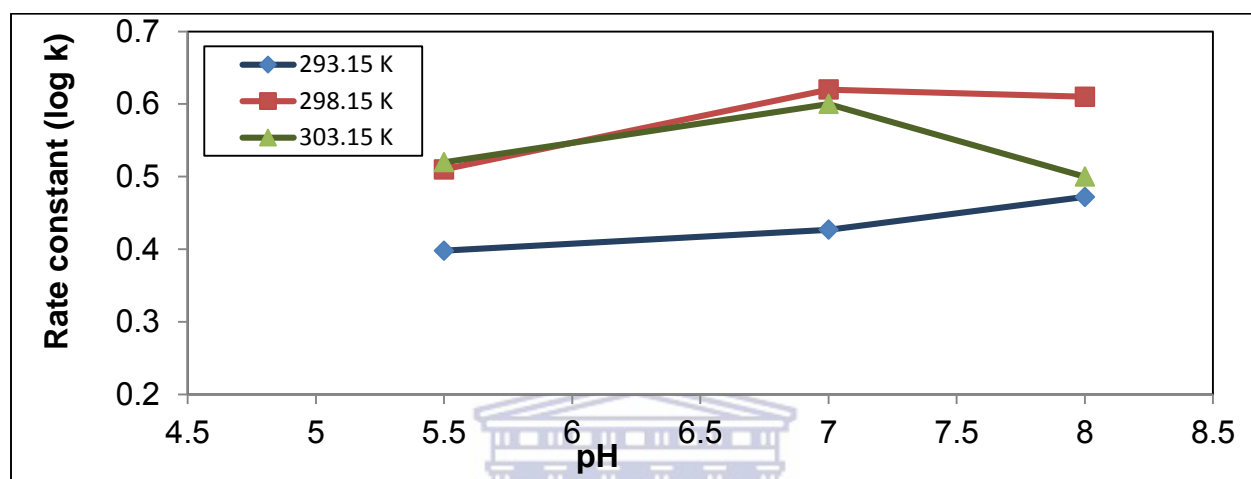


Figure 5.9 Rate constant (log k) vs pH of the complexation of  $Hg^{2+}$  with HA in aqueous phase.

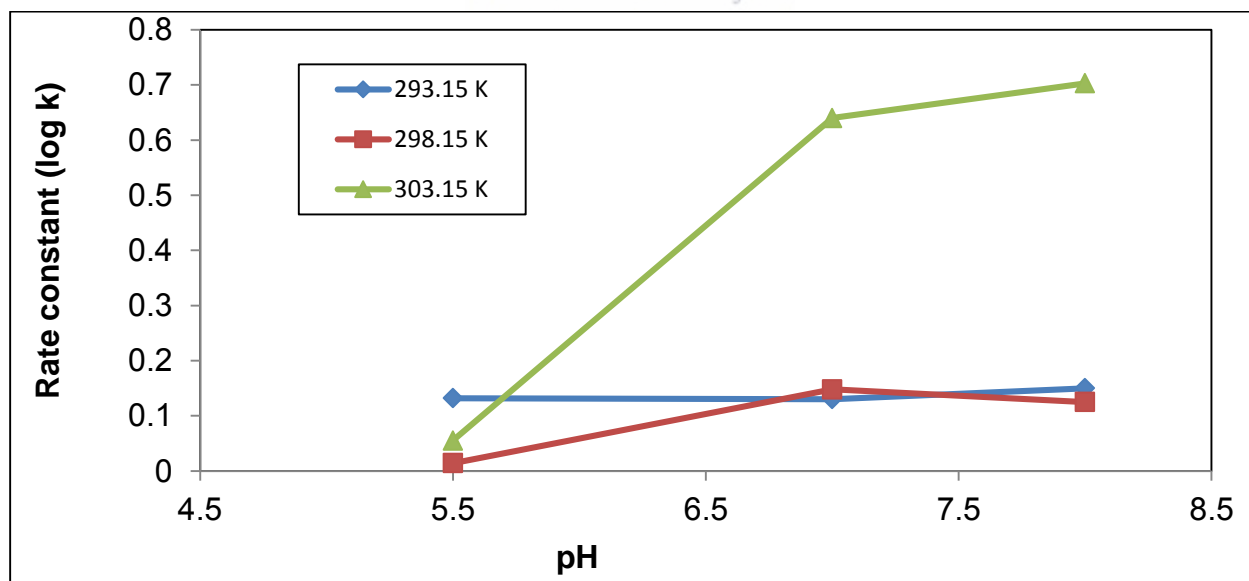


Figure 5.10 Rate constant (log k) vs pH of the complexation of Hg with HA in soil.

At pH 7.0 and 8.0 there was a decrease in the rate constant values in the aqueous phase at 303.15 K (Figure 5.11). There was a general increase of rate constants with an increase in temperature in the soil (Figure 5.12).

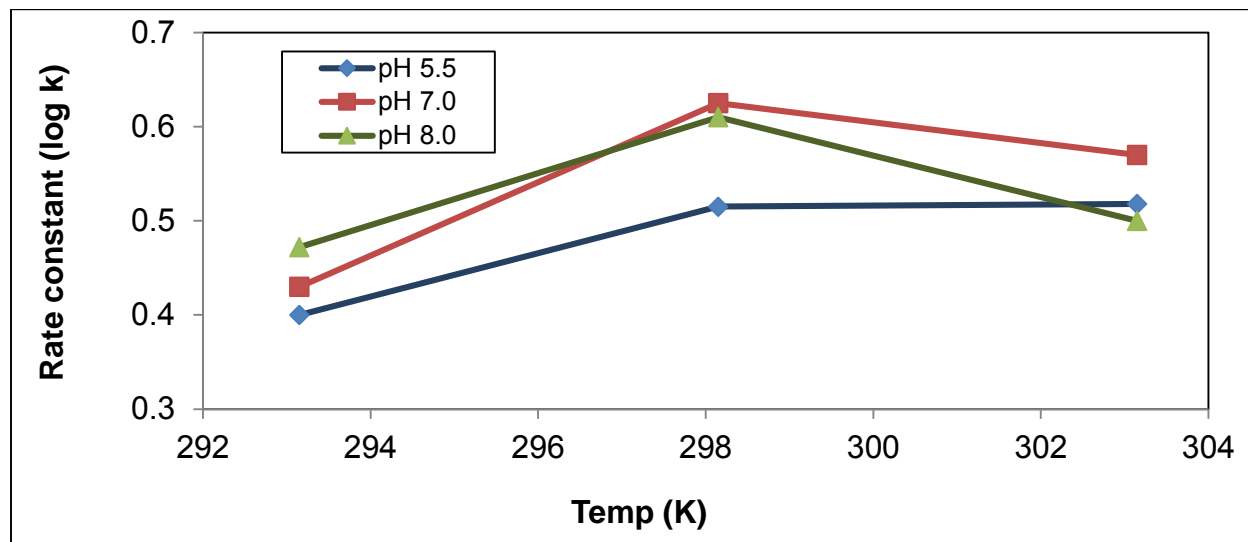


Figure 5.11 Rate constant (log k) vs temperature of the complexation of  $Hg^{2+}$  with HA in aqueous phase.

UNIVERSITY of the  
WESTERN CAPE

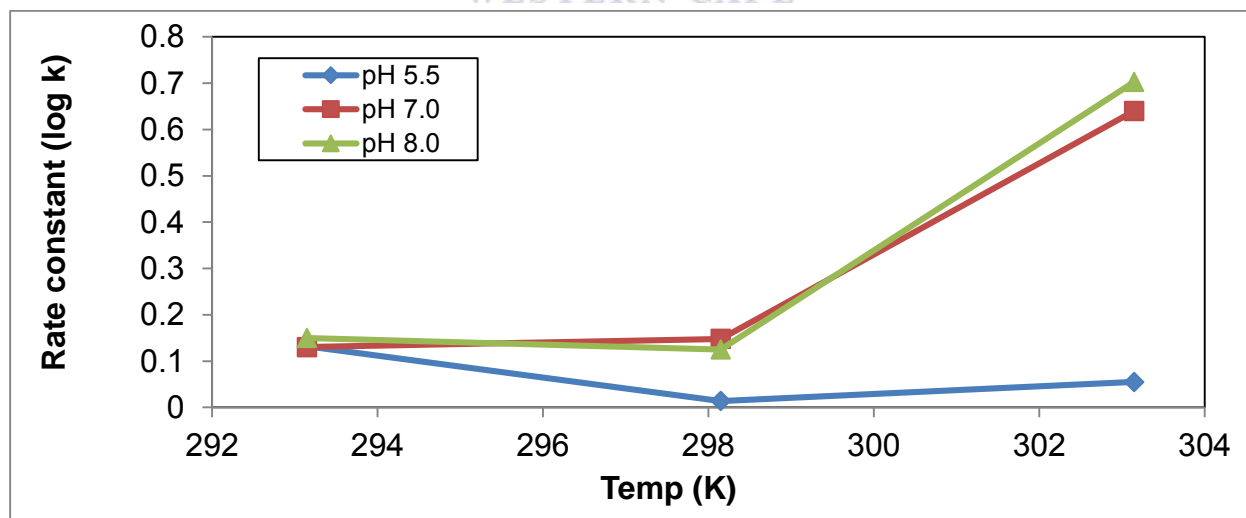
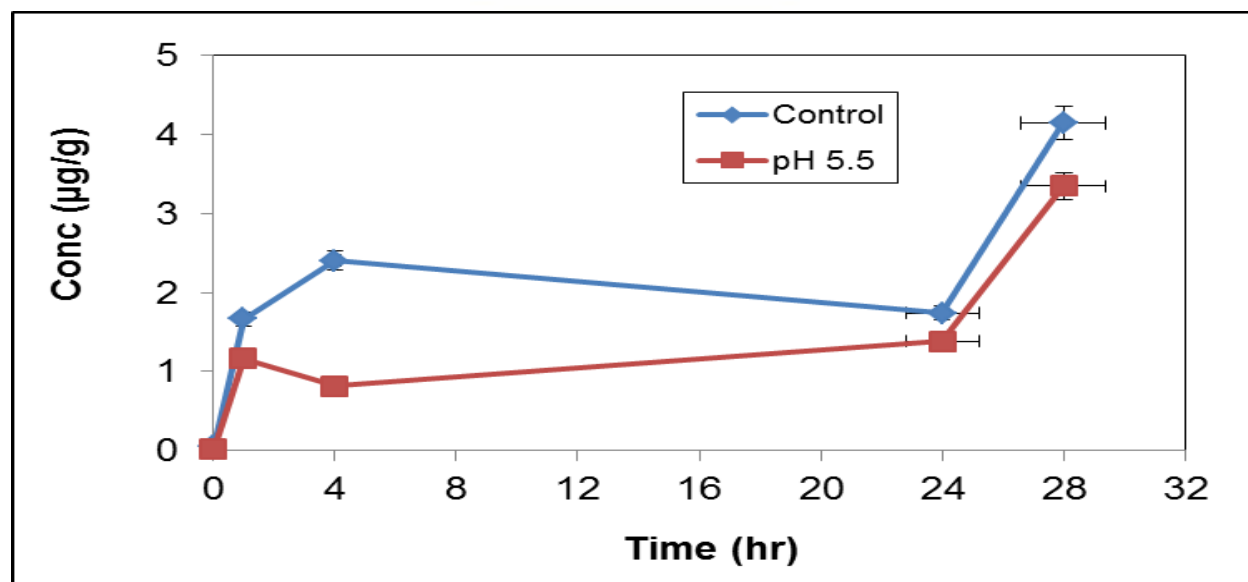


Figure 5.12 Rate constant (log k) vs temperature of the complexation of  $Hg^{2+}$  with HA in soil.

## 5.5 COMPLEXATION PROCESSES IN AQUEOUS PHASE AND SOIL: DISCUSSION

Mercury in soil can exist in various forms, such as dissolved or free metal ( $\text{Hg}^0$ ) or complexed, bound to organic ligands (HA) or precipitated as the sulphide or hydroxide. Adsorption to soil is reported to be inhibited in the presence of  $\text{Cl}^-$ , which results in complex formation with  $\text{Hg}^{2+}$ , and with the resulting complex exhibiting a lower affinity for the surface (Schuster, 1991; Davis *et al.*, 1997). Previous studies (Schuster, 1991; Davis *et al.*, 1997) have reported that  $\text{Cl}^-$  concentrations of  $> 14 \mu\text{g/mL}$   $\text{Hg}^{2+}$  is enough for all available Hg to be in the  $\text{HgCl}_2$  form, and that at higher pH values  $\text{Cl}^-$  can act as a desorbing agent. It is regarded as one of the most mobile and persistent complexing agents for Hg. As  $\text{Cl}^-$  occurs in all natural soil and water systems, it was added to the experimental systems.

In the control sample it was found that  $\text{Hg}^{2+}$  complexed to soil without HA present (Figure 5.1). When comparing the control (low pH and no HA added) and the sample at pH 5.5 (low pH but with HA added), it was found that within the first 24 hr adsorption to soil was higher in the control but after that the concentration in the sample at pH 5.5 steadily increased to a maximum at 28 hr (Figure 5.13).



**Figure 5.13** Comparison of the control and soil sample at 293.15 K. (error bars represent standard error).

The addition of HA may result in an inhibition of metal adsorption to the soil because of strong complex formation with the metal ion or by competing with the metal ion for available adsorption sites on the soil. It could also lead to enhanced adsorption if the ligand is capable of strong complex formation and possesses a substantial affinity for the solid surface (Schuster, 1991; Davis *et al.*, 1997; Arias *et al.*, 2004). In the low pH range the hydroxo complexes are the active sites in the adsorption of  $Hg^{2+}$  to soil.

In the present study Hg binding to soil happened faster at pH 7.0 and pH 8.0 and higher concentrations than at pH 5.5 (Figure 5.14–5.15). After 28 hours however a maximum is reached at all pH values and temperatures except at pH 8.0 at 303.15 K where the Hg concentration in the soil decreased.

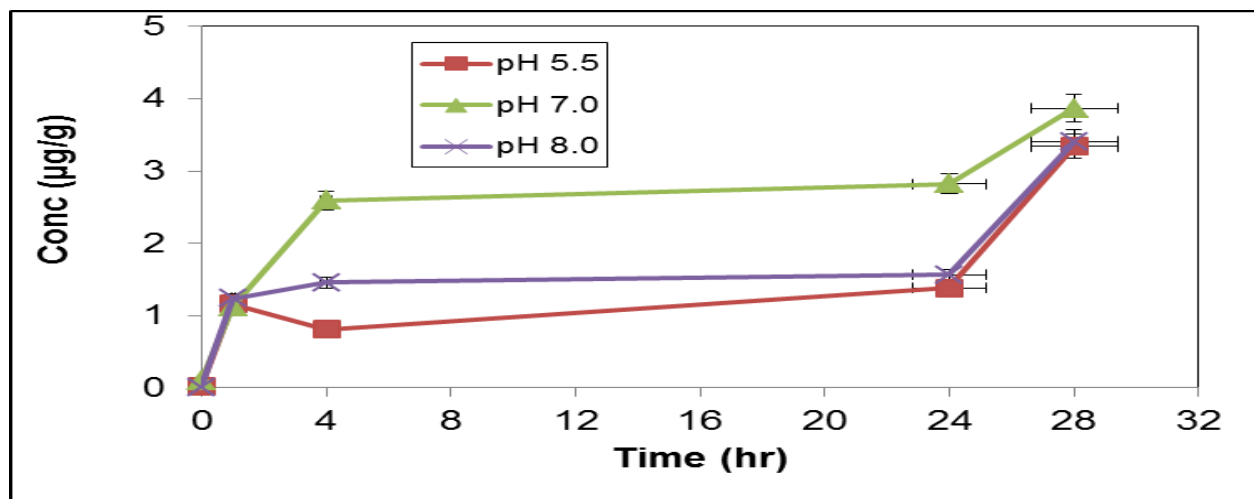


**Figure 5.14** Comparison of the soil sample at different pH values at 293.15 K (error bars represent standard error).

Adsorption to soil increases with increasing pH. Mercury also exhibits a great affinity for HA in soil and the type of interaction that will dominate depends on the type of HA and the pH of the system (Schuster, 1991; Davis *et al.*, 1997; Arias *et al.*, 2004).



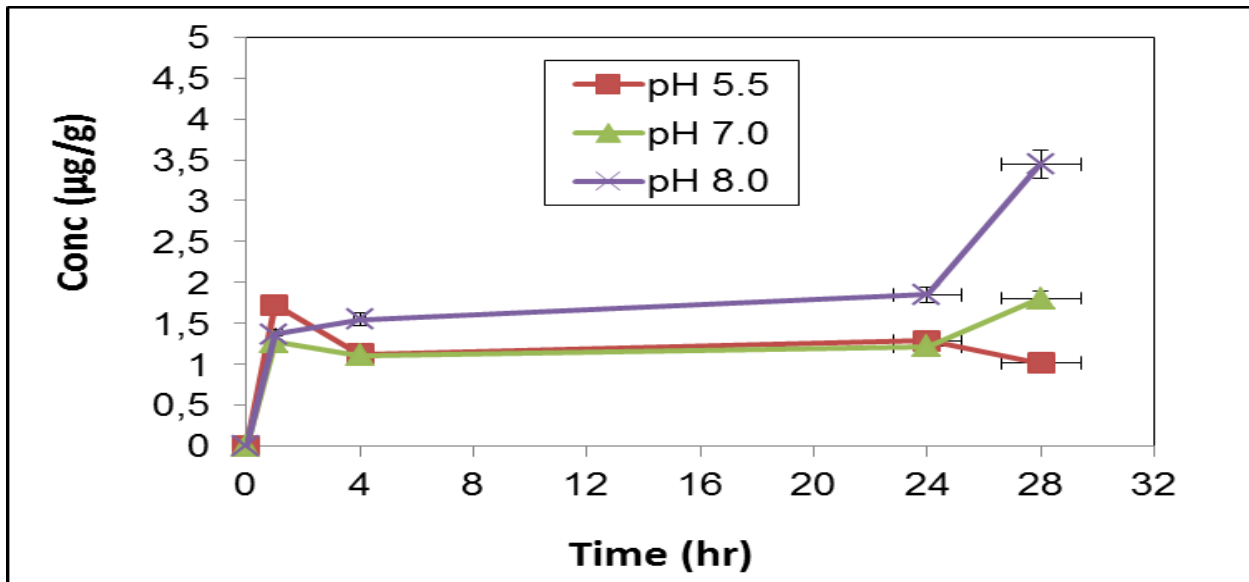


Figure 5.15 Comparison of the soil sample at different pH values at 298.15 K (error bars represent standard error).

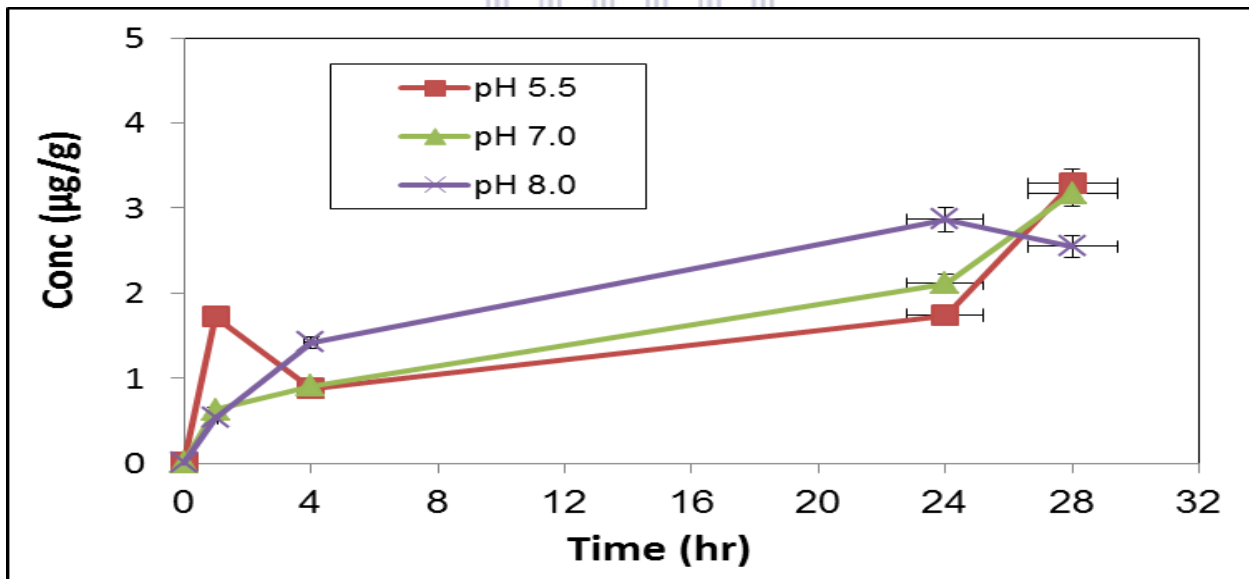


Figure 5.16 Comparison of the soil sample at different pH values at 303.15 K (error bars represent standard error).

There is a decrease in concentration of  $Hg^{2+}$  in soil at pH 8.0 after 28 hours. Increased temperature and pH thus play an important role in Hg desorption and volatilization from soils.

Dominating complexation processes would be formation of organic complexes and the rapid adsorption of Hg to soil surfaces. The processes that may thus dominate during the adsorption of Hg in soil are the formation of complexes with Cl<sup>-</sup> (at low pH), Hg(OH)<sub>2</sub> (at higher pH) which may precipitate, complexation with HA and sorption/desorption to soil. Reduction of Hg<sup>2+</sup> to Hg<sup>0</sup> may also take place and the possibility that it increases with increasing pH (Matthiessen, 1998; Serudo *et al.*, 2007; Yang *et al.*, 2007).

At 4–24 hr there is an equilibrium condition in the complexation process. In previous studies using X-ray absorption fine structure Absorption studies it was found that Hg is complexed to thiol (two reduced organic S groups), a third reduced S from an organic sulfide and when these groups were saturated to one carbonyl-O and amino-N (Haitzer *et al.*, 2002; Skyllberg *et al.*, 2006). The ratio of Hg with HA also plays an important role in the binding of Hg to the different groups in HA. At low ratio of Hg/HS organic thiols were found to be the primary binding sites and carbonyls at high Hg/HS ratios (Haitzer *et al.*, 2002). Initial reaction of Hg with HA takes place almost immediately and this could be with interaction of all available functional groups such as the more abundant but weakly bound carbonyl and amine as well as the less abundant strongly bound reduced thiols. The weakly bound complexes could over time be replaced by Hg transferred to the stronger thiol binding sites within the HS (Miller *et al.*, 2009).and generally the lowest concentration values are obtained during this period. These interactions shows Hg<sup>2+</sup> equilibrates as it forms stronger bonds, explains the persistent rate conditions found in the present study.

Summary: Processes in soil:

(1) Adsorption in soil with no HA



(2) Volatilisation and evaporation from soil (no HA, at high temp)



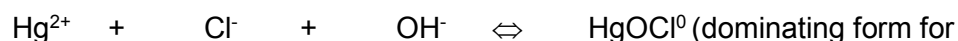
(3) Complexation in aqueous phase and soil

(a) low pH

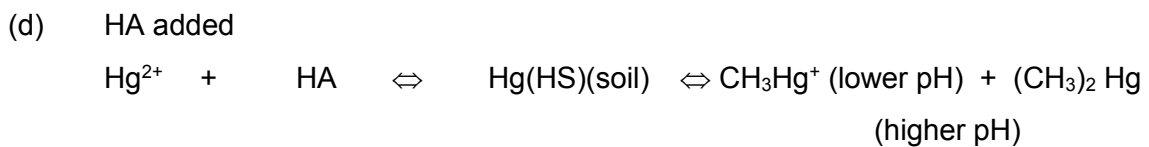
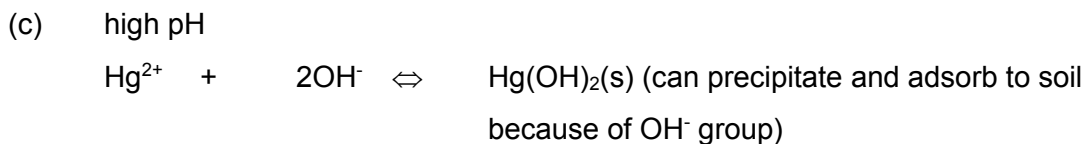


(no tendency to adsorb or very weakly retained soil)

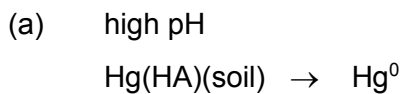
(b) neutral pH



maximum adsorption to soil due to greater covalency of HgOH<sup>+</sup>)



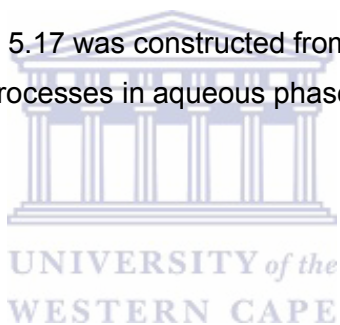
(4) Volatilisation and evaporation from soil (HA added)

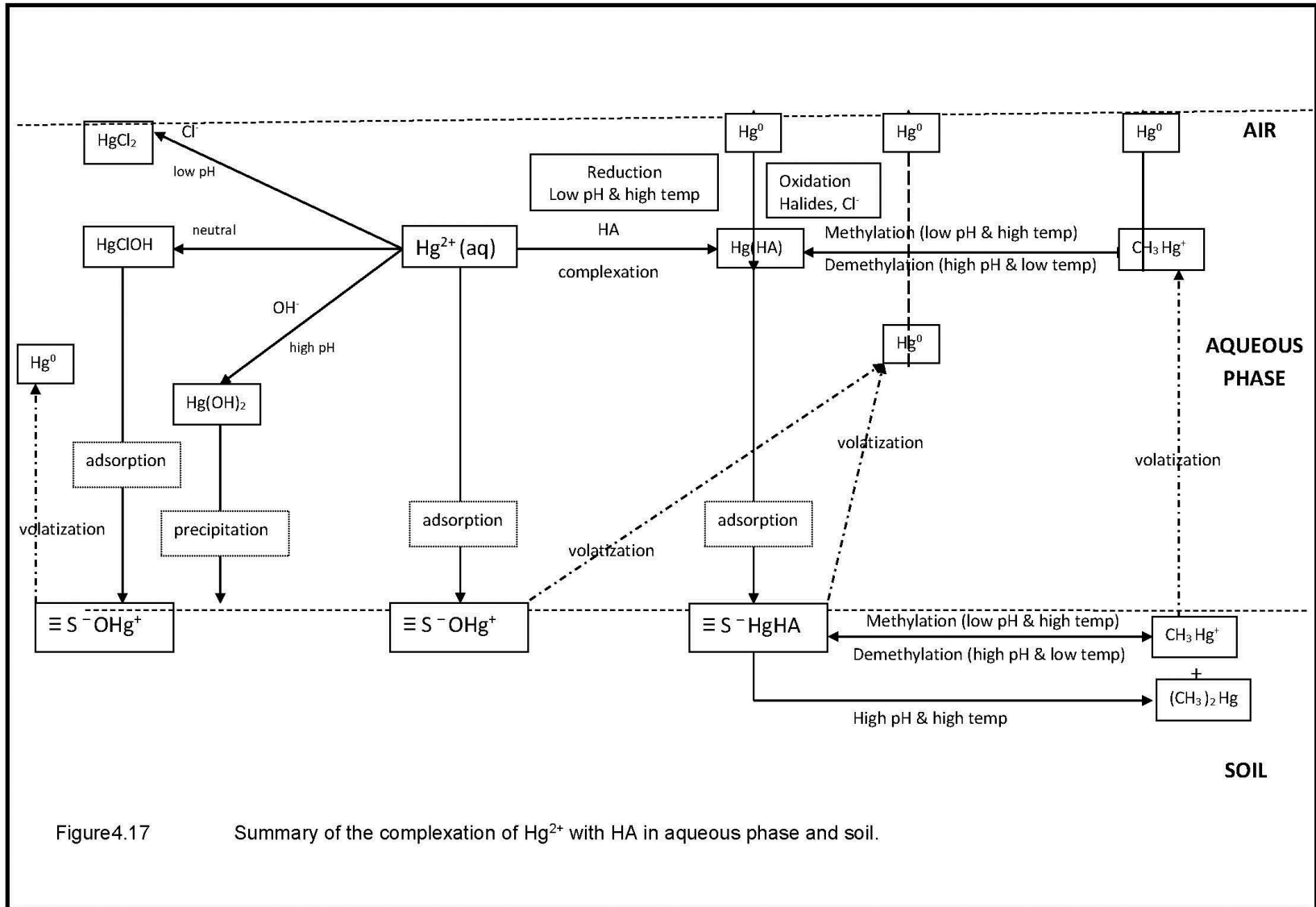


(b) methylation/demethylation (occurs at high pH and high temp)



The diagram represented in Figure 5.17 was constructed from the summarised data, to gain an understanding of the complexing processes in aqueous phase and soil.





## 5.6 BIOACCUMULATION OF MERCURY IN EARTHWORMS (BIOTA): BIOAVAILABILITY STUDIES

Earthworms play an important role in soil decomposition (Gudbrandsen *et al.*, 2007) and maintenance. Earthworms eat their way through soil, digest it and deposit it as waste, thereby aerating and mixing the soil (Ernst *et al.*, 2008). This process enhances the uptake of nutrients in the soil by plants. Earthworms can survive high-level of exposure by regularly crawling out of the exposure mixture. This practice decreases their contact time with the contaminated soil (Gudbrandsen *et al.*, 2007). Earthworms also have the ability to bioaccumulate toxins at high levels and up to 20 times higher than the levels in the soil. In turn they form the basis of many food chains, thereby passing these high levels on to the wildlife that feed on them. This poses a serious risk of secondary poisoning of these predators due to bio-magnification (Kamitani and Kaneko, 2007). Because of the intricate relationship between earthworms and the soil and its contaminants, they can serve as useful biological indicators of soil contamination (Veiga *et al.*, 1999; Dai *et al.*, 2004). Kinetic studies are important as they yield important information about the length of exposure and toxicity of earthworms to heavy metals. There are few reported studies that have considered the kinetics of Hg uptake by earthworms (Nahmani *et al.*, 2007).

The impact of dissolved HA on the bioavailability of Hg<sup>2+</sup> was also investigated by exposing earthworms to the metals in a fixed amount of HA in controlled laboratory conditions. Bioavailability experiments were carried out to study the complexation Hg with HA in earthworms. Earthworms were the biota selected for the study of the uptake of Hg<sup>2+</sup> in the presence of HA under different physical conditions (Section 3.1.1 and 4.1.1). Results of the study was published in SpringerPlus Open, DOI10.1186/s40064-016-2282-6 as *Bioaccumulation of total mercury in the earthworm Eisenia Andrei* by authors Shirley Le Roux, Priscilla Baker and Andrew Crouch. All other results are in Appendix C, pg 88-92.

### 5.6.1 BIOAVAILABILITY STUDIES: DISCUSSION

The present study was carried out to investigate short-term exposure of earthworms to Hg<sup>2+</sup> under different physic-chemical conditions. Prior to the experiment the earthworms were carefully selected to be uniform in size, adult with a well-developed clitella. Previous studies have found that earthworms could survive highly contaminated soil of up to 22 µg/g Hg and

concentrations of up to 6.5 µg/g Hg have been found in earthworms (Burton *et al.*, 2006: Ernst *et al.*, 2008). Colacevich *et al.*, (2011) found that long term exposure of earthworms to Hg-contaminated soil of up to 1287 mg/kg dry wt does not cause earthworm mortality. One of the most important parameters that determines uptake of Hg by earthworms is pH (Burton *et al.*, 2006: Ernst *et al.*, 2008). Veiga *et al.*, (1999) found that methylation could occur in the gut of earthworms, but upon analysis found only about 1% MeHg in the total Hg in the tissues. The ability of earthworms to convert Hg<sup>2+</sup> to MeHg was also indicated by the speciation results obtained by Santoyo *et al.*(2011).

Survival of earthworms in the present study was not good, especially at high pH and temperatures. Earthworms prefer acidic soil and a cool moist environment. Soil texture is also important, and the grain size of the soil used in this study could have been too large. The earthworms were also not fed during the experimental period and a lack of essential elements could have contributed to the earthworms not surviving.



## CHAPTER 6

### SUMMARY AND CONTRIBUTION to NEW KNOWLEDGE

#### 6.1 INTRODUCTION

The complexation of  $\text{Hg}^{2+}$  with HA is a complex process and involves many simultaneous ligand exchanges. The main objective of this study was to determine the impact of HA on the bioavailability of  $\text{Hg}^{2+}$  by studying the complexation of  $\text{Hg}^{2+}$  with HA in aquatic systems, soil/sediments and biota. To this end, analytical methods involving the use of HPLC-ICP-MS and HPLC-EC respectively were developed for speciation of Hg. Reaction rates of the Hg–HA complexation was determined to obtain insight into the mobility of Hg in the environment. It was considered important to determine the effect of the reaction rates of Hg–HA complexation on processes such as speciation and bioavailability, and ultimately the behaviour of Hg as an environmental pollutant.

A hydrogel sensor system was developed for the study of the complexation of Hg with HA by entrapment of HA into the hydrogel to produce a hydrogel-HA sensor. A detailed evaluation of the electrochemistry and analytical performance of the hydrogel-HA sensor towards the detection of  $\text{Hg}^{2+}$ , and by extension  $\text{Pb}^{2+}$ , was done.

#### 6.2 SUMMARY OF THE COMPLEXATION OF $\text{Hg}^{2+}$ WITH HA IN AQUEOUS PHASE/SOIL/BIOTA

The complexation of  $\text{Hg}^{2+}$  with HA in aqueous media, aqueous media and soil as well as aqueous media/soil/biota interface was determined under environmental conditions typical for South Africa. The methodology employed included validation of the HPLC-ICP-MS method adapted for the study against the standard method employed by the CSIR (Council for Scientific Research; Natural Resources and the Environment). The method was tested against a subset of sediment samples from the Westbank area, Western Cape, South Africa supplied by the CSIR. These findings were reported in *S. Afr. J. Chem.*, 2016, 69: *Determination of mercury in selected polluted sediments using HPLC-ICP-MS in Westbank area, Western Cape, South Africa* by authors Shirley Le Roux, Priscilla Baker and Andrew Crouch.

The process of complexation of Hg with HA in aqueous phase was found to be fast, and the reaction rates increased with an increase in pH and temperature. The complexation of Hg was found to follow pseudo first-order kinetics over a short reaction time (1-24 hr), consistent with those previously reported in literature (Miller et al., 2009). Generally, a much faster decrease in Hg concentration was recorded at pHs 7 and 8, and there was thus increased complexation compared to the control (no HA, low pH) and at pH 5.5 (low pH). At higher pH the binding of Hg with HA was increased due to increased proton competition for the Hg<sup>2+</sup> binding sites (Haitzer et al., 2003). Such an increase is predictable because of the exchange properties of the H<sup>+</sup> ions—as the pH increases the degree of ionisation of the carbonyl groups increases (Helal et al., 2007). Data obtained from Arrhenius plots confirmed that, due to the high value of E<sub>c</sub>, the complexation of Hg<sup>2+</sup> and HA is temperature dependent. The slope of the graphs of the rate constant against 1/T differs at the different pH values. . These results are important because they verify the temperature dependence of the complexation process and that different complexation processes may dominate at lower pH values compared to higher pHs.

Reaction rates were positively impacted by higher temperature and pH sensitive due to the increased volatility of the Hg at higher temperature. At pH 8 the precipitation of Hg(OH)<sub>2</sub> lead to a decrease in Hg<sup>2+</sup> concentration. Another process that decreases the concentration of Hg<sup>2+</sup> at increasing pH is the reduction of Hg<sup>2+</sup> to Hg<sup>0</sup> (Matthiessen, 1998; Serudo et al., 2007; Yang Yong-kui et al., 2007). These important results are summarized in Table 3.9 as well as Figure 3.13 and contribute to new knowledge as it clearly demonstrate the relationship between reaction rates and the effect of pH and temperature on the complexation of Hg<sup>2+</sup> and HA.

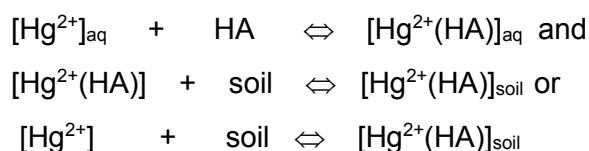
Evaluation of the complexation of Hg in soil and soil in contact with water (as in lakes and rivers etc) are relevant to the environment. Metals from anthropogenic sources in the atmosphere deposits onto the soil via wet or dry precipitation and metals dissolved in water systems eventually deposits in the soil/sediments in contact with it. Mercury deposits in sediments, which complexes and thus immobilizes this toxic metal, but this does not guarantee that the metals are safely removed from aquatic systems. Metals can be reintroduced into the aquatic systems if the solubility, mobility and bioavailability increase due to a change in different environmental factors such as pH, salt concentration, the presence of complexing agents, and temperature. Sediments can be a long-term source of Hg to surface waters. In the present study it was plainly demonstrated that the complexation of Hg<sup>2+</sup> in aqueous phase/soil showed a sharp decrease in the Hg<sup>2+</sup> concentration in the aqueous phase and a corresponding increase of the



Hg<sup>2+</sup> concentration in the soil. There is very little variation of this trend. After prolonged exposure of Hg to soil there was a total loss of Hg<sup>2+</sup> of 7–34% from the original spiked value at higher temperatures and pH values (as summarized in the table below). The experiment at 273.15 K at pH 5.5 showed the smallest loss of 5% and at pH 8.0 the greatest loss. A higher concentration of Hg is thus bound to soil at lower pH. Soil pH is one of the strongest influencing factors for the formation of humic-bound Hg. Acidic soils with lower soil pH or lighter soil texture contain higher amounts Hg-HA (Gabriel and Williamson, 2004; Gui-fen *et al.*, 2006).

This decrease was ascribed to the Hg complexing with the HA as well as the soil.

E.g.



These results are important since they demonstrate the role higher temperatures play in the adsorption of Hg on soils; this trend was illustrated by the biggest loss of total Hg<sup>2+</sup> of 34% of the original spiked value (aqueous phase and soil) at 303.15 K. High temperatures thus lead to a decrease of Hg adsorption on soil. The loss could also be due to abiotic reduction of Hg<sup>2+</sup> to Hg<sup>0</sup> and volatilization from soil which was favoured by presence of HA and higher temperatures (Allard *et al.*, 1991; Gabriel and Williamson, 2004; Rodríguez Martín-Doimeadios *et al.*, 2004; Yang *et al.*, 2007; Serudo *et al.*, 2007). These investigations led to the important mechanisms for Hg as set out in the diagram (Figure 5.17). The complexation of Hg<sup>2+</sup> and HA in aqueous phase/soil at different temperature and pH values was clearly summarized in a diagram and reported for the first time in Figure 5.17 and constitute an important contribution to new knowledge.

As an application study we introduced biota (earthworms) to the wetted soil ecosystem in a controlled study. Earthworms are important bioindicators of soil contamination and very important in soil processes and maintenance. Some constant trends were observed in the study of the uptake of Hg<sup>2+</sup> by selected invertebrates, earthworms, (*Eisenia andrei*). There is a sharp decrease in the Hg<sup>2+</sup> concentration in aqueous phase and a corresponding increase in the soil and earthworms. The greatest increase in concentration was in the earthworms. The earthworms were able to absorb the metal quickly; uptake of Hg<sup>2+</sup> takes place almost immediately and then increased over the sampling period. The rate constant was influenced by

pH and temperature. At very high pH the rate of  $\text{Hg}^{2+}$  uptake decreased. Uptake of  $\text{Hg}^{2+}$  was also better in soil with HA added and at lower temperatures.

Accumulation of  $\text{Hg}^{2+}$  in earthworms was less effective at pH 8.0. pH is highlighted in literature as one of the most important parameters that determines uptake of Hg by earthworms (Burton et al. 2006; Ernst et al. 2008). The absorption of Hg in these experiments especially over the shorter time periods was attributed to absorption via the dermal route. The fluctuation observed in absorption profiles over the extended time period, could be attributed to mixed absorption via dermal as well as the gut route, which are influenced by different physical parameters. Distribution profile of  $\text{Hg}^{2+}$  in presence of HA in soil, earthworms and remaining in aqueous phase as reported in table 6.3 taken from SpringerPlus Open, DOI10.1186/s40064-016-2282-6 as *Bioaccumulation of total mercury in the earthworm Eisenia Andrei* by authors Shirley Le Roux, Priscilla Baker and Andrew Crouch.

### 6.3 DEVELOPMENT OF A HYDROGEL SENSOR

The polysulphone hydrogel was prepared and synthesized as described by Muya *et al.* (2014). The 1mmol AuNP was prepared as described by Mailu *et al.* (2010). The hydrogel sensor was prepared in this study by CV attachment of the AuNP and hydrogel on to the GCE. The Au functionalized electrode was used for chemical attachment of the hydrogel. Attachment of the AuNP and hydrogel onto the GCE was characterized by the use of CV, SWV, AFS and Raman. Using these techniques provided ample proof that a stable GCE/AuNP/hydrogel was synthesized. The prepared electrode was used to entrap HA into the sensor to produce a stable GCE/Au/hydrogel—HA sensor to be used for the study of the complexation of  $\text{Hg}^{2+}$ . CV scans confirmed the attachment of HA to the hydrogel system as the peaks due to the AuNP and hydrogel disappeared after incubation of HA.

The stable novel hydrogel system was used to determine  $\text{Hg}^{2+}$  and to verify the robustness of the system was also used to determine  $\text{Pb}^{2+}$ . The CV and SWV scan of both  $\text{Hg}^{2+}$  and  $\text{Pb}^{2+}$  clearly showed the development of the  $\text{Hg}^{2+}$ --HA and  $\text{Pb}^{2+}$ --HA complexes at a unique potential compared to the standard potential of the free metal. The sensor also shows excellent results for Hg and Pb with LOD of 0.02  $\mu\text{mol/L}$  and sensitivity of 0.1-0.3  $\mu\text{mol/L}$ . The effect of the complexation was monitored using UV/VIS spectroscopy and found to concur with the CV/SWV investigation of the complexation. The disappearance of the free metal, from the electrolytic solution that the GCE/Au/Hydrogel/HA sensor was exposed to, was followed by UV/Vis

analysis. An increase in UV/Vis absorbance trend, for  $M^{2+}$  ion concentration, provided complimentary corroboration for the electrochemically driven complexation of  $M^{2+}$  ion by the HA ligand entrapped in the sensor matrix. The complexation of  $Hg^{2+}$  by HA ligand entrapped in the GCE/Au/Hydrogel/HA sensor showed strong affinity for  $Hg^{2+}$  and  $Pb^{2+}$  as evident by the high complexation values,  $\log K = 4.75$  and  $\log K = 3.04$  respectively. The complexation values for Hg using the sensor are in good agreement with values established by High-performance liquid chromatography (HPLC)  $\log K = 2.9$  to  $4.80$  (at different temperatures) in this study. This novel sensor constitute a major breakthrough in the determination of  $Hg^{2+}$  and by extension other  $M^{2+}$  metals and is a major contribution to new knowledge.

#### 6.4 RECOMMENDATIONS

Development of new cost-effective speciation methods in analytical chemistry, for trace level analysis, especially in analyzing environmental samples, is important. The speciation of Hg was achieved using various analytical methods. Good results were recorded for Hg analysis. The findings of the research carried out in this study could contribute to Hg research in South Africa, where there are grave concerns regarding the levels of Hg in the environment. A particular area of concern is, for example, anthropogenic sources (emission from the use of coal as energy source)—although recent legislation in South Africa (e.g. the National Air Quality Act) requires monitoring of the distribution of metals, including Hg species, as part of controlling pollution from industrial processes. There remains, however, little reported information on Hg levels in South Africa's water, soil and biota. Future work will include monitoring Hg levels in water, soil and biota in collaboration with other accredited laboratories in South Africa. The establishment of a laboratory that would follow the correct procedures for handling Hg and other trace metals in order to train other aspiring chemist. The use of the hydrogel- HA sensor in the determination of other metal will also be investigated. In the present study HA was used as a ligand but humic substance consist of fulvic as well as humic substance. Future work will investigate the complexation of fulvic acid with metals as well as the development of a hydrogel-FA sensor.

Numerous earlier studies have focused on the complexation of  $Hg^{2+}$  with various ligands in aqueous phase, but the kinetics of such complexation reactions has often been overlooked. Hence, a need was identified to study the effects of Hg–HA complexation kinetics in order to understand processes such as Hg speciation and bioavailability. In this study, the rate constants of the Hg–HA complexation reaction in aqueous phase were determined over a

period of 24 hr and found to increase from 0.04 to 0.11 hr<sup>-1</sup> with an increase in pH and temperature. The rate constant recorded from results taken over a shorter period of time (4 hr) also followed the expected trend very well, i.e., an increase in reaction rate with an increase in pH. The reaction rates determined over 4 hr were found to increase from 0.173–0.501 hr<sup>-1</sup> with an increase in pH. The Hg–HA complexation reaction thus slows down over time. Results obtained from experiments carried out over shorter reaction times also more closely followed first-order kinetics. Deviation from first-order kinetics occurred as soon as 7 hr after the start of reaction. Complexation of Hg<sup>2+</sup> with HA in aqueous phase and soil was fast, and most of the Hg transferred to the soil within the first 4 hr of the start of the complexation reaction. The complexation of Hg with aqueous phase/soil under different conditions was studied to determine how these conditions influence such interactions. With an increase in pH and temperature the rate constant in soil increased from 0.087 to 0.154 hr<sup>-1</sup>. It was determined that while Hg binds to soil almost immediately, there is a change in the trend under higher pH and temperature conditions. Under these conditions, the Hg could be reintroduced into the environment. These investigations led to the proposed mechanisms for Hg in the environment figure 3.13 and figure 5.17.

The uptake of Hg<sup>2+</sup> by earthworms *Eisenia andrei* was found to be highest at 293.15 K and 298.15 K (with HA added), with absorption of 84% of the total spiked value. This high uptake of Hg<sup>2+</sup> was ascribed to the more favourable conditions of low temperature and low pH here. The earthworms absorbed high concentrations of Hg (up to 5 µg/mL) and uptake was greater in samples containing HA than in the control (no HA). This is of concern, because of the vital role of earthworms at the bottom of the food chain. The study also revealed that earthworms are susceptible to the dissolved metal. High temperature was less favourable for Hg<sup>2+</sup> uptake; at 303.15 K only 11% in the control (no HA) and 33% of the spiked value was absorbed. The presence of the HA made the Hg<sup>2+</sup> more bioavailable for the uptake of Hg. It was found that prevailing physical conditions play an important role in determining the dominant type of ligand interaction with Hg. Complexation of Hg–HA was fast, and transfer of Hg from aqueous phase to soil took place within 24 hr. Contaminated water systems may thus exhibit deceptively lower Hg concentrations, because of this quick transfer to the sediment. In the study of the uptake of Hg<sup>2+</sup> by the selected invertebrates (earthworms *Eisenia andrei*), it was determined that the presence of HA is significant for the bioavailability of Hg.

## BIBLIOGRAPHY

**ALLARD, B., ARSENIÉ, I.** (1991) Abiotic reduction of mercury by humic substances in aquatic system—an important process for the mercury cycle. *Water, Air and Soil Pollution* 56, 457–464

**ÁLVAREZ, F.F., RODRÍGUEZ, M.T., ESPINOSA, A.J.F., DABÁN, A.G.** (2004) Physical speciation of arsenic, mercury, lead, cadmium and nickel in inhalable atmospheric particles. *Analytica Chimica Acta*, 524, 33–40

**ANDERSEN, A.** (1979) Mercury in soils. In: Nriagu JW (ed): *The biochemistry of mercury in the environment*. Amsterdam. Elsevier, North-Holland Biomedical Press, 79–112

**ANDERSEN, A., JULSHAMN, K., RINGDAL, O., MORKORE, J.** (1987) Trace elements intake in the Faroe Islands II. Intake of mercury and other elements by consumption of pilot whales (*Globicephalus meleanus*). *Science of The Total Environment* 65, 63–68

**ARIAS, M., BARRAL, M.T., DA SILVA-CARVALHAL, J., MEJUTO, J.C., RUBINOS, D.** (2004) Interaction of Hg(II) with kaolin–humic acid complexes. *Clay Minerals* 39, 35–45

**ARNOLD, R.E., LANGDON, C.J., HODSON, M.E., BLACK, S.** (2003) Development of a methodology to investigate the importance of chemical speciation on the bioavailability of contaminants to *Eisenia andrei*. *Pedobiologia* 47, 633–639

**ASADPOUR-ZEYNALI, K., AMINI, R.** (2017) A novel voltammetric sensor for mercury(II) based on mercaptocarboxylic acid intercalated layered double hydroxide nanoparticles modified electrode. *Sensors and Actuators B:Chemical* 246, 961-968

**ATKINS, P. W.** (1996) *The elements of Physical Chemistry*. Oxford: Oxford University Press

**BAHRAM, M., HOSEINZADEH, F., FARHADI, K., SAADAT, M., NAJAFI-MOGHADDAM, P., AFKHAMI, A.** (2014) Synthesis of gold nanoparticles using pH-sensitive hydrogel and its application for colorimetric determination of acetaminophen, ascorbic acid and folic acid. *Colloids and surfaces A: Physicochemical and Engineering Aspects* 441,517-524

**BARCELÓ, D.** (1993) Environmental Analysis: techniques, applications and quality assurance; Amsterdam: Elsevier Science Publishers

**BARRATT, G.J., COMBRINK, J.** (2002) An assessment of the degree of mercury (Hg) bio-transformation in two river systems following discharges from a mercury recovery plant. Water SA (Special Edition):WISA Proceedings 2002

**BATLEY, G.E.** (1999) Quality assurance in environmental monitoring. Marine Pollution Bulletin (Great Britain) 39, 1–12

**BERNAUS, A., GAONA, X., van REE, D., VALIENTE, M.** (2006) Determination of Hg in polluted soils surrounding a chlor-alkali plant. Direct speciation by X-ray absorption spectroscopy techniques and preliminary geochemical characterisation of the area. Analytica Chimica Acta, 565, 73–80

**BEYER, W.N., CROMARTIE, E., MOMENT, G.B.** (1985) Accumulation of methylmercury in the earthworm, *Eisenia foetida*, and its effect on regeneration. Bulletin of Environmental Contamination and Toxicology 157–162

**BLANCO, R.M., VILLANUEVA, M.T., URÍA, J.E.S., SANZ-MEDEL, A.** (2000) Field sampling, preconcentration and determination of mercury species in river waters. Analytica Chimica Acta 419, 137–144

**BLOOM, N.S., GROUT, A.K., PRESTBO, E.M.** (2005) Development and complete validation of a method for the determination of dimethyl mercury in air and other media. Analytica Chimica Acta 546, 92–101

**BLOOM, N.S., FITZGERALD, W.F.,** (1988) Determination of volatile mercury species at the pictogram level by low-temperature gas chromatography with cold-vapour atomic fluorescence detection. Analytica Chimica Acta 208, 151–161

**BOUDOU, A., RIBEYRE, F.** (1985) Experimental study of trophic contaminants of *Salmo gairdneri* by two mercury compounds: HgCl<sub>2</sub> and CH<sub>3</sub>HgCl. Analysis at the organism and organ levels. Water, Air and Soil Pollution 26, 137–148

**BUELL, P., GIRARD, J.** (1994) Chemistry: An Environmental Perspective. New York: Prentice Hall

**BURTON, D.T., TURLEY, S.D., FISHER, D. J., GREEN, D.J., SHEDD, T.R.** (2006) Bioaccumulation of total mercury and monomethylmercury in the earthworm *Eisenia fetida*. *Water, Air and Soil Pollution* 170, 37–54

**CABAÑERO, A.I., MADRID, Y., CĂMARA, C.** (2004) Selenium and Hg bioaccessibility in fish samples: an in vitro digestion method. *Analytica Chimica Acta* 526, 51–61

**CALISI, A., ZACCARELLI, N., LIONETTO, M.G., SCETTINO, T.** (2013) Integrated biomarker analysis in the earthworm *Lumbricus terrestris*: Application to the monitoring of soil heavy metal pollution. *Chemosphere* 90, 2637–2644

**CANET, L., SETA, P.** (2001) Extraction and separation of metal cations in solution by supported liquid membrane using lasalocid A as carrier. *Pure Applied Chemistry IUPAC* 73, no. 12, 2039–2046

**CAPITÁN-VALLVEY, L.F., CANO RAYA, C., LÓPEZ LÓPEZ, E., FERNÁNDEZ-RAMOS, M.D.** (2004) Irreversible optical test strip for Hg determination based on neutral ionophore. *Analytica Chimica Acta* 524, 365–372

**CHANNA, K., ODLAND J.O., KOOTBODIEN, T., THEODOROU, P., NAIK, I., SANDANGER, T.M., RÖLLIN, H. B.** (2013) Differences in prenatal exposure to mercury in South African communities residing along the Indian Ocean. *Science of The Total Environment* 463-464, 11–19

**CLARKSON, T.W.** (1993) Mercury: Major issues in environmental health. *Environmental Health Perspectives* 100, 31–38

**COLACEVICH, A., SIERRA, M. J., BORGHINI, F., MILLÁN, R., SANCHEZ–HERNANDEZ, J. C.** (2011) Oxidative stress in earthworms short– and long–term exposed to highly Hg–contaminated soils. *Journal of Hazardous Materials* 194, 135–143

**CONAWAY, C.H., SQUIRE, S., MASON, R.P., RUSSEL FLEGAL, A.** (2003) Mercury speciation in the San Francisco Bay estuary. *Marine Chemistry* 80, 199–225

**COX, C., CLARKSON, T.W., MARSH, D.O., AMIN-ZAKI, L., TIKRITI, S., MYERS G.G.** (1988) Dose-response analysis of infants prenatally exposed to methyl mercury: an application of a single compartment model to single-strand hair analysis. *Environmental Research* 49, 318–332

**CRAIG, P.J., JENKINS, R.O., STOJAK, G.H.** (1999) The analysis of inorganic and methyl mercury by derivatisation methods: opportunities and difficulties. *Chemosphere* 39, 1181–1197

**CRUMP, K.S., KJELLSTROM T., SHIPP., A.M., SILVERS, A., STEWART, A.** (1995) Influence of prenatal mercury exposure upon scholastic and psychological test performance: benchmark analysis of a New Zealand cohort. *Risk Analysis* 18, 701–713

**CUKROWSKA, E. M., GOVENDER, K., VILJOEN, M.** (2004) Ion mobility based on column leaching of South African gold tailings dam with chemometric evaluation. *Chemosphere* 56, 39-50

**DABEK-ZLOTORZYNSKA, E., LAI, E.P.C., TIMERBAEV, A.R.** (1998) Capillary electrophoresis: the state-of-the-art in metal speciation studies. *Analytica Chimica Acta* 359, 1–26

**DAI, J., BECQUER, T., ROUILLER, J.H., REVERSAT, G., BERNHARD-REVERSAT, F., NAHMANI, J., LAVELLE, P.** (2004) Heavy metal accumulation by two earthworm species and its relationship to total and DTPA-extractable metals in soils. *Soil Biology and Biochemistry* 36, 91–98

**DALVIE, M.A., EHRLICH, R.** (2005) Community mercury levels in the vicinity of peri-urban waste disposal sites and fossil fuel burning operations. *Environment International* 32, 493–499

**DA SILVA, M.P., PROCOPIO, J.R., HERNANDEZ, L.** (1997) Reversed-phase high-performance liquid chromatography of pyrrolidinedithiocarbamate complexes of mercuric species using amperometric and coulometric detection. *Journal of Chromatography* 761, 139–146

**DAVIDSON, P.W., MYERS, G.J., COX, C., WILDING, G.E., SHAMLAYE, C.F., HUANG, L.S., CERNICHIARI, E., SLOANE-REEVES, J., PALUMDO, D., CLARKSON, T.W.** (2006) Methylmercury and neurodevelopment: longitudinal analysis of the Seychelles child development cohort. *Neurotoxicology and Teratology* 28, 529–535

**DAVIES, T.C., MUNDALAMO, H. R.** (2010) Environmental health impacts of dispersed mineralisation in South Africa. *Journal of African Earth Sciences* 58, 652–666



**DAVIS, A., BLOOM, N.S., QUE HEE, S.S.** (1997) The environmental geochemistry and bioaccessibility of mercury in soils and sediments: a review. *Risk Analysis* 17, 557–569

**DIETZ, R., RIGET, F., CLEEMANN, M., AARKROG, A., JOHANSEN, P., HANSEN, J.C.** (2000) Comparison of contaminants from different trophic levels and ecosystems. *Science of The Total Environment* 245, 221–231

**do NASCIMENTO, F. H., MASINI, J. C.** (2012) Complexation of Hg(II) by humic acid studied by square wave stripping voltammetry at screen-printed gold electrodes. *Talanta* 100, 57–63

**DURRIEU, G., MAURY-BRACHET, R., BOUDOU, A.** (2005) Goldmining and mercury contamination of the piscivorous fish *Hoplias aimara* in French Guiana (Amazon basin). *Ecotoxicology and Environmental Safety* 60, 315–323

**EMTEBORG, H., SNELL, J., QIAN, J., FRECH, W.** (1999) Sources of systematic errors in mercury speciation using Grignard reagents and capillary gas chromatography coupled to atomic spectrometry. *Chemosphere* 39, 1137–1152

**ERNST, G., ZIMMERMANN, S., CHRISTIE, P., FREY, B.** (2008) Mercury, cadmium and lead concentrations in different ecophysiological groups of earthworms in forest soils. *Environmental Pollution* 156, 1304–1313

**FERNANDEZ, R.G., BAYON, M, M., GARCÍA ALONSO ,J.I., SANZ-MEDEL, A.** (2000) Comparison of different derivatization approaches for mercury speciation in biological tissues by gas chromatography/inductively coupled plasma mass spectrometry. *Journal of Mass Spectrometry* 35, 639–646

**FITZGERALD, W.F., LAMBORG, C.H., HAMMERSCHMIDT, C.R.** (2007) Marine biogeochemical cycling of mercury. *Chemical Reviews* 107, 641–662

**FROST, M.S., DEMPSEY, M.J., WHITEHEAD, D.E.** (2017) The response of citrate functionalised gold and silver nanoparticles to the addition of heavy metal ions. *Colloids and Surfaces A: Physicochemical and Engineering Aspects* 518, 15-24

**GABRIEL, M.C., WILLIAMSON, D.G.** (2004) Principal biogeochemical factors affecting the speciation and transport of mercury through the terrestrial environment. *Environmental Geochemistry and Health* 26, 421–434

**GAO, C., HUANG, X.** (2013) Voltammetric determination of mercury(II). Trends in Analytical Chemistry 51,1-12

**GÅRDFELDT, K., MUNTHE, J., STRÖMBERG, D., LINDQVIST, O.** (2003) A kinetic study on the abiotic methylation of divalent mercury in the aqueous phase. Science of The Total Environment 304, 127–136

**GERBERSMANN, C., HEISTERKAMP, M., ADAMS, F.C., BROEKAERT, J.A.C.** (1997) Two methods for the speciation analysis of mercury in fish involving microwave-assisted digestion and gas chromatography-atomic emission spectrometry. Analytica Chimica Acta 350, 273–285

**GHANEI-MOTLAGH, M., TAHER, M.A., HEYDARI, A., GHANEI-MOTLAGH, R., GUPTA, V.K.** (2016) A novel voltammetric sensor for sensitive detection of mercury(II) ions using glassy carbon electrode modified with graphene-based ion imprinted polymer. Material Science and Engineering C 63, 367-375

**GRIEB, T.M., DRISCOLL, C.T., GLOSS, S.P., SCHOFIELD, C.L., BOWIE, G.L., PORCELLA, D.B.** (1990) Factors affecting mercury accumulation in fish in the upper Michigan Peninsula. Environmental Toxicology and Chemistry 9, 919–930

**GRINBERG, P., CAMPOS, R.C., MESTER, Z., STURGEON, R.E.** (2003) A comparison of alkyl derivatization methods for speciation of mercury based on solid phase microextraction gas chromatography with furnace atomization plasma emission spectrometry detection. Journal of Analytical Atomic Spectrometry 18, 902–909

**GU, B., BIAN, Y., MILLER, C. L., DONG, W., JIANG, X., LIANG, L.** (2011) Mercury reduction and complexation by natural organic matter in anoxic environments. Environmental Sciences 108(4), 1479-1483

**GUDBRANDSEN, M., SVERDRUP, L.E., AAMODT, S., STENERSEN, J.** (2007) Short-term pre-exposure increases earthworm tolerance to mercury. European Journal of Soil Biology 43, S261–S267

**GUI-FEN, Y.U., HONG-TAO, W.U., XIN, J, WEN-XIANG, H.E., CHANG-LE, Q.** (2006) Relationships between humic substance-bound mercury contents and soil properties in subtropical zone. Journal of Environmental Sciences 18, 951–957

**GUIOCHON, G.A., BEAVER, L.A.** (2004) Progress and future of instrumental analytical chemistry applied to the environment. *Analytica Chimica Acta* 524(1–2), 1–14

**HAITZER, M., AIKEN, G.R., RYAN, J.N.** (2002) Binding of Mercury(II) to dissolved organic matter: the role of the mercury-to-DOM concentration ratio. *Environmental Science and Technology* 36, 3564–3570.

**HAITZER, M., AIKEN, G.R., RYAN, J.N.** (2003) Binding of Mercury(II) to aquatic humic substances: Influence of pH and source of humic substances. *Environmental Science and Technology* 37, 2436-2441.

**HAN, S., GILL, G.A.** (2005) Determination of mercury complexation in coastal and estuarine waters using competitive ligand exchange method. *Environmental Science and Technology* 39, 6607–6615

**HARRIS, D.C.** (2003) *Quantitative Chemical Analysis*. New York: W.H. Freeman and Company

**HARVEY, D.** (2000) *Modern Analytical Chemistry*. Boston: McGraw-Hill

**HASSAN, R.Y.A., KAMEL, M.S., HASSAN, H.N.A., KHALED, E.** (2015) Voltammetric determination of mercury in biological samples using crown ether/multiwalled carbon nanotube-based sensor. *Journal of Electroanalytical Chemistry* 759, 101-106

**HELAL, A.A., IMAM, D.M., KHALIFA, S.M., ALY, H.F.** (2007) The binding constants of heavy metal humate and fulvate complexes. *Journal of Saudi Chemical Society* 11, 191–198

**HEZARD, T., FAJERWEG, K., EVRARD, D., COLLIÈRE, V., BEHRA, P.** (2012) Gold nanoparticles on glassy carbon using cyclic voltammetry: Application to Hg(II) trace analysis. *Journal of Electroanalytical Chemistry* 664, 46-52

**HIGHT, S.C., CHENG, J.** (2006) Determination of methyl Hg and estimation of total Hg in seafood using high performance liquid chromatography and inductively coupled plasma-mass spectrometry: method development and validation. *Analytica Chimica Acta* 567, 160–172

**HOBBELEN, P.H.F., KOOLHAAS, J.E., VAN GESTEL, C.A.M.** (2006) Bioaccumulation of heavy metals in the earthworms *Lumbricus rubellus* and *Aporrectodea caliginosa* in relation to total and available metal concentrations in field soils. *Environmental Pollution* 144, 639–646

**HOUSEROVÁ, P., MATĚJČEK, D., KUBÁŇ, V.** (2007) High-performance liquid chromatographic/ion-trap mass spectrometric speciation of aquatic mercury as its pyrrolidinedithiocarbamate complexes. *Analytica Chimica Acta* 596, 242–250.

**HUGHES, D. L., AFSAR, A., HARWOOD, L.M., JIANG, T., LAVENTINE, D.M., SHAW, L.J., HODSON, M.E.** (2017) Adsorption of Pb and Zn from binary metal solutions and in the presence of dissolved organic carbon by DTPA-functionalised, silica-coated magnetic nanoparticles. *Chemosphere* 183,519-527

**INZA, B., RIBEYRE F., MAURY-BRACHET R., BOUDOU, A.** (1997) Tissue distribution of inorganic mercury, methylmercury and cadmium in the Asiatic clam (*Corbicula fluminea*) in relation to the contamination levels of the water column and sediment. *Chemosphere* 35, (12), 2817–2836

**IPOLYI, I., MASSANISSO, P., SPOSATO, S., FODOR, P., MORABITO, R.** (2004) Concentration levels of total and methylmercury in mussel samples collected along the coasts of Sardinia Island (Italy). *Analytica Chimica Acta* 505, 145–151

**ISSARO, N., ABI-GHANEM, C., BERMOND, A.** (2009) Fractionation studies of mercury in soils and sediments: A review of the chemical reagents used for mercury extraction. *Analytica Chimica Acta* 631, 1–12

**JAROSINSKA, D., BARREGÅRD, L., BIESIADA, M., MUSZYNSKA-GRACA, M., DADKOWSKA, B., DENBY, B., PACYNA, J., FUDALA, J., ZIELONKA, U.** (2006) Urinary mercury in adults in Poland living near a chloralkali plant. *Science of The Total Environment* 368, 335–343

**JOHNSTON, P., STRINGER, R., FRENCH, M.C., VALLETTE, J.** (1991) Contamination of soils and sediments in the vicinity of a mercury recovery plant. *Bulletin of Environmental Contamination and Toxicology* 46, 74-78

**KADING, T. J., MASON, R.P., LEANER, J.J.** (2009) Mercury contamination history of an estuarine floodplain reconstructed from a <sup>210</sup>Pb-dated sediment core (Berg River, South Africa). *Marine Pollution Bulletin* 59, 116–122

**KAMITANI, T., KANEKO, N.** (2007) Species-specific heavy metal accumulation patterns of earthworms on a floodplain in Japan. *Ecotoxicology and Environmental Safety* 66, 82-91

**KAYALVIZHY, E., PAZHANISAMY, P.** (2016) Swelling behavior of poly(N-cyclohexylacrylamide-co-Acrylamide/AMPSNa) gold Nanocomposite hydrogels. International Journal of Biological Macromolecules <http://dx.org/10.1016/j.ijbiomac.2016.01.047>

**KEITH, L.H.** (1991) Environmental Sampling and Analysis. A Practical Guide. USA: Lewis Publishers

**KHWAJA, A.R., BLOOM, P.R., BREZONIK, P.L.** (2006) Binding constants of divalent mercury in soil humic acids and soil organic matter. Environmental Science and Technology 40, 844–849

**KUBÁŇ, P., HOUSEROVÁ, P., KUBÁŇ, P., HAUSER, P.C., KUBÁŇ, V.** (2007) Mercury speciation by CE: a review. Electrophoresis 28, 58–68

**KUHN, G.** (2003) Closeout summary report on the monitoring programme, findings and conclusions reached during the period from 30/09/2002 to March 2003. Gerry Kurn Environmental and Hygiene, Piketberg, RSA.

**LANDALUZE, J.S., de DIEGO, A., RAPOSO, J.C., MADARIAGA, J.M.** (2004) Methylmercury determination in sediments and fish tissues from the Nerbioi-Ibaizabal estuary (Basque Country, Spain). Analytica Chimica Acta 508, 107–117

**LANGSETH, W.** (1986) Determination of organic and inorganic mercury compounds by reverse-phase high-performance liquid chromatography after extraction of the compounds as their dithizonates. Analytica Chimica Acta 185, 249–256.

**LAPORTE, J.M., TRUCHOT., J.P., RIBEYRE, F., BOUDOU, A.** (1997) Combined effects of water pH and salinity on the bioaccumulation of inorganic mercury and methylmercury in the shore crab *Carcinus maenas*. Marine Pollution Bulletin (Great Britain) 34, 880–893

**LAWRENCE, A.L., MASON, R.P.** (2001) Factors controlling the bioaccumulation of mercury and methylmercury by the estuarine amphipod *Leptocheirus plumulosus*. Environmental Pollution 111, 217–231

**LEHTONEN, T., PEURAVUORI, J., PIHLAJA, K.** (2000) Characterisation of lake- aquatic humic matter isolated with two different sorbing solid techniques: tetramethylammonium hydroxide treatment and pyrolysis–gas chromatography/mass spectrometry. Analytica Chimica Acta 424, 91–103

**LIVENS, F.R.** (1991) Chemical reactions of metals with humic material. *Environmental Pollution* 70, 183-208

**MAILU, S.N., WARYO, T.T., NDANGILI, P.M., NGECE, F.R., BALEG, A. A., BAKER, P.G., IWUOHA, E.I.** (2010) Determination of Anthracene on Ag-Au Alloy Nanoparticles/Overoxidized-Polypyrrole Composite Modified Glassy Carbon Electrodes. *Sensors*, 10, 9449-9465,doi:10.3390/s101009449

**MALESUIK, M.D., CARDOSO, S.G., BAJERSKI, L., LANZANOVA, F.A.** (2006) A stability-indicating high performance liquid chromatographic (HPLC) assay for the simultaneous determination of atorvastatin and amlodipine in commercial tablets. *Journal of Association of Official Analytical Chemists International* 89, 359–364

**MANAHAN, S.** (1996) *Environmental Chemistry*. Michigan: Lewis Publishers

**MARCZAK, M., WOLSKA, L., CHRZANOWSKI, W., NAMIEŚNIK, J.** (2002) Microanalysis of Volatile Organic Compounds (VOC) in water samples. *IDS-Water-White Paper*

**MASEKOAMENG, K.E., LEANER, J., DABROWSKI, J.** (2010) Trends in anthropogenic mercury emissions estimated for South Africa during 2000-2006. *Atmospheric Environment* 55, 4118–4125

**MASON, R.P.** (2007) Proceedings of 'Analytical Methods in Mercury Speciation' Workshop 2007. University of the Witwatersrand, Johannesburg

**MATTHIESSEN, A.** (1998) Reduction of divalent mercury by humic substances: kinetic and quantitative aspects. *Science of The Total Environment* 213, 177–183

**MAURY-BRACHET, R., DURRIEU, G., YANNICK, D., BOUDOU, A.** (2006) Mercury distribution in fish organs and food regimes: significant relationships from twelve species collected in French Guiana (Amazonian basin). *Science of the Total Environment* 368, 262–270

**McDONALD, S., BISHOP, A.G., PRENZLER, P.D., ROBARDS, K.** (2004) Analytical chemistry of freshwater humic substances. *Analytica Chimica Acta* 527, 105–124

**MILLER, C.L., SOUTHWORTH, G., BROOKS, S., LIANG, L., BAOHUA, GU.** (2009) Kinetic controls on the complexation between mercury and dissolved organic matter in a contaminated environment. *Environmental Science and Technology* 43, 8548–8553

**MINGANTI, V., CAPELLI, R., DRAVA, G., DE PELLEGRINI, R.** (2007) Solubilization and methylation of HgS, PbS and SnS by iodomethane: a model experiment for the aquatic environment. *Chemosphere* 67, 1018–1024

**MIRETZKY, P., BISINOTI, M.C., JARDIM, W.F.** (2005) Sorption of mercury (II) in Amazon soils from column studies. *Chemosphere* 60, 1583–1589

**MONPERRUS, M., KRUPP, E., AMOUROUX, D., DONARD, O.F.X., RODRIGUEZ MARTIN-DOIMEADIOS, R.C.** (2004) Potential and limits of speciated isotope-dilution analysis for metrology and assessing environmental reactivity. *Trends in Analytical Chemistry* 23, 261–272

**MONPERRUS, M., TESSIER, E., POINT, D., VIDIMOVA, K., AMOUROUX, D., GUYONEAUD, R., LEYNAERT, A., GRALL, J., CHAUVAUD, L., THOUZEAU, G., DONARD, O.F.X.** (2007) The biogeochemistry of mercury at the sediment–water interface in the Thau Lagoon. 2. Evaluation of mercury methylation potential in both surface sediment and the water column. *Estuarine Coastal and Shelf Science* 72, 485–496

**MONTES-BAYÓN, M., DeNICOLA, K., CARUSO, J.A.** (2003) Liquid chromatography–inductively coupled plasma mass spectrometry. *Journal of Chromatography* 1000, 457–476

**MORAES, P. M., SANTOS, F. A., CAVECCI, B., PADILHA, C. C.F., VIEIRA, J. C. S., ROLDAN, P. S., PADILHA, P. M.** (2013) GFAAS determination of mercury in muscle samples of fish from Amazon, Brazil. *Food Chemistry* 141, 2614–2617

**MOREDA-PIÑEIRO, A., BERMEJO-BARRERA, A., BERMEJO-BARRERA, P.** (2004) New trends involving the use of ultrasound energy for the extraction of humic substances from marine sediments. *Analytica Chimica Acta* 524, 97–107

**MORITA, M., YOSHINAGA, J., EDMONDS, J.S.** (1998) The determination of mercury species in environmental and biological samples. *Pure and Applied Chemistry* 70(8), 1585–1615

**MORRISON, R.T., BOYD, R.N.** (1983) *Organic Chemistry*. USA: Allyn and Bacon

**MOSCOSO-PÉREZ, C., MOREDA-PIÑEIRO, J., LÓPEZ-MAHÍA, P., MUNIATEGUI-LORENZO, S., FERNÁNDEZ-FERNÁNDEZ, E., PRADA-RODRÍGUEZ, D.** (2004) Hydride generation atomic fluorescence spectrometric determination of As, Bi, Sb, Se(IV) and Te(IV) in

aqua regia extracts from atmospheric particulate matter using multivariate optimization. *Analytica Chimica Acta* 526, 185–192

**MUYA, F. N., PHELANE, L., BAKER, P.G. L., IWUOHA, E. I.** (2014) Synthesis and Characterization of Polysulfone Hydrogels. *Journal of Surface Engineered and Advanced Technology* 4, 227-236

**MUYA, F. N., SUNDAY, C. E., BAKER, P., IWUOHA, E.** (2016) Environmental remediation of heavy metal ions from aqueous solutions through hydrogel adsorption: a critical review. *Water science and technology* 73(5), 983-992

**MYERS, G.J., DAVIDSON, P.W., COX, C., SHAMLAYE, C., CERNICHIARI, E., CLARKSON, T.W.** (2000) Twenty-seven years studying the human neurotoxicity of methylmercury exposure. Paper presented at 'Mercury as a Global Pollutant': 5<sup>th</sup> International Conference, Rio de Janeiro (Brazil), May 23–28; *Environmental Research* 83, 275–285

**NAHMANI, J., HODSON, M.E., BLACK, S.** (2007) A review of studies performed to assess metal uptake by earthworms. *Environmental Pollution* 145, 402–424

**NAVARRO, P., RAPOSO, J.C., ARANA, G., ETXEBARRIA, N.** (2006) Optimisation of microwave assisted digestion of sediments and determination of Sn and Hg. *Analytica Chimica Acta* 566, 37–44

**NEVADO, J.J.B., MARTÍN-DOIMEADIOS, R.C.R., BERNARDO, F.J.G., MORENO, M.J.** (2005) Determination of mercury species in fish reference materials by gas chromatography-atomic fluorescence detection after closed-vessel microwave-assisted extraction. *Journal of Chromatography* 1093, 21–28

**ODIN, M., RIBEYRE, F., BOUDOU, A.** (1997) Depuration processes after exposure of burrowing mayfly nymphs (*hexagenia rigida*) to methylmercury and cadmium from water column or sediment: effects of temperature and pH. *Aquatic Toxicology* 37, 125–137

**OOSTHUIZEN, J., EHRLICH, R.** (2001) The impact of pollution from a mercury processing plant in KwaZulu-Natal, South Africa, on the health of fishing-eating communities in the area: an environmental health risk assessment. *International Journal of Environmental Health Research* 11, 41–50



**OOSTHUIZEN, M.A., JOHN, J., SOMERSET, V.** (2010) Mercury exposure in a low-income community in South Africa. *South African Medical Journal* 100, 366–371

**PACYNA, J. M., PACYNA, E. G., STEENHUISEN, F., WILSON, S.** (2003) Mapping 1995 global anthropogenic emissions of mercury. *Atmospheric Environment* 37 (Suppl 1), 109–117

**PACYNA, E.G., PACYNA, J.M., FUDALA, J., STRZELECKA-JASTRZAB, E., HLAWICZKA, S., PANASIUK, D.** (2006) Mercury emissions to the atmosphere from anthropogenic sources in Europe in 2000 and their scenarios until 2020. *Science of The Total Environment* 370, 147–156

**PACYNA, E.G., PACYNA, J.M., SUNDSETH, K., MUNTHE, J., KINDBOM, K., WILSON, S., STEENHUISEN, F., MAXSON, P.** (2010) Global emission of mercury to the atmosphere from anthropogenic sources in 2005 and projections to 2020. *Atmospheric Environment* 44, 2487–2499

**PAGER, CS., GASPER, A.** (2002) Possibilities of determination of mercury compounds using capillary zone electrophoresis. *Microchemical Journal* 73, 53–58

**PAPU-ZAMXAKA, V., MATHEE, A., HARPHAM, T., BARNES, B., RÖLLIN, H., LYONS, M., JORDAAN, W., CLOETE, M.** (2010) Elevated mercury exposure in communities living alongside the Inanda Dam, South Africa. *Journal of Environmental Monitoring* 12, 472–477

**PAPU-ZAMXAKA, V., HARPHAM, T., MATHEE, A.** (2010) Environmental legislation and contamination: The gap between theory and reality in South Africa. *Journal of Environmental Management* 91, 2275–2280

**PARKER, J. I., BLOOM, N.S.** (2005) Preservation and storage techniques for low-level aqueous mercury speciation. *Science of the Total Environment* 337, 253–263

**PATNAIK, P.** (2004) *Dean's Analytical Chemistry Handbook*. Boston: McGraw-Hill

**PONE, J.D.N., HEIN, K.A.A., STRACHER, G. B., ANNEGARN, H.J., FINKLEMAN, R.B., BLAKE, D.R., McCORMACK, J.K., SCHROEDER, P.** (2007) The spontaneous combustion of coal and its by-products in the Witbank and Sasolburg coalfields of South Africa. *International Journal of Coal Geology* 72, 124–140

**POOLE, C.F., SCHUETTE, S.A.** (1984) *Contemporary Practice of Chromatography*. Amsterdam: Elsevier Science.

**Ph. QUEVAUVILLER.** (1999) Certification of methylmercury in sediments: from controversial facts to scientific evidence. *Chemosphere* 39, 1153–1165

**PRIYADARSHINI, E., PRADHAN, N.** (2017) Gold nanoparticles as efficient sensors in colorimetric detection of toxic metal ions: A review. *Sensors and Actuators B: Chemical* 238, 888-902

**QUINTANA, M., KLOUDA, A.D., GONDIKAS, A., OCHSENKÜHN-PETROPOULOU, M., MICHALKE, B.** (2006) Analysis of size characterized manganese species from liver extracts using capillary zone electrophoresis coupled to inductively coupled plasma mass spectrometry. *Analytica Chimica Acta* 573/4, 172–180

**RABENSTEIN D.L.** (1978) The chemistry of methylmercury toxicology. *Journal of Chemical Education* 55, 291–296

**RAPSOMANIKIS, S., CRAIG, P.J.** (1991) Speciation of mercury and methylmercury compounds in aqueous samples by chromatography-atomic absorption spectrometry after ethylation with sodium tetraethylborate. *Analytica Chimica Acta* 248, 563–567

**RASHED, M.N.** (2010) Monitoring of contaminated toxic and heavy metals, from mine tailings through age accumulation, in soil and some wild plants at Southeast Egypt. *Journal of Hazardous Materials* 178, 739–746

**RODRÍGUEZ MARTÍN-DOIMEADIOS, R.C., TESSIER, E., AMOUROUX, D., GUYONEAUD, R., DURAN, R., CAUMETTE, P., DONARD, O.F.X.** (2004) Mercury methylation/demethylation and volatilization pathways in estuarine sediment slurries using species-specific enriched stable isotopes. *Marine Chemistry* 90, 107–123

**RUBINSON, J.F., RUBINSON, K.A.** (1998) *Contemporary Chemical Analysis*. New Jersey: Prentice Hall

**SÁNCHEZ, D.M., MARTIN, R., MORANTE, R., MARÍN, J., MUNUERA, M.L.** (2000) Preconcentration speciation method for mercury compounds in water samples using solid phase extraction followed by reversed phase high performance liquid chromatography. *Talanta* 52, 671–679

**SANTOYO, M.M., FLORES, C.R., TORRES, A.L., WROBEL, K., WROBEL, K.** (2011) Global DNA methylation in earthworms: A candidate biomarker of epigenetic risks related to the presence of metals/metalloids in terrestrial environments. *Environmental Pollution* 159, 2387–2392

**SCHNITZER, M., KHAN, S.U.** (1978) *Soil Organic Matter*. Volume 8. Amsterdam: Elsevier Science

**SCHUSTER, E.** (1991) The behaviour of mercury in the soil with special emphasis on complexation and adsorption processes. A review of the literature. *Water, Air and Soil Pollution* 56, 667–680

**SERUDO, R.L., de OLIVEIRA, L.C., ROCHA, J.C., PATERLINI, W.C., ROSA, A.H., da SILVA, H.C., BOTERO, W.G.** (2007) Reduction capability of soil humic substances from the Rio Negro basin, Brazil, towards Hg(II) studied by a multimethod approach and principal component analysis (PCA). *Geoderma* 10, 1016–1020

**SIMON, O., BOUDOU, A.** (2001) Direct and trophic contamination of the herbivorous carp *Ctenopharyngodon idella* by inorganic mercury and methylmercury. *Ecotoxicology and Environmental Safety* 50, 48–59

**SIZMUR, T., HODSON, M.E.**, (2009) Do earthworms impact metal mobility and availability in soil? - A review. *Environmental Pollution* 157, 1981-1989

**SJÖBLOM, Å., MEILI, M., SUNDBOM, M.** (2000) The influence of humic substances in the speciation and bioavailability of dissolved mercury and methylmercury, measured as uptake by *Chaoborus larvae* and loss by volatilization. *Science of The Total Environment* 261, 115–124

**SKOOG, D.A., WEST, D.M., HOLLER, F.J., CROUCH, S.R.**, (2004) *Fundamentals of Analytical Chemistry*. USA: Brooks/Cole, Cengage Learning

**SKYLLBERG, U., BLOOM, P.R., QIAN, J., LIN, C., BLEAM, W.F.** (2006) Complexation of mercury(II) in soil organic matter: EXAFS evidence for linear two-coordination with reduced sulphur groups. *Environmental Science and Technology* 40, 4174–4180

**SOBRI, S., ROY, S., KALMAN, E., NAGYP, P., LAKATOS, M.** (2008) Growth of gold particles on glassy carbon from a thiosulphate –sulphite aged electrolyte. *Pertanika Journal of Science and Technology* 16 (1), 41 -48

**SPIRO, T.G., STIGLIANI, W.M.** (1996) *Chemistry of the Environment*. New York: Prentice Hall

**STEENBERGEN, N.T.T.M., IACCINO, F., DE WINKEL, M., REIJNDERS, L., PEIJNENBURG, W.J.G.M.** (2005) Development of a biotic ligand model and a regression model predicting acute copper toxicity to the earthworm *Aporrectodea caliginosa*. *Environmental Science and Technology* 39, 5694–5702

**STOICHEV, T., MARTIN-DOIMEADIOS, R.C.R., TESSIER, E., AMOUROUX, D., DONARD, O.F.X.** (2004) Improvement of analytical performances for mercury speciation by on-line derivatization, cryofocussing and atomic fluorescence spectrometry. *Talanta* 62, 433–438

**STOICHEV, T., AMOUROUX, D., MARTIN-DOIMEADIOS, R.C.R., MONPERRUS, M., DONARD, O.F.X., TSALEV, D.L.** (2006) Speciation analysis of mercury in aquatic environment. *Applied Spectroscopy Reviews* 41, 591–619

**SUNDA, W.G., HUNTSMAN, S.A.** (1998) Processes regulating cellular metal accumulation and physiological effects: phytoplankton as model systems. *Science of The Total Environment* 219, 165–181

**TIPPING, E.** (2004) *Cation binding by humic substances*. Cambridge Environmental Chemistry Series. Cambridge: Cambridge University Press

**TIPPING, E.** (2007) Modelling the interactions of Hg(II) and methylmercury with humic substances using WHAM/Model VI. *Applied Geochemistry* 22, 1624-1635

**ULLRICH, S.M., TANTON, T.W., ABDRAHITOVA, S.A.** (2001) Mercury in the aquatic environment: a review of factors affecting methylation. *Critical Reviews in Environmental Science and Technology* 31, 241–293

**VAN NIEKERK, H.J., VILJOEN, M.J.** (2005) Causes and consequences of the Merriespruit and other tailings-dam failures. *Land Degradation and Development* 16, 201–212

**VAN WIJNGAARDEN, E., BECK, C., SHAMLAYE, C.F., CERNICHIARI, E., DAVIDSON, P.W., MYERS, G.J., CLARKSON, T.W.** (2006) Benchmark concentrations for methyl mercury

obtained from the 9-year follow-up of the 'Seychelles Child Development Study'. *NeuroToxicology* 27, 702–709

**VEIGA, M.M., HINTON, J., LILLY, C.** (1999) Mercury in the Amazon: a comprehensive review with special emphasis on bioaccumulation and bioindicators. Proc. NIMD (National Institute for Minamata Disease) Forum 99, Minamata, Japan

**WAGNER, N.J., HLATSHWAYO, B.** (2005) The occurrence of potentially hazardous trace elements in five Highveld coals, South Africa. *International Journal of Coal Geology* 63, 228–246

**WALCARIUS, A., MATHIEU, E., DELACOTE, C.** (2004) Uptake of inorganic Hg(II) by organically modified silicates: influence of pH and chloride concentration on the binding pathways and electrochemical monitoring of the processes. *Analytica Chimica Acta* 508, 87–98

**WATRAS, C.J., BACK, R.C., HALVORSEN, S., HUDSON, R.J.M., MORRISON, K.A., WENTE, S.P.** (1998) Bioaccumulation of mercury in pelagic freshwater food webs. *Science of The Total Environment* 219, 183–208

**WESTÖÖ, G.** (1967) Determination of methylmercury in fish, egg, meat, and liver. *Journal Acta Chemica Scandinavia* 21, 1790–1800

**WHALIN, L., KIM, E., MASON, R.** (2007) Factors influencing the oxidation, reduction, methylation and demethylation of mercury species in coastal waters. *Marine Chemistry* 107, 278–294

**WILSON, S.J., STEENHUISEN, F., PACYNA, J.M., PACYNA, E.G.** (2006) Mapping the spatial distribution of global anthropogenic mercury atmospheric emission inventories. *Atmospheric Environment* 40, 4621–4632

**WU, F. C., EVANS, R. D., DILLON, P.J., CAI, Y.R.** (2007) Rapid quantification of humic and fulvic acids by HPLC in natural waters. *Applied Geochemistry* 22, 1598–1605

**YANG, Y., ZHANG, C., SHI, X., LIN, T., WANG, D.** (2007) Effect of organic matter and pH on mercury release from soils. *Journal of Environmental Sciences* 19, 1349–1354

## APPENDIX A

### WATER EXPOSURE: COMPLEXATION OF $\text{Hg}^{2+}$ WITH HA IN AQUEOUS PHASE MONITORED OVER 72 hr AT 293.15 K, 298.15 K AND 303.15 K

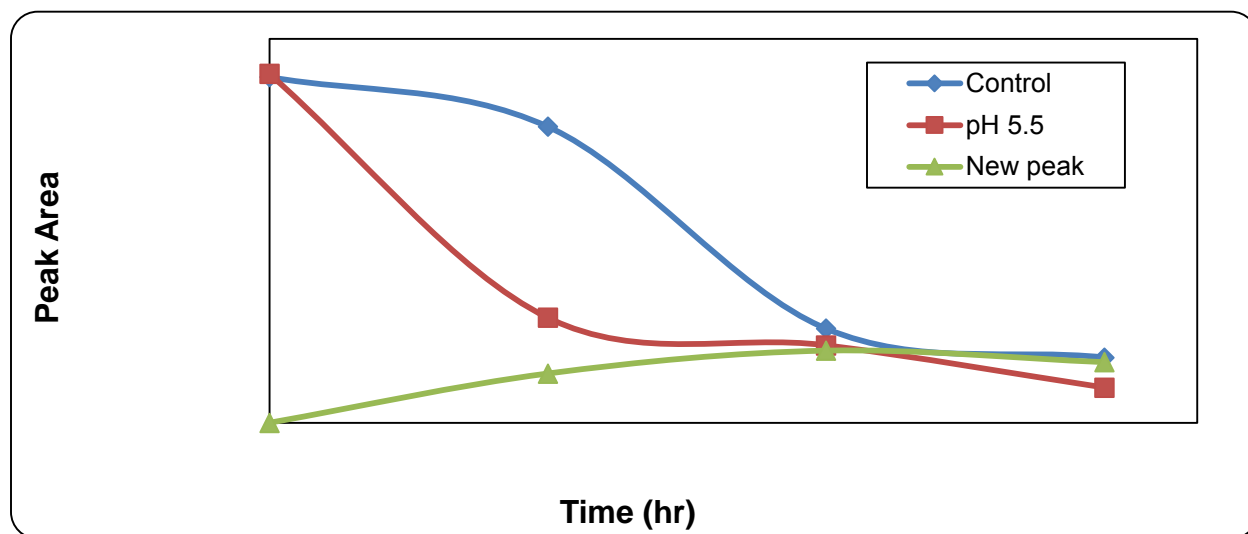


Figure A.1 Complexation of  $\text{Hg}^{2+}$  with HA at pH 5.5 at 293.15 K.

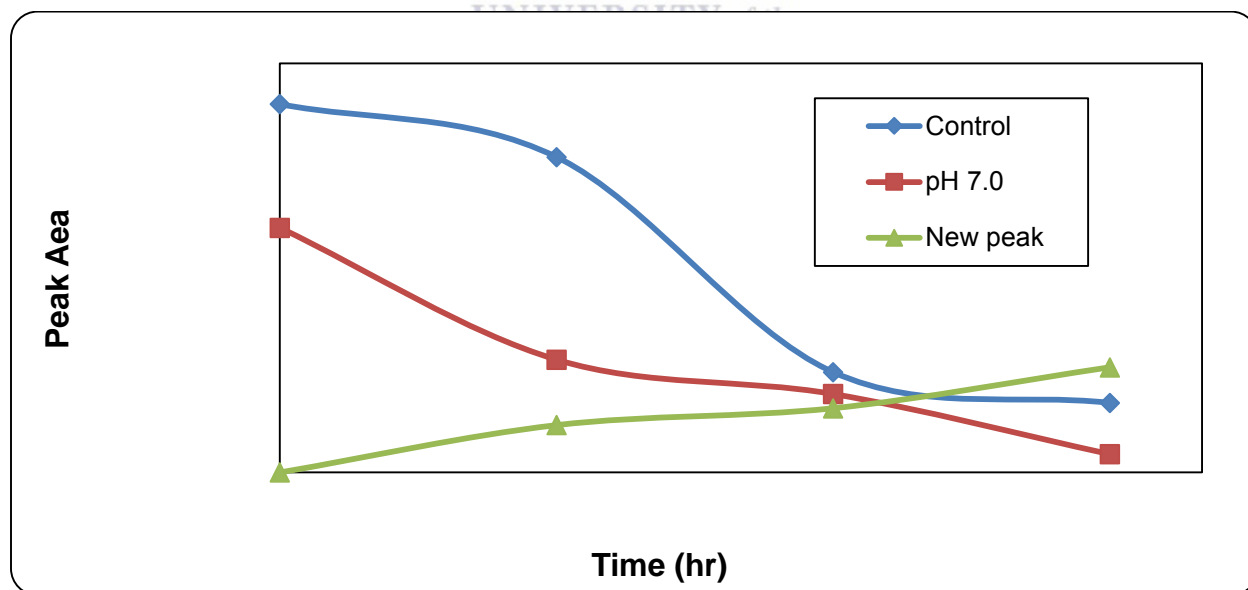


Figure A.2 Complexation of  $\text{Hg}^{2+}$  with HA at pH 7.0 at 293.15 K.

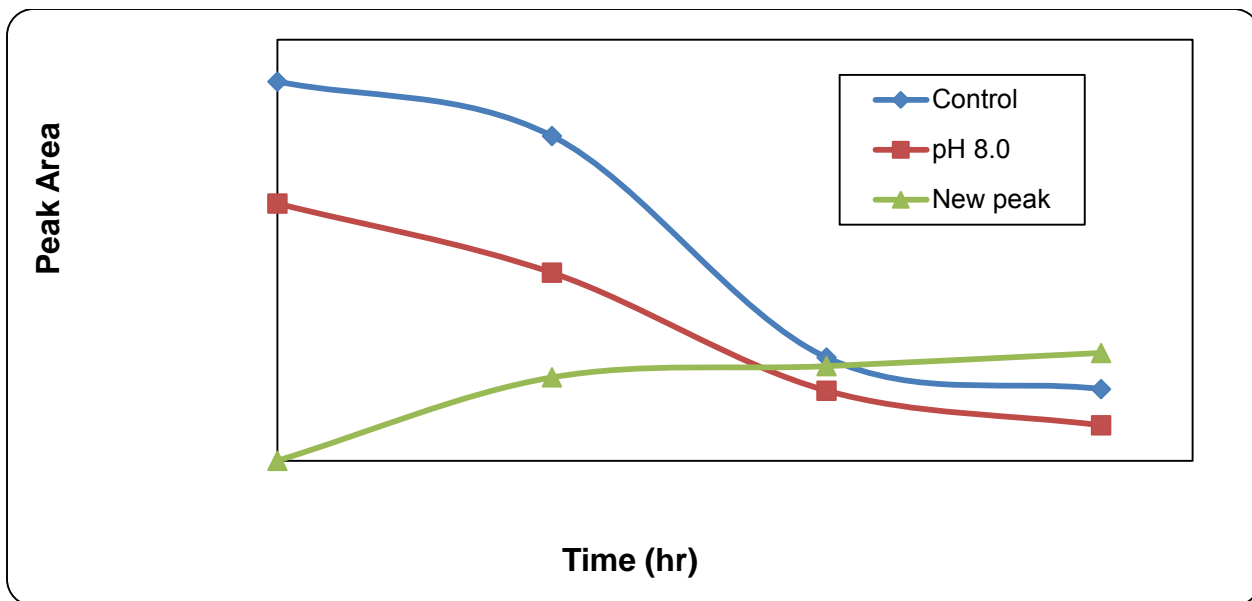


Figure A.3 Complexation of  $\text{Hg}^{2+}$  with HA at pH 8.0 at 293.15 K.

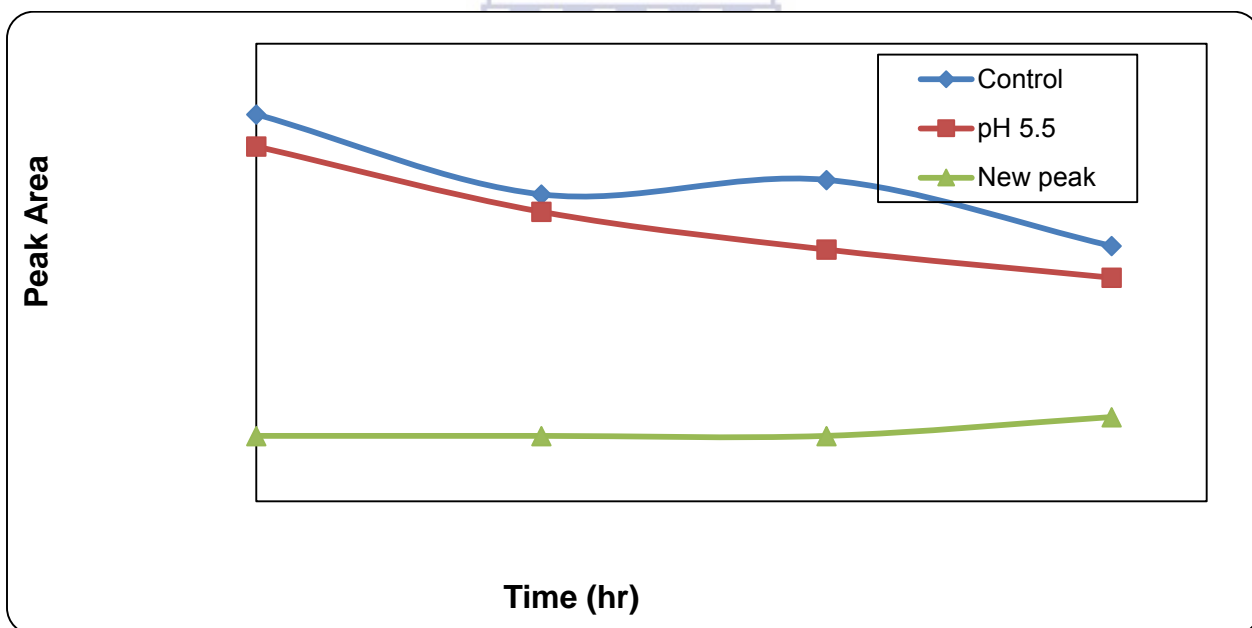


Figure A.4 Complexation of  $\text{Hg}^{2+}$  with HA at pH 5.5 at 298.15 K.

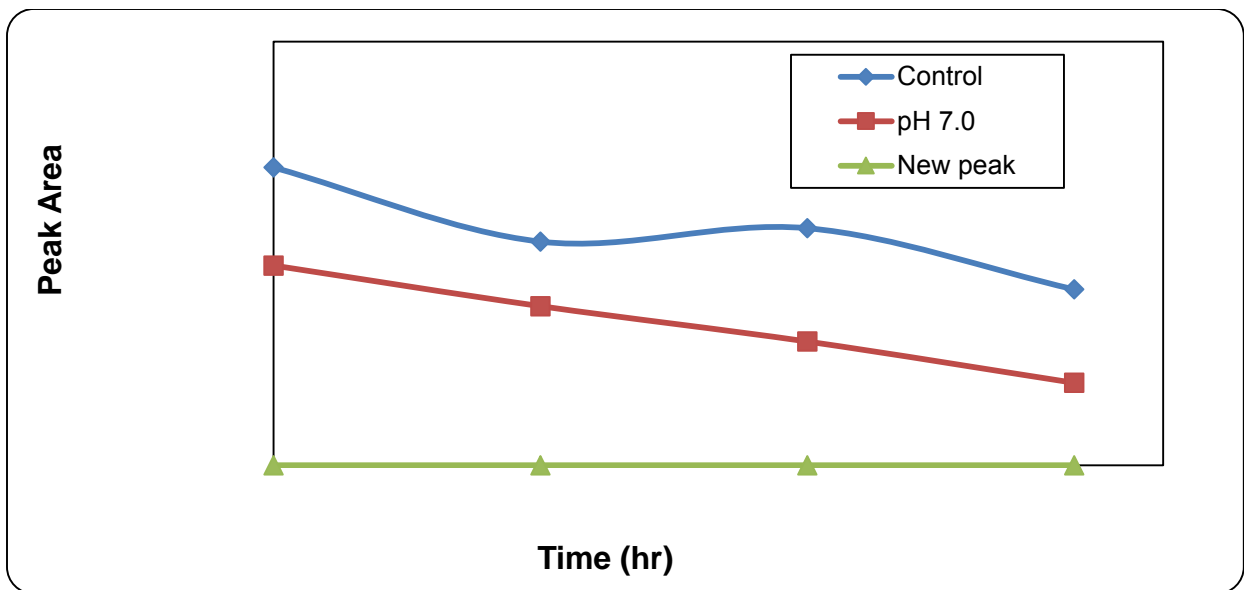


Figure A.5 Complexation of  $\text{Hg}^{2+}$  with HA at pH 7.0 at 298.15 K.

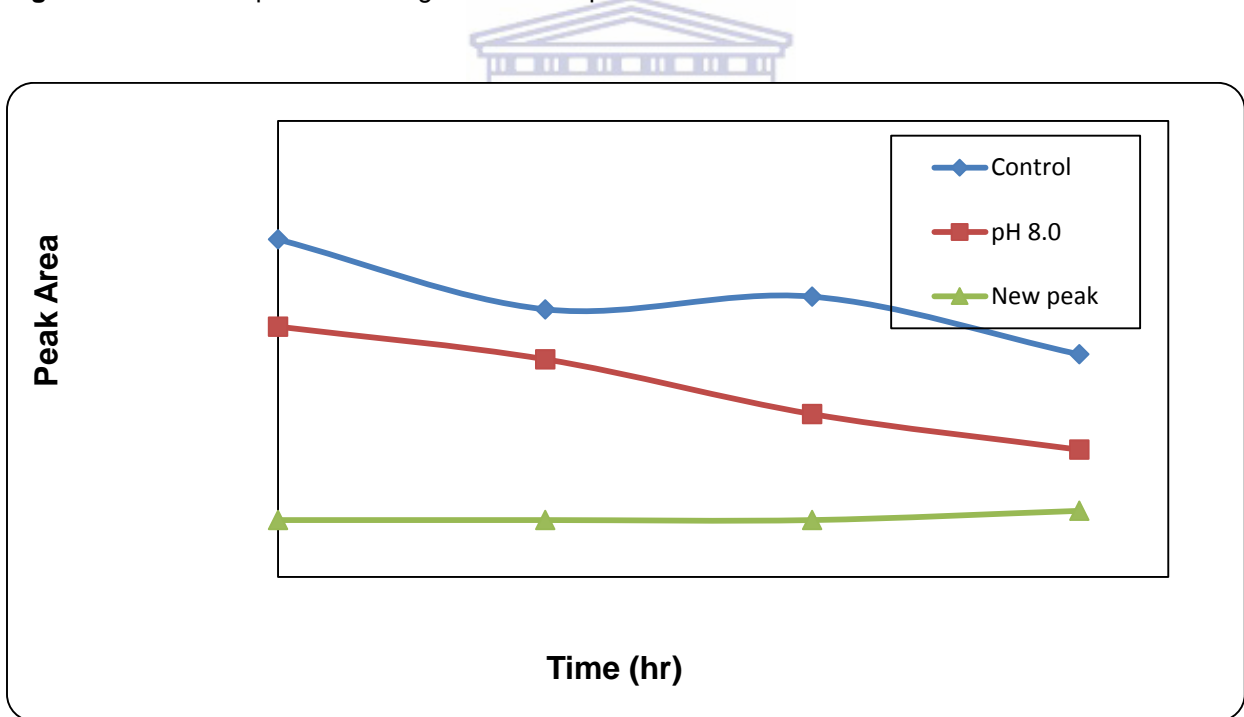


Figure A.6 Complexation of  $\text{Hg}^{2+}$  with HA at pH 8.0 at 298.15 K.



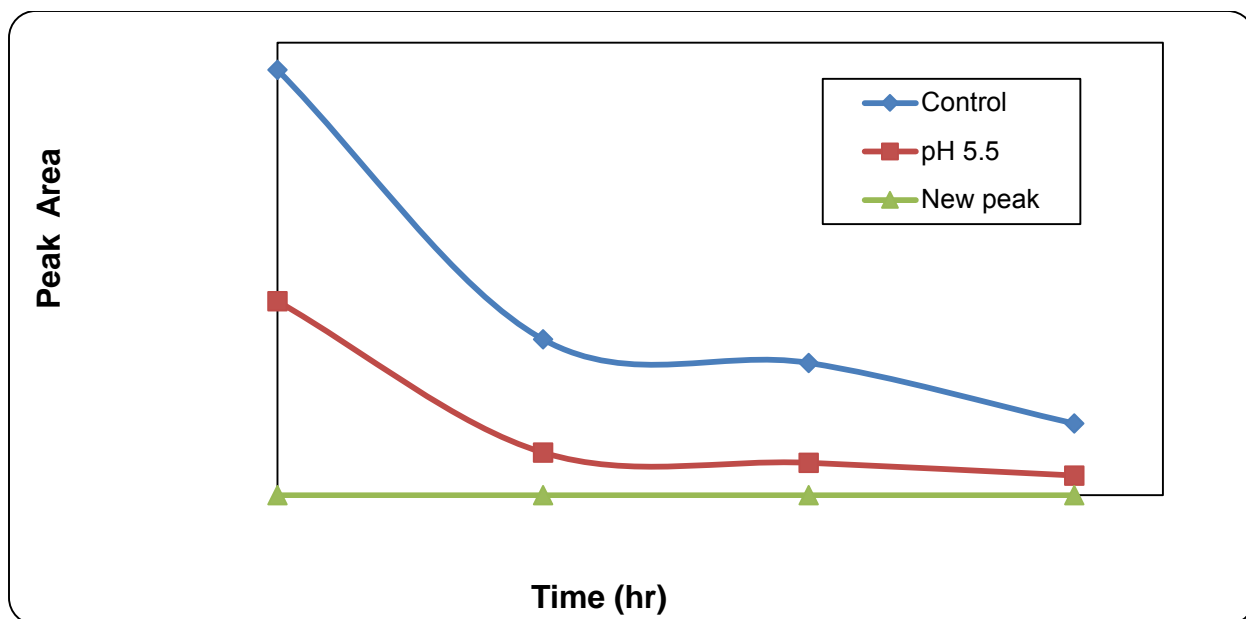


Figure A.7 Complexation of  $\text{Hg}^{2+}$  with HA at pH 5.5 at 303.15 K.

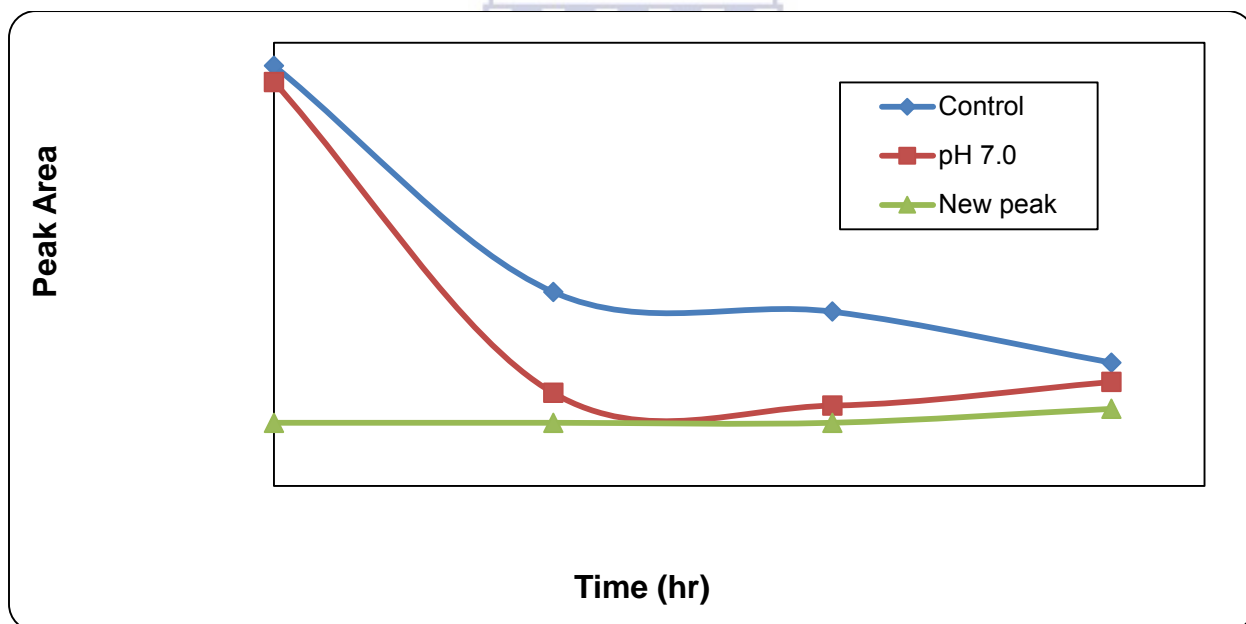


Figure A.8 Complexation of  $\text{Hg}^{2+}$  with HA at pH 7.0 at 303.15 K.

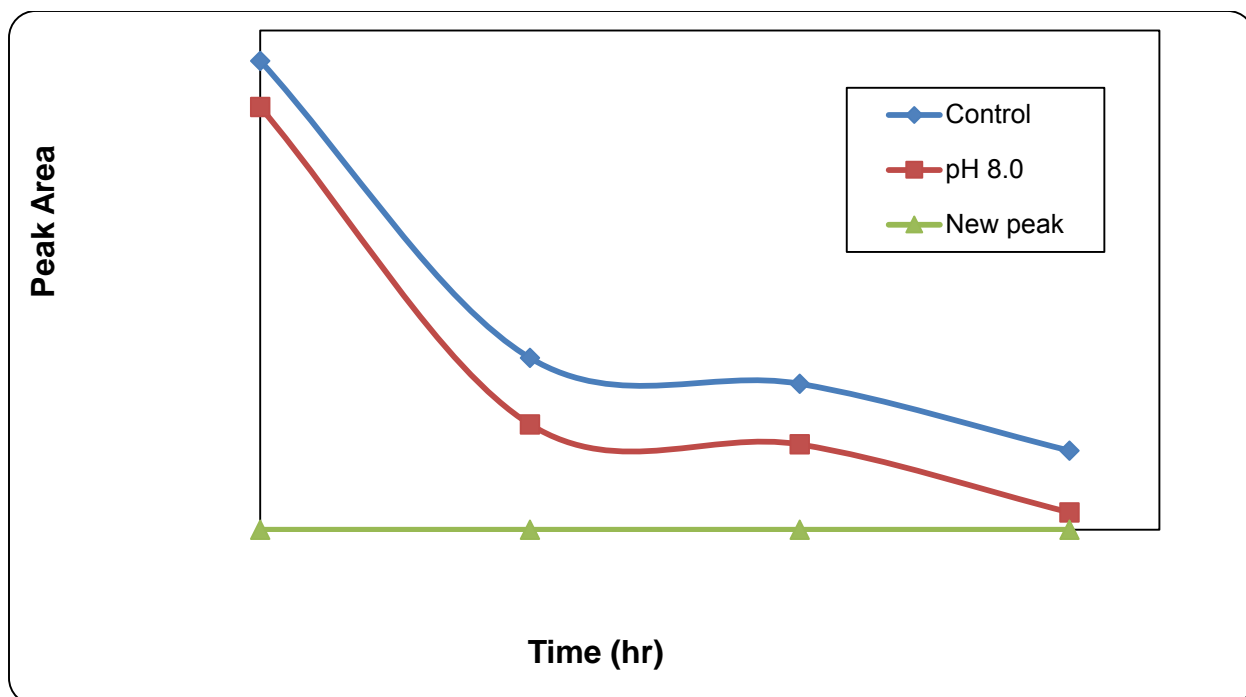


Figure A.9 Complexation of  $\text{Hg}^{2+}$  with HA at pH 8.0 at 303.15 K.

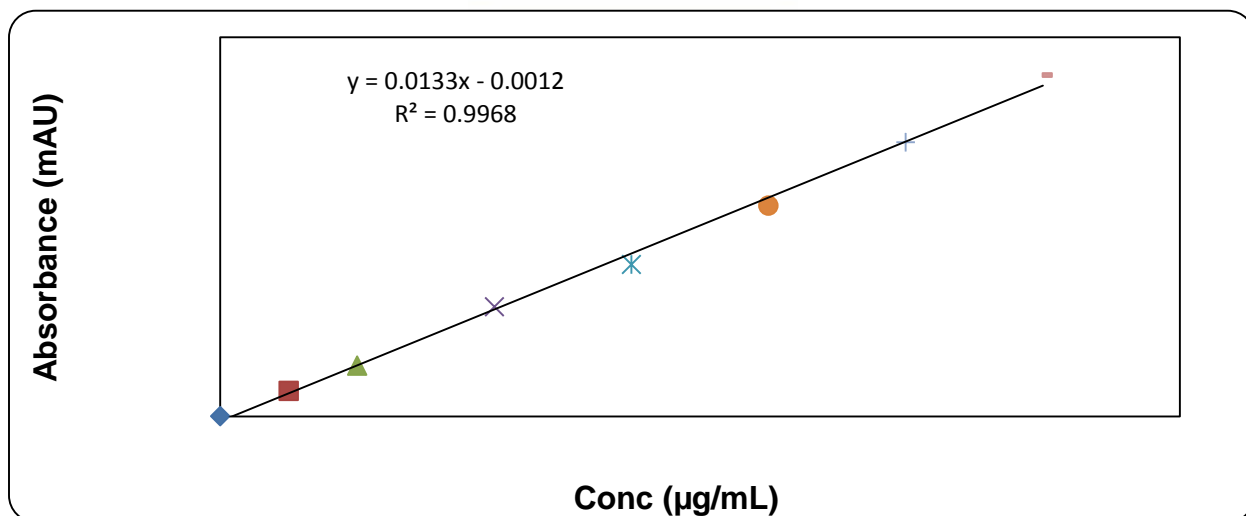


Figure A.10 Calibration curve of  $\text{Hg}^{2+}$  determined with hydride generation method.

**Table A. 1** Results of the calibration curve of Hg<sup>2+</sup> determined with hydride generation method

Number of standards	Concentration (µg/mL)	Absorbance (mAU)
1	0.0	0.001
2	0.5	0.006
3	1	0.012
4	2	0.026
5	3	0.035
6	4	0.050
7	5	0.065
8	6	0.081



**Table A. 2** Results of the complexation of Hg<sup>2+</sup> with HA at 293.15 K obtained with hydride generation method

Sample	initial	1hr	2hr	3 hr	4 hr
Control	0.018	0.016	0.014	0.011	0.009
pH 5.5	0.012	0.012	0.010	0.006	0.005
pH 7.0	0.015	0.011	0.010	0.008	0.006
pH 8.0	0.016	0.011	0.010	0.008	0.005

**Table A. 3** Results of the complexation of  $\text{Hg}^{2+}$  with HA at 298.15 K obtained with hydride generation method

<b>Sample</b>	<b>initial</b>	<b>1hr</b>	<b>2 hr</b>	<b>3 hr</b>	<b>4 hr</b>	<b>5 hr</b>
Control	0.018	0.015	0.014	0.011	0.008	0.005
pH 5.5	0.015	0.014	0.012	0.010	0.008	0.005
pH 7.0	0.016	0.013	0.011	0.009	0.006	0.006
pH 8.0	0.017	0.015	0.011	0.007	0.004	0.007

**Table A. 4** Results of the complexation of  $\text{Hg}^{2+}$  with HA at 303.15 K obtained with hydride generation method

<b>Sample</b>	<b>initial</b>	<b>1hr</b>	<b>2hr</b>	<b>3 hr</b>	<b>4 hr</b>	<b>5 hr</b>
Control	0.018	0.015	0.012	0.008	0.006	0.002
pH 5.5	0.015	0.011	0.008	0.005	0.004	0.001
pH 7.0	0.012	0.007	0.005	0.005	0.001	0.001
pH 8.0	0.014	0.008	0.006	0.005	0.002	0.001

UNIVERSITY of the  
WESTERN CAPE

## APPENDIX B

### WATER AND SOIL EXPOSURE: COMPLEXATION OF Hg<sup>2+</sup> WITH HA IN AQUEOUS PHASE AND SOIL MONITORED OVER 48 hr AT 298.15 K

**Table B.1** Data of the complexation of Hg<sup>2+</sup> with HA in aqueous phase at 298.15 K

Time (hr)	Control (Hg <sup>2+</sup> )/μg/mL	Hg <sup>2+</sup> and HA at a salinity of 35 μg/mL and pH 5.5	Hg <sup>2+</sup> and HA at a salinity of 35 μg/mL and pH 7.0	Hg <sup>2+</sup> and HA at a salinity of 35 μg/mL and pH 8.0
0	4.31	4.60	4.71	4.50
1	4.05	3.30	3.80	3.70
4	3.40	3.05	3.39	3.50
24	3.20	3.30	3.10	3.10
28	2.05	1.60	1.60	1.80

**Table B.2** Data of the complexation of Hg<sup>2+</sup> with HA in the soil samples at 298.15 K

Time (hr)	Control (Hg <sup>2+</sup> )/μg/g	Hg <sup>2+</sup> and HA at a salinity of 35 μg/mL and pH 5.5	Hg <sup>2+</sup> and HA at a salinity of 35 μg/mL and pH 7.0	Hg <sup>2+</sup> and HA at a salinity of 35 μg/mL and pH 8.0
0	0.046	0.007	0.005	0.006
1	0.915	1.731	1.278	1.366
4	1.163	1.130	1.112	1.549
24	1.211	1.294	1.224	1.850
28	2.242	2.806	2.654	2.185

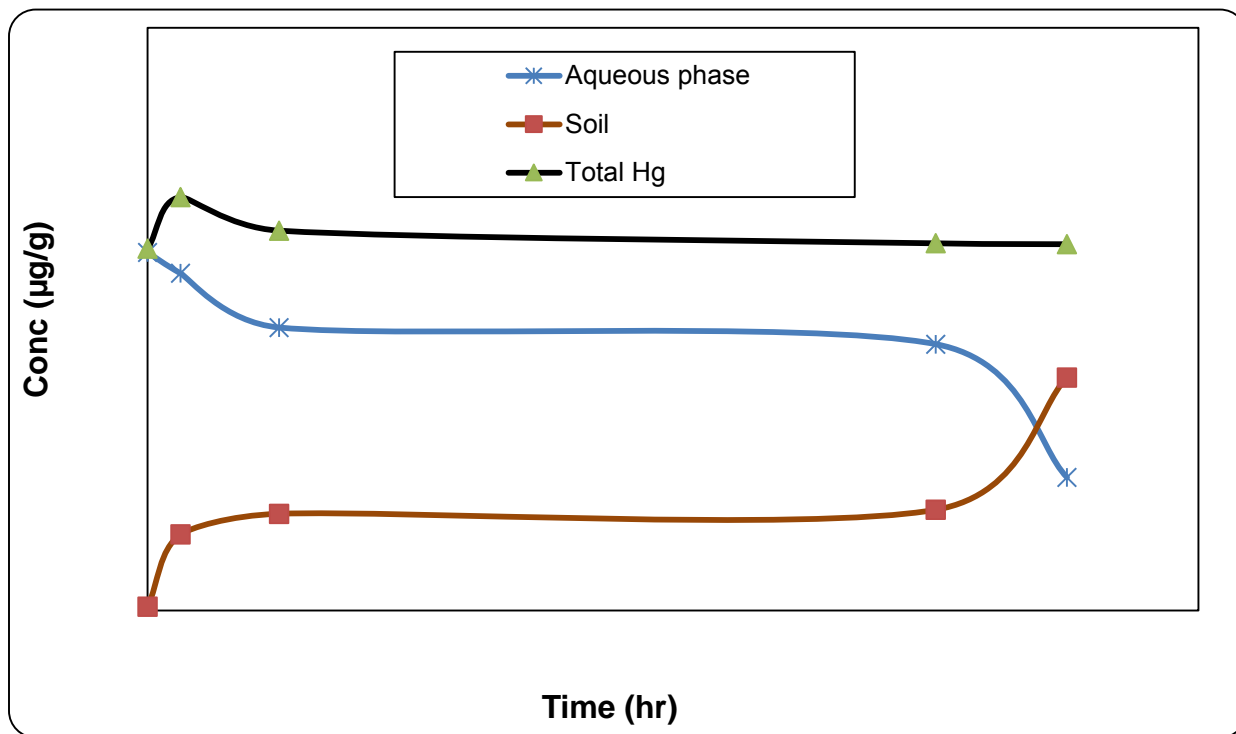


Figure B.1 Complexation of Hg<sup>2+</sup> with HA in aqueous phase and soil of the control at 298.15 K.

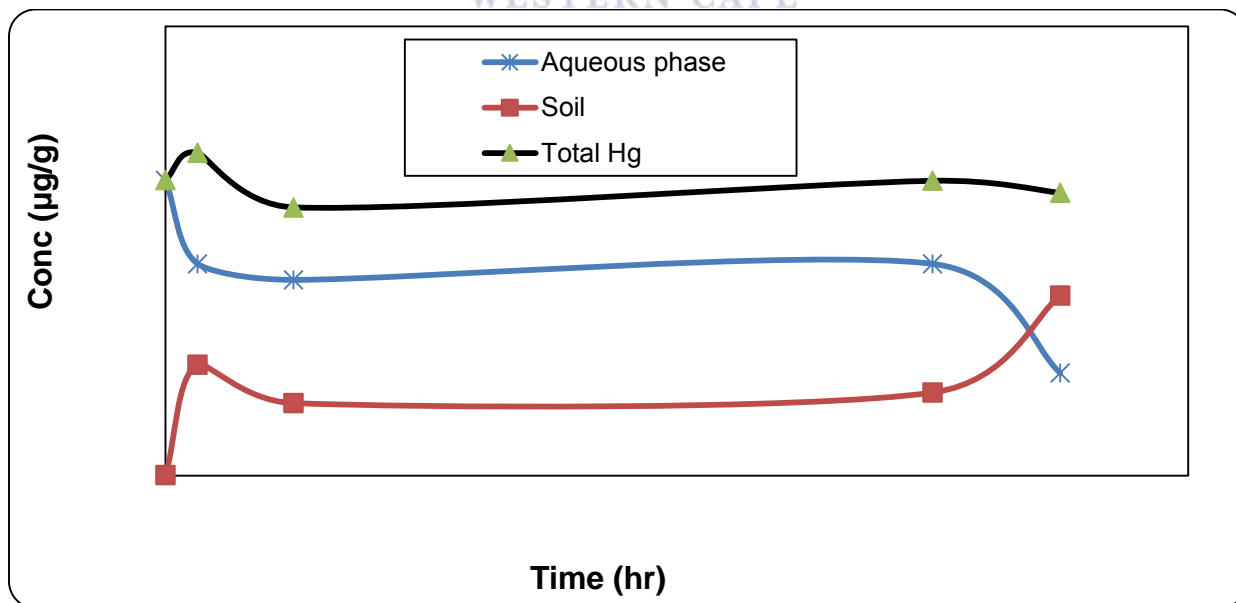


Figure B.2 Complexation of Hg<sup>2+</sup> with HA in aqueous phase and soil at pH 5.5 at 298.15 K.

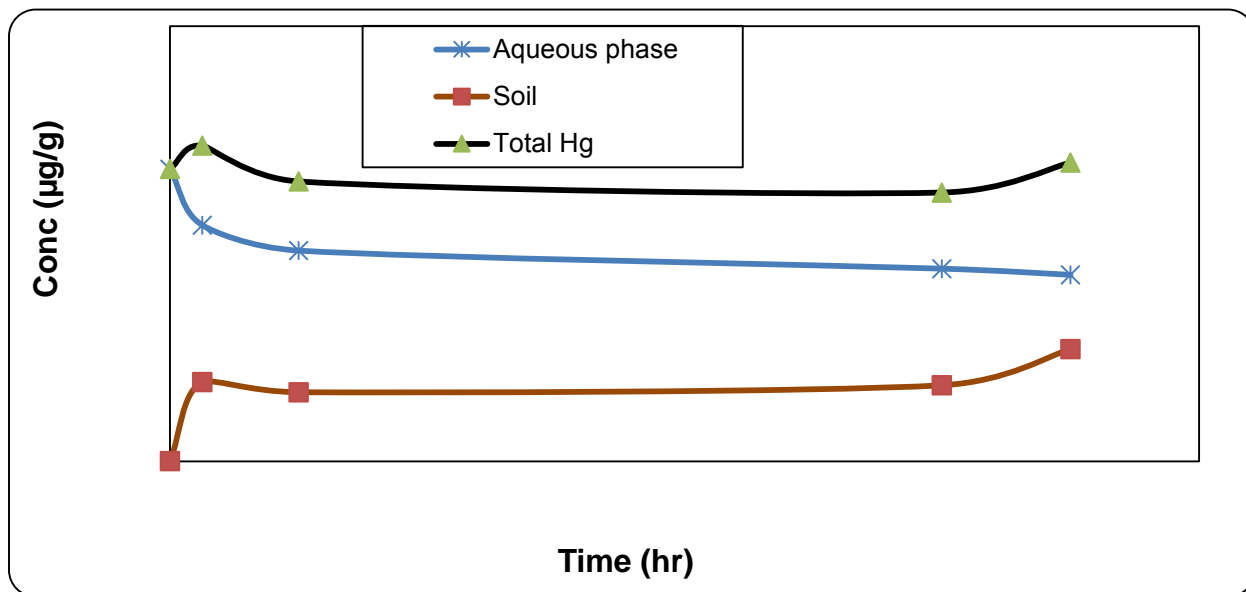


Figure B.3 Complexation of  $\text{Hg}^{2+}$  with HA in aqueous phase and soil at pH 7.0 at 298.15 K.

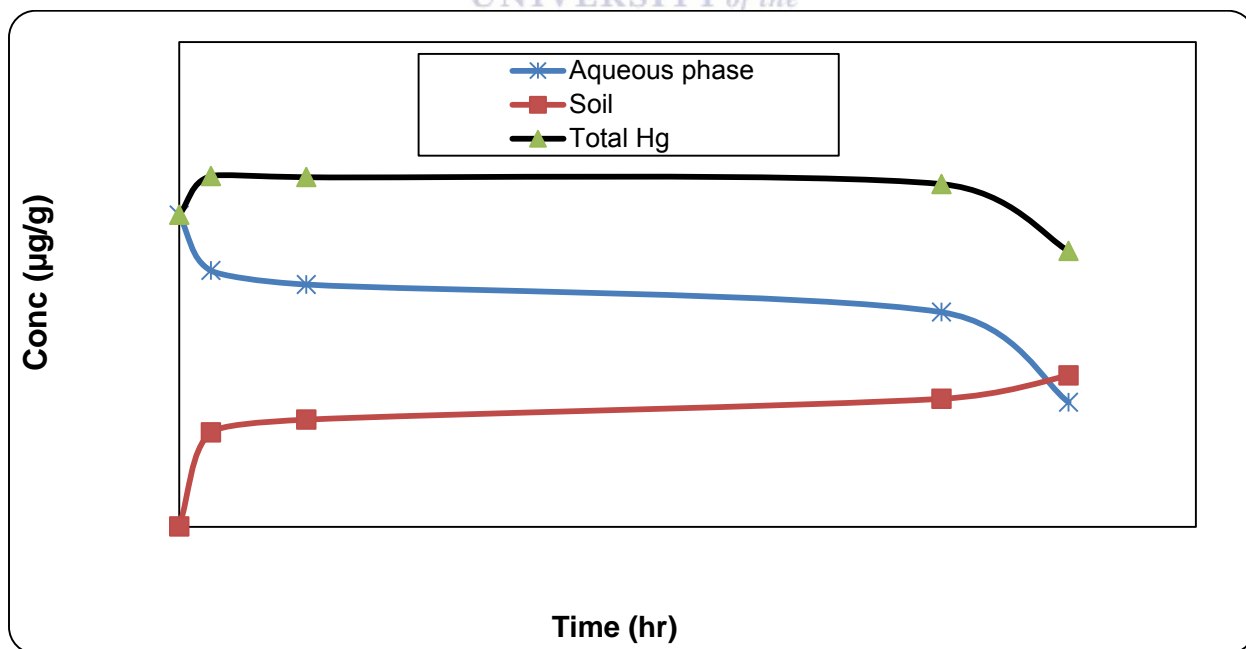
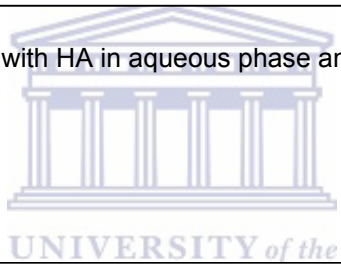


Figure B.4 Complexation of  $\text{Hg}^{2+}$  with HA in aqueous phase and soil at pH 8.0 at 298.15 K.

**Table B.3** Data of the complexation of Hg<sup>2+</sup> with HA in aqueous phase at 303.15 K

Time (hr)	Control (Hg <sup>2+</sup> )/ $\mu\text{g/mL}$	Hg <sup>2+</sup> and HA at a salinity of 35 $\mu\text{g/mL}$ and pH 5.5	Hg <sup>2+</sup> and HA at a salinity of 35 $\mu\text{g/mL}$ and pH 7.0	Hg <sup>2+</sup> and HA at a salinity of 35 $\mu\text{g/mL}$ and pH 8.0
0	4.47	3.95	3.71	3.21
1	3.45	3.25	2.71	2.32
4	2.65	2.75	2.32	1.62
24	1.21	1.92	0.98	0.56
28	0.75	0.85	0.82	0.73

**Table B.4** Data of the complexation of Hg<sup>2+</sup> with HA in the soil samples at 303.15 K

Time (hr)	Control (Hg <sup>2+</sup> )/ $\mu\text{g/g}$	Hg <sup>2+</sup> and HA at a salinity of 35 $\mu\text{g/mL}$ and pH 5.5	Hg <sup>2+</sup> and HA at a salinity of 35 $\mu\text{g/mL}$ and pH 7.0	Hg <sup>2+</sup> and HA at a salinity of 35 $\mu\text{g/mL}$ and pH 8.0
0	0.007	0.006	0.009	0.005
1	0.774	1.726	0.632	0.532
4	2.001	0.880	0.909	1.422
24	2.754	1.740	2.115	2.865
28	3.500	3.290	3.179	2.552



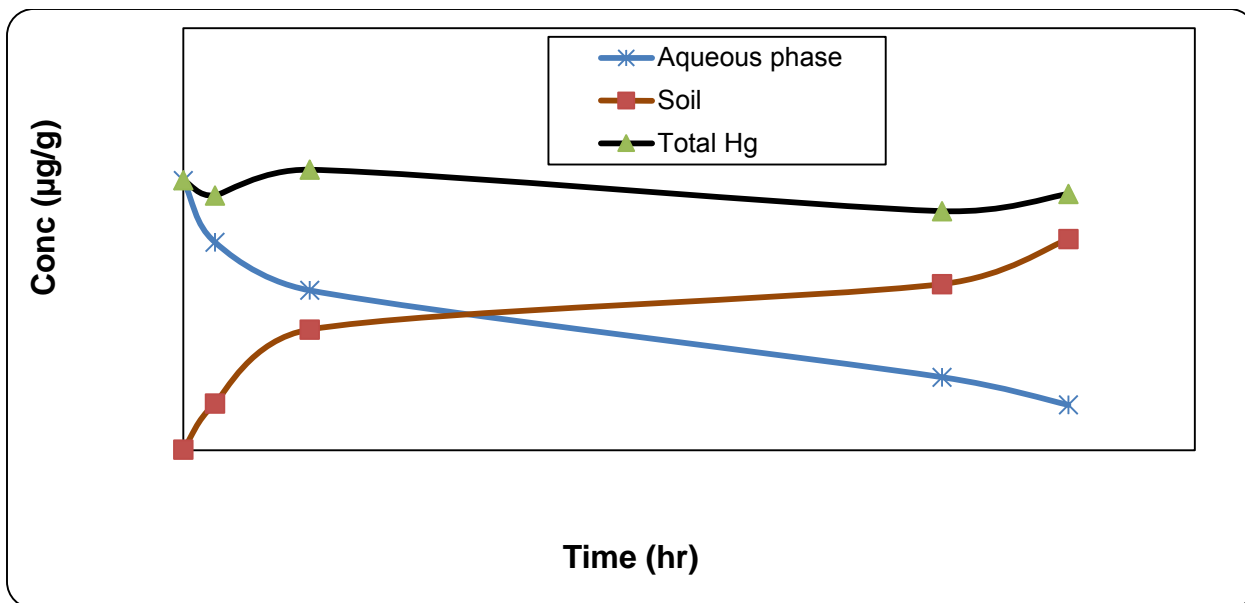


Figure B.5 Complexation of Hg<sup>2+</sup> with HA in aqueous phase and soil at the control at 303.15 K.

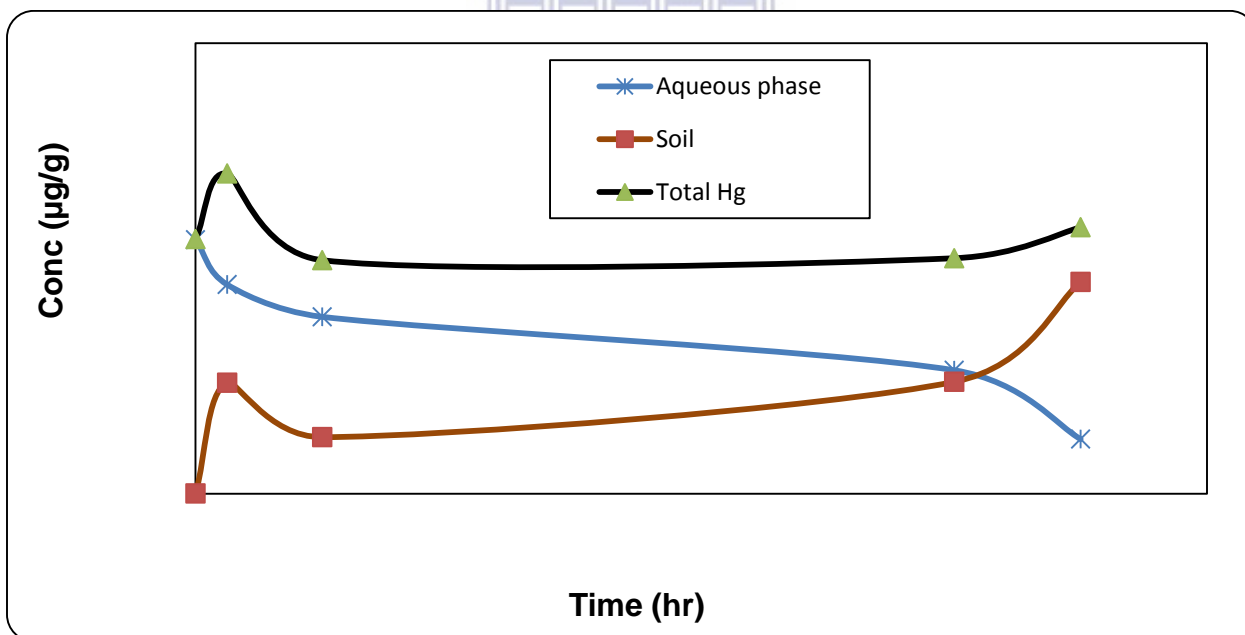


Figure B.6 Complexation of Hg<sup>2+</sup> with HA in aqueous phase and soil at pH 5.5 at 303.15 K.

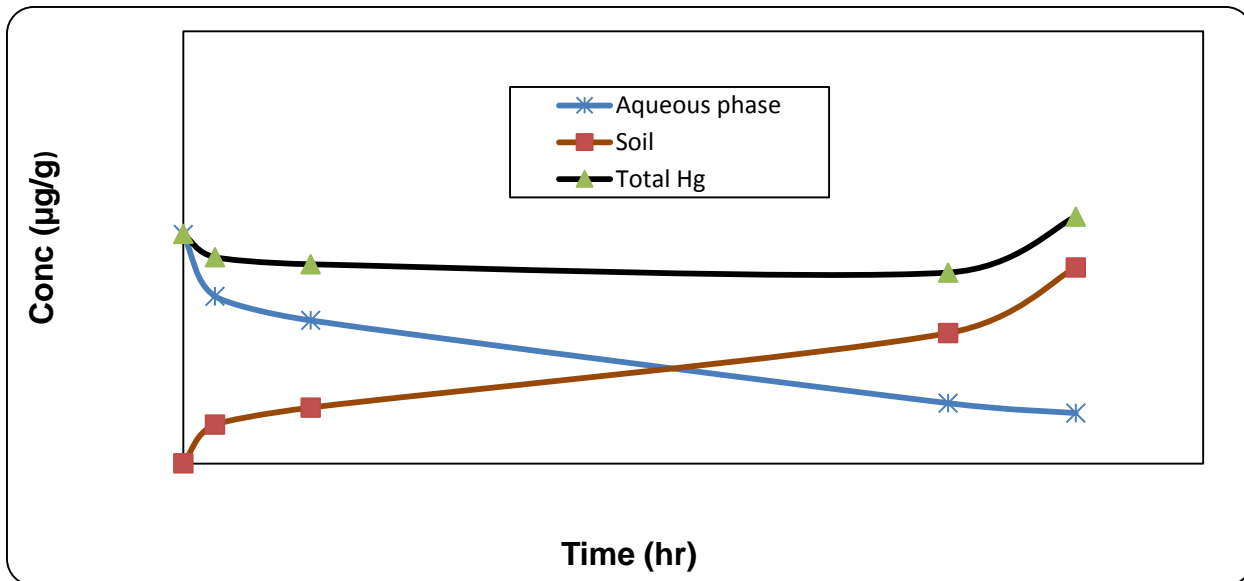


Figure B.7 Complexation of  $\text{Hg}^{2+}$  with HA in aqueous phase and soil at pH 7.0 at 303.15 K.

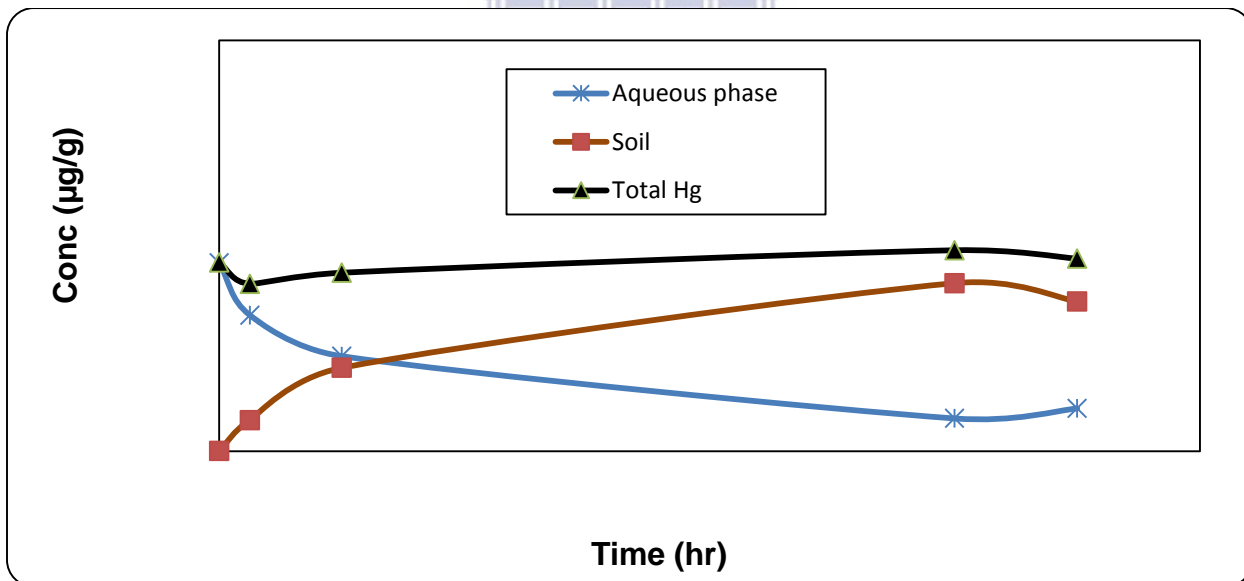


Figure B.8 Complexation of  $\text{Hg}^{2+}$  with HA in aqueous phase and soil at pH 8.0 at 303.15 K.

## APPENDIX C

### BIOAVAILABILITY STUDIES: DETERMINATION OF THE COMPLEXATION OF Hg<sup>2+</sup> WITH HA IN AQUEOUS PHASE, SOIL AND EARTHWORMS *Eisenia andrei* at 293.15 K, 298.15 K AND 303.15 K.

**Table C.1** Data of the complexation and adsorption of Hg<sup>2+</sup> in aqueous phase, soil and earthworms of the control at 293.15 K.

Time (hr)	Aqueous phase (µg/mL)	Soil (µg/g)	Earthworms (µg/g)
0	0.097	0.004	0.580
1	0.193	0.199	1.640
4	0.121	0.576	3.573
24	0.046	0.255	2.151
28	0.041	0.311	4.382
48	0.014	0.363	3.732

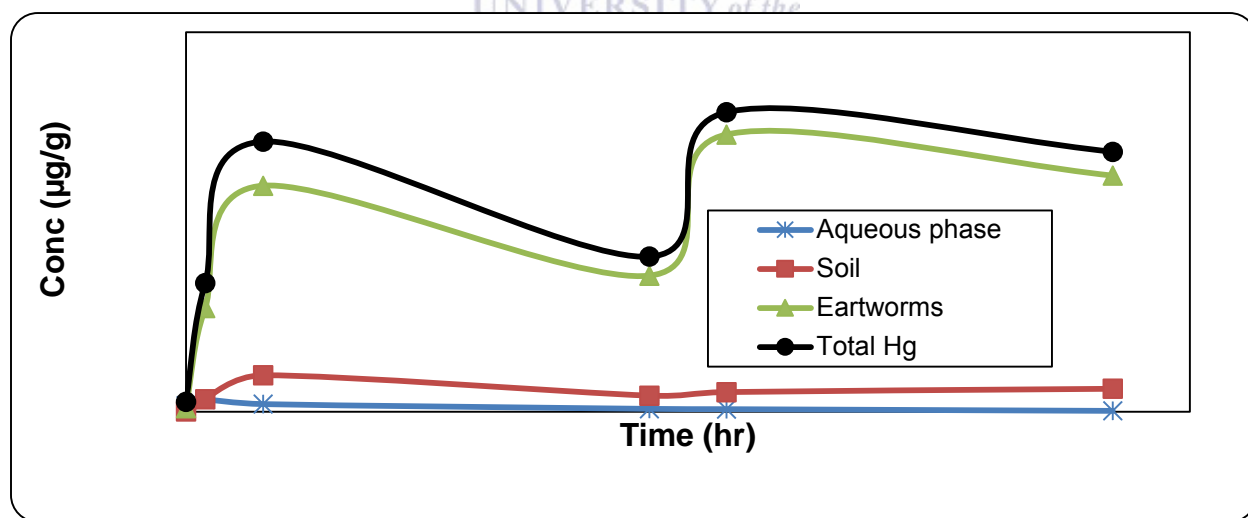


**Figure C.1** Complexation and adsorption of Hg<sup>2+</sup> in aqueous phase, soil and earthworms in the control sample at 293.15 K.

**Table C.2** Data of the complexation of  $Hg^{2+}$  with HA in aqueous phase, soil and earthworms pH 7.0 at 293.15 K

	Aqueous phase ( $\mu\text{g/mL}$ )	Soil ( $\mu\text{g/g}$ )	Earthworms ( $\mu\text{g/g}$ )
0	0.176	0.010	0.006
1	0.008	0.240	3.717
4	0.096	0.215	4.644
24	0.032	0.268	4.202
28	0.008	0.299	3.317
48	0.024	0.245	3.732

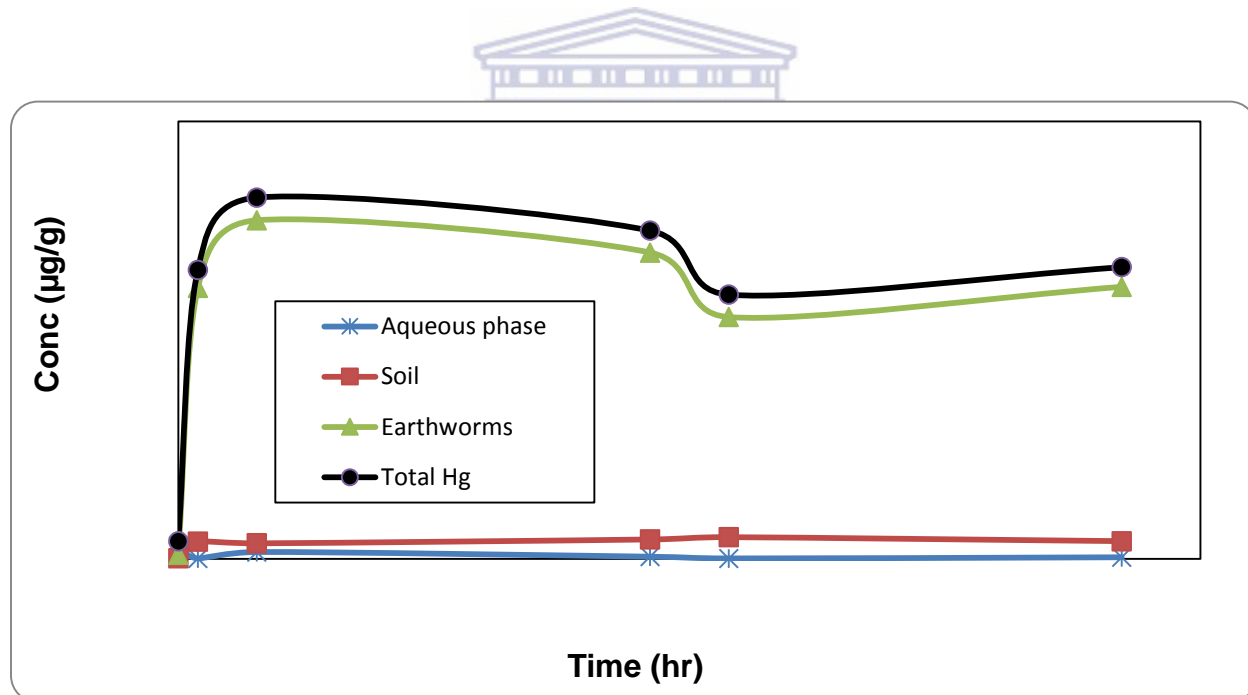


**Figure C.2** Complexation of  $Hg^{2+}$  with HA in aqueous phase, soil and earthworms at 293.15 K at pH 7.0.

**Table C.3** Data of the complexation of  $\text{Hg}^{2+}$  with HA in aqueous phase, soil and earthworms at pH 8.0 at 293.15 K

Time (hr)	Aqueous phase ( $\mu\text{g/mL}$ )	Soil ( $\mu\text{g/g}$ )	Earthworms ( $\mu\text{g/g}$ )
0	0.135	0.001	0.006
1	0.065	0.476	2.170
4	0.055	0.598	3.062
24	0.026	0.659	3.127
28	0.020	0.595	2.166
48	0.019	0.65	2.417

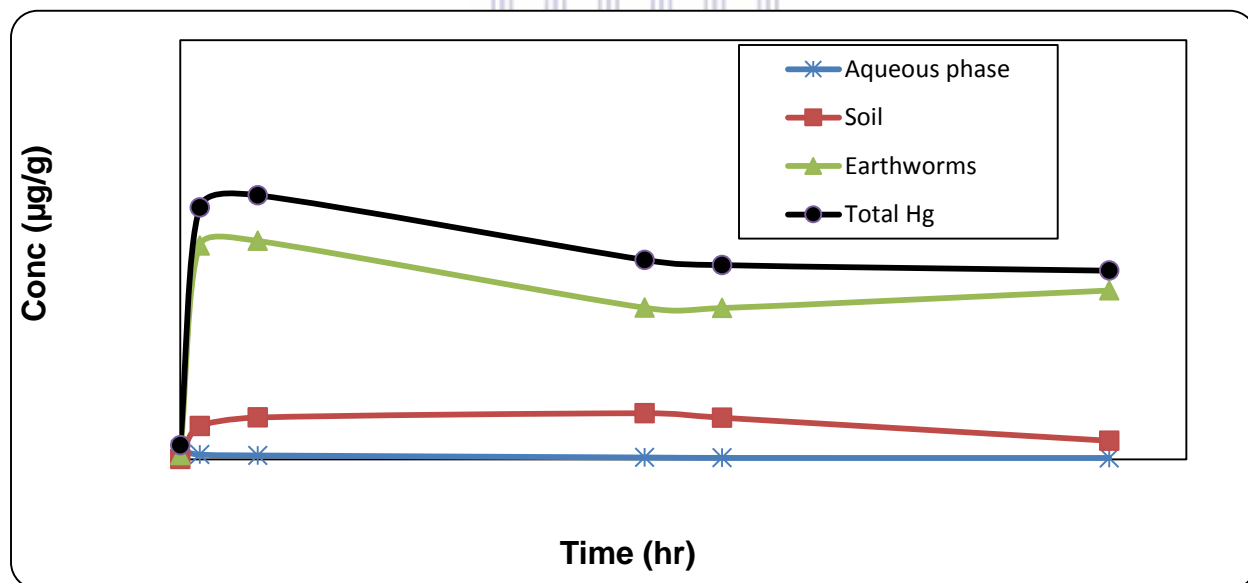


**Figure C.3** Complexation of  $\text{Hg}^{2+}$  with HA in aqueous phase, soil and earthworms at 293.15 K at pH 8.0.

## COMPLEXATION OF Hg<sup>2+</sup> WITH HA IN SOIL AND EARTHWORMS AT 298.15 K

**Table C.4** Data of the complexation and adsorption of the Hg<sup>2+</sup> in the control in soil and earthworms at 298.15 K

Time (hr)	Soil (µg/g)	Earthworms (µg/g)
0	0.116	0.019
1	0.126	0.066
4	0.133	0.112
24	0.105	0.242
28	0.134	0.223
48	0.103	0.172

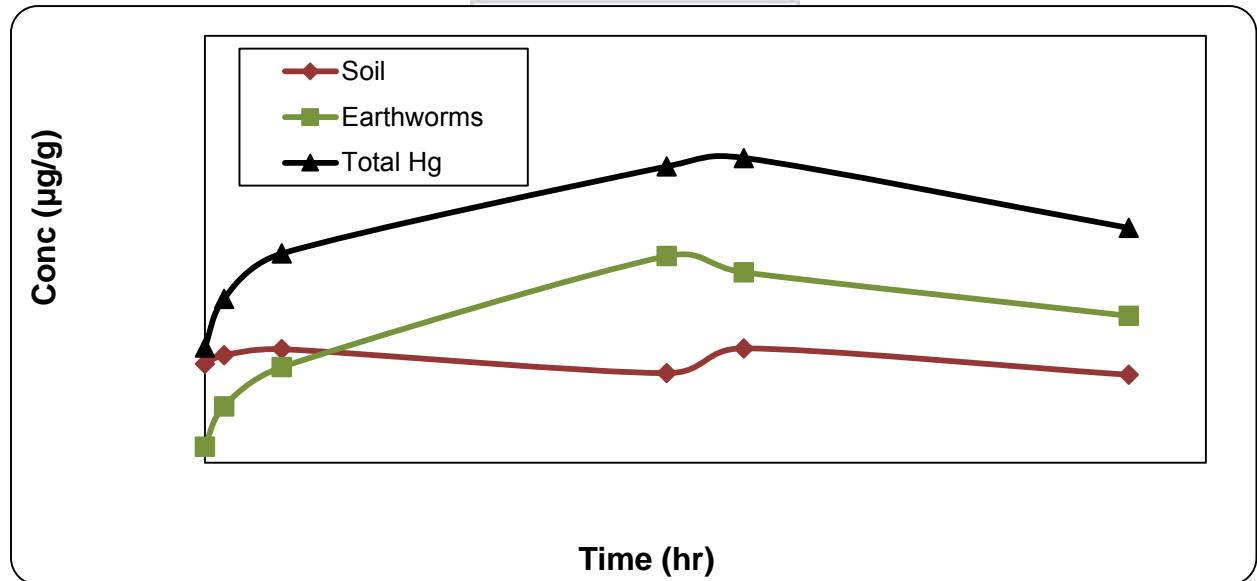


**Figure C.4** Complexation and adsorption of Hg<sup>2+</sup> in soil and earthworms in the control group at 298.15 K.

## COMPLEXATION OF Hg<sup>2+</sup> WITH HA IN SOIL AND EARTHWORMS AT 303.15 K

**Table C.5** Data of the adsorption and complexation of the Hg<sup>2+</sup> in soil and earthworms of the control group at 303.15 K

Time (hr)	Soil (µg/g)	Earthworms (µg/g)
0	0.004	0.019
1	0.231	0.066
4	0.185	0.023
24	0.108	0.047
28	0.023	0.045
48	0.123	0.055

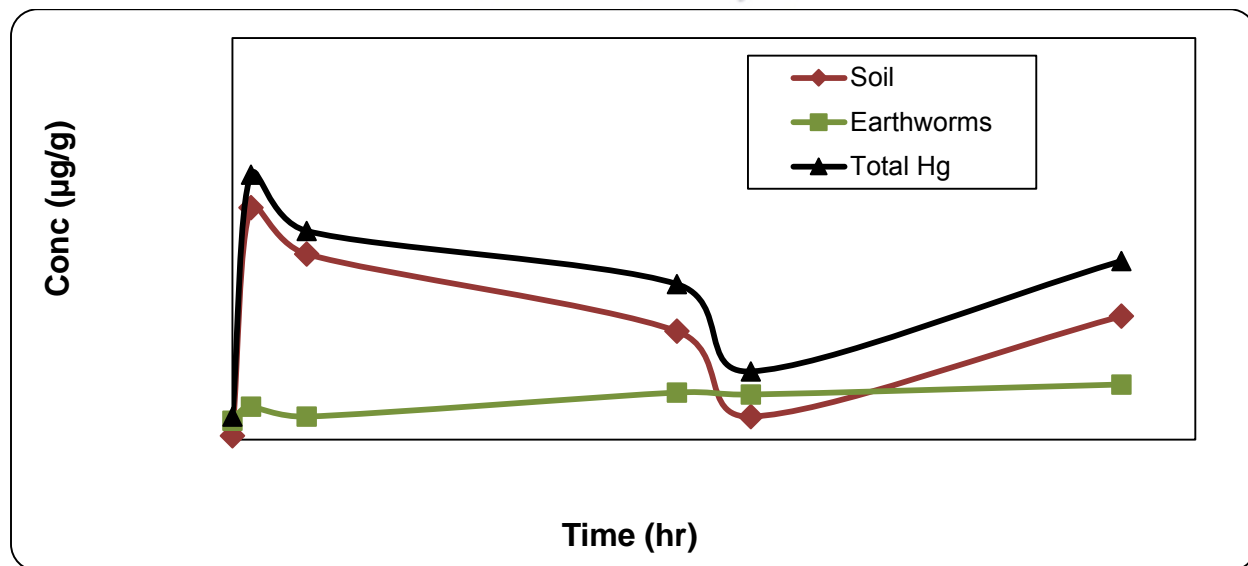
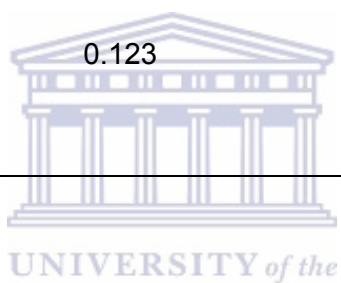


**Figure C.5** Complexation and adsorption of Hg<sup>2+</sup> in the control group in soil and earthworms at 303.15 K.